HIGH-TEMPERATURE DRYING OF *PINUS RADIATA* BOARDS IN A BATCH KILN

A Thesis

Submitted in Fulfilment of the Requirement for the Degree
of
Doctor of Philosophy in Chemical and Process Engineering
to
the University of Canterbury

by

Pang Shusheng

Department of Chemical and Process Engineering

University of Canterbury

1994

Acknowledgements

My sincere thanks are due to:

Professor R.B. Keey, the principal supervisor, for his most valuable help in carrying out this project, in obtaining the scholarships and in the financial support. Dr J.C.F. Walker, the co-supervisor, who has helped me greatly in understanding and tackling the problems on wood properties. The advice, comments and encouragement from Professor R.B. Keey and Dr J.C.F. Walker and their willingness to discuss any problems I have ever had are most acknowledged.

Dr T.A.G. Langrish of Sydney University for his help in computer programming and for the discussion in preparing this thesis.

Mr W.R. Miller, Mr A.N. Haslett and Mr I.G. Simpson of New Zealand Forest Research Institute Ltd (now Mr W. Miller has left NZFRI) for their help and arrangement in conducting the drying experiments.

Dr R.M. Allen, Mr A.C. Allen and Mr J. Thompson of this Department for their help in using the computer systems.

The Department of Chemical and Process Engineering of this University and the New Zealand Ministry of External Relation and Trade through this University for providing the scholarships, the New Zealand Public Good Science Found for the financial support (under contract UOC 302).

Mrs Daphne Keey for her enthusiastic hosting in New Zealand and in England while I was attending an overseas conference.

Finally, my wife, Li Jingge, for the understanding of my long hours absence from home when preparing this thesis and my daughter, Dimeng, for her cheering me up especially when the things went tough.

Contents

Summary

In New Zealand, high-temperature drying (i.e. drying at temperatures higher than 100°C) of softwood boards, particularly *Pinus radiata,* is widely used because it gives much faster drying than is possible at lower temperatures. However, drying defects limit its use where the quality is important. This thesis presents studies on understanding and describing the high-temperature drying of the softwood board in a batch kiln. These studies include: (1) the investigation of wood physical characteristics and properties, which are related to drying; (2) the mathematical simulation of moisture movement and heat-transfer within a board; (3) the experimental studies on drying a single board; (4) the kiln-wide analysis of drying a stack of boards and (5) the evaluation of the airflow reversals.

(1) On examining the structure of softwood and the movement of liquid material in a tree, the botanical phenomena have been related to the drying of the wood. Pits aspiration is the main factor affecting the movement of moisture in the wood during drying. In green sapwood, the bordered pits are usually open, so liquid materials are able to transport from one tracheid to another towards the drying surface of a board on drying. The pits around the wounded region will close (aspirate) when the wood is damaged in some way such as the stand is fell or the timber is sawn out. In coniferous species, the formation of the heartwood is usually accompanied by the aspiration of tracheid pits and losses of moisture. The sapwood is more permeable both to liquid and gas flows than heartwood. These features of wood have made it possible to develop a mathematical model to simulate the drying of a single board.

In modelling of the process of timber drying, some wood properties and physical parameters are used, including the equilibrium moisture content of wood, heat of sorption of timber, permeability of wood, wood basic density and moisture content *etc.* These have been reviewed from literature or measured in the drying experiments.

(2) In the model, the drying is essentially expressed by two processes: in the first one liquid water evaporates and water vapour moves towards the drying surface and in the second one, only bound water and water vapour remain. In the drying of heartwood, as the liquid movement is insignificant, an evaporative front is assumed to withdraw into the wood from the start of drying. At this front, all the liquid water evaporates until the evaporative front has reached the mid-layer of the board. In subsequent drying, bound

water diffusion and water vapour movement control the drying. With the drying of sapwood, there is an initial period when the drying is dominated by the liquid water flow towards the drying surface. However, in a thin layer close to surface the drying is very rapid as the wood cells are damaged during the milling process. When the liquid is no longer funicular just beneath this thin dry layer, the evaporative front will withdraw further into the material and the subsequent drying is similar to that of heartwood. This model has been used to predict the moisture content and temperature profiles within the board.

Board, which contains mixed sapwood and heartwood, comprise a significant proportion of a kiln stack of boards. The drying of such boards has been simulated by dividing the whole drying into three phases according the positions of evaporative fronts from both the sapwood and heartwood sides. These calculations show that a mixed board dries more slowly than a board consisting of entirely heartwood or sapwood.

(3) Tests were carried out at New Zealand Forest Research Institute (NZFRI) to dry a single board of sapwood, heartwood and mixed sap and heartwood. In the drying, the temperatures at different depths of a board were monitored to give temperature variations both with distance from the surface and with elapsed time. From the tests, the differences in temperature profiles between the drying of a sapwood, heartwood and mixed wood board have been found. The changes in average moisture content have been calculated by measuring the sample weight during drying. Separate samples were dried to examine moisture gradients within a board by cutting the sample into slices at different stages of drying. These results have been used to test the proposed mathematical model.

(4) The results produced from the mathematical model of drying a single board of entire sapwood and entire heartwood have been simplified by using the concept of characteristic drying curves. This concept was developed by Keey for the drying of slabform particulate materials. In this thesis, this concept has been extended in that the falling-rate drying is expressed by two separate curves. These two curves are distinguished from the point when the evaporative front reaches the mid-layer of the board. By taking moisture mass balance between the boards and airstream in a kiln, a method has been proposed to calculate the variations in external humidity and in local mean moisture content of the boards. The profile of external temperature through a kiln stack has been simulated by considering the heat conservation.

(5) By employing the models proposed in this thesis, an investigation has been made to examine the influence of airflow reversals both on the drying of a single board and on the

drying of a kiln-stack. With this study, the current policy of reversing air flow has been evaluated and recommendation has been made to improve the drying operation.

In the kiln-wide analysis and evaluation of airflow reversals, the variations of external transfer process has been taken into account. The external mass-transfer coefficients over a single board vary with distance from the leading edge, having a peak value about the leading edge and reaching an asymptotic value towards the trailing edge. The board average mass-transfer coefficient across a kiln stack reveals a higher value over the first two or three rows of boards in the stack, while the coefficients onwards are virtually constant except for a slight reduction over the last row of board due to the edge effect.

The convective heat transfer coefficients in the airstream have been calculated from the experimental data of mass-transfer coefficients by using Chilton-Colburn analogy. The radiative heat has been taken into consideration. The higher value of heat-transfer coefficient than that predicted from the analogy is consistent with the early experimental results by other authors.

Chapter 1

Introduction

When describing the dependence of mankind civilization on the utilization of wood, Panshin states (1964):

> *The more technologically advanced man has become, the more diverse and sophisticated uses he has found for wood.*

This may be recognised by the fact that in the known history, man used the wood first for shelter, for weapons, for fire to cook, then for transportation by wheel and boat, and last for large structures and luxury furniture. The progress in using wood has been accompanied by the development of wood processes, one of which is wood seasoning or drying.

A freshly felled tree contains varying amount of water, being possibly as high as twice of its wood material, or as low as 40% in some other cases. However, wood will eventually lose most of this water either artificially or naturally to reach an equilibrium with its surroundings. The corresponding equilibrium moisture content can be as low as 6% in very dry, hot weather (30°C, 30% relative humidity) or as high as 20% in damp warm conditions (20°C, 90% relative humidity). Therefore, although green wood may be used for framing or roofing timbers, wood for most uses must first be dried. There are some important reasons for drying the wood prior to use (Walker, 1993; Koch, 1972):

- Wood shrinks as it loses moisture with moisture content below a value of about 30% (fibre saturation point). Drying will make the wood stable and minimise its movement in use.
- Drying reduces the possibilities of stain or decay developing during transport, storage or use.
- Dry wood is less susceptible to damage by insects than wet wood.
- Most strength properties of wood increase as it is dried below the fibre saturation point.
- Glued wood products perform better when assembled from dry wood.
- Prior drying usually makes treatment of wood with preservatives more successful.

Some other benefits of drying the wood include the reduction of shipping weight, and the increase of thermal insulation and electrical resistance.

Wood seasoning is probably most important for timber (lumber) and its products, as they are often used for interior use under humidities and temperatures dictated by human comfort (Keey and Ashworth, 1979). If the timber is dried inappropriately, some problems will occur in use. For example, if a 0.5 m wide board having a moisture content above 30% is used in construction and left to equilibria with typical ambient conditions (20°C and 60% relative humidity), then it will shrink 0.021 m at the time when the board reaches that equilibrium. Also if the board is loaded, the strength of the green board is only two third of that of a dry board with equilibrium moisture content of 10% in the above surroundings (NZ Ministry of Forestry, 1988).

Before the kiln seasoning came into use, all timber were dried in the open air, a process which is usually referred to as air seasoning or air drying. In air seasoning, the boards are piled in a stack with separating stickers. The air horizontally entering a stack (due to wind action) picks up moisture from the wood, and in doing so, is cooled tending to fall to the bottom and finally escaping away, to be replaced by the fresh air. In order to obtain rapid air-drying, vertical channels or chimneys are arranged. This allows moisture-laden air to fall and encourages a continuous flow of air through the pile.

Even though much care has been exercised, air seasoning of wood is largely dependent on the vagaries of wind, sun and rain, and so is extremely difficult to control. The duration of the air drying 25 mm thick timber may last from 40 to 150 days for most softwoods such as pine species to reach a moisture content of approximately 20% while cypress may needs over 200-275 days (Brown and Bethel, 1966).

In contrast to air-seasoning, timber drying kilns provide a means of overcoming the limitations imposed by natural climate. In the kiln drying, the stacks of boards are loaded into a chamber, in which the dry-bulb temperature, humidity of the air and the air velocity through the stack can be controlled. With higher drying rates obtainable in the drying kilns, timbers can be kiln-dried faster than by air-drying. The 25 mm thick lumber mentioned above now needs only 3-7 days (10-20 days for cypress) with the USA typical schedules for conventional kiln-drying of pine species timber (Brown and Bethel, 1966).

The timber drying kiln may be classified in various ways: (1) based on the method of charging; (2) based on the type of air circulation or (3) based on the temperature of circulated air.

On the basis of charging, the kilns may be classified as either progressive or compartment-type (batch) kiln. In progressive kilns, trucks of boards are loaded into one end of the kiln, they progress through, and are finally discharged from the other end of the kiln. The moisture content of boards' in these kilns decreases progressively from initial value to the required value. In the batch kiln, on the other hand, the boards are loaded into kiln until it is full. The kiln is then closed and drying starts. All of the boards are discharged at the end of the drying run. Before the Second World War, there were a number of progressive kilns in operation in various countries, but these have almost disappeared in favour of the batch kilns (Brown, 1965).

On the basis of air circulation, kilns may be described as natural circulation kilns or forced circulation kilns. Natural circulation kilns are designed to provide air movement by natural means (Brown and Bethel, 1966). This type of kiln is very rare recently. Although natural circulation kilns can save some energy without fans, most of the modern kilns are designed as forced circulation kilns to achieve higher and controlled drying rates. Forced circulation kilns provide the air flow through a stack by fans mounted inside the kiln.

Historically, drying kilns have been operated at temperatures below 100°C. This type of kiln is now referred to as a conventional kiln (or low temperature kiln) in order to distinguish them from newly developed kiln in which air temperatures are greater than 100°C. The latter is usually called a high-temperature kiln. Since the high temperature drying can significantly reduce the drying time and save energy compared with conventional lower temperature kilns (Hanson, 1988), it has been actually studied for over two decades. However, due to drying defects such as checking, distortion and the lack of complete understanding of the process, the high-temperature drying, as a commercial practice, has been restricted to permeable softwoods such as southern pine (*Pinus palustris, P. elliottii, etc.*) in the USA and *Pinus radiata* in Australia and New Zealand. The temperatures used are usually below 150°C.

There are two processes of high-temperature drying. The first uses mixtures of air and steam. The air is brought in by the fans and heated by the coils within the kiln while low-temperature steam may be injected for deliberate humidification. The operation is controlled by the dry-bulb and wet-bulb thermometers placed within the kiln. The air velocity is controlled by the fan speed. During drying, the kiln is tightly sealed except for several vents which allow a proportion of exhausted damp air to be replaced with fresh air. This process is widely adopted in New Zealand and Australian to dry the of *Pinus radiata*. The second process uses superheated steam, i.e., steam above the boiling point of

water. In this system, the steam occupies the kiln to the complete exclusion of air. The steam can give up its superheat without condensing and thus act as a dry media. There is no air present and the process is only controlled by dry-bulb temperature. This process is usually used in the USA to dry southern pine (*Pinus palustris, P. elliottii, etc.*) (Culpepper, 1990).

This thesis will present the studies on the drying of softwood board, specifically *Pinus radiata*, in a forced circulation high-temperature batch kiln. In the following discussion, this type of kiln will be called a high temperature kiln for short.

1.1 Description of the Drying Operation in A High-Temperature Kiln

Figure 1.1a is a photograph of a high-temperature kiln manufactured by Windsor Engineering Ltd., New Zealand while Figure 1.1b provides a simplified, schematic end view of the kiln. Before drying, the wet boards are stacked edge by edge, layer on layer with separating stickers. Then a weight of 1000 kg m^{-2}, which is recommended by New Zealand Forest Research Institute (NZFRI), is placed on the top of the stack and the stack is ready to be loaded into the kiln. When the kiln is full, it is tightly sealed and the drying starts by turning on the fans. During drying, the air driven by the fans passes through the heating coils and is heated up to the desired temperature. As the hot air flows between the boards layers in the stack, it gives off the heat to the surfaces of boards to evaporate the moisture in wood and at the same time carries away the moisture vapour. In this way, the timber is dried continuously. The dry-bulb and wet-bulb temperatures are monitored and regulated to obtain the required drying rates. The air temperature is controlled by changing the temperature or flux of the heating medium in the heating coils, while the relative humidity is adjusted by the extent to which the vents are opened or by injecting low-pressure steam. In the commercial practice, the airflow direction is usually reversed every few hours during drying by switching over the fan direction. When all of the boards have reached 2 - 3% (MC) below the required final moisture content, the drying stops and the boards will then be conditioned with fully saturated steam. When this has been done, the drying is finally accomplished and the boards are ready to be dispatched.

In New Zealand, high-temperature kiln drying has become a preferred practice to dry the plantation grown softwood boards, such as *Pinus radiata*. By applying techniques developed at NZFRI (Williams and Kininmonth, 1984; Haslett and Simpson, 1990), timbers of 50mm thick or less can be successfully dried at a dry-bulb temperature of

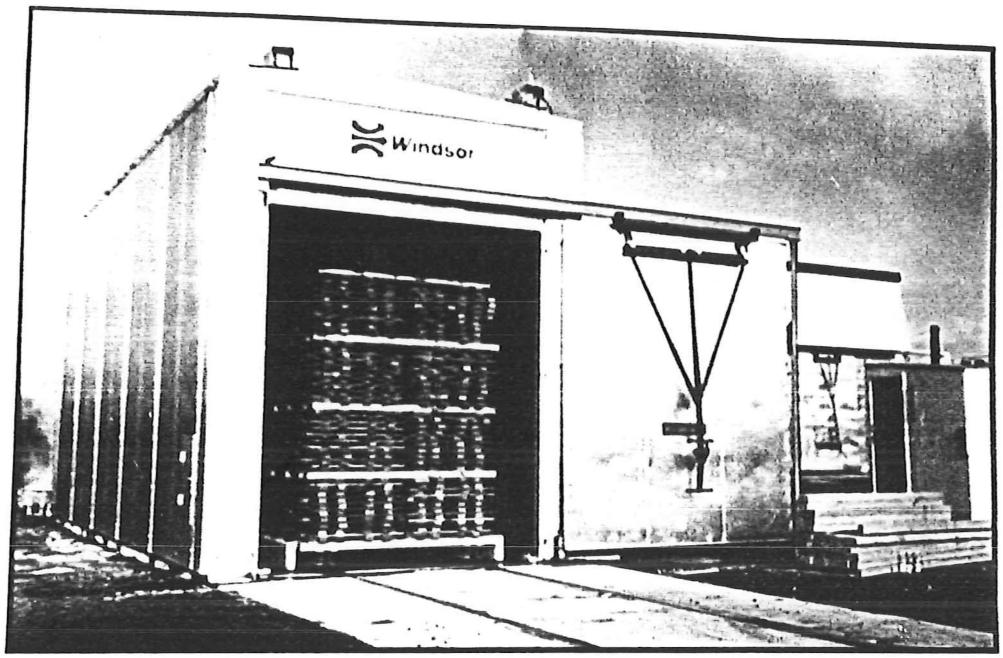

(a). Photograph of a high-temperature kiln by Windsor Engineering Ltd.

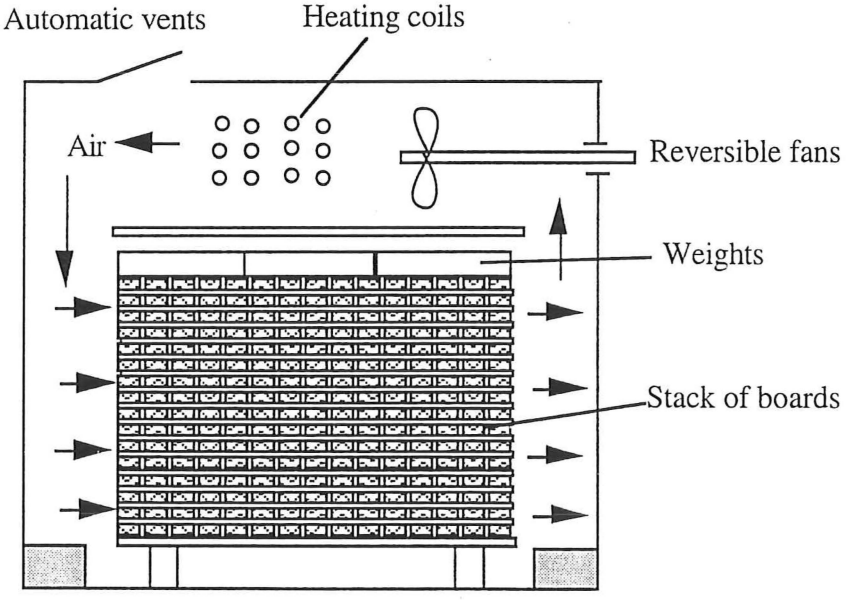

(b). The simplified, schematic end view of the high-temperature kiln.

Figure 1.1. A high-temperature kiln to dry New Zealand *Pinus radiata* boards.

120°C and a wet-bulb temperature of 70°C without significant degrade. However, when using higher temperatures than 120°C, or drying the boards with thickness greater than 50 mm or other species of wood, some problems become significant.

1.2 Problems in High-Temperature Kiln Drying

Two major problems are usually encountered with the rapid drying in the high-temperature kiln: (1) drying defects such as checking, distortion *etc.*, and (2) uneven moisture-content distribution across a stack.

1.2.1 Drying Defects

Drying defects occur during or after drying and represent a loss of board quality by reducing the tensile strength, distortion or spoiling the appearance of the material. Distortion has been restricted by placing weights on the top of the stack before drying. Checking, however, is a major defect restricting the utilization of higher temperatures to achieve even higher drying rates, although reconditioning immediately after drying is effective for the drying at temperatures of 120/70°C. This technique is recommended by Williams and Kininmonth (1984) and Haslett and Simpson (1990) to minimise the internal checks subsequently developing in the middle region of a board. Williams and Kininmonth (1984) show that of every 60 checks, half occur within 100 mm from the ends and rest between 100 and 200 mm with conditioning, while without reconditioning half the checks in every 60 have been found beyond 500 mm from the ends. However, no board was observed to be free of checking at both ends. Haslett and Simpson (1990) extended the HT (high-temperature) schedules to the drying of 100x100 mm furniture squares. Squares are more susceptible to internal checking than 50 mm boards. They developed a HT schedule capable of drying sapwood squares while restricting the internal checks to less than 5% of the board length. For heartwood, internal checks could be restricted to places near the ends by steaming at a critical point in the drying process. However, there is a problem with mixed sap and heartwood since the critical time for the steaming could vary from heartwood to sapwood during the same drying conditions.

Some analysis of stress development and check formation has been performed by Pang *et al.* (1992c). Causes of this defect are considered to be the excessive induced stress or strain and this may be further traced to differential shrinkage due to moisture-content and temperature gradients within the board. During drying, heat is transferred from the airstream to the surface of the board and then through the material, resulting in outward

movement of the moisture. This movement is only possible when a moisture-content gradient exists. During the initial stages of drying, the shell of the timber dries and attempts to shrink (when the moisture content falls below the fibre saturation point, X_{FSP}), while the core has not yet begun to dry to any extent and to shrink (the moisture content is still above X_{FSP}). As a result, the shell is restrained from shrinkage by the core. The shell goes into tension and the core into compression. If drying in the shell progresses too rapidly, it is stretched irrecoverably and dries in a permanently stretched condition, without attaining full shrinkage. It would be expected that surface or sub-surface checks occur during this stage of drying if the strain induced by stress exceeds the fracture limit of the material.

As drying progresses further, the core begins to loose moisture and attempts to shrink. However, the shell has been set in a permanently swollen condition which prevents normal shrinkage in the core. This causes the stresses within the board to reverse. The core goes into tension and the shell into compression. The tensile stresses in the core may be severe enough to cause or contribute to internal checks of the board.

When green wood is heated it may expand or shrink depending upon the growth stresses and the intensity of heating. As growth stresses are believed to be low for *Pinus radiata* relative to the strength of the material, the release of the growth stresses should be insignificant. Therefore, the dimensional changes are primarily caused by normal thermal expansion and by contraction due to loss in moisture from the wood substance. Such changes in dimensions may be significant in the preheating period and would contribute to the total strains during subsequent drying.

1.2.2 The Uneven Moisture-Content Distribution

Recently higher temperatures of air than 130°C have been tried in commercial kilns in New Zealand. However, noticeable nonuniformity in moisture-content profile during the high-temperature drying has been found across a kiln stack. On one occasion, the author accompanied a staff of NZFRI when he examined the moisture-content variation in a stack of *Pinus radiata* boards dried at a sawmill near Rotorua. Within the same stack, some boards were as dry as 5-6% moisture content, whereas some others were still wet with moisture content of 40-50%. Although this may be an extreme example, the difference of 20-30% in moisture content through a stack is not unusual in practice despite that the kilns are operated with airflow reversals.

On the basis of previous work (Pang, Keey and Langrish, 1991, 1992a and 1992b; Ashworth, 1977; Keey and Ashworth, 1979), it is believed that the variation in moisture content within a stack could be caused by the variations in external conditions as well as the differences in internal structure of the boards. As the air flows across the boards, the dry-bulb temperature drops and humidity increases in the airflow direction. It is also observed that the external mean mass-transfer coefficient decreases and tends towards an asymptotic value over the following boards behind the front one or two rows (Kho, Keey and Walker, 1989; Langrish *et al.*, 1992). Consequently, the boards in the front of the stack dry rapidly while those towards the end of the stack dry somewhat slowly without airflow reversals.

The differences in the internal structure of the boards will also affect the ease of drying. The heartwood has a lower initial moisture content, but the wood is less permeable and the liquid flow is insignificant due to the extent of pit aspiration in the greenwood. In contrast, the permeability, both to liquid and gas flow, is higher for the much wetter sapwood. When the board consists of both sapwood and heartwood, the moisture movement becomes complicated as some moisture migrates through the heartwood layer while other moisture moves across the sapwood zone. Since the ease of drying the board is closely related to the permeability of wood, the permeabilities both to liquid and gas flows become very important factors.

Booker (1989) has observed that the permeability varies with directions (radial, tangential or longitudinal), so the timber orientation in the different sawn direction will also affect the drying behaviour of the board. Since the radial permeability to liquid flow in green sapwood is much lower than that in tangential direction, when a board is exactly flat-sawn, the liquid flow perpendicular to the airflow direction may not be as high as that in a quarter-sawn board.

Although the above problems have been observed from early application of the high-temperature drying technique, these have not yet been fully understood and no satisfactory systematical studies have been published to quantitatively describe them. This situation is largely due to the complexities of the problems (Puiggali and Quintard, 1992; Kayihan, 1993).

1.2.3 The Complexities of the Problem

The complexities of the problem are mainly from two aspects involved in the drying: (1) the wood has a complex anatomy and is biologically diverse; (2) the drying rates vary across each board and throughout the kiln and the stacking of the boards is irregular to some extent.

Since the wood originally comes from a tree stem, understanding of the wood behaviour will be traced to the structure and composition of a living tree. Therefore, when seeking to tackle any problem in this field, it should be born in mind that in dealing with wood one is confronted not with a man-made material, manufactured to exact and reproducible specifications, but with a variable substance whose basic nature is by and large beyond man's control. The complexities can be recognised by the fact that trees may grow in different sites, different environmental surroundings such as climate, soil, moisture and growing space etc., and above all the trees are affected by genetic factors. Fortunately, not all of species of trees become commercial important. For example, in the United States, only 80 species out of 1027 are recognised as valuable for commercial use (Panshin, 1964; USDA, 1987). In New Zealand, and to a lesser extent, in Australia this can be seen more clearly where one species of plantation softwood, *Pinus radiata*, dominates the market (Kininmonth and Whitehouse, 1991). Today in New Zealand nearly 90% of the total area planted is in this species (Ministry of Forestry, 1988) — a position which seems unlikely to be challenged in foreseeable future by any of the hundred or more major forest trees. This is partially due to its good growth rates, disease resistance and partially, possibly more importantly, due to its capability of meeting requirements for a wide range of end uses.

The operation and associated irregularities also affect the drying in some ways. For example, it is found that it is beneficial to heat up the whole stack to near 100°C in as short a time as possible prior to the initial stage of drying (NZ Ministry of Forest, 1990). Also it has been observed that the irregularities of piling the boards and uneven distribution of airstream through the stack affect the drying to some extent (Kho, *et al.*, 1989; Culpepper, 1990; Kayihan, 1993).

However, with some improvements in the management of tree plantation, in boards preparation and in kiln operation, the complexities can be reduced to minimum so that systematical studies are able to be carried out with a review to quantitatively interpret the drying phenomenon.

1.3 The Objective of the Study

From the above discussion, it is apparent that in order to solve the problems encountered with the high-temperature kiln drying, we need first to understand the mechanisms of drying — moisture movement and heat transfer within a board, and then to quantitatively describe the drying process both with a single board and in the kiln-wide scale. The objectives of this study are:

- The examination of the physical characteristics and properties of wood. In this way we can see how the moisture could move during drying and what differences emerge between sapwood and heartwood with respect of the moisture movement (Chapter 2 and Chapter 4).
- The development of a comprehensive model to simulate the moisture movement and heat transfer within a single board, which can be applied to sapwood, heartwood and mixed sap/heartwood (Chapter 3 and Chapter 9). This model, based on the physical characteristics of wood, can be used to produce a picture of moisture-content and temperature profiles. These profiles will be verified by experimental data (Chapter 6).
- The modification of the model to produce a simplified description to carry out an analysis of drying on a kiln-wide scale. By using this analysis, moisture-content variations and external-condition changes can be predicted (Chapter 7) and the optimum operation conditions (airflow reversals) recommended for commercial operation (Chapter 8).

1.4 Assumptions

In this study, the following assumptions will be made:

- *Pinus radiata* is taken as an example of softwood.
- The wood comes from well-managed plantation forests with selected seedlings, which will tend to yield timber with less biodiversity (Keey, 1993).
- The boards are arranged in well-boxed stacks, with uniform stickers height and board thickness.
- The kiln is well-sealed and operated, so that the an uniform airstream flow through a stack results.

1.5 References

1. Ashworth, J.C. 1977. The Mathematical Simulation of Batch-Drying of Softwood Timber. Ph.D. Thesis. Chemical Engineering, University of Canterbury, Christchurch, New Zealand.

2. Booker, R.E. 1990. Changes in Transverse Wood Permeability during Drying of *Dacrydium cupressinum and Pinus radiata.* *New Zealand J. Forest Sci.*, 20(2) pp231-244.

3. Brown, N.C. and Bethel, J.S. 1966. "*Lumber*". 2nd edn. John Wiley & Sons, Inc. New York.

4. Brown, W.H. 1965. "*An Introduction to the Seasoning of Timber*". Pergamon Press. New York.

5. Culpepper, L. 1990. "*High-Temperature Drying—Enhancing Kiln Operations*". Miller Freeman Publications, Inc., San Francico.

6. Hanson, O.P. 1988. "*Contemporary Timber Drying*". British Timber Research and Development Association (TRADA). Buckinghamshire, England.

7. Haslett, T. and Simpson, I. 1990. Multi-Client Drying Project Compares HT and Conventional Drying. New Zealand Forest Research Institute, Rotorua. Wood Drying No.10 (unpublished).

8. Kayihan, F. 1993. Adaptive Control of Stochastic Batch Lumber Kilns. *Computers Chem. Engng.* 17(3) pp265-273.

9. Keey, R.B. and Ashworth, J.C. 1979. The Kiln Seasoning of Softwood Timber Boards. *The Chemical Engineers*, Aug./Sep., pp593-607.

10. Keey, R.B. 1993. Comments on Adaptive Control of Stochastic Batch Lumber Kilns by Kayihan. Private Communication.

11. Kho, P.C.S., Keey, R.B. and Walker, J.C.F. 1989. Effects of Minor Irregularities and Air Flows on Drying Rate of Softwood Timber Boards in Kilns. *Proc. of 2nd IUFRO International Wood Drying Symposium.* Seattle, Washington. pp150-157.

12. Kininmonth, J.A. and Whitehouse, L.J. 1991. "*Properties and Use of New Zealand Radiata Pine*", Vol.1: Wood Properties, New Zealand Ministry of Forestry, Forest Research Institute, Rotorua, New Zealand.

13. Koch, P. 1972. "*Utilization of the Southern Pine*". Agriculture Handbook No.420. USDA, Washington.

14. Langrish, T.A.G., Kho, P.C.S., Keey, R.B. and Walker, J.C.F. 1992. Experimental Measurements and Numerical Simulation of Local Mass-Transfer Coefficients in Timber Kiln. *Drying Technology*, 10(3) pp753-782.

15. Pang Shusheng, Keey, R.B. and Langrish, T.A.G. 1991. Modelling of the High-Temperature Kiln Drying of *Pinus radiata* Boards. Research Report No.1. Chemical and Process Engineering, University of Canterbury, Christchurch, New Zealand (unpublished).

16. Pang Shusheng, Keey, R.B. and Langrish, T.A.G. 1992a. Modelling of Temperature Profiles within Boards during High-Temperature Drying of *Pinus radiata* Timber. in Mujumdar, A.S. (ed.): "*Drying'92*", Elsevier, Part A: pp417-433.

17. Pang Shusheng, Keey, R.B. and Langrish, T.A.G. 1992b. Moisture Movement in Softwood Timber at Elevated Temperatures. *Proc. of 3rd IUFRO Wood Drying Symposium*, Vienna, Austria, pp112 - 122.

18. Pang Shusheng, Keey, R.B., Walker, J.C.F. and Langrish, T.A.G. 1992c. The Stress Development and Check Formation within Boards of Pinus radiata during High-Temperature Drying. Research Report No.3. Chemical and Process Engineering, University of Canterbury, Christchurch, New Zealand (unpublished).

19. Panshin, A.J., Zeeuw, C.D. and Brown, H.P. 1964. "*Textbook of Wood Technology*". 2nd edn. McGraw-Hill Book Co., New York.

20. Puiggali, J.R. and Quintard, M. 1992. Properties and Simplifying Assumptions for Classical Drying Models. in Mujumdar, A.S. (ed.): "*Advances in drying*". Vol.5, pp109-144. Hemisphere Publishing Co., New York.

21. NZ Ministry of Forestry. 1988. "*New Zealand Radiata Pine*". NZ Ministry of Forestry, Forest Research Institute, Rotorua, New Zealand.

22. USDA. 1987. "*Handbook of Wood and Wood Based Materials for Engineers, Architects and Builders*". Hemisphere Publishing Co., New York.

23. Walker, J.C.F. 1993. "*Primary Wood Processing: Principles and Practice*". Chapter 8: The Drying of Timber. Chapman and Hall, London.

24. Williams, D.H. and Kininmonth, J.A. 1984. High-Temperature Kiln Drying of Radiata Pine Sawn Timber. New Zealand Forest Service, Forest Research Institute Bulletin No.73, Rotorua, New Zealand (unpublished).

Chapter 2

Physical Characteristics of Softwood

Wood is a hygroscopic material, which will adsorb or give up moisture, according to the surrounding conditions. It is, however, heterogeneous since it consists of a highly complex mass of vascular fibre tissue which nature intended to provide the tree with the means to live (Brown, 1965). The behaviour of wood during drying and afterwards, varies with the species and within species. Therefore, to understand the drying process, it is necessary to understand the structure and some physical characteristics of wood which are related to drying.

Timbers are classified into softwoods and hardwoods. Botanically, softwoods include the timbers from the needle-leaved trees, most of which are evergreen (Butterfield, 1993). Hardwoods, on the other hand, generally mean the deciduous trees with broad-leaves. The difference in drying behaviour between softwoods and hardwoods lies mainly in the different structure and some physical properties rather than the true hardness as their names might indicate. In fact, 'soft' and 'hard' in the names have lost the meaning of hardness as a scientific term. Although the average specific gravity of commercially important domestic hardwoods (0.50) is greater than that of softwoods (0.41), hardwoods are by no means harder than softwoods, as considerable overlap occurs in the range of specific gravities (softwoods: 0.29 - 0.60; hardwoods: 0.32 - 0.81) (Lewin and Goldstein, 1991). Thus, some softwoods are 'harder' than some hardwoods and some hardwoods 'softer' than some softwoods. This thesis will, as mentioned in the previous chapter, only examine softwoods, specifically New Zealand plantation species *Pinus radiata*. Since the tissues of wood are closely related to their functions in a tree stem, the growth of a tree will briefly be discussed first.

2.1 Growth of the Tree

When a seed of the tree has germinated, it sends down into the earth roots which will draw up mineral salts in solution. These are the basis of the tree's food. The germinated seeds also send upwards a stem which will ultimately form the trunk and therefore the subsequent timber. The stem will increase in height and girth, year after year, until maturity is reached. For *Pinus radiata* planted in New Zealand, the trees will grow in

around 30 years to produce mature timber. In a living tree, wood in stem performs the functions of conduction, support, and storage (Lewin and Goldstein, 1991). The conduction role involves the movement of water from the roots up the woody stem to the leaves. The heights of trees and their weights, not only of the stem but associated branches and foliage, as well as external loading (e.g., wind), require a strong support system. The third main function of wood is the storage of food in the form of starch.

The tree depends on carbon, oxygen and hydrogen to live. These are provided and conducted in the following manner: Initially, roots send upwards water soluble minerals salts through *sapwood*, which is the wood layer beneath the bark, to the leaves. In the leaves, a complicated system of photosynthesis produces carbonhydrates taht contribute to the growth of woody material (Figure 2.1a).

Immediately under the bark may be found a narrow zone of thin-walled cells, which is known as the *cambium.* The cambium is essential for the continuing growth of the tree since wood is produced in it. As the crown of the tree gets larger with more leaves and branches, the stem increases in diameter to support the extra load. More wood is added by cambium to trunk and the stem thickens (Butterfield, 1993).

2.1.1 Growth ring

In each growing season, trees develops a new layer of wood over the entire stem between the existing wood and the bark. This new addition of wood is termed a *growth ring*. In the temperate zones such as New Zealand, trees usually grow rapidly early in the season, and the rate of growth slows down appreciably as the season advances. During the early period, the portion of the growth formed in the same ring has large-diameter and thin-wall cells which are quite porous. This part of the ring is commonly designated as *earlywood* or *springwood.* Later in the season, denser and hence frequently darker wood with cells of small-diameter and thick-wall is produced. This part is termed *latewood* or *summerwood.*

Growth rings of *Pinus radiata* are distinct due to the visible differences between earlywood and latewood. The proportion of latewood typically ranges from 10% near the pith to 50% in the outerwood. The transition from earlywood to latewood is gradual compared with that found in species such as Southern pine or Douglas fir (Cown, 1989).

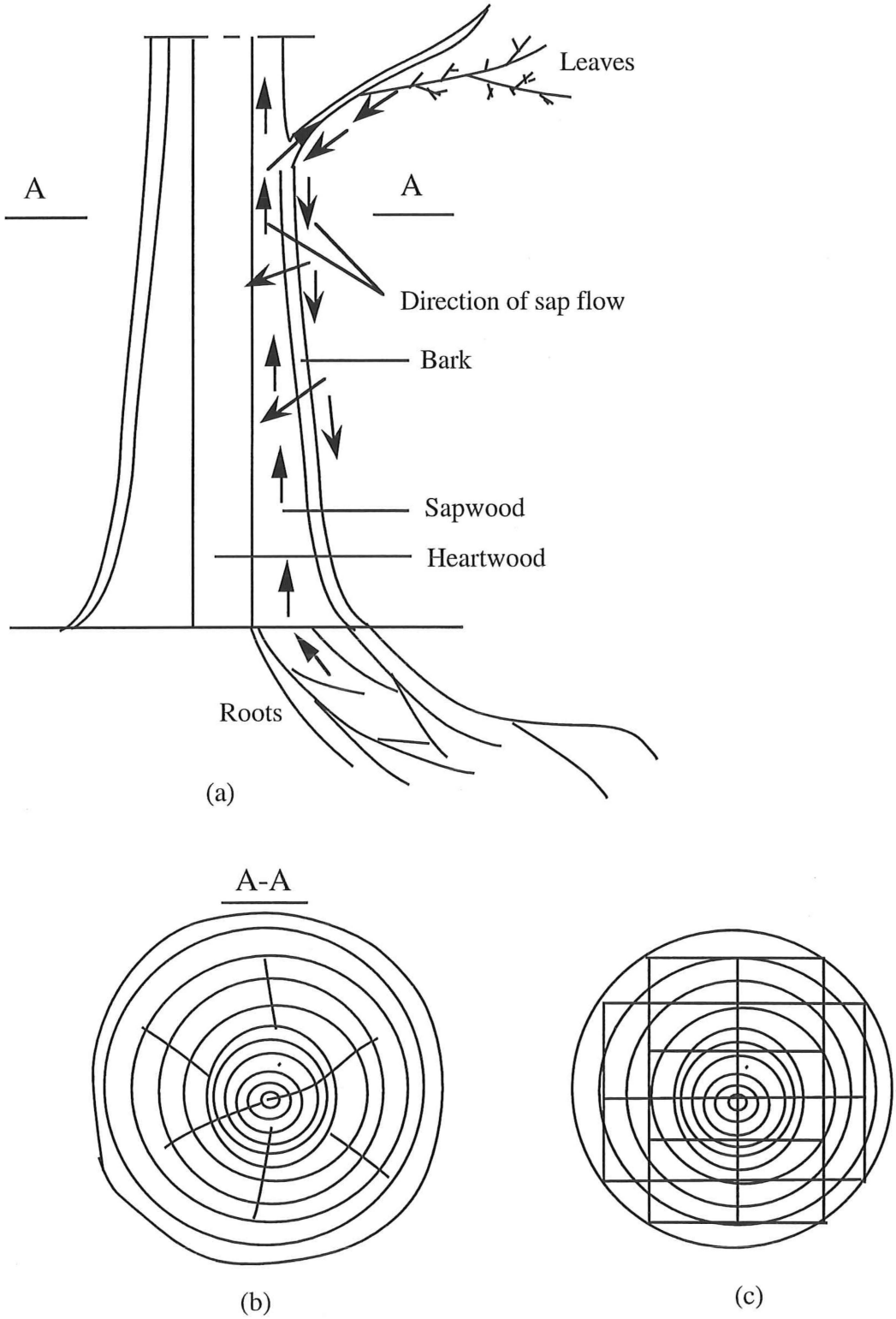

Figure 2.1 The sectional scanning of a living tree and the log.

(a). the cross-section cut along the pith of a living tree and the moisture movement;

(b). the cross-section cut at straight angle to tree pith;

(c). the sawn-patter to produce commercial timbers (NZ Ministry of Forestry, 1991).

2.1.2 Sapwood and Heartwood

As a tree grows, the outer rings of wood immediately under the bark form the sapwood. This newly formed wood performs the roles of support, conduction and storage. Generally speaking, the sapwood is recognised by its lighter colour. In a very young sapling the proportion of sapwood to heartwood is very high. As the trees grow, the fractional amount of sapwood decreases as the food-storage cells die and is species-dependent. The subsequent death of these cells is usually accompanied by some physical and chemical changes, which may correspond to the onset of dark-coloured heartwood formation. The reasons for heartwood formation is not yet fully understood. However, it is observed that during the production of heartwood starch is hydrolysed to sugar which in turn breaks down, and is oxidized and polymerized to yield phenolics. Extractives (resin) are formed and deposited (Brown, 1965; Cown, 1989; Butterfield, 1993). Another important change associated with heartwood formation is that the connections between the cells (*bordered pits*) become blocked (aspirated) and coated with resins, thus decreasing the permeability of wood. With advancing tree age, the heartwood becomes 'enriched' with resin produced by sapwood and transported towards the pith by the resin canals. The heartwood of mature stems can have high resin content, especially near the pith.

Table 2.1. The tree heartwood and sapwood contents in *Pinus radiata* (After Cown, 1989)

Tree Age (year)	% of tree volume	
	Heartwood	Sapwood
10	0	100
20	10	90
30	20	80
40	30	70
50	40	60

Pinus radiata is characterised by a typically wide sapwood zone. The creamy white sapwood can be distinguished from the deeper creamy, sometimes pinkish heartwood when freshly cut. However, unlike many other species, *Pinus radiata* does not show a sharp contrast in the colour of its sapwood and heartwood when dry: both of them tend to be light brown or chestnut brown. Research conducted at New Zealand Forest Research Institute (NZFRI) has shown that heartwood formation for *Pinus radiata* begins at the age

of 12 and 14 years and advances outwards from the pith at a constant rate of about half a growth ring each year with slightly slower rate in the South Island (Cown and McConchie, 1983). However, crops harvested at 25 to 35 years still do not have a high proportion of heartwood (Table 2.1).

2.2 The Structure of Softwood

One of the differences between softwoods and hardwoods is that anatomical structure of softwood is relatively simple. A diagram of the microstructure of *Pinus radiata* is shown in Figure 2.2 in three directions: longitudinal, radial and tangential. The longitudinal direction, which is also termed the axial direction, is parallel with the stem pith. The radial direction is the direction along the radii of growth rings, or normal to the bark, while the tangential direction is perpendicular to the longitudinal and radial directions, being tangential to the growth rings. In Figure 2.2, face A is the transverse section, in which the cut ends of longitudinal cells can be observed. Face B is the plane parallel with the grain and radial direction, which is termed the radial/longitudinal section. In this surface, wood rays can be seen. Face C is perpendicular to both plane A and plane B, i.e., parallel with the grain and tangential direction. In this tangential/longitudinal plane, longitudinal cells are cut sideways and rays cut endwise.

Seven possible softwood cell types may be present (Table 2.2, Lewin and Goldstein, 1991). However, most softwoods mainly contain two cell types: axial tracheids and ray parenchyma.

Table 2.2. Softwood cell types (Lewin and Gold stein, 1991)

Functions	Longitudinal	Transverse
Support, conduction, or both	1. longitudinal tracheid 2. strand tracheid	1. ray tracheid
Storage or serration	1. longitudinal parenchyma 2. epithelial	1. ray parenchyma 2. epithelial

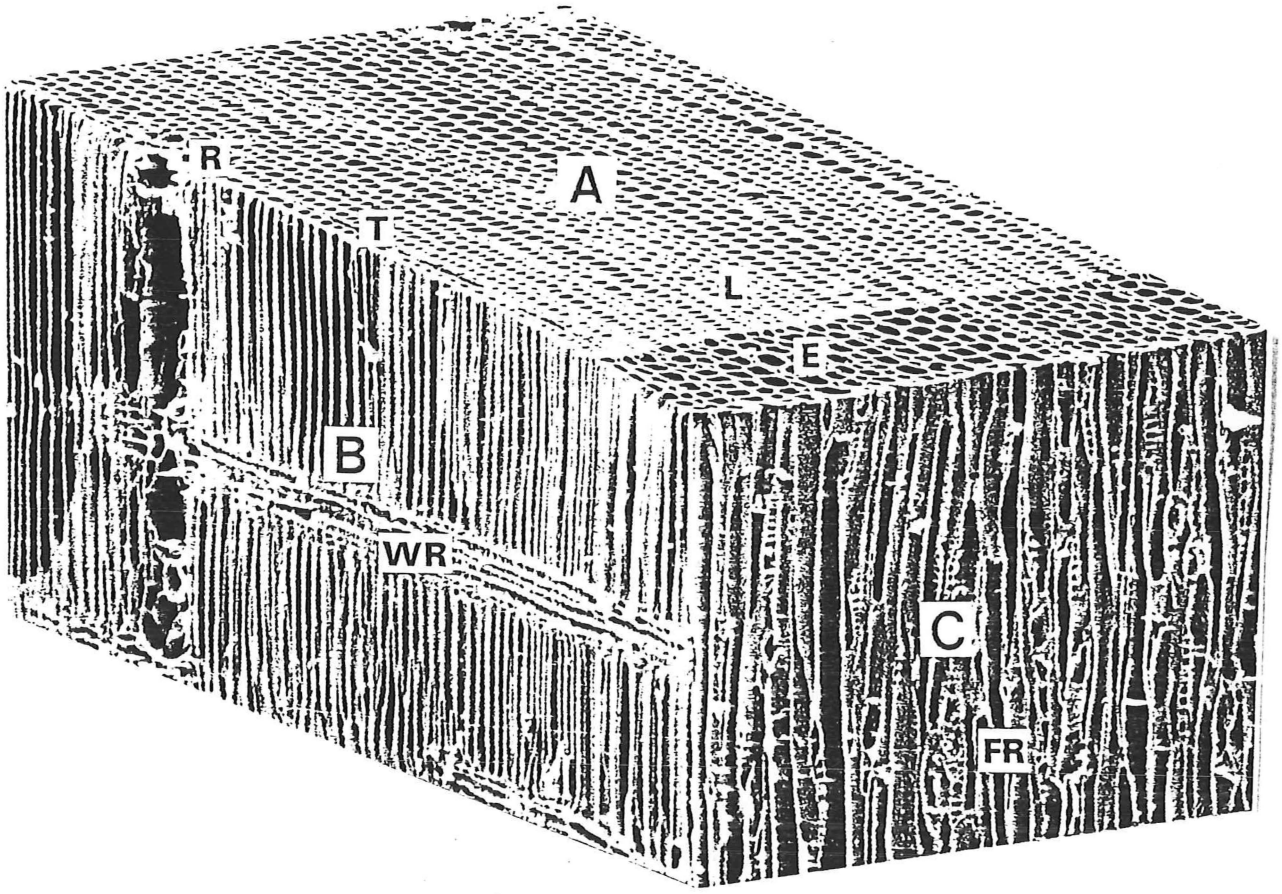

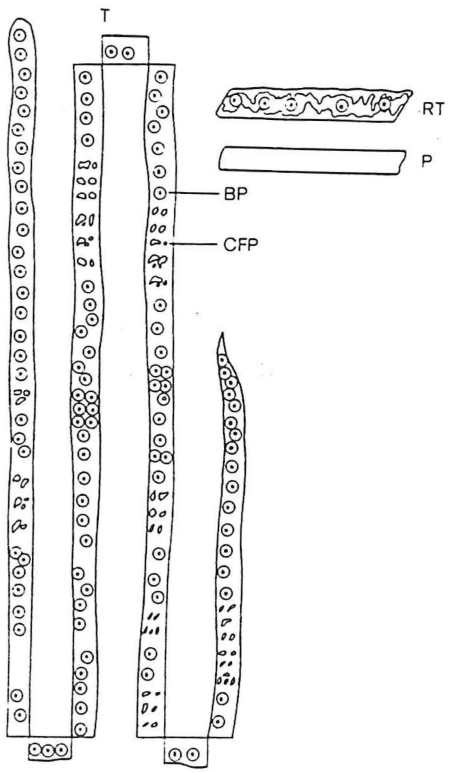

Figure 2.2 (above). The microstructure of *Pinus radiata* wood in three directions. (After Kininmonth and Whitehouse, 1991)
Face **A** Transverse: T - cut ends of tracheids; L - latewood; E - earlywood; R - resin canal
Face **B** Radial/Longitudinal: WR - wood ray
Face **C** Tangential/longitudinal: FR - fusiform ray.

Figure 2.3 (left). The structure of cells. (After Kininmonth and Whitehouse, 1991)
T - Tracheid about 3 mm long; BP - Bordered pits; CFP Pits to ray parenchyma (cross-field pits); RT - Ray tracheids with dentations of variable size; P - Parenchyma cell.

2.2.1 Longitudinal Tracheids

Longitudinal tracheids are the most important cell type since they occupy more than 95% of the wood by volume in *Pinus radiata* (Kininmonth and Whitehouse, 1991). They are aligned in the radial direction. These cell are relatively long, four- to six- sided prismatic hollow elements, with closed ends. Their long axes are parallel to the longitudinal direction. In the cross-sectional view, earlywood tracheids are generally hexagonal and latewood tracheids rectangular. Also, earlywood has noticeable thinner cell-wall and larger lumens. In a longitudinal view, earlywood tracheids are end-rounded in the radial plane and end-pointed in the tangential plane, while latewood tracheids are end-pointed in both planes (Howard and Manviller, 1969). Another difference between earlywood tracheids and latewood tracheids is that the tracheids have the same tangential diameter but the radial diameter for latewood is much smaller than that of earlywood. The measured dimensions of longitudinal tracheids for *Pinus radiata* are given by Kininmonth and Whitehouse (1991) as:

tangential diameter (μm):	38.35 (range 21.80-56.60)
wall thickness (μm):	3.45 (range 1.20-6.60)
length (mm):	2.72 (range 0.73-4.78)

A significant feature of the longitudinal tracheids is that there are a number of pits on the cell walls (Figure 2.3). These pits are required to conduct the liquid both longitudinally and transversely. In a living tree, the adjacent longitudinal tracheids are connected through the bordered pits and the sap can be conducted from one tracheid to another until the leaves are reached. The pits-to-ray cells allow the liquid material to move in radial direction. Most of these pits appear on radial walls of the longitudinal tracheids; on tangential walls, pits are rare and occur only in cells close to the ring boundary.

2.2.2 Resin Canals

Resin canals have a relatively complicated structure, in which resin is conveyed and deposited. In *Pinus radiata*, both longitudinal and radial canals are found in the wood. Longitudinal resin canals have a diameter normally five to six cells while radial ones are slightly smaller in diameter. They are lined with thin-walled epithelium and are surrounded by epithelial cells, which is in turn surrounded by a layer of short longitudinal parenchyma cells. Such units have simple pits to connect to the radial resin canals. Radial resin canals have a similar structure to that of the longitudinal canals, but are surrounded

by transverse epithelial and ray parenchyma cells. Although resin canals occupy only about 1% of wood by volume (Panshin *et al.*, 1964), it may become significant under high temperature drying in the conduction of moisture vapour in wood where moisture contents are less than 30%. With these values of moisture content the bordered pits on the longitudinal tracheids are all aspirated while the resin deposited in the canals has been 'cleared away' at drying temperatures above 100°C. The mechanism of such process is far from being completely understood. Alternatively, the effect of resin canals on drying can be taken into account by using the measured gas permeability of dry wood for the moisture vapour movement when the moisture content is below fibre saturation point.

2.2.3 Wood Rays

Wood rays consist of the structure formed by transverse-oriented cells. They radiate from the medulla or pith like the spokes of a wheel and their functions are to store food, and to convey liquids to wherever needed within the bole of the tree. The rays of most softwoods uniseriate (arranged in a single vertical column) or part biseriate with resin canals (spindle-shaped, tapering at both ends), as occurs in *Pinus radiata*. Uniseriate rays are composed either entirely of ray parenchyma or both ray parenchyma and ray tracheids. A uniseriate ray has one or more cells (1-21 for *Pinus radiata*) in height, and does not contain resin canal. Multiseriate or past biseriate rays contain a resin canal and are characterized by a spindle shape. The rays are connected to the longitudinal cells by cross-field pits (CFP, Figure 2.3).

In white pine (*Pinus strobus L.*), the proportion of wood rays is about 6% of wood volume (Panshin et al., 1964), but *Pinus radiata* contains only about 4% with the longitudinal tracheids occupying over 95% of the volume. Wood rays contribute to the conduction of moisture in the radial direction and are important in seasoning, since they govern to a great extent, shrinkage and checking.

2.2.4 Pit Structure

As discussed in section 2.1, in a living tree the sap must be conducted from roots up to the leaves and across the stem. The movement of sap from tracheid to tracheid is performed through a disk-like (or dome-like) structure called pits. Most of these pits appear as pit pairs, i.e., one on either side of the double wall between adjacent cells.

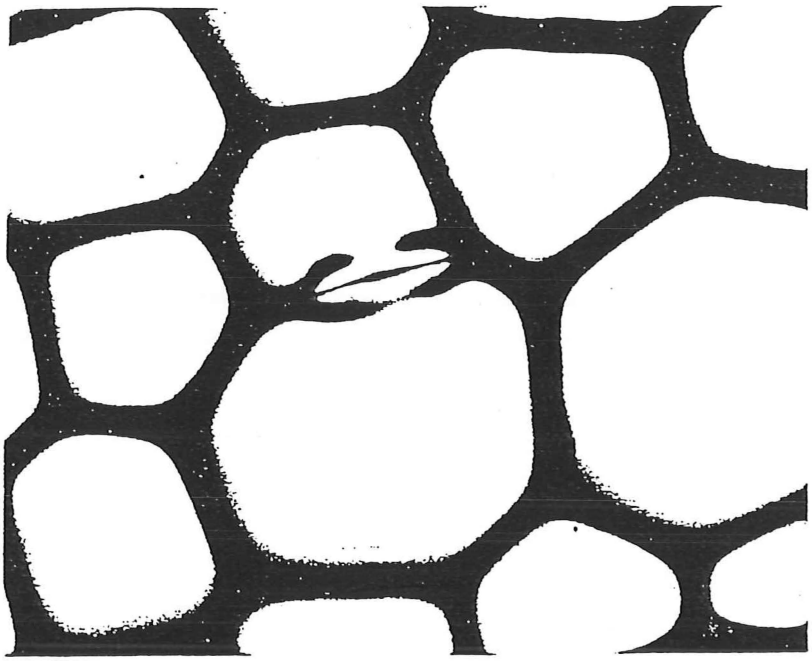

Figure 2.4. A bordered pit between two tracheids in *Pinus radiata* earlywood. (After Booker, 1986)

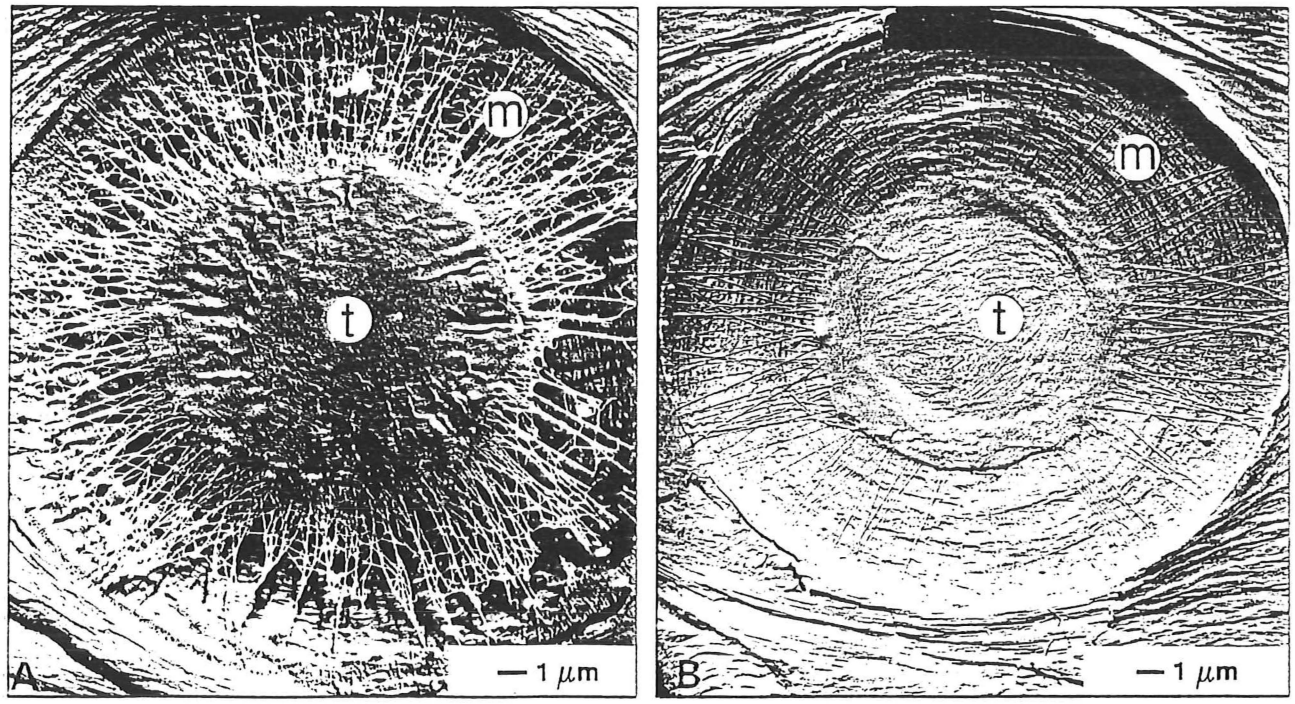

Figure 2.5. A bordered pit in earlywood of *Pinus radiata* sapwood revealing structural changes: A - unaspirated state; B - aspirated state. (After Kininmonth and Whitehouse, 1991). In the Figure: t - torus; m - margo.

Bordered pits

Since pit pairs between longitudinal tracheids are bordered, these pits are usually called *bordered pits* (Figure 2.4). The structure of such a bordered pit pair (unaspirated) is shown in Figure 2.5A. The dome-like structure is called the *pit border* or *pit chamber* and the circular opening is termed the *pit aperture*. Removal of the pit border exposes the *pit membrane*. The central impermeable area is the *torus* and surrounding the torus is the web-like region called the *margo*. Since bordered pits appear in pairs between adjacent tracheids, the liquid in the lumen of one tracheid can flow through the aperture, the margo and finally out through the aperture on the other side into the lumen of the adjacent tracheid. This process of liquid flow from one tracheid to another can occur when the pit is open, or unaspirated.

In the sapwood of a living tree, in its passage from roots to leaves, water is literally "pulled" up a stem by capillary action in the form of fine columns that completely fill the tracheids or lumens under a large tensile force initiated in the leaves. However, where a gas bubble develops within a tracheid (e.g., the tree stem is damaged in some way), the water column will be broken and the capillary pressure will fall. In response, the small bubble expands and forces the torus in the bordered pit pair rapidly and deeply into the surrounding pit apertures. This makes the pit aspiration virtually irreversible. In this way, the conducting pathways around the bubble are blocked and the wood in adjacent area is protected. Therefore the important feature of the bordered pit pair in relation to drying is that when the pit is open or unaspirated, it allows the liquid to flow through tracheids, however when it is closed or aspirated it blocks the passage and significantly reduces the ease of liquid flow within the material. Although detailed studies show some differences between latewood and earlywood both in pit structure and numbers (fewer, smaller pits in latewood, Kininmonth and Whitehouse, 1991; Lewin and Goldstein, 1991), the related physical properties will be taken as an average of these features over the whole growth ring. Thus the pit behaviours mentioned above can be applied to the whole ring.

Pitting between tracheids and ray parenchyma

On the longitudinal tracheids walls can be seen some pits which connect to the ray parenchyma cells. The structure of this type of pit has not yet been fully examined.

In general, these pits are relatively simple compared to bordered pits. They comprise a more or less straight-sided hole down though the wall as far as the outer surface (primary wall), which forms an external closing membrane. Unlike the bordered pit pairs, this membrane is holopermeable, allowing the passage of moisture without being blocked (Kininmonth and Whitehouse, 1991).

2.3 Summary

Bordered pits, when open or unaspirated, allow fluid to flow between tracheids. However, when aspirated or closed, the permeability of the timber to the movement of fluid is hindered markedly. In this case, moisture can only move through resin canals and rays or by diffusion through cell-wall tissue.

In the heartwood of coniferous trees (such as *Pinus radiata*), the moisture content is low and the bordered pits generally aspirate, so even in green heartwood type pits are normally aspirated both before and after sawing (Harris, 1954). However, the pits in sapwood are usually not aspirated while the sapwood is green, since the pits are needed for the transport of liquid nutrients. The pits aspirate only when the sapwood is dried or damaged in some way, as when the timber is felled or sawn.

2.4 References

1. Booker, R.E. 1989. Hypothesis to Explain the Characteristic Appearance of Aspirated Pits. Paper presented at 2nd Pacific Region Wood Anatomy Conference, Laguna, Philippines.

2. Butterfield, B.G. 1993. The Structure of Wood: An Overview. in Walker, J.C.F. (ed): "*Primary Wood Processing: Principles and Practice*". Chapman and Hall, London.

3. Cown, D.J. and McConchie, D.L. 1980. Wood Property Variations in an Old-Crop Stand of Radiata Pine. *New Zealand J. of Forest Science*, 10(3) pp508-520.

4. Cown, D.J.and McConchie, D.L. 1983. Radiata Pine Wood Properties Survey (1977-1982). New Zealand Forest Research Institute Bulletin No.50. Rotorua, New Zealand.

5. Cown, D.J. 1989. Wood Characteristics of New Zealand Radiata Pine and Douglas Fir: Suitability for Processing. New Zealand Forestry Corporation Ltd. Wellington.

6. Harris, J.M. 1954. Formation of Heartwood of Radiata Pine. *New Phytol*, 53(3) pp517 - 524.

7. Howard, E.T. and Manwiller, F.G., 1969. Anatomical Characteristic of Southern Pine Stemwood. *Wood Sci.*, 2(2), pp77-86.

8. Kininmonth, J.A. and Whitehouse, L.J. 1991. "*Properties and Uses of New Zealand Radiata Pine: Volume 1-Wood Properties*". New Zealand Ministry of Forestry, New Zealand Forest Research Institute, Rotorua, New Zealand.

9. Brown, W.H. 1965. "*An Introduction to the Seasoning of Timber*". Pergamon Press. New York.

10. Lewin, M. and Goldstein, I.S. 1991. "*Wood Structure and Composition*". Marcel Dekker, Inc. New York.

11. Panshin, A.J., Zeeuw, C.D. and Brown, H.P. 1964. "*Textbook of Wood Technology*". 2nd edn. McGraw-Hill Book Co., New York.

12. Puiggali, J.R. and Quintard, M. 1992. Properties and Simplifying Assumptions for Classical Drying Models. in Mujumdar, A.S. (ed.): "*Advances in drying*". Vol.5, Hemisphere Publishing Co., New York.

13. NZ Ministry of Forestry. 1988. "*New Zealand Radiata Pine*". NZ Ministry of Forestry, Forest Research Institute, Rotorua, New Zealand.

Chapter 3

Simulation of Moisture Movement and Heat-Transfer within a Board during Drying

The modelling of the drying process of a board involves studies in two areas although these are related to each other: (1) the simulation of external transfer processes and (2) the internal transfer processes. The measurement and prediction of the external mass-transfer process has been studied by Keey and colleagues (Kho *et al.*, 1989, 1990; Langrish *et al.*, 1992, 1993). In this chapter, the internal moisture mass- and heat-transport processes will be investigated and a mathematical model will be proposed based on physical characteristics of the timber and transport properties of moisture.

The drying process of a board at high-temperatures (HT) can be interpreted as simultaneous heat and moisture transfer with local thermodynamic equilibrium at each point within the timber. The moisture within wood can be identified as three phases: liquid water (or free water) in the wood cell lumens, bound water in the cell walls and water vapour (Skaar, 1988). The moisture content and temperature profiles in a board are believed to be the dominant causes for drying defects such as checking (Pang *et al.*, 1992; Johnson, 1989; Puiggali, *et al.*, 1993) and fundamental for any kiln-wide analysis (Kayihan, 1993; Pang and Keey, 1994). A number of mathematical models have been published in the past two decades to simulate the drying process. These models can be divided into three categories: diffusional, empirical and models based on transport properties and physical phenomena related to the material.

3.1 Literature Review

3.1.1 The Diffusional Model

In this model it is assumed that moisture migrates by diffusion due to the moisture content gradient, which can be described by the Fick's second law. This model was the earliest attempt to quantify the drying of wood (Rosen, 1984). Recently it has been realised that using the diffusion equation to describe overall moisture movement in wood is possibly misleading. This can be recognised from the definition of diffusion in Fick's law

(Sherwood, 1929) and the states of the moisture present in the wood. Since each state of moisture (liquid water, bound water or water vapour) has a different mechanism to move in wood during drying, it is impossible to describe the overall moisture using a unique single relationship. The diffusional model is usually now used only to describe the stress development after some modification due to its relative simplicity (Morén, 1989; Salin, 1989; Puiggali *et al.*, 1993).

By using the Fick's second law, Sherwood (1929) suggested that the following relationship could describe the drying behaviour of wood:

$$\frac{\partial X}{\partial \tau} = \frac{\partial (D \partial X / \partial z)}{\partial z} \tag{3.1}$$

where X is the local moisture content, τ is the time, z is the distance coordinate perpendicular to the airstream and D is the diffusion coefficient.

To solve equation (3.1), some further assumptions were made:

- the coefficient D in the equation is constant;
- initial moisture content in wood is uniform;
- surface resistance to moisture movement is negligible, i.e., surface fibres attain equilibrium with the surrounding air as soon as drying starts.

In this way, equation (3.1) can be solved to give the moisture-content profile, given the following initial and boundary conditions:

$$\tau = 0,\ X = X_i \tag{3.2}$$

$$z = \pm \delta,\ X = X_e \tag{3.3}$$

This model was modified and solved afterwards by many other researchers. Stamm (1964) has demonstrated that below fibre-saturation point moisture movement will be controlled by diffusion and will appear as if it were a diffusion phenomenon (Rosen, 1984). Choong and Skaar (1969, 1972) have taken into account the surface resistance to moisture movement during drying and solved equation (3.1) with corresponding boundary conditions by analytical techniques. Collignan *et al.*, (1993) have noticed that the diffusion coefficient may be different for different stage of drying. They have proposed correlations to calculate diffusion coefficients which may vary with moisture content, wood density and air temperatures.

As this type of model cannot reflect the true picture of moisture content distribution and it is strongly dependent on the experiments to determine the coefficient, D, other attempts have been made to provide a framework for the drying process.

3.1.2 Empirical Model

Empirical models were developed initially in order to provide information for kiln design rather than to describe the true moisture or temperature profiles, since the mechanisms and driving forces were only rough estimates in most cases.

Bramhall (1976) has developed a model that allows for changes in drying conditions. He suggested that the pressure difference is the driving force for the moisture movement, but for overall moisture-content changes he assumeed that the driving force is the difference between the saturation pressure of water vapour at dry-bulb temperature (p^s_{db}) and that at wet-bulb temperature (p^s_{wb}),

$$\frac{d<X>}{d\tau} = \frac{p^s_{db} - p^s_{wb}}{R} = \frac{\Delta p}{R} \tag{3.4}$$

where $<X>$ is the local average moisture content and R is the resistance, which is a function of average moisture content and can be found from experiment. When the moisture content approaches the equilibrium value, the resistance becomes so great that the drying rate is almost zero. Therefore, by breaking the drying schedule into several incremental periods of constant conditions, equation (3.4) can be solved implicitly to determine the dry-bulb temperature and hence the drying time to achieve the final desired moisture content. This method takes the dry-bulb temperature changes as the criterion to evaluate the moisture content and needs experimental data on similar types of wood material.

Rosen (1980) developed another empirical model to characterize drying under constant external conditions. The characteristic moisture content, E, is defined as

$$E = \frac{<X> - X_e}{X_o - X_e} \tag{3.5}$$

where X_o and X_e are the critical and equilibrium moisture contents respectively.

This characteristic moisture content is determined by

$$E = 1 - E_o \int_0^{\tau} (-a\tau^{1/b}) d\tau \qquad (3.6)$$

in which a and b are experimentally dependent factors, and the coefficient E_o is estimated from these factors as

$$E_o = \frac{a^b}{b\Gamma(b)} \qquad (3.7)$$

This model has been solved by Rosen (1978, 1982). From the experimental results, one can obtain the factors a and b and coefficient E_o. Then, the moisture content at different drying times can be predicted.

Another empirical attempt was made by Milota and Tschernitz (1990) for the drying of loblolly pine (*Pinus taeda L.*) at high-temperatures. They assume that the drying can be divided into two periods: an initial constant drying period and a falling-rate period. During the constant drying period, they suggest a fitted equation to predict the drying rate, F_{cr}, which is only a function of wet-bulb depression $(T_d - T_w)$ at a fixed air velocity:

$$F_{cr} = [0.01208 + 0.006797(T_d - T_w) - 2.482x10^{-5}(T_d - T_w)^2] f_v \qquad (3.7)$$

The influence of air velocity is reflected by the parameter f_v, which is obtained from

$$f_v = (\frac{v}{1329})^{0.3} \quad (v<1329) \qquad (3.8)$$

$$f_v = (\frac{v}{1329})^{0.5} \quad (v>1329) \qquad (3.9)$$

For the drying in falling-rate period, the drying rate, F_m, is fitted from the drying curves as a function of moisture content:

$$F_m = \{[S_T(M - M_e)]^{-n} + (F_{cr})^{-n}\}^{-1/n} \qquad (3.10)$$

where S_T is the slope of the asymptote through the point at equilibrium moisture content, M_e, and n is a factor which determines the curve shape at different external conditions. Both S_T and n are dependent on the air temperature, humidity and velocity.

Since the empirical attempts are mainly based on experimental data rather than drying theory, they are not reliable when extrapolating beyond the data range. They are only usable for the particular drying problems selected.

3.1.3 Transport-Based Model

In the first attempts to express the drying process with a transport-based model, Luikov's equations (1966) describing heat- and mass-transfer process in capillary-porous bodies were used (Lowery, 1972, Thomas, *et al.*, 1980; Basilico, *et al.*, 1982). These equations have the following form (Rosen, 1987):

$$\frac{\partial T}{\partial \tau} = \frac{1}{\rho_S C_P} \nabla (\kappa \nabla T) + \frac{\xi \lambda}{C_P} \frac{\partial X}{\partial \tau} \tag{3.11}$$

$$\frac{\partial X}{\partial \tau} = \nabla (D \nabla X) + \nabla (D\delta \nabla T) + \nabla (D\delta_p \nabla p) \tag{3.12}$$

$$\frac{\partial p}{\partial \tau} = \nabla (D_{fl} \nabla p) - \frac{\xi}{\nu} \frac{\partial X}{\partial \tau} \tag{3.13}$$

In these equations,

ξ is the evaporation criterion, being equal to the ratio of the vapour diffusion coefficient in wood to the coefficient of total diffusion of moisture;

δ is the thermomigration coefficient, being equal to the ratio of moisture content gradient to temperature gradient in the absence of moisture transfer in wood;

δp is the filtration motion diffusion coefficient of water vapour-gas mixture; and

ν is the capillary capacity constant.

Since the equations (3.11) to (3.13) are non-linear and contain coefficients, which need to be determined from experiment, this model is very complex and is strongly dependent on experimental data. Also, as the bound water is not distinguished from liquid water, the model needs to be modified to take into account of the effect of bound water, particularly when the moisture content is below fibre-saturation point (Puiggali and Quitard, 1992).

Recently, the studies have described the drying process by considering different mechanisms for each state of moisture and by applying heat- and mass-transfer principles separately (Kayihan, 1982; Plumb *et al.*, 1985; Stanish, *et al.*, 1986; Perré *et al.*, 1988; Chen and Pei, 1989). In these models, the wood is considered as a hygroscopic porous material body with the material being treated as homogeneous. When solving the

equations, the sapwood board is taken as an example for evaluation of the model. Since the physical properties (such as pits aspiration) and their differences (e.g., sapwood and heartwood) play an important role in the drying behaviour, these models need further modification in order to simulate the drying in practical cases. These models are usually complex, thus their application have been restricted.

The object of this work is to propose a model based on the physical features of wood and on the transport properties during drying. This model should have a relatively simple form but can be applied to many practical situations of drying.

3.2 A Physical Model to Simulate Moisture Movement and Heat-Transfer within a Board during HT Drying

Stanish, Schajer and Kayihan (1986) used their model to predict temperature profiles in board of southern pine (*Pinus palustris Mill, Pinus echinata, etc.*) and Douglas fir (*Pseudotsuga menziesii*) during high temperature drying. The resulting simulation is complex. However, their simulation results indicate that the centre-line temperature approaches a plateau of about 100°C and remains there for a substantial part of the drying process. Further, from the experimental results of HT drying of *Pinus radiata* and yellow poplar (*Liriodron tulipifera* L.), Northway (1989) and Beard *et al.*, (1982, 1985) show that the temperatures at different depths of the board initially reach a temperature about 100°C and then start to rise progressively of above 100°C. This feature of the temperature-time profiles at different depths in the timber suggests the presence of a receding evaporative plane at the boiling point of water (about 100°C).

Another implication of the results both from the simulation by Stanish *et al.*, (1986) and the drying tests (Beard *et al.*, 1985; Northway, 1989) is that the centre of the board is not significantly above atmospheric pressure, since this would require a higher boiling temperature for the water. This result contradicts the simulation of Perré, Fohr and Arraud (1988) who predicted centre-line pressures in the drying of spruce (*Picea rubens* Sarg.) of up to 2.4 times atmospheric pressure. *Pinus radiata* is very permeable compared with many coniferous species, and a significant pressure rise within the board is less likely.

The effects of total pressure gradients in the wet core of the board were neglected in the timber drying model of Bonneau (1991). In this study these gradients will also be neglected in the core regions of the board. In the following discussion, a view of the drying process for heartwood and sapwood in *Pinus radiata* will briefly described and

mathematical expressions for the transfer processes and phase equilibria will then be presented with the method of the solution. The simulation results will be given in Chapter 6 after all of the physical properties of wood and external transport process have been presented in Chapter 4 and Chapter 6.

3.2.1 The Physical Processes of Drying for a Softwood, *Pinus radiata*

From the discussion in Chapter 2, it is known that the properties of softwood timber vary substantially from sapwood to heartwood. The bordered pits in the cell walls between longitudinal tracheids generally aspirate when coniferous trees such as *Pinus radiata* form heartwood. This process significantly retards liquid flow within the timber. However, the pits in sapwood are usually not aspirated when the sapwood is green, since the pits are required for the transport of liquid material. They aspirate only when the sapwood is dried. This aspiration process is irreversible (Booker, 1989).

This difference is relevant to the drying of timber because the degree of pit aspiration governs the permeability of the timber to the flow of liquid. The permeability of the timber to liquid flow becomes very low once the pits are aspirated and the pits are blocked.

The process of high-temperature drying of *Pinus radiata* heartwood can be divided into three periods. During the first and second period, it is postulated that there exists an evaporative plane at which all the free water evaporates. This plane will recede into the material as drying proceeds (Figure 3.1). The evaporative plane divides the material into two parts, a wet zone beneath the plane and a dry zone above it. Above the plane, moisture is assumed to exist as bound water and water vapour. Bound water will be in local thermodynamic equilibrium with the vapour pressure of water at the local temperature (Stanish *et al.*, 1986). In the wet zone, the moisture content remains at the initial value and the vapour partial pressure remains constant being equal to that at the evaporative plane.

Initially, when the evaporative plane has barely receded into the wood, the external transfer process controls the drying. However, as the plane withdraws, the internal resistance becomes significant. Then the drying becomes internally control. This transition point will be called the first critical point, before which the drying is the first period of drying and after which the second period. After the evaporative plane has reached the centre-layer of the board, drying is controlled by bound-water diffusion and water vapour flow. The subsequent drying will be called the third drying period.

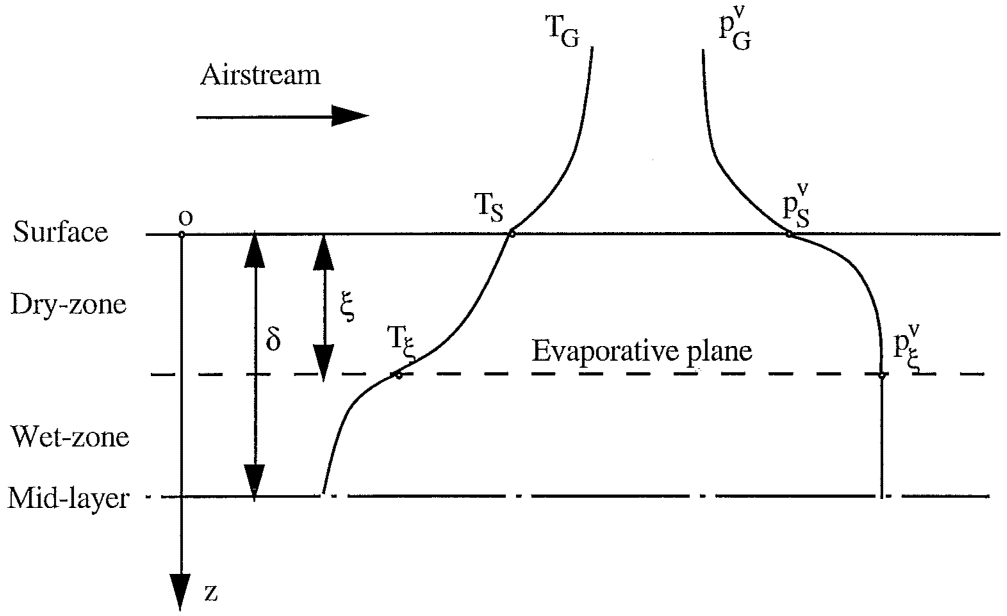

Figure 3.1. The evaporative plane model for the HT drying of softwood board.

In the drying of sapwood boards, the flow of liquid moisture close to the surface is insignificant. During the milling process, the surfaces of the board were damaged and the continuous water column is broken, so a evaporative will withdraw beneath the surface to create cavitation to generate sufficient tension for liquid flow. Therefore, at the beginning of the first drying period of sapwood, the evaporative plane recedes into the material very quickly. However, when the plane reaches a certain distance ξ_o from the surface, most of the pits inside this position are not yet aspirated and the flow of liquid is not negligible. The liquid flow towards the surface will keep the evaporative plane at the position ξ_o until the moisture content at the plane decreases to the minimum value for liquid continuity. After this, the plane starts to recede into the material and the second period of drying starts. The main difference between the drying behaviour of sapwood and heartwood during the first period is that the liquid flow in the wet zone for sapwood has a significant influence on the receding velocity of the evaporative plane. Thereafter, in the second and third periods of drying the drying process for sapwood is similar to that for heartwood.

3.2.2 Heat and Moisture Mass Balance Equations

The heat- and mass-conservation equations in the dry zone during the first and second periods and within the whole material during the third period are as follows: -

$$C_P \rho_S \frac{\partial T}{\partial \tau} = \frac{\partial}{\partial z}(\lambda \frac{\partial T}{\partial z}) - \Delta H_{vb} \frac{j_{wv}}{\partial z} \qquad (3.14)$$

and

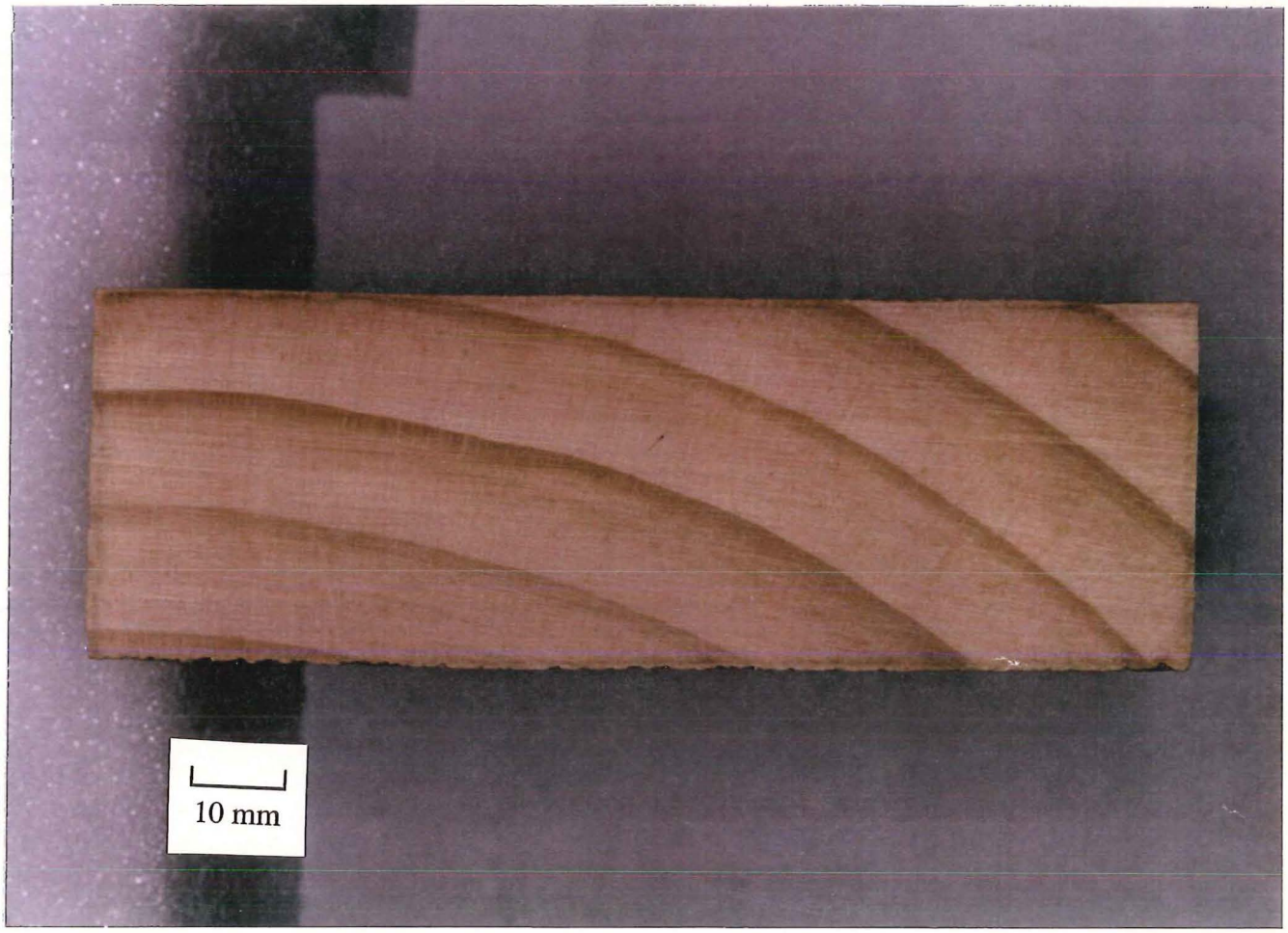

A section through a flat-sawn sapwood board showing a stain line about 1 mm below the surface. The dimension of kiln brown stain is corresponding to the thin dry layer. It is believed that this line represents the position of the evaporative plane during the first period of drying with sapwood when a thin drying has formed adjacent to the surface. Xyloses and other water-soluble components would migrate to the evaporative plane when these substances can oxidise in contact with the air.

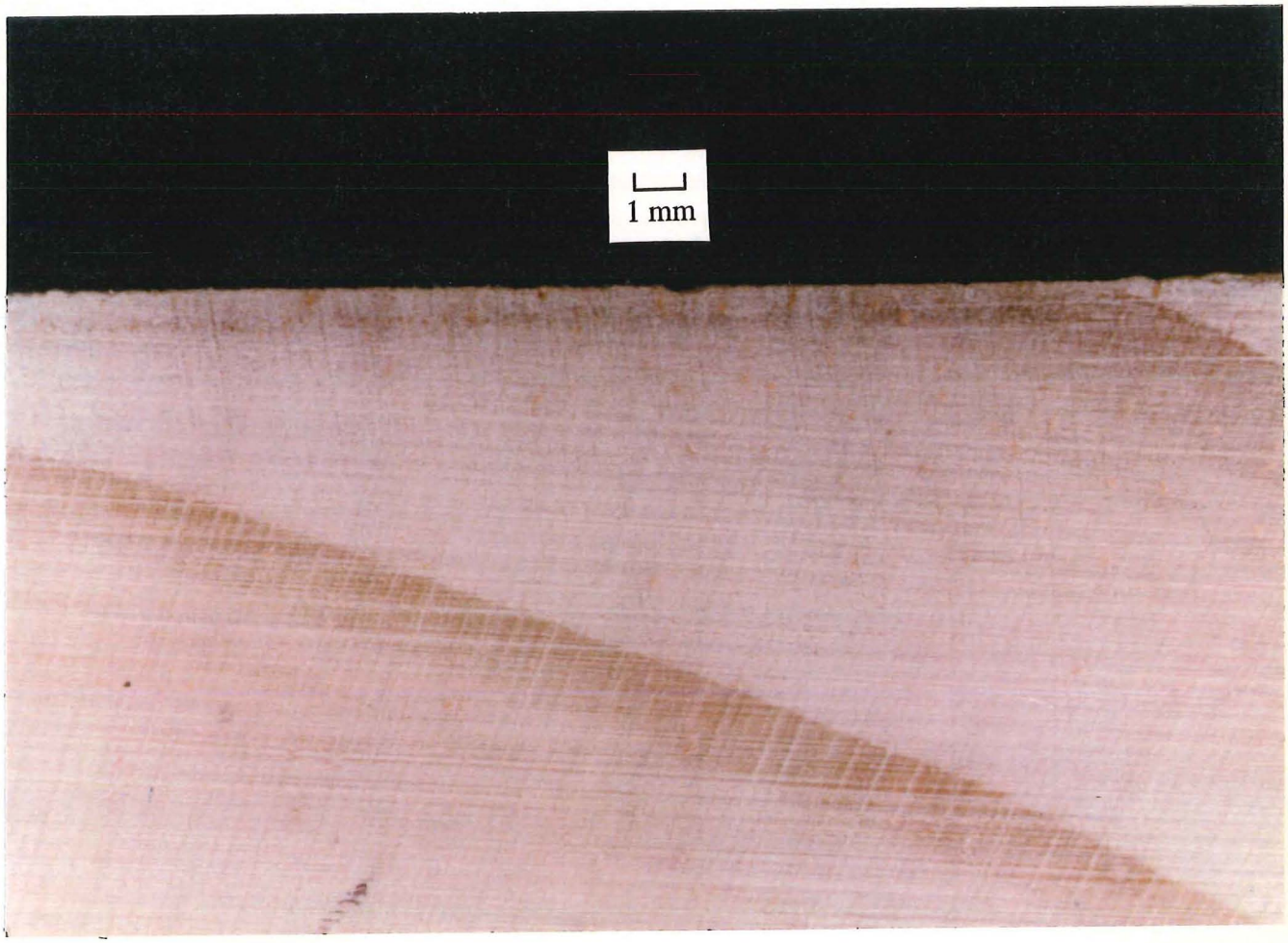

A section through a flat-sawn sapwood board showing a stain line about 1 mm below the surface. The dimension of kiln brown stain is corresponding to the thin dry layer. It is believed that this line represents the position of the evaporative plane during the first period of drying with sapwood when a thin drying has formed adjacent to the surface. Xyloses and other water-soluble components would migrate to the evaporative plane when these substances can oxidise in contact with the air.

$$- \rho_S \frac{\partial X}{\partial \tau} = \frac{\partial}{\partial z}(j_{wv} + j_{wb}) \qquad (3.15)$$

where C_P is the specific heat capacity of moist wood (J kg^{-1} K^{-1});
X is the local moisture content in the wood (kg kg^{-1});
ρ_S is the basic density of wood (kg m^{-3});
T is the temperature (K);
τ is the time (s);
z is the space coordinate measured normal to the surface of the board (m);
λ is the thermal conductivity of the moist wood (W m^{-1} K^{-1});
j_{wv} is the water vapour flux (kg m^{-2} s^{-1});
j_{wb} is the bound water flux (kg m^{-2} s^{-1}); and
ΔH_{vb} is the latent heat of vaporization of bound water (J kg^{-1}).

3.2.3 Moisture Vapour Movement

If the flux of water vapour is assumed to be proportional to the gradient of the vapour partial pressure, then the vapour flux in the dry zone is given by

$$j_{wv} = - E_v \frac{\partial p^v}{\partial z} \qquad (3.16)$$

in which, E_v is the effective permeability to vapour flow (s); and
p^v is the vapour partial pressure (Pa).

The effective permeability to vapour flow, E_v, may be related to the commonly measured permeability, K_G (m^2), by the equation: -

$$E_v = \frac{K_G \rho_G}{\mu_G} \qquad (3.17)$$

where ρ_G and μ_G are the density (kg m^{-3}) and viscosity (kg m^{-1} s^{-1}) of the vapour respectively.

The vapour partial pressure can be calculated as a function of local temperature and moisture content using the relationship given by Simpson and Rosen (1981) with some modification for the particular species of wood, *Pinus radiata.*

3.2.4 Bound Water Movement

If we use the chemical potential as the driving force for bound-water movement, then the bound-water flux can be expressed as (Stanish, 1986; Stanish et al, 1986) : -

$$j_{wb} = - D_b (1 - \varepsilon) \frac{\partial \mu_b}{\partial z} \tag{3.18}$$

where μ_b is the chemical potential of bound water (J kg^{-1});
D_b is the bound water transfer coefficient (kg s m^{-3}); and
ε is the fractional void space.

For the local thermodynamic equilibrium, the chemical potential of bound water, μ_b is the same as that for the vapour, μ_v and it follows:

$$M_v \frac{\partial \mu_b}{\partial z} = M_v \frac{\partial \mu_v}{\partial z} = - S \frac{\partial T}{\partial z} + V \frac{\partial p^v}{\partial z} \tag{3.19}$$

The entropy, S is a state function of temperature and pressure.

When the vapour obeys the Ideal Gas Laws, the above relationship can be converted into an equation in which the chemical potential is related to local temperature and pressure as follows:

$$\frac{\partial \mu_b}{dz} = \frac{\partial \mu_v}{\partial z}$$
$$= \frac{1}{M_v} \{ - [S_o + C_{PV} \ln(\frac{T}{T_o}) - R \ln(\frac{p^v}{P_o})] \frac{\partial T}{\partial z} + \frac{RT}{p^v} \frac{\partial p^v}{\partial z} \} \tag{3.20}$$

where C_{PV} is the specific heat of vapour (J kg^{-1} K^{-1});
R is the universal gas constant, R = 8.314 J mol^{-1} K^{-1};
T_o, P_o and S_o are the datum temperature (K), atmosphere pressure (Pa) and reference entropy (J mol^{-1} K^{-1}).

For water vapour at temperature of 298.15 K and one atmosphere (101325 Pa), Stanish (1986) gives the average value of entropy (S_o) as 187 J mol^{-1} K^{-1}. Therefore, the bound water flux can be calculated by inserting equation (3.20) into equation (3.18).

$$j_{wb} = -\frac{D_b\,(1 - \varepsilon)}{M_v}\{-[187 + 35.1\,ln(\frac{T}{298.15}) - 8.314\,ln(\frac{p^v}{101325})]\frac{\partial T}{\partial z} + 8.314\,\frac{T}{p^v}\,\frac{\partial p^v}{\partial z}\} \qquad (3.21)$$

In the wet zone there are no significant vapour flows, so the fluxes j_{wv} and j_{wb} are zero in this region. Also, there is no liquid flow in this zone within heartwood, and the moisture content below the evaporative plane is everywhere equal to the initial moisture content.

3.2.5 Liquid Water Movement in the Wet Zone of Sapwood

For sapwood, however, the moisture content is initially high, so when water evaporates at the evaporative plane, unbound water beneath the plane will flow towards it due to the liquid pressure gradient. The pressure gradient in the liquid is assumed to be the consequence of capillary action between the liquid and gas phases within the voids of the wood. This process can be described by Darcy's law. In wood drying, the body forces are small compared to the pressure gradient and can be ignored (Spolek, 1981; Comstock, 1967). Thus the liquid water flux within the wood (j_{wf}) is obtained as

$$j_{wf} = -E_l\frac{\partial p_l}{\partial z} \qquad (3.22)$$

where p_l is the pressure in liquid phase (Pa); and
E_l is the effective permeability to liquid flow (s), which may also be related to the commonly measured permeability, K_l (m^2), by the equation: -

$$E_l = \frac{K_l\,\rho_l}{\mu_l} \qquad (3.23)$$

in which ρ_l and μ_l are the density (kg m^{-3}) and viscosity (kg m^{-1} s^{-1}) of liquid water respectively.

In any lumen partially filled with water, a meniscus forms between the liquid and gas phases. Thus a force balance equation can be obtained as:

$$p_g = p_l + p_c \qquad (3.24)$$

or

$$p_l = p_g - p_c \qquad (3.25)$$

where p_c is the capillary pressure, so

$$\frac{\partial p_l}{\partial z} = -\frac{\partial p_c}{\partial z} \tag{3.26}$$

It has been found that both the capillary pressure p_c (Spolek and Plumb, 1981) and the liquid permeability K_l (Stanish *et al.*, 1986) are functions of the saturation S_a, which is defined by

$$S_a = \frac{\text{Liquid Volume}}{\text{Void Volume}} = \frac{X - X_{FSP}}{X_{max} - X_{FSP}} \tag{3.27}$$

where X_{max} is the moisture content of the wood if the entire void structure were filled with liquid and X_{FSP} is the moisture content at the fibre-saturation point when the lumens are devoid of any liquid water.

For softwoods, Spolek and Plumb (1981) assume that the capillary pressure is a simple algebraic function of saturation

$$p_c = A\, S_a^{-B} \tag{3.28}$$

where A and B are constants. For southern pine, Spolek and Plumb give (1981)

A = 12400 Pa, and B = 0.61

We will assume that these values can describe the capillary behaviour of *Pinus radiata* also.

Stanish *et al.* (1986) correlate the permeability (K_l) of the unsaturated wood to that measured at saturation (K_l^s) by the expression:-

$$K_l = K_l^s \{1.0 - \cos[\frac{\pi}{2}\frac{(S_a - S_{amin})}{(1.0 - S_{amin})}]\} \tag{3.29}$$

where S_{amin} is the minimum saturation for liquid flow within the wood.

From equations (22), (26), (27) and (28), the relationship between the liquid water flux and the local moisture content becomes

$$j_{wf} = -\frac{A\ B\ E_l\ (X_{max} - X_{FSP})^B}{(X - X_{FSP})^{(1+B)}}\ \frac{\partial X}{\partial z} \tag{3.30}$$

The equation for moisture conservation enables the change in moisture content with time to be related to the gradient of this flux as follows: -

$$\rho_S \frac{\partial X}{\partial \tau} = -\frac{\partial j_{wf}}{\partial z} \tag{3.31}$$

The equation for the movement of liquid water in the wet zone has a similar form to that for heat conduction (equation 3.15). By combining equations (3.30) and (3.31) we obtain

$$\rho_S \frac{\partial X}{\partial \tau} = \frac{\partial}{\partial z}\left(\eta \frac{\partial X}{\partial z}\right) \tag{3.32}$$

where the apparent moisture-diffusion coefficient η is given by

$$\eta = \frac{A\ B\ E_l\ (X_{max} - X_{FSP})^B}{(X - X_{FSP})^{(1+B)}} \tag{3.33}$$

3.2.6 Boundary Conditions at the Surface and the Receding Velocity of the Evaporative Plane

The external mass-transfer coefficient (β) affects the boundary conditions at the surface of the boards, and the total vapour flux from the surface (j_{tot}) is given by

$$j_{tot} = -\frac{d}{d\tau}[\langle X \rangle \rho_S\ \delta] = \beta (p_S^v - p_G^v) \tag{3.34}$$

in which $\langle X \rangle$ is the local average moisture content (kg kg^{-1});
δ is the half-layer board thickness (m);
p_S^v is the partial pressure of moisture vapour at board surface (Pa); and
p_G^v is the bulk-gas value of the moisture vapour partial pressure (Pa).

The velocity of the evaporative plane has been predicted from the local moisture mass balance around the plane. If the evaporative plane recedes a distance $\Delta\xi$ during a time interval $\Delta\tau$, the moisture loss in this region should be equal to the time interval multiplied

by the flux difference between the vapour just above the plane ($j_{wv\xi}$) and the liquid water just beneath it ($j_{wf\xi}$). That is

$$\Delta\xi\, \rho_S\, (X_\xi - X_{FSP}) = -\, (j_{wv\xi} - j_{wf\xi})\, \Delta\tau \qquad (3.35)$$

where X_ξ is the moisture content just beneath the plane.

We can use equations (3.14) to (3.35) to predict the temperature, T, and the moisture content, X, in both the dry and wet zones, the bound water flux (j_{wb}) and the water vapour flux (j_{wv}) in the dry zone, and the liquid water flux in the wet zone (j_{wf}) for sapwood. We can solve the model numerically if the initial and boundary conditions, the various transport coefficients and physical properties of wood are known. The method adopted will be described in the next section.

3.3 Solving the Model Using A Numerical Method

We will solve the equations in the model in the following order. First, the heat conservation equation (3.14) will be solved for the temperature profiles within the timber. This enables the water vapour flux (j_{wv}, equation 3.16) and the bound-water flux (j_{wb}, equation 3.21) to be calculated in the dry zone, so the mass conservation equation (3.15) can be solved in the dry zone. For sapwood, the moisture content in the wet zone can be estimated from equations (3.32) and (3.33). These equations are non-linear and inter-linked. For example, the water vapour flux appears in the heat conservation equation. Therefore, the above procedure was repeated until all the temperatures change from iteration to iteration by less than 0.001 K.

3.3.1 Solving the Heat Conservation Equation for the Temperature Profiles

From equation (3.14), the general form of this equation is: -

$$C_P\, \rho_S \frac{\partial T}{\partial \tau} = \frac{\partial}{\partial z}\left(\lambda \frac{\partial T}{\partial z}\right) + \Phi \qquad (3.36)$$

where Φ is a source term involving the latent heat of vaporization. In the dry zone during the first and the second periods, and within the whole material during the third period

$$\Phi = - \Delta H_{vb} \frac{\partial j_{wv}}{\partial z} \tag{3.37}$$

In the wet zone, $\Phi = 0$, while at the evaporative plane

$$\Phi = - \Delta H_{vw} \frac{j_{wv\xi}}{(\Delta z - \Delta z_{\xi})} \tag{3.38}$$

where ΔH_{vw} is the latent heat of vaporization of liquid water, $j_{wv\xi}$ is the vapour flux just above the evaporative plane and $(\Delta z - \Delta z_{\xi})$ is the distance to the node just beneath it when the temperature is calculated.

The board is divided into 2J uniformly spaced nodes, as shown in Fig.3.2. The temperature at a node j is obtained from those at the adjacent nodes by a fully implicit discretization of Equation (3.35) (Patankar, 1980). The result is: -

$$b_j T_j^n = a_{j+1} T_{j+1}^n + a_{j-1} T_{j-1}^n + r_j \tag{3.39}$$

for $j = 2, \cdots\cdots, J-1$

The various coefficients in the equation are given by

$$a_{j+1} = \frac{\lambda_{j+1}}{(\Delta z)_{j+1}} \tag{3.40}$$

$$a_{j-1} = \frac{\lambda_{j-1}}{(\Delta z)_{j-1}} \tag{3.41}$$

$$a_j^o = [\frac{\rho_S C_P \Delta z}{\Delta \tau}]_j \tag{3.41}$$

$$b_j = a_{j+1} + a_{j-1} + a_j^o \tag{3.42}$$

where Δz is the size of the distance increment and $\Delta \tau$ is the size of the time step.

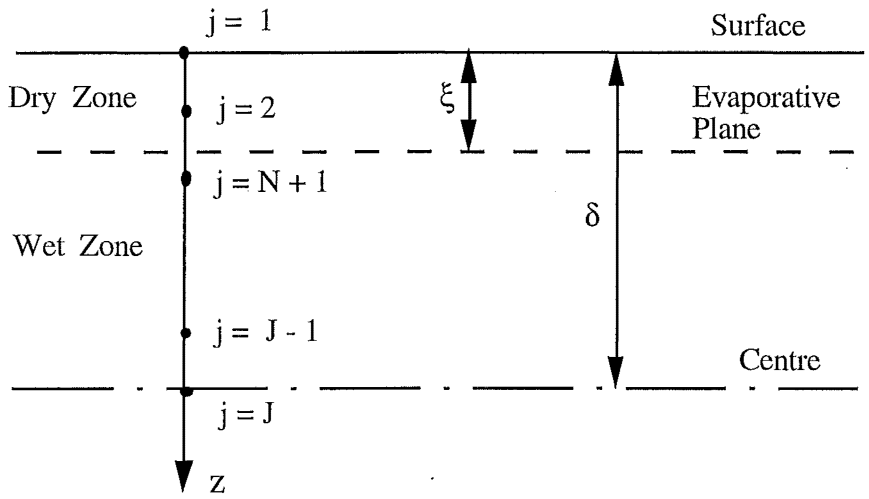

Figure 3.2. The grid points over a half-width of the board

The source term in equation (3.39) becomes

$$r_j = a_j^o \; T_j^o + \Phi_j \, \Delta z \tag{3.43}$$

Rearranging equation (3.39), it follows that

$$- a_{j-1} \, T_{j-1}^n + b_j \, T_j^n - a_{j+1} \, T_{j+1}^n = r_j \tag{3.44}$$

The boundary conditions are required in order to obtain the full solution of equation (3.39).

From the heat balance at the surface of the board, the heat-transfer equation becomes

$$b_1 \, T_1^n - a_2 T_2^n = r_1 \tag{3.45}$$

with

$$r_1 = h \, T_G + a_1^o \, T_1^o + \Phi_1 \, \Delta z \tag{3.46}$$

and

$$b_1 = a_2 + \; a_1^o \; + h \tag{3.47}$$

where h is the heat transfer coefficient to the board surface (W m^{-2} K^{-1}), and T_G is the bulk gas temperature (K).

At the centre of the board, since the temperature profile is symmetrical about the mid-layer, we know that

$$T^n_{J+1} = T^n_{J-1} \tag{3.48}$$

$$a_{J+1} = a_{J-1} \tag{3.49}$$

Therefore the heat-transfer equation at the centre of the board becomes

$$-2\, a_{J-1}\, T^n_{J-1} + b_J\, T^n_J = r_J \tag{3.50}$$

All the heat-transfer equations at any point in time may be represented in matrix notation as

$$\begin{bmatrix} b_1 & -a_2 & 0 & 0 & \cdots\cdots & 0 \\ -a_1 & b_2 & -a_3 & 0 & \cdots\cdots & 0 \\ & \cdots\cdots & \cdots\cdots & \cdots\cdots & & \\ 0 & \cdots\cdots & 0 & -a_{J-2} & b_{J-1} & -a_J \\ 0 & \cdots\cdots & 0 & 0 & -2a_{J-1} & b_J \end{bmatrix} \begin{bmatrix} T_1 \\ T_2 \\ \cdot \\ \cdot \\ \cdot \\ T_{J-1} \\ T_J \end{bmatrix} = \begin{bmatrix} r_1 \\ r_2 \\ \cdot \\ \cdot \\ \cdot \\ r_{J-1} \\ r_J \end{bmatrix} \tag{3.51}$$

This tridiagonal system of equations was solved using a subroutine from Press *et al.* (1986).

3.3.2 Solving the Mass Conservation Equation for the Moisture Content in the Wet Zone

Again, we use a fully implicit discretization of equation (3.32) using the technique described by Patankar (1980). The result is: -

$$d_j\, X^n_j = c_{j+1}\, X^n_{j+1} + c_{j-1}\, X^n_{j-1} + q_j \tag{3.52}$$

for j = N+2, ••••••, J-1

The various coefficients are given by

$$c_{j+1} = \frac{\eta_{j+1}}{(\Delta z)_{j+1}} \tag{3.53}$$

$$c_{j-1} = \frac{\eta_{j-1}}{(\Delta z)_{j-1}} \tag{3.54}$$

$$c_j^o = (\frac{\rho_S \Delta z}{\Delta \tau})_j \tag{3.55}$$

$$d_j = c_{j+1} + c_{j-1} + c_j^o \tag{3.56}$$

and the source term becomes

$$q_j = c_j^o X_j^o \tag{3.57}$$

Boundary conditions are needed to give the full solution of equation (3.52) for all nodes in the wet zone.

The moisture transfer equation for the two nodes just beneath the evaporative plane and the point at the plane becomes

$$- c_\xi X_\xi^n + d_{N+1} X_{N+1}^n - c_{N+2} X_{N+2}^n = q_{N+1} \tag{3.58}$$

in which,

$$c_\xi = \frac{\eta_\xi}{(\delta z)_\xi} \tag{3.59}$$

At the centre of the board, the moisture content profile is symmetrical about the mid-layer, so we can write a similar equation to equation (3.45) for heat-transfer, as follows: -

$$- 2\, c_{J-1} X_{J-1}^n + d_J X_J^n = q_J \tag{3.60}$$

Equations (3.58) to (3.60) may be rearranged in matrix notation as

$$\begin{bmatrix} d_{N+1} & -c_{N+2} & 0 & 0 & \cdots\cdots & 0 \\ -c_{N+1} & d_{N+2} & -c_{N+3} & 0 & \cdots\cdots & 0 \\ & \cdots\cdots & \cdots\cdots & \cdots\cdots & & \\ 0 & \cdots\cdots & 0 & -c_{J-2} & d_{J-1} & -c_J \\ 0 & \cdots\cdots & 0 & 0 & -2c_{J-1} & d_J \end{bmatrix} \begin{bmatrix} X_{N+1} \\ X_{N+2} \\ \cdot \\ \cdot \\ \cdot \\ X_{J-1} \\ X_J \end{bmatrix} = \begin{bmatrix} q_{N+1} \\ q_{N+2} \\ \cdot \\ \cdot \\ \cdot \\ q_{J-1} \\ q_J \end{bmatrix} \quad (3.61)$$

At first, the moisture content (X_ξ) at the evaporative plane will be greater than the minimum value (X_{min}) for liquid continuity. Before the plane begins to recede, the moisture content at the plane will decrease and the moisture content in the wet zone will change correspondingly. However, an equation to relate explicitly the moisture content just beneath the plane to that just above it (the fibre-saturation point) cannot be stated, so we have to adjust the moisture content just below the plane to satisfy mass conservation within the whole wet zone. Here, the total moisture loss from the wet zone during a time interval, $\Delta\tau$, should equal the liquid flux just beneath the evaporative plane, $(j_{wf})_\xi^+$ multiplied by this time interval. This gives

$$\left[\sum_{N+2}^{J-1} \Delta z\,(X_j^n - X_j^o)\,\rho_S\right] + 0.5\,\Delta z\,\rho_S\,[(X_{N+1}^n - X_{N+1}^o) + (X_J^n - X_J^o)] - \Delta\tau\,(j_{wf})_\xi^+$$

$$= 0 \quad (3.62)$$

In solving this equation, the secant method is applied at each time step. Once the moisture content at the evaporative plane has decreased to the minimum value for liquid continuity (X_{min}), it will remain constant and equal to X_{min}.

3.3.3 The Moisture Content Just Above the Evaporative Plane

The moisture content at the node just above the evaporative plane may be estimated from a local mass balance in the vicinity of the evaporative plane (Fig. 3.3). At the evaporative plane, we postulate a moisture content jump between the wet-side value, $X_\xi = X_{min}$, and the dry-side value X_{FSP} at fibre saturation. This contrivance is an approximation to what

we believe to be the actual profile: a very rapid transition over perhaps one or two tracheids widths.

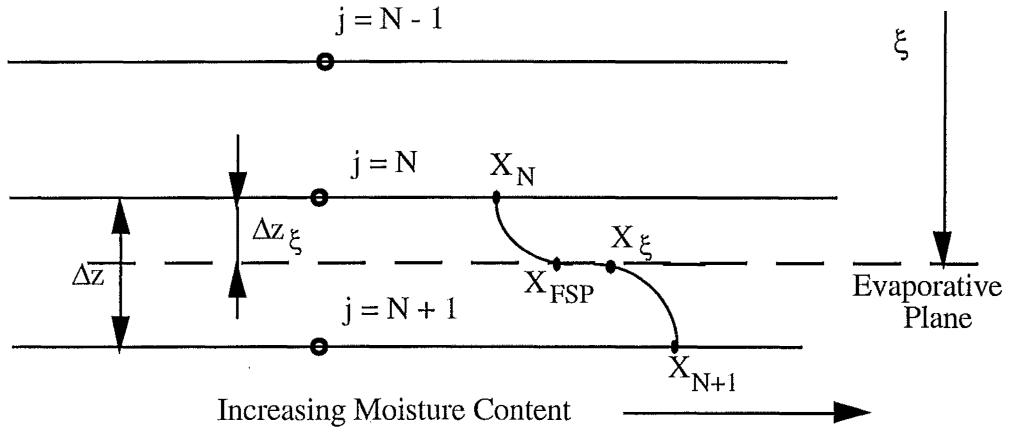

Figure 3.3 The vicinity of the evaporative plane.

For the area between nodes N and N+1, the mass balance equation is : -

$$\langle X_N \rangle \Delta z = (\Delta z - \Delta z_\xi) \frac{(X_\xi + X_{N+1})}{2} + \Delta z_\xi \frac{(X_{FSP} + X_N)}{2} \qquad (3.63)$$

where $\langle X_N \rangle$ is the average moisture content in the region between node N+1 just beneath the evaporative plane and the node N just above it. The variables $\langle X_N \rangle$, Δz_ξ and X_N will vary with time, so equation (3.63) may be differentiated to give

$$\Delta z \frac{\partial \langle X_N \rangle}{\partial \tau} = 0.5 (X_{FSP} + X_N - X_{N+1} - X_\xi) \frac{\partial \xi}{\partial \tau} + 0.5 (\Delta z - \Delta z_\xi) \left(\frac{\partial X_{N+1}}{\partial \tau} + \frac{\partial X_\xi}{\partial \tau}\right) + 0.5 \Delta z_\xi \frac{\partial X_N}{\partial \tau} \qquad (3.64)$$

Another mass conservation relationship for the region between node N and node N+1 can be obtained from equation (3.15), as follows: -

$$\Delta z \rho_S \frac{\partial \langle X_N \rangle}{\partial \tau} = - [(j_{wf})_{N+1} - (j_{wv} + j_{wb})_N] \qquad (3.65)$$

By combining equations (3.64) and (3.65), the moisture content at the node just above the evaporative plane may be obtained by solving the equation,

$$- \frac{(j_{wf})_{N+1} - (j_{wv} + j_{wb})_N}{2\rho_S} = [- X_{N+1} - X_\xi + X_{FSP} + X_N] \frac{\partial \xi}{\partial \tau}$$

$$+ (\Delta z - \Delta z_{\xi}) \left(\frac{\partial X_{N+1}}{\partial \tau} + \frac{\partial X_{\xi}}{\partial \tau}\right) + \Delta z_{\xi} \frac{\partial X_N}{\partial \tau} \qquad (3.66)$$

where $(j_{wv} + j_{wv})_N$ is the vapour and bound-water fluxes at the node just above the evaporative plane and $(j_{wf})_{N+1}$ is the liquid flux at the node just below the plane. Solving equation (3.66) for the moisture content X_N ensures that the solution proceeds smoothly when the evaporative plane moves across a node point in a time step.

When solving the model using numerical method, the wood density, initial moisture content will be chosen from measured values. The permeabilities of wood both to liquid (sapwood) and to gas are quite variable and the measured values span a range of two orders (Booker, 1989). Therefore these will be fitted in the experimental range to give a close match between predicted and measured values in temperature profiles and the drying times at average moisture content of about 10%. This point corresponds to the drying at the end of second period when the evaporative plane has just reached the mid-layer of the board. At this point, both predicted and measured temperatures at the centre of the board start to rise approaching the surface temperature. Also, the bound-water diffusion coefficient has been chosen so that the calculated and measured temperature profiles agreed closely.

The specific heat capacity C_P, (Kayihan, 1982) and the thermal conductivity λ, (Stanish, *et al.*, 1986) of moist wood have been predicted from the following correlations: -

$$C_P = 4184 \frac{X + 0.324}{1.0 + X} \qquad (3.67)$$

$$\lambda = \frac{\rho_S}{1000} (0.4 + 0.5 X) + 0.024 \qquad (3.68)$$

Other properties and parameters of wood used in the model will be given in next chapter, while the external transfer process and properties of moisture air and water vapour will be presented in Chapter 5.

3.4 Conclusion

By solving the model proposed in section 3.2 using the numerical method of section 3.3, we are able to predict the variations of the temperatures and moisture contents both with position and with drying times for the high-temperature drying of individual *Pinus radiata* boards. In this model, it is postulated for heartwood that an evaporative plane at the moisture boiling point sweeps through the timber. In the case of the much wetter sapwood board, we assume that at first the liquid flows maintain an evaporative plane just below the surface until the moisture is no longer funicular. Thereafter, drying proceeds in a similar way to heartwood. Once the timber is below the fibre-saturation point, cell-wall diffusion controls. These assumptions are in accordance with models for pit aspiration (Booker, 1990). The parameters involved in the model are measurable and have specific physical meanings. These parameters can be either chosen directly from measured data or fitted within the experimental range.

This model is based on the simultaneous heat- and mass-transfer properties with local thermodynamics equilibrium, and also it considers the physical features of pit aspiration and the differences between sapwood and heartwood in relation to drying. Therefore, this model can reflect the picture of moisture movement and heat transfer in wood during drying. However, this model is relatively simple compared to any existing models based on the transport properties.

In the model, a thin dry layer for sapwood is proposed to identify the sapwood drying. This idea is based on the botanical phenomenon of the green wood and is supported by the drying behaviour observed in drying tests. Recently, independent research (Laytner, 1994) indicates that a 0.5 to 1.5 mm staining layer close to the surface is inevitable for the sapwood drying. This dimension corresponds to the thin dry layer. The staining can be explained by the liquid water flow towards this evaporative front beneath the drying surface. As the liquid water evaporates at the front, the chemicals are left there causing the wood staining.

3.5 Nomenclature

a	coefficient in equations (3.7), (3.7) and (3.39 to 3.51)
A	constant in equation (3.28), Pa
b	coefficient in equations (3.7), (3.7) and (3.39 to 3.50)
B	constant in equation (3.28)
c	coefficient in equations (3.52 to 3.61)
C_P	specific heat capacity of moist wood, J kg^{-1} K^{-1}
d	coefficient in equations (3.52 to 3.61)
D	diffusion coefficient in equation (3.12), cm^2 s^{-1}
D_b	bound water transfer coefficient, kg s m^{-3}
D_{fl}	filtration motion diffusion coefficient in equation (3.13), cm^2 s^{-1}
E_l	effective permeability to liquid flow, s
E	characteristic moisture content in equation (3.6)
E_o	coefficient in equation (3.7)
E_v	effective permeability to vapour flow, s
Fcr	drying rate in constant-rate period in equation (3.7), lb ft^{-2} h^{-1}
F_m	drying rate in the falling-rate period in equation (3.8), lb ft^{-2} h^{-1}
f_v	factor for air velocity influence in equation (3.7)
ΔH_{vb}	latent heat of vaporization of bound water, J kg^{-1}
ΔH_{vw}	latent heat of vaporization of liquid water, J kg^{-1}
j_{wb}	bound water flux, kg m^{-2} s^{-1}
j_{wf}	liquid water flux, kg m^{-2} s^{-1}
j_{wv}	water vapour flux, kg m^{-2} s^{-1}
K_l	permeability of unsaturated wood, m^2
K_l^s	permeability of saturated wood, m^2
M	moisture content in equation (3.10), % (dry basis)
M_e	equilibrium moisture content in equation (3.10), % (dry basis)
M_v	molar mass of water vapour, kg mol^{-1}
n	factor in equation (3.10)
p_c	capillary pressure, Pa
p_l	liquid pressure, Pa
p, p^v	vapour pressure, Pa
p_{db}^s	saturation pressure of water vapour at dry-bulb temperature in equation (3.4), Pa
p_{wb}^s	saturation pressure of water vapour at wet-bulb temperature in equation (3.4), Pa

P total pressure, Pa

q source term in equation (21)

r source term in equation (16)

R resistance to moisture movement in equation (3.4), Pa kg kg^{-1}

S entropy, J mol^{-1} K^{-1}

S_a saturation

S_{amin} minimum saturation for liquid flow

S_T slope of the asymptote of the drying curve
in equation (3.10), lb ft^{-2} h^{-1}/%

T temperature, K

T_d dry-bulb temperature in equation (3.10), °F

T_w wet-bulb temperature in equation (3.10), °F

v air velocity in equations (3.8) and (3.9), ft min^{-1}

X local moisture content, kg kg^{-1}

$<X>$ average moisture content, kg kg^{-1}

X_e equilibrium moisture content in equation (3.5), kg kg^{-1}

X_{FSP} moisture content at the fibre-saturation point, kg kg^{-1}

X_i initial moisture content, kg kg^{-1}

X_{max} moisture content if entire void structure were filled with water, kg kg^{-1}

X_o critical moisture content in equation (3.5), kg kg^{-1}

z space coordinate measured normal to the surface, m

Δz distance interval, m

Greek

ε void fraction

λ thermal conductivity of moist wood, W m^{-1} K^{-1}
latent heat of vaporization in equation (3.11), J kg^{-1}

μ_b chemical potential of bound water, J kg^{-1}

μ_v chemical potential of water vapour, J kg^{-1}

μ_l viscosity of water, kg m^{-1} s^{-1}

μ_G viscosity of gas, kg m^{-1} s^{-1}

ρ_l density of water, kg m^{-3}

ρ_S density of dry wood, kg m^{-3}

τ time, s

$\Delta\tau$ time step, s

ξ distance of the evaporative plane from the surface, m

κ thermal conductivity in equation (3.11), W m^{-1} K^{-1}

Subscript

G	in the airstream
S	at the board surface
j	node point
ξ	at the position of evaporative plane

Superscript

n	time step
o	previous

3.6 References

1. Adesanya, B.A., Nanda, A.K. and Beard, J.N. 1988. Drying Rates During High-Temperature Drying of Yellow Poplar. *Drying Technology*, 6(1) pp95-112.

2. Beard, J.N., Rosen, H.N. and Adesanya, B.A. 1982. Heat Transfer during the Drying of Lumber. *Proc. 3rd Drying Sympusium*, Vol.1, pp110-122.

3. Beard, J.N., Rosen, H.N. and Adesanya, B.A. 1985. Temperature Distribution in Lumber during Impingement Drying. *Wood Sci. and Techn.* 19, pp277-286.

4. Bosilica, C., Moyne, C. and Martin, M. 1982. High-Temperature Convective Drying of Softwood: Moisture Migration Mechanism. *Proc. 3rd International Drying Symposium*, Vol.1, pp46-55.

5. Bonneau, P. 1991, Modélisations du Séchage d'un Matériau Hétérogène: Application à un bois de résineux, Ph.D. Thesis, University of Bordeaux, France, 245 p.

6. Booker, R. E. 1990. Changes in Transverse Wood Permeability during the Drying of *Dacrydium cupressinum* and *Pinus radiata*. *NZ J. Forest. Sci.* 20(2) pp231 - 244.

7. Booker, R. E. 1989. Hypothesis to Explain the Characteristic Appearance of Aspirated Pits. *Proc. Second Pacific Region Wood Anatomy Conference*, Forest Products Research and Development Institute, Laguna, Philippines.

8. Booker, R. E. 1979. A Comparison of the Radial, Tangential and Axial Permeabilities of Radiata Pine. New Zealand Forest Service, Forest Research Institute, Rotorua, New Zealand, Timber Drying Report No. 39 (unpublished).

9. Bramhall, G. 1976. Semi-Empirical Method to Calculate Kiln-Schedule Modification from Some Lumber Species. *Wood Sci.*, 8(4) pp213-222.

10. Chen, P. and Pei, D.C.T. 1989. A Mathematical Model of Drying Processes. *Int. J. Heat Mass Transfer,* Vol.32, No.2, pp297-310.

11. Choong, E.T. and Skaar, C. 1969. Separating Internal and External Resistance to Moisture Removal in Wood Drying. *Wood Sci.,* 1(4) pp200-202.

12. Choong, E.T. and Skaar, C. 1972. Diffusion and Surface Emissivity in Wood Drying. *Wood and Fibre*, 4(2) pp80-86.

13. Collignan, A., Nadeau, J.P. and Puiggali, J.R. 1993. Description and Analysis of Timber Drying Kinetics. *Drying Technology*, 11(3) pp487-506.

14. Comstock, G.L. 1967. Longitudinal Permeability of Wood to Gases and Nonswelling Liquids. *Forest Product J.*, 17(10) pp41-46.

15. Cown, D. J. and McConchie, D. L. 1983. Radiata Pine Wood Properties Survey (1977 - 1982). New Zealand Forest Research Service, Forest Research Institute Bulletin No. 50, Rotorua, New Zealand (unpublished).

16. Johnson, J.A. 1989. Stress Development. *Proc. IUFRO Wood Drying Symposium*, Seattle, Washington, pp269-280.

17. Kayihan, F. 1982. Simulation Heat and Mass Transfer with Local Three-Phase Equilibria in Wood Drying. *Proc. 3rd International Drying Symposium*, Vol.1, Birmingham, pp123 - 134.

18. Kayihan, F. 1983. Adaptive Control of Stochastic Batch Lumber Drying. *Computers Chem. Engng.*, Vol.17, No.3, pp265-273.

19. Kho, P. C. S., Keey, R. B. and Walker, J. C. F. 1989. Effect of Minor Board Irregularities and Air Flows on the Drying Rate of Softwood Timber Board in Kilns. *Proc. IUFRO International Wood Drying Symposium*, Seattle, Washington, pp150-157.

20. Langrish, T. A. G., Kho, P. C. S., Keey, R. B. and Walker, J. C. F. 1992. Experimental Measurement and Numerical Simulation of Local Mass-Transfer Coefficients in timber Kilns. *Drying Technology*, 10(3) pp753-782.

21. Langrish, T.A.G., Keey, R.B., Kho, P.C.S. and Walker, J.C.F. 1993. Time-Dependent Flow in Arrays of Timber Boards: Flow Visualization, Mass-Transfer Measurement and Numerical Simulation. *Chem. Eng. Sci.*, 48(12), pp2211-2223.

22. Laytner, F. 1994. Staining Radiata's Reputation. *NZ Forest Industries*, 25(4), pp55.

23. Lowery, D.P. 1972. Vapour Pressure Generated in Wood During Drying. *Wood Sci.*, 5(1) pp73-80.

24. Luikov, A.V. 1966. "*Heat and Mass Transfer in Capillary-Porous Bodies*". Pergamon Press, New York.

25. Milota, M.R. and Tschernitz, J.L. 1990. Correlation of Loblolly Pine Drying Rates at High-Temperatures. *Wood and Fibre Sci.*, 22(3) pp298-313.

26. Moren, T.J. 1989. Check Formation During Low Temperature Drying on Scots Pine: Theoretical Consideration and Some Experimental Results. *Proc. IUFRO International Wood Drying Symposium*, Seattle, Washington, pp97-100.

27. Pang Shusheng, Keey, R.B. and Langrish, T.A.G. 1992a. Modelling of Temperature Profiles within Boards during High-Temperature Drying of *Pinus radiata* Timber. in Mujumdar, A.S. (ed.): *Drying'92*, Elsevier, Part A: pp417-433.

28. Pang Shusheng, Keey, R.B., Walker, J.C.F. and Langrish, T.A.G. 1992b. The Stress Development and Check Formation within Boards of *Pinus radiata* during High-Temperature Drying. Research Report No.3. Chemical and Process Engineering, University of Canterbury, Christchurch, New Zealand (unpublished).

29. Pang Shusheng and Keey, R.B. 1994. The Drying Kinetics of Impermeable Heartwood Board of *Pinus radiata* at Elevated Temperatures. to be presented at International Drying Symposium, IDS '94, Brisbane, Australia.

30. Patankar, S. 1980. "*Numerical Heat Transfer and Fluid Flow*". Hemisphere, New York.

31. Perré, P., Fohr, J. P. and Arnaud, G. 1988. A Model of Drying Applied to Softwood: The Effect of Gaseous Pressure Above the Boiling Point. *Proc. Sixth International Drying Symposium IDS '88*, Versailles, pp279.

32. Plumb, O.A., Spolek, G.A. and Olmstead, B.A. 1985. Heat and Mass Transfer in Wood During Dying. *Int. J. Heat Mass Transfer,* Vol.28, No.9, pp1669-1678.

33. Press, W. H., Flannery, B. P., Teukolsky, S. A. and Vetterling, W. T. 1986. "*Numerical Recipes. The Art of Scientific Computing*". Cambridge University Press, Cambridge, MA.

34. Puiggali, J.R. and Quitart, M. 1992. Properties and Simplifying Assumptions for Classical Drying Models. in Mujumdar, A.S. (ed.): "*Advances in Drying*", Vol.5. Hemisphere Publishing Co., Washington.

35. Puiggali, J.R., Nadeau, J.P. and Sales, C. 1993. Assessment of Timber Drying Schedules by Evaluation of Damage Risks. *Drying Technology*, 11(3) pp507-524.

36. Rosen, H.N. 1980. Empirical Model for Characterizing Wood Drying Curves. *Wood Sci.*, 12(4) pp201-206.

37. Rosen, H.N. 1978. Evaluation of Drying Times, Drying Rates and Evaporative Fluxes When Drying Wood with Impinging Jets. *Proc. 1st International Drying Symposium,* pp192-200.

38. Rosen, H.N. 1982. Function Relations and Approximation Techniques for Characterizing Wood Drying Curves. *Wood Sci.*, 15(1) pp49-55.

39. Rosen, H.N. 1987. Recent Advances in the Drying Solid Wood. in Mujumdar, A.S. (ed.): "*Advances in Drying*", Vol.4, Hemisphere Publishing Co., Washington.

40. Salin, J.G. 1989. Prediction of Checking, Surface Discolouration and Final Moisture Content by Numerical Method. *Proc. IUFRO International Wood Drying Symposium*, Seattle, Washington, pp222-225.

41. Sherwood, T.K. 1929. The Drying of Solids — I. *Indus. and Eng. Chem.*, 21(1) pp12-16.

42. Siau, J. F. 1984. "*Transport Processes in Wood*". Spring-Verlag, Berlin and New York.

43. Simpson, W. T. and Rosen, H. N. 1981. Equilibrium Moisture Content of Wood at High Temperature. *Wood and Fibre*, 13(3) pp150-158.

44. Skaar, C. 1988. "*Wood-Water Relations*". Spring-Verlag, New York.

45. Spolek, G. A. and Plumb, O. A. 1981. Capillary Pressure in Softwood. *Wood Science and Techn*, Vol. 15, pp189 - 199.

46. Stamm, A.J. 1964. "*Wood and Cellulose Science*". Ronald Press, New York.

47. Stanish, M. A., Schajer, G. S. and Kayihan, F. 1986. A Mathematical Model of Drying for Hygroscopic Porous Media. *AIChE J.*, 32(8) pp1301-1311.

48. Stanish, M.A. 1986. the Roles of Bound Water Chemical Potential and Gas Phase Diffusion in Moisture Transport through Wood. *Wood Sci. and Techn.*, 19(1), pp53-70.

49. Thomas, H.R., Lewis R.W. and Morgan, K. 1980. An Application of the Finite Element Method to the Drying of Timber. *Wood and Fibre,* 1(4) pp237-243.

Chapter 4

The Physical Properties and Thermodynamic Parameters of Wood

In the proposed mathematical model, various physical properties and thermodynamic parameters of wood, air, water and water vapour are used in the equations. These properties and parameters of wood include the moisture isotherm on drying, the heat of sorption heat for wood, the initial moisture content of green wood and wood permeability to both gas and water flows. In order to solve the model, these properties and parameters for *Pinus radiata* and those of air, water and vapour need to be determined as well as the variation of these parameters during drying. In this chapter, the equilibrium moisture content (desorption process) and sorption heat of wood will be discussed in detail, while the other parameters will be described briefly or cited from the literature.

4.1 The Equilibrium Moisture Content for *Pinus radiata*

The equilibrium moisture content (X_e) is defined as that moisture content at which the material neither gains nor loses moisture at a given condition of temperature and humidity. The value of X_e for a material depends upon the physical nature of the material and the surrounding air of temperature and humidity. At a fixed relative humidity and temperature, the amount of moisture retained by a body is also affected by whether the equilibrium has been approached by wetting (adsorption) or by drying (desorption) (Keey, 1978).

In wood processing and in the use of wood products, accurate prediction of X_e is important for controlling the quality and matching the products to conditions to which they are exposed. In the simulation of the timber drying process, knowledge of the X_e-temperature-relative humidity relationship is useful to determine one factor from the other two. X_e is the limiting value for drying which is approached asymtotically.

The X_e-temperature-relative humidity data of wood at a temperature range of 30°F and 270 °F (-1°C and 132°C) can be found in the Wood Handbook by the Wood Products Laboratory of the U. S. Department of Agriculture. A correlation to predict equilibrium moisture content of wood is also proposed by Simpson (1971,1973), and Simpson and

Rosen (1981). These predictions have widely been used in studies of timber drying. Simpson obtained the coefficients in the correlation from adsorption data (1971, 1973) at temperatures between 30°F and 210°F (-1°C and 99°C). Afterwards, Simpson and Rosen (1981) extrapolate the correlation to high-temperatures (215-302°F) (102°C - 150°C). In the Wood Handbook, there is no indication as to whether the data are for adsorption or for desorption. However, the data agree very well with Simpson's prediction. These predictions are assumed to be a general guide for most practical purposes for wood of any species.

For the wood of *Pinus radiata*, one of the most popular commercial species grown in New Zealand, Cunningham and Sprott (1984) have given the experimental data of X_e both for adsorption and for desorption, and have suggested an equation to predict the values of X_e. They measured X_e at a temperature of 15°C and there is no temperature-correction in their equation for varying temperatures.

The objective of this section is to develop expression(s) to predict the value of X_e for *Pinus radiata* in a desorption process (drying) with a correction for temperature effects. The development is based on the existing correlation by Simpson and the data by Cunningham and Sprott.

4.1.1 Comparison of the Prediction for X_e with Recent Data for *Pinus radiata*

Using the sorption theory of Hailwood and Horrobin (1946), Simpson (1971, 1973) has developed a correlation to predict the equilibrium moisture content of wood. The form of the correlation is as follows:

$$X_e = \frac{18}{W}\left[\frac{K_1 K_2 \psi}{1 + K_1 K_2 \psi} + \frac{K_2 \psi}{1 - K_2 \psi}\right] \qquad (4.1)$$

where X_e is the equilibrium moisture content (kg kg^{-1}), ψ is the relative humidity, and K_1, K_2 and W are temperature-dependent coefficients.

The coefficients were correlated by Simpson (1971) using adsorption data and are related functions of temperature T_F (°F):

$$K_1 = 3.73 + 3.642X10^{-2}\, T_F - 1.547X10^{-4}\, T_F^2 \qquad (4.1a)$$

$$K_2 = 0.674 + 1.053X10^{-3}\, T_F - 1.714X10^{-6}\, T_F^2 \qquad (4.1b)$$

$$W = 216.9 + 1.961X10^{-2}\, T_F + 5.720X10^{-3}\, T_F^2 \qquad (4.1c)$$

For *Pinus radiata*, Cunningham and Sprott (1984) measured X_e at a temperature of 15°C both for adsorption and for desorption processes in four cases: the wood was untreated, boric treated, *CCA* treated and *AAC* treated.

A comparison of X_e data by Cunningham and Sprott for *Pinus radiata* with the predictions by other authors is shown in Figure 4.1 and Table 4.1. In the comparison, a temperature of 15°C is used in all predictions. It can be seen from both the figure and table that Simpson's prediction agrees very well with the data of the Wood Handbook, and these predictions are very close to the adsorption data by Cunningham and Sprott. However, significant differences appear between these predictions and the desorption data for *Pinus radiata* in all of the four cases. This means that Simpson's correlation can be applied to predict X_e for *Pinus radiata* in a wetting process (adsorption) without significant error, but will underpredict X_e in a drying process (desorption) for the wood. The deviation for using Simpson's correlation in a drying process varies from around 2% MC at 10% relative humidity to 4.0% MC above 60% relative humidity.

From the measured data by Cunningham and Sprott, it can also be shown that the X_e values in desorption processes for the four cases are very close, so it may be possible to develop a single correlation to predict the values in each case of drying.

4.1.2 Prediction of Equilibrium Moisture Content for *Pinus radiata* with Temperature Correction

During drying, the equilibrium moisture content varies with temperature and relative humidity, so these variations need to be quantified when it is used to describe the drying process. In the desorption process (drying), a modified correlation may be obtained by accepting the form of Simpson's correlation (equation 4.1). In order to predict the values of equilibrium moisture content of *Pinus radiata*, the coefficients in the correlation will be obtained by fitting the correlation to the measured data by Cunningham and Sprott (1984). In this way these coefficients, K_1, K_2 and W are re-defined as:

$$K_1 = A_1 + 0.04773\, T_C - 5.012X10^{-4}\, T_C^2 \qquad (4.1d)$$

$$K_2 = A_2 + 1.698X10^{-3}\, T_C - 5.553X10^{-6}\, T_C^2 \qquad (4.1e)$$

$$W = A_3 + 0.6942\, T_C + 0.01853\, T_C^2 \qquad (4.1f)$$

in above equations T_C is the temperature (°C).

By fitting equation (4.1) with new coefficients (equations 4.1d to 4.1f) to Cunningham's measured data for desorption with the technique of nonlinear least squares, the values of A_1, A_2, A_3 are predicted as:

$A_1 = 9.864$
$A_2 = 0.7196$
$A_3 = 187.6$

Therefore the equilibrium moisture content of *Pinus radiata* can be predicted by the following equation:

$$X_e = \frac{18}{W}\left[\frac{K_1 K_2 \psi}{1 + K_1 K_2 \psi} + \frac{K_2 \psi}{1 - K_2 \psi}\right] \qquad (4.2)$$

where the coefficients are determined by

$$K_1 = 9.864 + 0.04773\, T_C - 5.012X10^{-4}\, T_C^2 \qquad (4.2a)$$

$$K_2 = 0.7196 + 1.698X10^{-3}\, T_C - 5.553X10^{-6}\, T_C^2 \qquad (4.2b)$$

$$W = 187.6 + 0.6942\, T_C + 0.01853\, T_C^2 \qquad (4.2c)$$

By using equation (4.2), the predicted values of X_e for *Pinus radiata* can be compared with Cunningham's data to examine the goodness of fit. The results are shown in Figure 4.2.

From the comparison, a very close match between the predictions of equation (4.2) and the experimental data at a temperature of 15°C can be seen. Significant errors occur only when the relative humidity is close to unity, the air being nearly saturated.

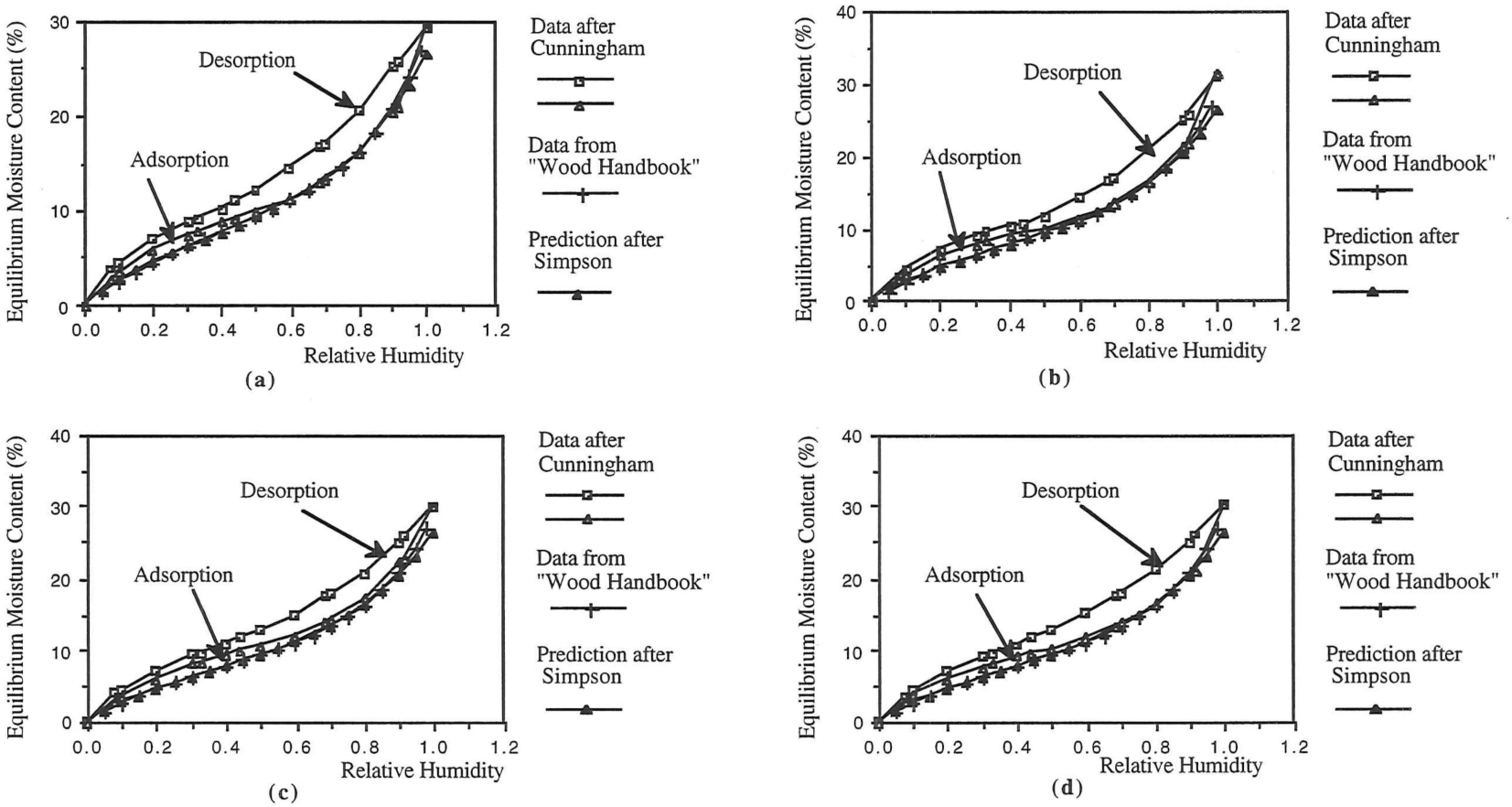

Figure 4.1. The comparison of the experimental results of the equilibrium moisture content by Cunningham and Sprott (1984) for *Pinus radiata* with the predicted results at 15°C for all species of wood by other authors.

(a). the wood is untreated; (b). the wood is boron treated; (c). the wood is *CCA* treated;
(d). the wood is *ACC* treated.

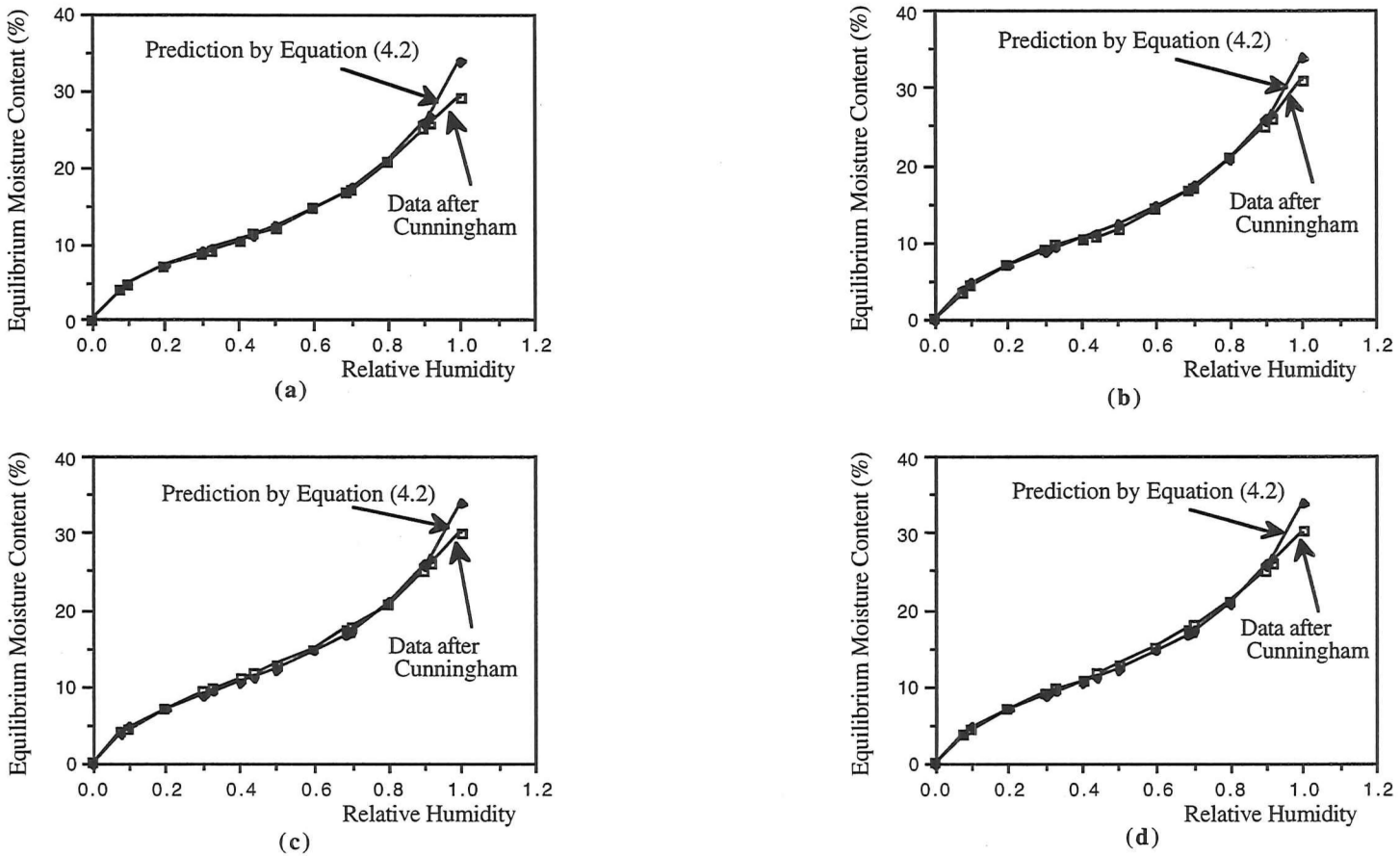

Figure 4.2. The comparison of the prediction of the equilibrium moisture content at 15°C for *Pinus radiata* by the correlation developed in this paper with the experimental results by Cunningham Sprott (1984).

(a). the wood is untreated; (b). the wood is boron treated; (c). the wood is *CCA* treated;
(d). the wood is *ACC* treated.

Table 4.1 The data of the equilibrium moisture content at the temperature of 15°C by different authors

Relative Humidity	X_e (%) in Adsorption Process for *P. radiata* after Cunningham and Sprott (1984)				X_e (%) in Desorption Process for *P. radiata* after Cunningham and Sprott (1984)				X_e (%) from "Wood Hand-book"	X_e (%) after Simpson (1971, 1981)
	Untreated	Boron treated	*CCA* treated	*AAC* treated	Untreated	Boron treated	*CCA* treated	*AAC* treated	All wood species	All wood species
0.1	3.57	3.75	3.54	3.96	4.58	4.38	4.38	4.38	2.5	2.72
0.2	5.84	6.25	6.04	6.04	7.08	7.08	7.08	7.08	4.6	4.61
0.3	7.52	7.92	8.15	7.71	8.75	9.17	9.38	9.17	6.2	6.2
0.4	8.78	9.17	9.38	9.17	10.21	10.42	11.04	10.83	7.8	6.96
0.5	10.00	10.00	10.63	10.21	12.08	11.88	12.92	12.92	9.4	9.35
0.6	11.26	11.46	12.08	11.67	14.58	14.38	15.00	15.21	11.1	11.19
0.7	13.36	13.54	14.38	13.75	17.08	17.08	17.71	17.92	13.3	13.44
0.8	16.05	16.46	17.29	16.25	20.63	20.83	20.63	21.25	16.2	16.35
0.9	20.42	21.46	22.29	20.63	25.00	25.00	25.00	25.00	20.7	20.37
1.0	29.17	31.17	30.00	30.42	29.17	31.17	30.00	30.42	26.8	26.47

4.1.3 Conclusion

By accepting the form of Simpson's correlation and fitting the model to Cunningham's experimental data at a temperature of 15°C, new coefficients have been obtained for Simpson's equation to predict the equilibrium moisture content in a drying process (desorption) for *Pinus radiata*. The prediction is in close agreement with the data. However, for a wetting process (adsorption) Simpson's correlation can be used without significant error.

Simpson (1971,1973) has determined the coefficients in his correlation from adsorption data, so the correlation should be corrected for a drying process. Unfortunately, Simpson's correlation has been cited by many authors without identifying whether the process is adsorption or desorption. Therefore errors may result when using his correlation to predict the equilibrium moisture content in a drying process.

4.2 The Heat of Sorption of Timber

The bonding of condensed moisture to its host material is reflected in a difference in heat content or enthalpy between that of the bound (H_W) and that of the free (H_W^o) moisture at the same temperature and total pressure. This enthalpy difference ($H_W - H_W^o$) is called the differential heat of sorption, $-\Delta H_W$, and is a function of the moisture content at given relative humidity and temperature. Pang, Langrish and Keey (1993) have presented some comments on the calculation of sorption heat of timber. This work is included here to complete solving the model.

4.2.1 A Review of Proposed Methods to Calculate the Heat of Sorption

Skaar (1988) has given correlations for the heat of sorption of timber, which are apparently based on fitting the results of Stamm and Loughborough (1935). They maintain that they could also use an equation for the differential heat of sorption together with equilibrium data which they measured themselves.

The correlation given by Skaar (1988) for the heat of sorption at temperatures near 50°C was:

$$-\Delta H_W = 1172\, exp(-14X) \qquad (4.3)$$

where X is the moisture content on a dry basis. The results given by Skaar (1988) compare closely with heats of sorption obtained from fundamental measurements made by Kelsey and Clarke (1956). They measured the total or integral heats of wetting, and calculated the heat of sorption by differentiating the curves of heat of wetting against moisture content. Their data are extensive, covering a range of moisture contents from 0.01 kg kg^{-1} to 0.26 kg kg^{-1}.

However, Rees (1948) has shown that the use of sorption data to calculate the heat of sorption at low moisture contents (below 10%) is subject to considerable errors. This suggests that Skaar (1988) may be mistaken in suggesting that heats of sorption can be calculated from sorption data with any great accuracy.

As a further example of this, one can use the sorption equilibrium relationship given by Simpson and Rosen (1981) to estimate the heat of sorption, and show that the use of this equation can lead to results which are inconsistent with those of Kelsey and Clarke (1956) and Skaar (1988). This will be demonstrated in the following way.

The difference may be calculated from a form of the Clausius-Clapeyron equation, which is derived by assuming that the vapour phase behaves as an ideal gas and that the molar volume of the condensed phase is negligible compared with that of the vapour (Smith and Van Ness, 1975):

$$\left[\frac{\partial \ln(p^v/p_s^v)}{\partial T}\right]_X = -\frac{1}{R}\left[\frac{H_w - H_w^o}{T^2}\right] \qquad (4.4)$$

where p^v is the partial pressure of water vapour, p_s^v is the saturation pressure, R is the universal gas constant and T is the absolute temperature. Since the enthalpy difference $(H_w - H_w^o)$, which is the heat of sorption, $-\Delta H_w$, is a function of the moisture content, the following relationship can be obtained for constant moisture content:

$$\Delta H_w = \frac{RT^2}{M_w}\left(\frac{\partial \ln \psi}{\partial T}\right)_X = -\frac{R}{M_w}\left[\frac{\partial \ln \psi}{\partial (1/T)}\right]_X \qquad (4.5)$$

in which the relative humidity (ψ)is defined as the ratio of the vapour pressure to the saturated vapour pressure. It follows that the heat of wetting can be found from the slope of a graph of $\ln \psi$ plotted against the reciprocal of the absolute temperature $1/T$ if sorption

data are available at various temperatures. Equation (4.5) will be referred to as the differential form of the Clausius-Clapeyron equation.

For small temperature intervals, it may be assumed that the heat of wetting is a constant. Thus, if data at two, fairly close temperatures (say 20°C difference) are known, then

$$\Delta H_w = \frac{R\, T_1\, T_2\, ln(\psi_1/\psi_2)}{M_w\,(T_1 - T_2)} \tag{4.6}$$

with $T_1<T_2$ and $\psi_1<\psi_2$. Equation (4.6) is an integral form of the Clausius-Clapeyron equation.

The free energy change (ΔG) is sometimes given as an approximation to the heat of wetting. The free energy change can be calculated from:

$$\Delta G = - R\, T\, ln\psi \tag{4.7}$$

4.2.2. The Sorption Equilibrium Relationship of Simpson and Rosen

Simpson and Rosen (1981) present an equation (4.1) for the sorption equilibrium of timber to predict equilibrium moisture content. This equation can be converted into a form to calculate relative humidity from known temperature at given equilibrium moisture content as done by Kayihan (1982)*.

$$\psi = \frac{1}{2}\left[Z_1 + \left(Z_1^2 + \frac{4}{K_1\, K_2^2}\right)^{1/2}\right] \tag{4.8}$$

In this equation, the factors Z_1, K_1, K_2 and other factors Z_2 and W are:

$$Z_1 = \frac{(1 - Z_2)}{K_2} - \frac{(1+Z_2)}{K_1\, K_2} \tag{4.8a}$$

$$Z_2 = \frac{18}{W\ X} \tag{4.8b}$$

$$K_1 = 3.37 + 3.642X10^{-2}\, T_F - 1.547X\ 10^{-4}\, T_F^2 \tag{4.8c}$$

$$K_2 = 0.674 + 1.053\ X10^{-3} T_F - 1.714\ X10^{-6}\, T_F^2 \tag{4.8d}$$

$$W = 216.9 + 1.961X10^{-2}\, T_F + 5.720X10^{-3}\, T_F^2 \tag{4.8e}$$

---

* Kayihan's paper contains proofreading error: $Z_1 = \frac{(1 - Z_2)}{K_2} + \frac{(1+Z_2)}{K_1\, K_2}$

In equations (4.8a) to (4.8e) T_F is temperature in degrees Fahrenheit, which can be related to the absolute temperature T in Kelvin by $T_F = 1.8\,(T - 237.15) + 32$. Equation (4.8) is valid over a range of temperatures from 0°C to 150°C and the maximum deviation between this equation and the equilibrium data reported in the Dry Kiln Operator's Manual (Rasmussen, 1961) and the Wood Handbook (U.S. FPL, 1974) is 1% moisture content. However, as discussed in foregoing section, the moisture content in this equation should be that for the adsorption process (wetting).

When calculating the heat of sorption from the differential form of the Clausius-Clapeyron equation, we need the partial derivative of $ln\psi$ with respect to temperature. We can estimate this by writing equation (4.8) in the form:

$$ln\psi = ln\frac{1}{2} + ln\left[Z_1 + \left(Z_1^2 + \frac{4}{K_1 K_2^2}\right)^{1/2}\right] = ln\frac{1}{2} + ln\, U \tag{4.9}$$

where the term $Z_1 + [Z + 4/(K_1 K_2^2)]^{1/2}$ is denoted by U. Then the partial derivative of $ln\psi$ with respect to temperature is:

$$\frac{\partial ln\psi}{\partial T} = \frac{1}{U}\frac{\partial U}{\partial T} \tag{4.10}$$

The factor U is a function of Z_1, K_1 and K_2 so the chain rule must be used to obtain its derivative with respect to temperature, as follows:

$$\frac{\partial U}{\partial T} = \frac{\partial U}{\partial Z_1}\frac{\partial Z_1}{\partial T} + \frac{\partial U}{\partial K_1}\frac{\partial K_1}{\partial T} + \frac{\partial U}{\partial K_2}\frac{\partial K_2}{\partial T} \tag{4.11}$$

The partial derivatives $\frac{\partial U}{\partial Z_1}$, $\frac{\partial U}{\partial K_1}$ and $\frac{\partial U}{\partial K_2}$ are:

$$\frac{\partial U}{\partial Z_1} = 1 + \frac{Z_1}{[Z_1^2 + 4/(K_1 K_2^2)]^{1/2}} \tag{4.12}$$

$$\frac{\partial U}{\partial K_1} = \frac{2}{[Z_1^2 + 4/(K_1 K_2^2)]^{1/2} K_1^2 K_2^2} \tag{4.13}$$

$$\frac{\partial U}{\partial K_2} = \frac{4}{[Z_1^2 + 4/(K_1 K_2^2)]^{1/2} K_1 K_2^3} \tag{4.14}$$

The partial derivatives $\partial K_1/\partial T$ and $\partial K_2/\partial T$ have the simple forms (with the temperatures in Kelvin):

$$\frac{\partial K_1}{\partial T} = 0.3216 - 1.002X\ 10^{-3}\ T \tag{4.15}$$

$$\frac{\partial K_2}{\partial T} = 4.731X\ 10^{-3} - 1.111X10^{-5}\ T \tag{4.16}$$

The partial derivative of Z_1 with respect to temperature is more complicated because Z_1 is a function of Z_2, K_1 and K_2. Further applications of the chain rule are required:

$$\frac{\partial Z_1}{\partial T} = \frac{\partial Z_1}{\partial Z_2}\frac{\partial Z_2}{\partial T} + \frac{\partial Z_1}{\partial K_1}\frac{\partial K_1}{\partial T} + \frac{\partial Z_1}{\partial K_2}\frac{K_2}{\partial T} \tag{4.17}$$

$$\frac{\partial Z_2}{\partial T} = \frac{\partial Z_2}{\partial W}\frac{\partial W}{\partial T} = -\frac{18}{X\ W^2}(-9.429 + 0.03706\ T) \tag{4.18}$$

$$\frac{\partial Z_1}{\partial Z_2} = -\frac{1}{K_1}(1 + \frac{1}{K_2}) \tag{4.19}$$

$$\frac{\partial Z_1}{\partial K_1} = -\frac{1}{K_1^2}\left[(1 - Z_2) - \frac{1 + Z_2}{K_2}\right] \tag{4.20}$$

$$\frac{\partial Z_1}{\partial K_2} = \frac{1 + Z_2}{K_1\ K_2^2} \tag{4.21}$$

These equations (4.10 to 4.21) enable the heat of sorption to be calculated from the equilibrium expression of Simpson and Rosen (1981) (equation 4.8) using the differential form of the Clausius-Clapeyron equation (equation 4.5).

4.2.3 Results and Discussion

4.2.3.1. A Comparison of the Results with the Literature

Figure 4.3 and 4.4 show the heat of sorption for wood at a temperature of 50°C plotted against moisture content and relative humidity respectively. The curves were calculated from the Clausius-Clapeyron equation in its differential and integrated forms (equation 4.5 and 4.6 respectively), the free energy change (equation 4.7) and the correlation of Skaar (1988). The integrated form of the Clausius-Clapeyron equation was calculated using a temperature difference $(T_2 - T_1)$ of 10 K. The free energy change is a poor estimate of the heat of sorption at all moisture contents and relative humidities. Also, the differential and integral form of the heat of sorption of timber agree closely and both show a peak value at a moisture content of about 0.05 kg kg^{-1}.

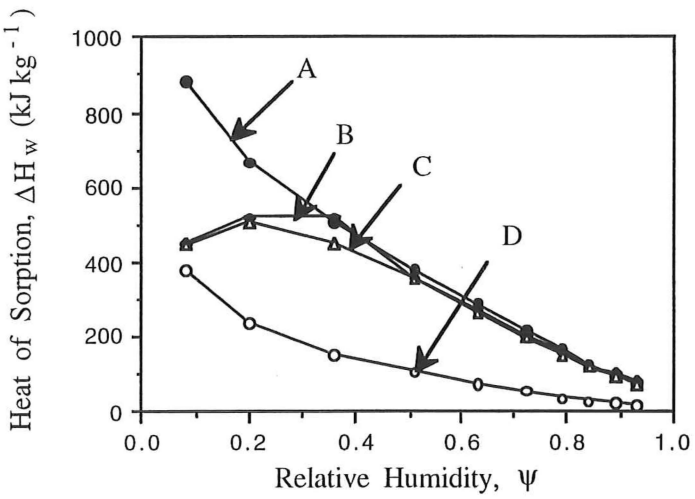

Figure 4.3. The heat of sorption for wood plotted against moisture content at a temperature of 50°C. The methods are:

A: after Skaar (1988), equation (4.3);

B: from the differential form of the Clausius-Clapeyron equation (equation 4.5);

C: from the integral form of the Clausius-Clapeyron equation (equation 4.6);

D: from the free energy change (equation 4.7).

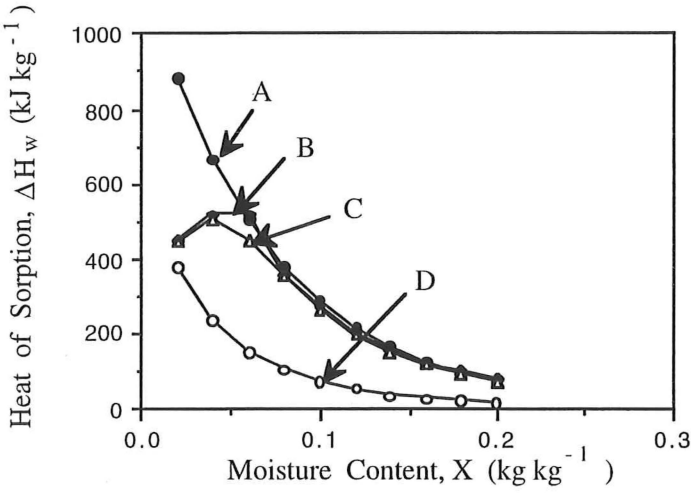

Figure 4.4. The heat of sorption for wood plotted against relative humidity at a temperature of 50°C. The methods are:

A: after Skaar (1988), equation (4.3);

B: from the differential form of the Clausius-Clapeyron equation (equation 4.5);

C: from the integral form of the Clausius-Clapeyron equation (equation 4.6);

D: from the free energy change (equation 4.7).

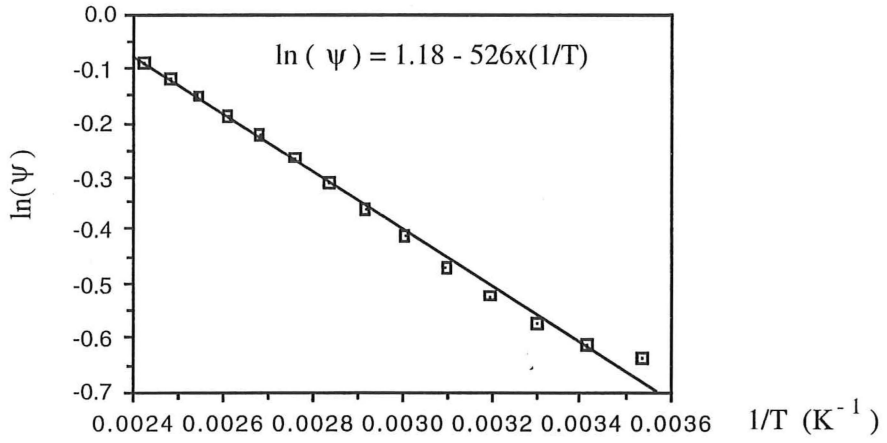

Figure 4.5. The sorption relationship for timber at a moisture content of 0.1 kg kg^{-1}.

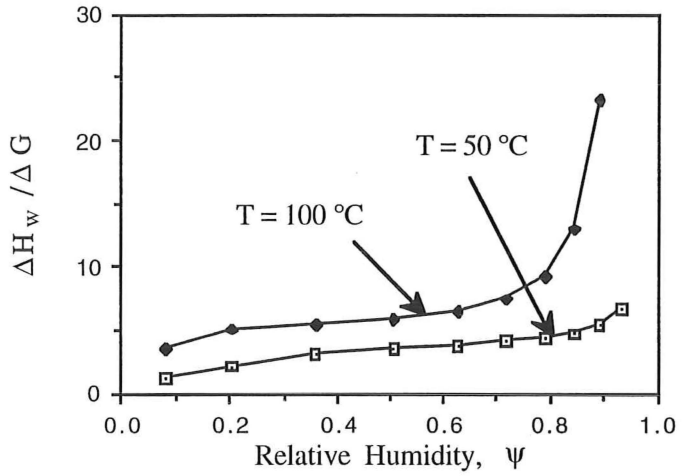

Figure 4.6. The ratio of the heat of sorption to the free energy change as a function of relative humidity.

However, the correlation of Skaar (1988) agrees with both forms of the Clausius-Clapeyron equation only above moisture contents of 0.07 kg kg^{-1} or relative humidities of 35%. This was not expected, as Skaar has fitted the results of Stamm and Loughborough (1935) and these authors used the integrated form of the Clausius-Clapeyron equation to give curve A in Figures 4.3 and 4.4. In addition, the equilibrium relationship given by Simpson and Rosen (1981) agrees with their sorption data well. For example, the relative humidities at a temperature of 200°F, moisture contents of 0.02 kg kg^{-1}, 0.06 kg kg^{-1} and 0.14 kg kg^{-1} are predicted to be 14.2%, 39.4% and 87.0% respectively from the equation of Simpson and Rosen (1981) compared with 15%, 40% and 90% respectively from the graph of Stamm and Loughborough (1935). These values agree within the uncertainty involved in reading the graph of Stamm and Loughborough (1935).

Noack, Schwab and Bartz (1973) show that adsorption isotherms for different species of timber differ significantly at high moisture contents, but the variations are much smaller at the low moisture contents and relative humidities where our results differ significantly from those of Stamm and Loughborough (1935). Therefore the variation in adsorption isotherms is unlikely to be the cause of the deviations which have been noted.

The deviations are most likely to be due to inaccurate nature of the sorption relationship at low moisture contents and echo the comments of Rees (1948) regarding the inappropriate use of equation (4.5) and (4.6) to calculate the heat of sorption. Direct measurement is more satisfactory. The direct measurements have been used in this work.

4.2.3.2. The Free Energy Change as an Approximation to the Heat of Sorption

If the free energy change (equation 4.7) were equal to the heat of sorption (equation 4.5), then:

$$\Delta H_w = - R \left[\frac{\partial ln\psi}{\partial 1/T}\right]_x = -R \left[\frac{ln\psi}{1/T}\right]_x \qquad (4.22)$$

For this equality to hold, the equilibrium relationship must have the following form:

$$ln\psi = a\left(\frac{1}{T}\right) \qquad (4.23)$$

where a is a constant. However the equilibrium relationship for timber has the form of the Antoine equation at given moisture content, as follows:

$$ln\psi = a\left(\frac{1}{T}\right) + b \qquad (4.24)$$

Here b is another constant at a given moisture content, and this is not zero for timber. An example is shown in Figure 4.5 at a moisture content of 0.1 kg kg^{-1}, where the constant b is 1.18.

Since b is non-zero for the sorption equilibrium of timber, this implies that the free energy change (equation 4.7) is an inappropriate estimate of the heat sorption of timber. Indeed, it will be inappropriate for any material for which the coefficient b is significantly non-zero.

This is emphasized by Figure 4.6, which shows the ratio of the heat of sorption to the free energy change at temperatures of 50°C and 100°C. The ratio of the two is very large, with the difference exceeding 100% over the full range of relative humidity. It is also notable that the difference increases with relative humidity and temperature.

Stamm and Loughborough (1935) discuss the difference between the heat of sorption and the free energy change. They attribute this difference to the entropy change (ΔS) accompanying the dimensional changes in timber on swelling. Their values for the entropy of sorption as a function of moisture content show a monotonic decrease with increasing moisture content with no negative values and only a slight variation with temperature. This variation with moisture content is consistent with the form of curve A in Figure 4.3 and 4.4 rather than those curves (B and C) derived from sorption data.

4.2.4. Conclusion

Two different methods for calculating the heat of sorption of timber are compared. One method uses thermodynamic expressions together with the sorption equilibrium relationship given by Simpson and Rosen (1981), while the other is based on the direct measurements made by Stamm and Loughborough (1935). The latter method is most reliable for moisture contents below 0.07 kg kg^{-1} while above this value these two methods agree closely.

The results presented by Skaar (1988) are reliable. The calculation based on sorption isotherms is also acceptable provided that the moisture content is 0.07 kg kg^{-1} or higher. At lower moisture content the calculation departs significantly from direct measurements.

4.3 Permeability to Liquid and Vapour Flows

4.3.1 The Data from Literature

The permeability of the wood to both vapour and liquid flows is likely to vary with factors such as species of the tree, the location of the wood in the tree trunk, the orientation of the sample, the density of the wood and seasonal changes. As the permeability is a most variable property of wood (Booker, 1990), a large range in the permeability values even for the same species can be found.

Table 4.2. The permeability of dry *Pinus radiata*

Author	Permeability to liquid, 10^{-18} m^2 (water resaturated)		Permeability to gas, 10^{-15} m^2			
	Sapwood		Sapwood		Heartwood	
	R.	T.	R.	T.	R.	T.
Booker* (1990)	540 ~4820 8000~46000	0.3~9.0 0.4~10	32~138		8.8~78.6	

* Note: Booker's data for permeability to gas were measured on oven-dry samples and it is likely that these values overestimate the permeability under drying conditions when the resin canals are less open.

Table 4.3. The permeability of green *Pinus radiata* sapwood

Author	Permeability to liquid, 10^{-18} m^2	
	R.	T.
Booker (1990)	30~168 18~144	189~326 169~774
Booker (1979)	38.7~114	217~281
Kininmonth (1991)	310~3800	2900

In Tables 4.2 and 4.3, R. stands for radial direction and T. represents tangential one.

Table 4.4 Wood permeabilities (Stanish *et al.* 1986)

Wood species	Permeability to liquid, 10^{-18} m^2	Permeability to gas, 10^{-15} m^2
Southern pine (*Pinus palustris* Mill,*Pinus eliottii* Engelm, etc.)	500	5
Pseudotsuga menziesii	500	1

Usually, the boards are sawn out in the direction parallel to the tree stem. In the drying of timber boards where the air sweeps over the long flat surfaces, nett moisture movement in the longitudinal direction is of minor consequence. Only radial and tangential

permeabilities are of interest as moisture is lost at right angles to the grain direction. Tables 4.2-4.4 give some data for the transverse permeabilities of *Pinus radiata* and other species of softwood.

Table 4.5. Species-dependent factors K_G^o and K_l^o (Perré,1988)

Timber species	Permeability to liquid, 10^{-18} m^2	Permeability to gas, 10^{-15} m^2
Maritime pine (a French species of pine)	1000 (in tangential direction)	0.08 (in tangential direction)
Spruce (*Picea*)	50 (in radial direction)	0.003 (in radial direction)

Table 4.6 Moisture-dependent factors k_v and k_l (Perré, 1988)

Moisture content range X, kg kg^{-1}	Permeability factor to liquid, k_l	Permeability factor to gas, k_v
0	0	1
$0 \sim X_{tr}$	$0.95\ (\frac{X}{X_{tr}})^2$	$0.95\ (1 - \frac{X}{X_{tr}})^2 + 0.05$
$X_{tr} \sim X_{sat}$	$0.95 + 0.05\ (\frac{X - X_{tr}}{X_{sat} - X_{tr}})$	$0.05\ (1 - \frac{X - X_{tr}}{X_{sat} - X_{tr}})$

In table 4.6, X_{tr}: transitional moisture content;

X_{sat}: moisture content at saturation estimated.

Perré (1988) gives some equations to correlate permeabilities. He splits the permeability into a constant part which is dependent only on the species and a variable part which depends on the moisture content. His equations are:

$$K_G = K_G^o\, k_G \tag{4.25}$$

$$K_l = K_l^o\, k_l \tag{4.26}$$

where K_G^o and K_l^o are the species-dependent factors for vapour and liquid flow respectively and k_G and k_l are the corresponding moisture-dependent terms. Some values of these factors are shown in Table 4.5 and 4.6. These values are for sapwood but extreme difficulties in measuring permeabilities in heartwood mean that values for heartwood are generally not available.

The transitional moisture content X_{tr} in Table 4.6 is a fitted value from Perré's drying test (Perré, 1988) with blocks of maritime pine sapwood, and is claimed to depend upon the degree of overlaping of the tracheids.

Perré (1988) gives the value of X_{sat} in Table 4.6 to be 1.33 kg kg^{-1} based on physical properties of Northern hemisphere coniferous sapwoods (Comstock and Cote, 1968). For *Pinus radiata*, a higher value may be estimated from a lower basic density and a higher cell-wall density of this species.

4.3.2 The Permeability in a Board

From the data for wood permeability measured by Booker (1990) and Kininmonth (1991) and those fitted results of Stanish *et al.* (1986) and Perré (1988), it can be seen that the values of permeability in tangential direction are significantly different from that in radial direction. Therefore, when a board is sawn in such a way that the growth rings are not parallel to the drying surface, the moisture moves at different rates in the radial and tangential directions towards the surface. If the ease of moisture movement is reflected by an effective normal permeability in this case, then this permeability may be related to both radial and tangential ones.

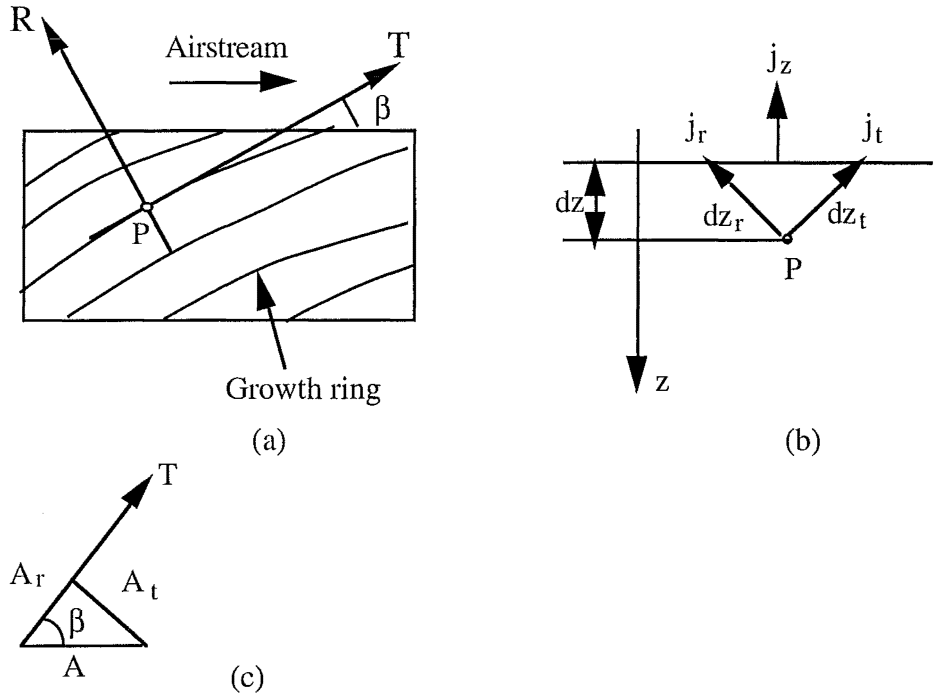

Figure 4.7. A board sawn with an angle between growth rings and airflow direction.
(a). the end view of a board sample; (b). the directions of moisture flow;
(c). the ares which the moisture flows through.

Suppose that the board is sawn out as shown in Figure 4.7a. The growth ring at point P has an angle of β to the airflow direction. A small element is taken out on which the cross-sectional area parallel to air flow is supposed to be A which the moisture flows through in direction normal to airstream (Figure 4.7c). The corresponding areas normal to radial and tangential directions are A_r and A_t respectively. The total flow rate of liquid or gas within board towards the surface, Q_z, is the sum of those in radial direction, Q_r, and tangential direction, Q_t:

$$Q_z = Q_r + Q_t \tag{4.27}$$

The flux in this direction is

$$j_{wz} = \frac{Q_z}{A} = \frac{1}{A}(Q_r + Q_t) \tag{4.28}$$

Since the fluxes in radial direction, j_{wr}, and tangential direction, j_{wt}, can be related to radial and tangential permeabilities and the flow rate can be calculated from the corresponding fluxes, it is found that

$$j_{wr} = E_r \frac{dp}{dz_r} \tag{4.29}$$

$$j_{wt} = E_t \frac{dp}{dz_t} \tag{4.30}$$

and $Q_r = j_{wr} A_r$ (4.31)

$$Q_t = j_{wt} A_t \tag{4.32}$$

From the geometric relationships in Figures 4.7b and 4.7c, it is known that

$$A_r = A\ cos\beta \tag{4.33}$$

$$A_t = A\ sin\beta \tag{4.34}$$

and

$$dz_r = \frac{dz}{cos\beta} \tag{4.35}$$

$$dz_t = \frac{dz}{sin\beta} \tag{4.36}$$

The effective permeability of liquid or gas flows in the direction normal to the surface is defined as:

$$E_z = \frac{j w_z}{dp/dz} \tag{4.37}$$

On introducing equations (4.28) to (4.36) into equation (4.37), one may obtain the effective permeability in the direction at right angle to board surface. It is related to the permeabilities of radial and tangential directions as follows:

$$E_z = E_r \cos^2\beta + E_t \sin^2\beta \tag{4.38}$$

Since the effective permeabilities E_i and normal measured permeabilities K_i are related directly by

$$E_i = \frac{\rho}{\mu} K_i \tag{4.39}$$

the normal measured permeability at right angle to board surface is related to those in radial and tangential directions with the same function form:

$$K_z = K_r \cos^2\beta + K_t \sin^2\beta \tag{4.40}$$

With flat-sawn timber, $\beta = 0$, so $K_z = K_r$ while for quarter-sawn, $\beta = 90°$, $K_z = K_t$.

Suppose that the radial permeability of *Pinus radiata* sapwood is 65×10^{-18} m^2 and the tangential permeability is 410×10^{-18} m^2 (Booker, 1991), the permeability in the direction normal to board surface are given in Table 4.7, which shows how the sawn angle to air flow direction affects the values.

Table 4.7. The variations of permeability normal to board surface with sawn angle to airflow ($K_r = 65 \times 10^{-18}$ m^2, $K_t = 410 \times 10^{-18}$ m^2)

β	0°	15°	30°	45°	60°	75°	90°
K_z, 10^{-18} m^2	65	88	151	238	324	387	410

Since the permeability is so variable and is affected by many factors, it needs to be adjusted within the measured range so that we can get a close match between the experimental results and predictions for temperature profiles.

4.4 The Fibre Saturation Point (X_{FSP})

The *fibre saturation point*, X_{FSP}, was first defined by Tiemann (1906) as the moisture content of wood at which the cell walls are saturated with bound water but no liquid water remains in capillary voids. He noted in his studies on the effect of moisture content on the strength properties of wood that below X_{FSP} the mechanical properties of wood (such as strength, Young's modules) increased with decreasing moisture content, but above this point these properties were independent of moisture content. Stamm (1964) extended this latter observation and interpreted X_{FSP} as the moisture content corresponding to the point where abrupt changes occur in physical properties of wood such as shrinkage, mechanical strength, electrical conductivity, and heat of wetting with changing moisture content.

Based on these two kinds of definition of fibre saturation point, some methods have been developed to determine the values of X_{FSP} for different species of wood. Stamm (1971) reviewed nine of them and concluded (1964, 1971) that for most species of wood the values of X_{FSP} range from 24% to 31% with most of them between 27% and 31%. The X_{FSP} should be corrected for different temperature on the basis of a decrease of 0.1% for each 1°C increase. For convenience, the value of 30% is assumed for North American woods at 20°C (Siau, 1984, Stamm and Nelson, 1961). Therefore a correlation can be proposed to calculate X_{FSP} at different temperatures (Siau, 1984) as follows:

$$X_{FSP} = 0.3 - 0.001\,(T - 293.15) \qquad (4.40)$$

Stamm recognised that X_{FSP} cannot be defined as the equilibrium moisture content corresponding to 100% relative humidity since such an equilibrium moisture content would result in total saturation of wood. It must be recognised that values of equilibrium moisture content given in a sorption isotherm above 98% relative humidity in fact only represent the extrapolation of values measured lower relative humidities.

4.5 Wood Basic Density

Wood *basic density* is a measure of the mass of dry wood substance per unit volume of green timber. As it is derived from the oven-dry weight and is independent of moisture content and shrinkage, the basic density is commonly used as a basis for comparison, to predict other density-related properties. Here in the proposed mathematical model, the basic density is used to avoid the complication since it is constant as the wood dries out. The other two densities, which are occasionally used, are *air-dry density* and *green density*. The air-dry density is measured with the timber moisture content in equilibrium with a standard atmosphere. For *Pinus radiata*, the standard atmosphere of 20°C, 65% relative humidity gives an equilibrium moisture content of approximately 12%. This density is of value for assessing the density of wood in use. The green density is the value for a freshly felled log and is of importance for estimating log volumes from weighbridge data. However, for *Pinus radiata*, in which the heartwood is significantly drier than sapwood, the green density decreases with tree age (as the proportion of heartwood increases) and so increases with the height in the tree.

Cown and McConchie (1983) have surveyed the studies undertaken between 1977 and 1982 in New Zealand on the *Pinus radiata* wood properties, and have presented complete data for the wood basic density.

4.5.1 Density Pattern

Cown and McConchie (1980) have examined ten 52-year-old trees in considerable detail and have proposed a pattern of variations in wood basic density (Figure 4.8). Within a tree, the basic density increases from centre of the stem outwards in all the height (e.g., from 386 kg m^{-3} to 480 kg m^{-3} at breast height). The cross-sectional mean density decreases with increasing height in the tree (e.g., from 438 kg m^{-3} at the base to 367 kg m^{-3} at a height corresponding to a stem with 10-rings). The overall mean average basic density for all the trees investigated is 420 kg m^{-3} (from 370 kg m^{-3} to 462 kg m^{-3}) while for the sawn timber, the mean basic density is 380 kg m^{-3}, ranging from 339 kg m^{-3} to 419 kg m^{-3}.

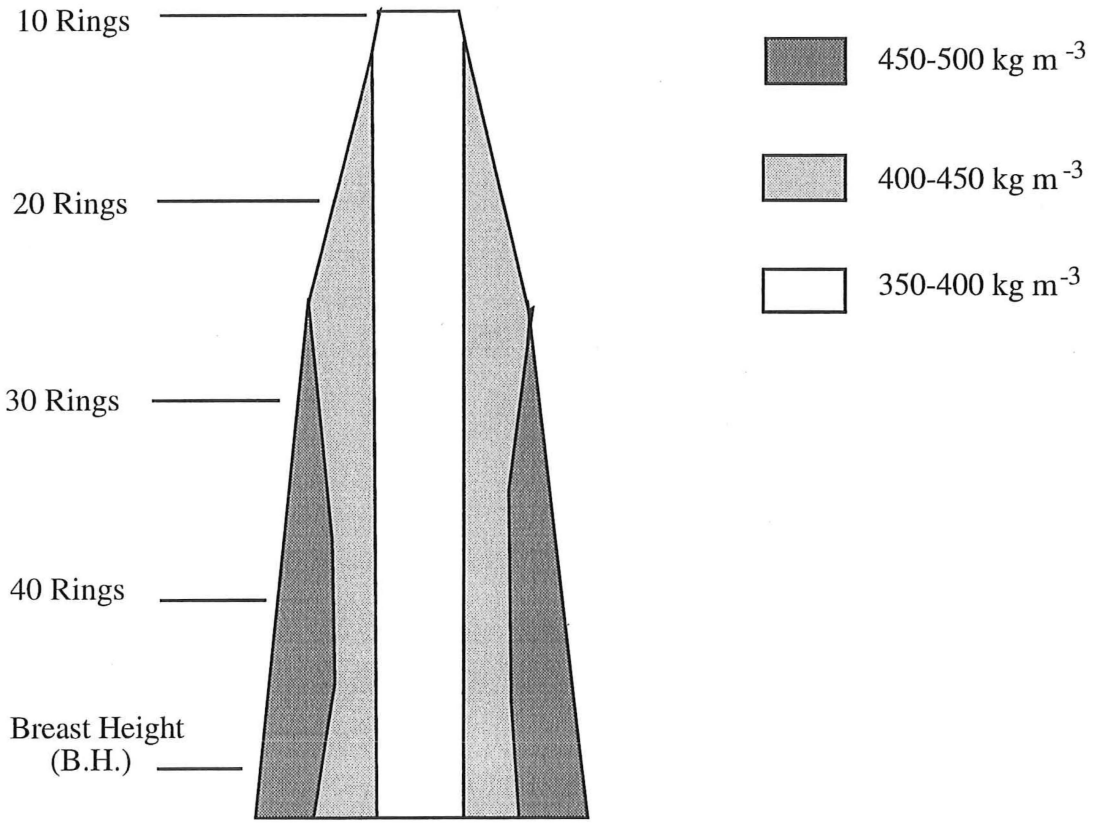

Figure 4.8. Mean within-tree basic density distribution (after Cown and McConchie, 1980).

4.5.2 Density variations with age and site

The above pattern of wood basic density applies to all the trees, but the values may vary with the age and the site where the tree grows. In New Zealand, the basic density of corewood (1-10 rings) varies from 360 kg m^{-3} in Southland and Canterbury regions to 405 kg m^{-3} in Auckland; and that of outerwood (21-25 rings) from 430 kg m^{-3} to 505 kg m^{-3}, with the same trend of increasing wood density on moving north. This variation leads the researchers to classify sites by three density zones using the outerwood values. Much of the South Island (apart from ares in Marlborough and Nelson) and Wellington region are in the low-density zone (<450 kg m^{-3}) while the northern part of North Island is the high-density zone (>475 kg m^{-3}) and the remaining areas form the medium-density zone (450-475 kg m^{-3}). In the same density zone, the density increases with age of the tree; for example, the sawn timber density varies from 350 kg m^{-3} in a 15-year-old tree to 400 kg m^{-3} for a 45-year-old tree in the low-density zone, while the density in the high-density zone and the medium-density zone yield the same tendency with values 30 and 15 kg m^{-3} higher.

Apart from the site and age, the growth rate and the orientation in earlywood or latewood may also contribute to the density variations. However, these influences are weakly and largely unpredictably related in populations of trees of the same age and same site (Kininmonth and Whitehouse, 1991), and no generalisation can be made.

4.6. The Green Moisture Content of Wood

The *green moisture content* (dry basis) of wood varies considerably among the species of trees, between heartwood and sapwood in the same tree, and even between logs cut from different height in the tree. In some cases, there may be seasonal variations in green moisture content (Skaar, 1987). Peck (1953) has reported the average green moisture content of sapwood and heartwood of 27 softwoods native to the United States. The value for conifer sapwood is 148.9%, ranging from 98% to 249%. This is almost three times higher than that for heartwood which has a mean value of 55.4%, ranging from 30% to 121%. Henderson and Choong (1968) have observed the mean moisture content variations from the trees felled at different seasons. However, Peck (1953) argues that the seasonal variation in tree moisture content is small and inconsistent in most species.

New Zealand *Pinus radiata* is characterised by a wide sapwood zone with high sapwood moisture content. Cown and McConchie (1980) have measured the average moisture content from the ten 52-year-old trees and have found that the moisture content of sapwood tended to increase somewhat from 135% in the lower half of the stem to 180% at a height corresponding to a stem with 10-rings. Figure 5.9 shows the radial distribution of green moisture content in 52-year-old radiata pine stem at different heights. The green moisture content in heartwood, however, was virtually constant at 40%. The green moisture contents for both sapwood and heartwood may be different among trees of different ages. For example, Booker and Langrish (1993) report an average green moisture content of 180% with fluctuation of ± 40% for the samples from trees between 7 and 28-year-old, and Kininmonth and Whitehouse (1991) give an average value for heartwood of 45%, ranging from 40% to 50%. Pang (1992) measured the green moisture content both for sapwood and heartwood of a 30-year-old crop from Kaingaroa Forest while he was conducting the drying tests at NZFRI. It was found the green moisture content of heartwood ranged from 34.7% to 38% and that of sapwood fell in a range of 116.4% and 139.2%. Theses values are comparably lower than those reported elsewhere in the literature. This may be due to the fact that the measurement was carried out two days after the boards were sawn out from the freshly felled log.

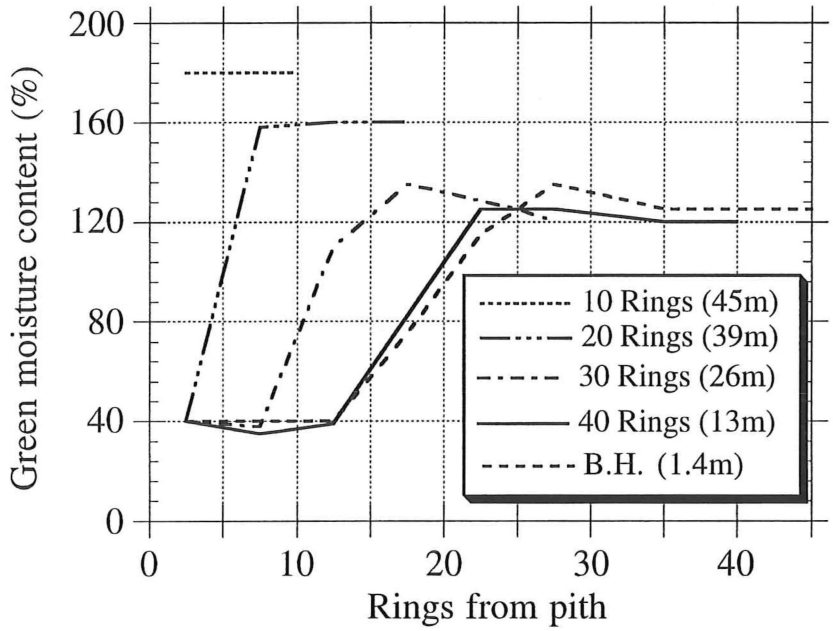

Figure 4.9. Radial moisture content distribution (after Cown and McConchie, 1980).

Since the green moisture content of heartwood is significantly different from that of sapwood, the mean whole tree's moisture content will be strongly dependent on the proportion of heartwood in a tree. Cown and McConchie (1983) report in their survey that there exists a very close relationship between the total number of growth rings and the average number of heartwood rings at breast height, This relationship may be used to evaluate the effect of age. Generally, *Pinus radiata* in New Zealand starts to form heartwood at between 12 and 14 years at the rate of about one half of a ring per annum in North Island, and a slightly slower rate in the South Island. However, this regional difference may be negligible with the anticipated rotation age for commercial *Pinus radiata* crops (25-35 years).

4.7 Notation

a constant in equations (4.23) and (4.24)

A sectional area parallel to air flow of en element, m^2

A_1, A_2, A_3 coefficients in equations (4,1d, 4.1e and 4.1f)

b constant in equation (4.24)

E effective permeability operated, s^{-1}

ΔG free energy change, kJ kg^{-1}

H_w enthalpy of bound moisture, kg mol^{-1}

H_w^o enthalpy of free moisture, kg mol^{-1}

ΔH_w differential heat of sorption kJ kg^{-1}

j_w moisture flux, kg m^{-1} s^{-1}

K wood permeability, m^2

K_1, K_2 coefficients in equations (4.1 and 4.2)

K_G^o species-dependent wood permeability to gas flow, m^2

K_L^o species-dependent wood permeability to liquid flow, m^2

k_G moisture-content correction factor for gas permeability

k_l moisture-content correction factor for liquid permeability

M_w molar weight of water vapour, kg mol^{-1}

p^v partial pressure of water vapour, P_a

p_S^v saturation partial pressure of water vapour, P_a

Q moisture flow rate, kg s^{-1}

R universal gas constant, 8.314 J $mol^{-1}K^{-1}$

T temperature, K

T_F temperature, °F

U factor in equation (4.9)

W factor in equations (4.1) and (4.2)

X moisture content of wood (dry basis), kg kg^{-1}

X_e equilibrium moisture content, kg kg^{-1}

X_{FSP} moisture content at fibre saturation point, kg kg^{-1}

X_{sat} moisture content at saturation, kg kg^{-1}

X_{tr} transition moisture content, kg kg^{-1}

Z_1, Z_2 factors in equations (4.8) to (4.21)

Greek

β ring angle to air flow direction

ψ relative humidity,--

Subscript

r radial direction

t tangential direction

z direction normal to air flow

$1,2$ two different conditions of temperature and relative humidity

4.8 References

1. Booker, R.E. 1979. A comparison of the Radial, Tangential and Axial Permeabilities of Two Radiata Pine. New Zealand Forest Service, Forest Research Institute, Timber Drying Report No.39 (unpublished).

2. Booker, R.E. 1990. Changes in transverse wood permeability during the drying of *Dacrydium cupressinum* and *Pinus radiata*. *New Zealand J. of Forestry Science*, 20(2) pp231-244.

3. Booker, R.E. 1991. Changes in Transverse Wood Permeability during the Drying of Rimu and Radiata Pine. paper presented at the 21st Annual Meeting of the Forest Research Institute, Rotorua, New Zealand.

4. Booker, R.E. and Langrish, T.A.G. 1993. The Percentage Saturation of Sapwood and Heartwood from *Pinus radiata* on the Central Plateau of New Zealand. submitted to *J. of Experimental Botany*.

5. Cown, D.J. and McConchie, D.L. 1980. Wood Property Variations in an Old-Crop Stand of Radiata Pine. *New Zealand J. of Forest Science*, 10(3) pp508-520.

6. Cown, D.J.and McConchie, D.L. 1983. Radiata Pine Wood Properties Survey (1977-1982). New Zealand Forest Research Institute Bullentin No.50. Rotorua, New Zealand (unpublished).

7. Cunningham, M. J., and Sprott, T. J. 1984. Sorption Properties of New Zealand Building Materials. Research Report, R43, Building Research Association of New Zealand (unpublished).

8. Forest Products Laboratory (USA). 1987. "*Handbook of Wood and Wood-Based Materials for Engineers, Architects, and Builders*". Hemisphere Publishing Co., New York.

9. Hailwood, A.J. and Horrobin, S. 1946. Absorption of Water by Polymers: Analysis in Terms of a Simple Model. *Trans. Faraday Soc.* 42B, pp84-102.

10. Keey, R. B. 1978. "*Introduction to Industrial Drying Operations*". Pergamon, Oxford.

11. Kelsey, K.E. and Clarke, L.N. 1956. The Heat of Sorption of Water by Wood. *Australian Journal of Applied Science,* 7 (2), pp160-175.

12. Kininmonth, J.A. and Whitehouse, L.J. 1991. "*Properties and Uses of New Zealand Radiata Pine: Volume 1-Wood Properties*". New Zealand Ministry of Forestry, New Zealand Forest Research Institute, Rotorua, New Zealand.

13. Noack, D., Schwab, E. and Bartz, A. 1973. Characteristics for a Judgment of the Sorption and Swelling Behaviour of Wood. *Wood Sci. Technol.* 7, pp218-236.

14. Pang Shusheng, Keey, R.B. and Langrish, T.A.G., 1992a. Modelling of Temperature Profiles within Boards during the High-Temperature Drying of *Pinus radiata* Timber. in Mujumdar, A.S.(ed.): *Drying'92*. Elsevier, Part A: pp417-433.

15. Pang Shusheng, Keey, R.B., Walker, J.C.F. and Langrish, T.A.G. 1992b. The Stress Development and Check Formation within Boards of *Pinus radiata* during

High-Temperature Drying. Research Report No.3. Department of Chemical and Process Engineering, University of Canterbury, Christchurch, New Zealand (Unpublished).

16. Pang Shusheng. 1992c. Temperature and Moisture-Content Profiles within a Board during High-Temperature Drying of *Pinus radiata*: Experimental Results and Comparison with Mathematical Model. Research Report to NZRFI. Department of Chemical and Process Engineering, University of Canterbury, Christchurch, New Zealand (unpublished).

17. Pang Shusheng, Langrish, T.A.G. and Keey, R.B. 1993. The Heat of Sorption of Timber. *Drying Technology,* 11(5), pp1071-1080.

18. Perré, P., Fohr, J.R. and Arnaud, G. 1988. A Model Applied to Softwoods: the Effect of Gaseous Pressure below the Boiling Point. *Proc. of 6th International Drying Symposium, Drying'88*, Versailles, pp279 - 286.

19. Rasmussen, E.F. 1961. "*Dry Kiln Operator's Manual*". U.S. Dept. Agric., Agric. Handbook 188. Washington, D.C.

20. Rees, W.H. 1948. Heat of absorption of water by cellulose, *J. Text. Inst.* 39(11), pp351-367.

21. Rosen, H. N. 1987. Recent Advances in the Drying of Solid Wood, in Mujumdar, A. S. (ed.): *Advances in Drying*, Vol.4, Hemisphere Publishing Co., New York.

22. Siau, J.F. 1984. "*Transport Process in Wood*". Springer-Verlag, Berlin.

23. Simpson, W.T. and Rosen, H.N. 1981. Equilibrium Moisture Content of Wood at High Temperatures. *Wood Fibre* 13(3), pp150-158.

24. Simpson, W. T. 1971. Equilibrium Moisture Content Prediction for Wood, *Forest Products J.*, 21(5), pp48-49.

25. Simpson, W. T. 1973. Predicting Equilibrium Moisture Content of Wood by Mathematical Models. *Wood and Fibre*, 5(1), pp41-49.

26. Skaar, C. 1988. "*Wood-water relations*". Springer-Verlag, Berlin.

27. Smith, J.M.; Van Ness, H.C. 1975. "*Introduction to Chemical Engineering Thermodynamics*". 3rd ed., McGraw Hill, New York.

28. Stamm, A.J.; Loughborough, W.K. 1935. Thermodynamics of the Swelling of Wood. *J. Phys. Chem.* 39, pp121-132.

29. Stamm, A.J. 1964. "*Wood and Cellulose Science*". Ronald, New York.

30. Stamm, A.J. 1971. Review of Nine Methods for Determining the Fibre Saturation Point of Wood and Wood Products. *Wood Science*, Vol.4, pp114-128.

31. Stanish, M.A., Schajer, G.S., and Kayihan F. 1986. A Mathematical Model of Drying for Hygroscopic Porous Media. *AIChE.J.* 32(8), pp1301-131.

32. Tiemann, H.D. 1906. Effect of Moisture upon Strength and Stiffness of wood. USDA For. Serv. Bull. 70.

33. U.S. Forest Products Laboratory. 1974. "*Wood Handbook*". USDA, Agric. Handbook 72. (Revised), For. Prod. Lab., Wisconsin.

Chapter **5**

Transfer Process in the Airstream and Physical Properties of Moist Air and Vapour

In the high-temperature drying of softwood, as drying rates increase dramatically the external heat- and mass-transfer processes play a more important role in drying than these do at low temperatures. The air flow and the mass-transfer process through arrays of timber boards as encountered in a kiln have been investigated by Keey and his colleagues (Kho *et al.*, 1989; Lee, 1990; Langrish, *et al.*, 1993). This chapter will briefly review their results following a description of the fundamentals of the external transfer process. Also, some physical properties of air and water vapour used in the proposed model will be discussed.

5.1 Fluid Flow, Heat- and Mass-Transfer Over A Sharp Edged Flat Plate

5.1.1 Fluid Flow and Transport Processes Over A Flat Plate

The fluid flow over a sharp-edged flat plate (Figure 5.1) is a topic which variety of papers and books have discussed (Massey, 1983; Schlichting, 1960). Here it is repeated for comparison with the flow over the truncated slabs, as encounted in a drying kiln. In Figure 5.1, just before the fluid contacts the plate, the flow is streamline, all of the fluid moving parallel to each other. This type of flow is called *laminar flow*. As soon as it flows over the plate, a very thin layer forms adjacent to the plate surface in which the fluid's velocity changes from zero right at the surface to almost 99% of the free-stream velocity. This thin layer close to the plate surface is known as the *boundary layer* (AB in Figure 5.1). Since the flow is retarded, disturbances in the layer are difficult to develop, and the flow is laminar. With the fluid moving further along the plate, the thickness of the boundary layer increases rapidly, and the boundary layer becomes turbulent (CD). However, beneath this turbulent boundary layer there still exists a thinner layer close to the solid surface (EF). This thinner layer is termed the *laminar sublayer* in which the flow is laminar.

The picture of fluid flow is relevant to heat- and mass-transfer through the fluid stream as most of the resistances both to heat and mass transport occur in the boundary layer, while in turbulent flow the laminar sublayer is predominant. Wherever there is temperature or concentration difference between fluid in main stream and that immediately above the solid surface, the heat or mass will be transferred through the fluid. For example, when the temperature and mass concentration at the plate surface are higher than those in the main stream, the heat is firstly transferred through the laminar layer mainly by conduction while the mass moves mainly by diffusion. Then the heat and mass are transferred through the main stream. If the flow in the whole section is laminar, the transfer rates both for heat and for mass are low as the resistances in boundary layer are great. In the turbulent region, on the other hand, these transport rates increase significantly due to the irregular motion of the fluid. The turbulent flow is characterized by the irregular velocity-fluctuations superimposed on the main stream. These rapid fluctuations, or eddies, carry entities of fluid, with their associated momentum, energy, and mass, from position to position and mix them with others, in an irregular manner. This increases the transport rates many times over those by conduction or diffusion in laminar flow.

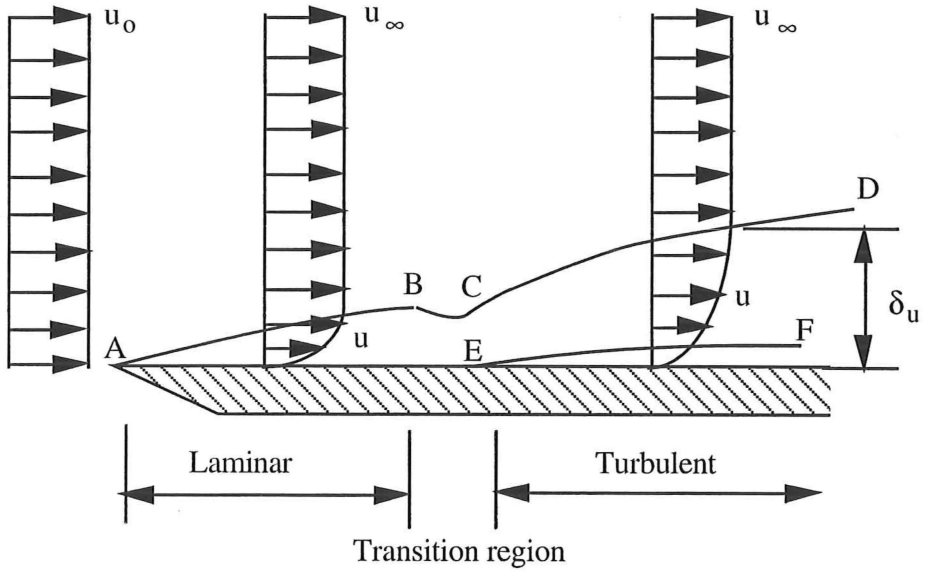

Figure 5.1 The fluid flowing over a sharp edged flat plate.

For both the laminar and turbulent flows, the heat- and mass-transfer processes at any point may be expressed in a general way:

$$q = -(k + E_H \rho C_P)\frac{dT}{dz} \tag{5.1}$$

$$N_A = -(D_{AB} + E_D)\frac{dc_A}{dz} \tag{5.2}$$

in which q and N_A are the heat- and mass-transfer rates, k and D_{AB} are thermal conductivity and molecular diffusivity of the fluid respectively while $E_H \rho C_P$ and E_D represent the transport properties associated with turbulence.

Since in turbulent flow both the thickness of the boundary layer and that of the laminar sublayer are difficult to calculate, and the domination of these layers are not yet fully understood, in practice, some simplifications have been made, one of which is the film theory (Treybal, 1968). This theory assumes that for both laminar and turbulent flows there is a film close to the solid surface in which all of the temperature or concentration gradient occurs, whereas in the main stream, the velocity, concentration and temperature are uniform and no further net transport occurs (Figure 5.2). The heat is transferred in this film by thermal conductivity and mass by diffusivity. Integrating equations (5.1) and (5.2) over the heat transfer film δ_T and mass transfer film δ_c respectively yields:

$$q = -\frac{k}{\delta_T}(T_I - T_\infty) = -h\,(T_I - T_\infty) \tag{5.3}$$

$$N_A = -\frac{D_{AB}}{\delta_c}(c_{AI} - c_{A\infty}) = -K_c\,(c_{AI} - c_{A\infty}) \tag{5.4}$$

where h is the heat-transfer coefficient and K_c is the mass-transfer coefficient based on molar concentration. Equations (5.3) and (5.4) enable the transfer process to be computed. However, in most cases, the coefficients need to be determined experimentally.

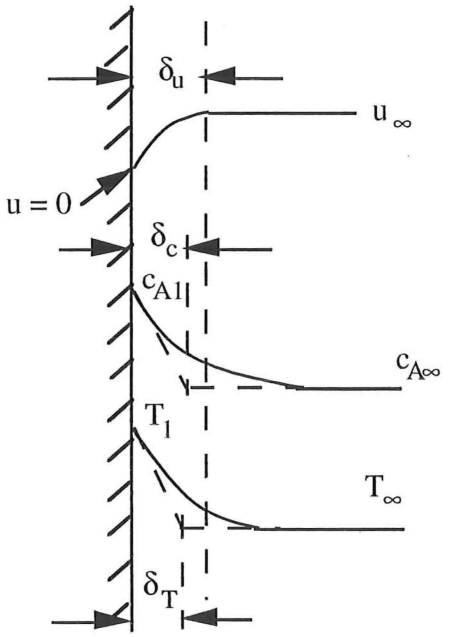

Figure 5.2 The fluid-dynamic, thermal and concentration films.

The heat- and mass-transfer coefficients may be obtained by employing the analogies among momentum, heat, and mass transport (Colburn, 1933; Chilton and Colburn, 1934). For example, where a laminar boundary layer is developing across a plate, the mass-transfer coefficient can be calculated (Schlichting, 1960; Langrish *et. al.*, 1993) by the expression

$$Sh_x = 0.332\ Re_x^{1/2}\ Sc^{1/3} \tag{5.5}$$

where $Sc = \nu/D_{AB}$ is the Schmidt number;
$Re_x = (u\ x)/\nu$ is the local Reynolds number based on the swept length x;
$Sh_x = (K_c\ x)/D_{AB}$ is the local Sherwood number;
K_c is the local mass-transfer coefficient;
ν is the kinematic viscosity of fluid;
x is the distance from the leading edge of the plate;
u is the bulk velocity of the main stream;
D_{AB} is the diffusivity of the fluid.

Whenever the boundary over the plate is turbulent, the following equation may be used (Langrish *et al.*, 1993) :

$$Sh_x = 0.0288\ Re_x^{4/5}\ Sc^{1/3} \tag{5.6}$$

5.1.2 Chilton-Colburn Analogy

Since there are similarities among momentum, heat and mass transport processes, these processes can be interrelated through the analogies, the simplest form of which is that suggested by Chilton and Colburn, *Chilton-Colburn analogy*. In this analogy, the three types of transfer processes are related to each other as:

$$j_H = j_D = \frac{C_f}{2} \tag{5.7}$$

where j_H, j_D are heat and mass transfer factors and C_f is the skin friction coefficient. These factors are defined by

$$j_H = St_T\ Pr^{2/3} \tag{5.8}$$
$$j_D = St_c\ Sc^{2/3} \tag{5.9}$$

$$C_f = \frac{2\tau_w}{\rho u^2} \tag{5.10}$$

In this way, the heat- and mass- transfer coefficients may be related to each other as:

$$K_c = \frac{h}{\rho C_p}\left(\frac{Pr}{Sc}\right)^{2/3} \tag{5.11}$$

For the water vapour-air system, by converting the mass-transfer coefficient based on the molar concentration into that based on differences in air humidity difference, *humidity potential*, equation (5.11) can be reduced to (Keey, 1978):

$$K_o = h\,\sigma/C_{PY} \tag{5.12}$$

Where σ is the *psychrometric coefficient* and C_{py} is humid specific heat. Keey has examined the variation of psychrometric coefficient with factors such as a humidity, substances of the system involved *etc.*. For the water vapour-air system he concluded that the value of psychrometric coefficient can be taken to be unity. The significance of equation (5.12) is that one of the two transfer coefficients can be calculated from the other. The local mass transfer coefficient is relatively easier of the two coefficients to measure in the arrays of timber stacks, so the heat transfer coefficient is usually derived.

5.1.3 Conversion of Mass Transfer Coefficients for Water Vapour-Air System

Fick's first law of diffusion may be applied to calculate the diffusion rate when water vapour escapes from a wet surface and diffuses in the bulk air stream. Assuming the physical properties and diffusion coefficient are uniform in the boundary layer and the air movement normal to the plate surface is negligible, the integrated form of Fick's first law is obtained as follows

$$N_A = \frac{D_{AB}\,c}{\delta}\ ln\left[\frac{c - c_{A\infty}}{c - c_{A\,I}}\right] \tag{5.13}$$

Where N_A is the diffusion rate of water vapour designated by A;
D_{AB} is the diffusivity of water vapour in the air represented by B;
c is the total molar concentration;
δ is the thickness of concentration boundary layer;
$c_{A\infty}$ is the vapour concentration in the main stream;

c_{AI} is the vapour concentration adjacent the wet surface.

Equation (5.13) can be directly used to estimate evaporation rates in laminar flow since the mechanism of the molecular diffusion is well known and can be described in terms of kinetic theory to give results which agree well with experimental data (Treybal, 1969). However, the flow process involving the momentum of eddies in the turbulent region is not so thoroughly known and hence cannot be so described. Therefore, the term $D_{AB}\, c/\delta$ in equation (5.13) is replaced by F, a *mass-transfer coefficient*, in order to describe the rate of mass-transfer through a combination of laminar film and turbulent zone.

Table 5.1 Relations among mass-transfer coefficients.

Concentration	Transport of A through non-transferring B (kg s^{-1} m^{-2})	Units of coefficients
partial pressure (Pa)	$N_A = \beta\, \Delta p_A$	s m^{-1}
molar fraction (mol mol^{-1})	$N_A = K_y\, \Delta y_A$	mol s^{-1} m^{-2}
molar concentration (mol m^{-3})	$N_A = K_c\, \Delta c_A$	m s^{-1}
mass concentration, (humidity)	$N_A = K_o\, \phi \Delta Y_A$	kg s^{-1} m^{-2}
Conversion		
$M_A F = \beta p_{BM} = M_A K_y \frac{p_{BM}}{P_t} = M_A K_c \frac{p_{BM}}{RT} = K_o \frac{M_A}{M_B}$		

In practice, the film theory is widely used to calculate the overall transport rates, so we can relate the mass-transfer coefficient, K_c, based on the molar concentration difference in film theory with the originally defined mass-transfer coefficient, F, by combining equation (5.13) and equation (5.4), as follows:

$$F = \frac{p_{BM}}{RT} K_c \qquad (5.14)$$

where p_{BM} is the logarithmic mean partial pressure of component B, the air in water vapour-air system, which is defined as:

$$p_{BM} = \frac{p_{B\infty} - p_{BI}}{ln(p_{B\infty}/p_{BI})} \qquad (5.15)$$

Since the concentration may be defined in a number of ways and the standards have not been established, the coefficient corresponding to each definition can be related to each other. Table 5.1 gives four of them, which are commonly used in the gas system.

In principle, each concentration can be chosen as the driving force for the calculation of transport rate although the molar concentration is widely used. However, in some cases, use of certain concentration is restricted due to other considerations or physical reality. For example, the humidity concentration of the water vapour in air is infinitly close to a saturated interface at temperatures above 100°C under atmospher in pressure. In this case, the humidity concentration makes the calculation of transport rate impossible.

5.2 The Air Flow and External Transport Process Over Array of Timber Boards

5.2.1 The Flow Pattern

Lee (1990) has performed a series of experiments to visualise the flow over a layer of short boards in a wind tunnel. The boards were stacked in a similar way to that in a commercial kiln. The dimensions of the sample boards were 100 x 25 x 225 mm. In the tests, the air velocities used were 0.2, 0.4 and 0.6 m s^{-1} and the gaps between adjacent boards (board gap) were 3, 5 and 10 mm to give dynamic similarity with the flow over board side-gaps in a kiln. A significant feature of the air flow over the boards is that eddies periodically formed in the gaps. These eddies then moved upward, deformed and finally moved forward along the board in the airstream (Figure 5.3). The periods of oscillation for eddy formation and upwards movement was observed to be 0.5-10 s. This cycle period seems to decrease with increasing air velocity and decreasing gap distance. Another noticeable feature of the flow is that the eddies over the first front board are always present at a certain distance from the leading edge. The position for the eddies to form over the first front board is proportional to $Re_x^{-1/2}$, about 20 mm from the leading edge at air velocity of 3 to 7 m s^{-1}. This distance is significantly less than that for the turbulent transition region predicted for a sharp-edged flat plate (Kho *et al.*, 1989; Lee, 1990; Massey, 1970).

Since there is a dynamic similarity between the flow in this experiment and that in a kiln stack of boards, the eddy formation, deformation and movement can be expected to occur over the truncated boards encountered in the kilns in which the board side-gaps are narrower and the velocities are greater (board side-gap of 1 to 5 mm and air velocity of 3 to 7 m s^{-1}). These processes will certainly enhance the turbulence of the air flow, reducing the thickness of the boundary layer or laminar sublayer, hence increase the transfer rates.

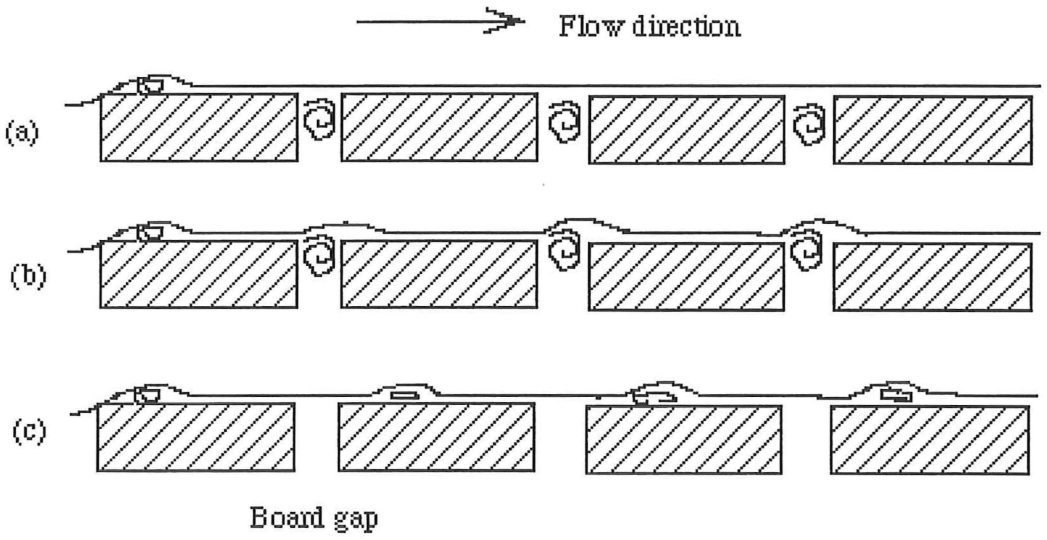

Figure 5.3 The visualized flow of air over a layer of timber boards. (after Lee, 1990)
(a). Generation of eddies in the board gaps and over the front board;
(b). Outward motion of the eddies in board gaps;
(c). Forward motion of the deformed eddies.

The air flow over arrays of timber boards has been numerically simulated by Langrish *et al.* (1993). In the simulation, the flow is considered as time-dependent and turbulent. In this way the Navier-Stokes equations are solved to give the flow pattern. The encouraging feature of the simulation is that the eddy formation and upward motion is predicted with oscillation period of 2 seconds for the air velocity of 0.6 m s^{-1} and with a gap of 10 mm between boards. This is in close agreement with the experimental observations. Also, in further simulations (Langrish, 1993) for an air velocity of 5 m s^{-1} and a 1 mm gap between boards, the oscillation period is predicted to be similar to the above experiments.

5.2.2 The External Transfer Coefficients

Local mass-transfer coefficients over a sample board in a stack within a pilot kiln have been experimentally measured by Kho Keey and Walker (1989, 1990). In the tests, a 100x25 mm truncated aluminium board coated with naphthalene was placed within a kiln stack, and the mass-transfer rate was determined by measuring the amount of sublimation from surface.The experiment was carried out at an air temperature of 41°C and air velocities of 3, 5 and 7 m s^{-1} respectively. The mass-transfer coefficient variations over the first three boards with distance from the leading edge of the first board are shown in Figure 5.4. From the measured mass-transfer coefficient profiles, some important features can be observed:

• The maximum mass-transfer coefficient occurs over the front of the first board 10-30 mm away from the leading edge. This is consistent with the presence of eddies above this board.
• The maximum values over successive boards occur at positions close to leading edges of each board, then reach an asymptotic value from 30-40 mm onwards. This phenomenon can again be explained by the influence of eddy formation, outward motion and forward movement. As the deformed eddies move along the board, they vanish into the airstream, hence the effect was diminished.
• From the second board on in the airstream direction, the coefficient profiles over each board are identical for a fixed air velocity, with higher values for higher air velocities.

In the experiments by Kho *et al.*(1989, 1990), the effects of minor board irregularities have also been investigated. The board gap of 5 mm was noticed to enhance the local mass-transfer coefficient about 20% over that for a 1 mm board gap. The influence of different heights of adjacent boards have been observed to change the local coefficients to varying extents. A lower leading board has a greater influence on the front portion of the sample board than that of a lower trailing board with the same height difference. Significant enhanced local mass-transfer coefficients for nearly the whole width of the sample board were measured when the sample aluminium board was lower than the adjacent ones.

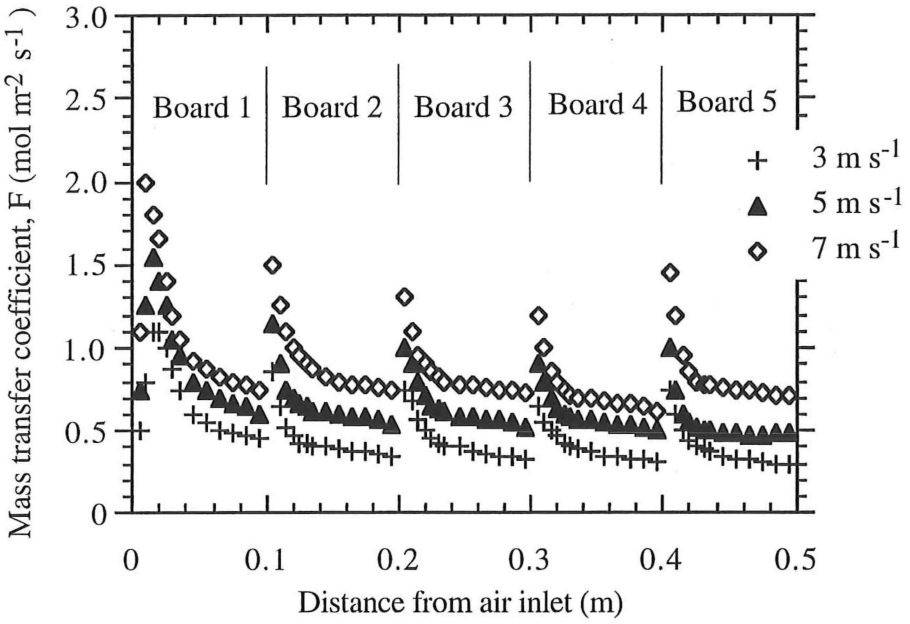

Figure 5.4 Local mass-transfer coefficient variation with distance from the leading edge for the first three boards with normal board gap of 1 mm and uniform board level. (From Kho, Keey and Walker, 1990)

When comparing the measured asymptotic mass-transfer coefficients with those predicted by the flat-plate correlations (equations 5.5 and 5.6), it is found that the turbulent correlation underpredicts the coefficient by 66% for air velocity of 3 m s^{-1}, 62% for 5 m s^{-1} and 82% for 7 m s^{-1} (Langrish *et al.*, 1993).

In the flow simulation performed by Langrish *et al.* (1993), the local mass-transfer coefficients have been predicted by using Chilton-Colburn analogy between skin friction and mass-transfer. The magnitude and variations of the calculated coefficients with distance are in reasonable agreement with experimental values, except that the enhancement at the leading edge of each board (especially over the first front board) are underpredicted, possibly because the treatment of the flow near the edge is oversimplified in the simulation.

An earlier experiment has been carried out by Stevens *et al.* (1956) to measure the external heat-transfer coefficient. They dried a very wet sample board in stack at dry-bulb temperature of 60°C and wet-bulb temperature of 50°C. The air velocities used veried from 0.46 m s^{-1} (1.5 ft s^{-1}) to 2.74 m s^{-1} (9 ft s^{-1}). By measuring the weight variations of the sample board, and on assuming that the board surface was at wet-bulb temperature,

the average heat-transfer coefficient was calculated and a correlation was suggested to predict heat-transfer coefficient at different air velocities:

$$h = 1.9 + 0.48\,u \qquad (5.16)$$

where h is heat-transfer coefficient (Btu ft^{-2} $°F^{-1}$ hr^{-1}) and u is the air velocity (ft s^{-1}).

On converting the British units into SI units, the above equation becomes:

$$h = 10.79 + 8.94\,u \qquad (5.17)$$

in which the units of h and u are W m^{-2} K^{-1} and m s^{-1}.

The heat-transfer coefficients calculated from this method are higher than those estimated from Chilton-Colburn analogy and the experimental data of Kho *et al.* (1989, 1990) at low temperatures. This is because that the heat-transfer coefficients from the analogy is a function of specific heat of humid air. The moist air at low temperatures has relatively lower values of specilic heat (due to lower values of humidity). However, at high temperatures where the humidity is high, these two methods are in agreement. For example, for air at dry-bulb temperature of 120°C and wet-bulb temperature of 70°C and with air velocity of 3 m s^{-1}, the heat-transfer coefficient from Stevens equation is 37.61 W m^{-2} K^{-1} while the value from the analogy and the experimental mass-transfer coefficient of 0.8 mol m^{-2} s^{-1} for the first front board is 35.52 W m^{-2} K^{-1}. The heat-transfer coefficients over succesive boards predicted from the analogy and measured mass-transfer coefficients are lower than this value (22.2 W m^{-2} K^{-1}).

5.3 Physical Properties of Water Vapour and Moist Air

5.3.1 Prediction of Humidity of the Air

The dampness of air is commonly represented by its fractional saturation or relative humidity ψ (Keey, 1978). The relative humidity is defined as the ratio of partial pressure of water vapour at a given condition to the saturated partial pressure at the same temperature.

Rosen and Simpson (1981) have compared two methods to calculate the relative humidity (*RH*) of the moist air by using adiabatic saturation temperature and wet-bulb temperature respectively. Their results show that the relative humidity based on the difference between dry-bulb and adiabatic saturation temperatures do not differ significantly from that based on the difference between dry-bulb and wet-bulb temperatures. The maximum difference for these two calculations is 0.54% (*RH*); on the average, the difference is ± 0.25% (*RH*). In this way, the adiabatic saturation temperature can be replaced by wet-bulb temperature without introducing significant error for timber drying to calculate humidity of the air (Rosen and Simpson, 1981):

$$Y_G = Y_{GS} - \frac{1.8(T_{GD} - T_{GW})\,(0.24 + 0.44\,Y_{GS})}{1351.4 + 0.792\,T_{GD} - 1.8\,T_{GW}} \tag{5.18}$$

where T_{GD} is the dry-bulb temperature (K);
T_{GW} is the wet-bulb temperature (K); and
Y_{GS} is the humidity of air when saturated with water vapour at the wet-bulb temperature, which may be estimated by following equation (Keey, 1978):

$$Y_{GS} = \frac{p_s^v}{1.61(P_t - p_s^v)} \tag{5.19}$$

In equation (5.19), P_t is the total pressure in the airstream. The saturation vapour partial pressure (p_s^v) at temperature T can be calculated by using fitted correlations from experimental data. For example, on using Yaw's suggestions (Kayihan, 1981), the partial pressure is estimated by

$$p_s^v = \frac{1.0133x10^5}{760}\,x10^{f(T)} \tag{5.20}$$

in which $f(T)$ is a function of temperature, T, which has a form as follows:

$$f(T) = 16.3737 - \frac{2818}{T} - 1.6908\ log_{10}(T) - 5.7546x10^{-3}\ T + 4.007x10^{-6}\ T^2 \qquad (5.21)$$

From the definition of relative humidity (Keey, 1978), we have:

$$\psi = \frac{p^v}{p_s^v} = \frac{1.61\ Y_G\ P_t}{(1 + 1.61\ Y_G)p_s^v} \qquad (5.22)$$

By using equations from (5.18) to (5.22), we can calculate saturation partial pressure at given temperatures, and calculate humidity and relative humidity when dry-bulb and wet-bulb temperatures are known.

5.3.2 Thermodynamic Relationships and Physical Properties of Air and Water Vapour

The thermodynamic relationships and physical properties of air and water vapour to be used in the proposed model are: the heat of vaporization of water, H_{wv}; specific heat of water vapour and that of air, C_{PV} and C_{PG} These parameters vary with temperature and pressure.

The heat of vaporization of liquid water can be correlated with temperature from the data in steam tables using the following polynomial (Stanish, 1986):

$$H_{wv} = 2.792x10^6 - 160\ T_G - 3.43\ T_G^2 \qquad (5.23)$$

When the moisture content is below the value for the fibre saturation point, some extra heat is needed to evaporate the bound water as some energy is needed to break the bond between water and wood substance. In this case, the heat of vaporization is the sum of heat for vaporization of liquid water and that for this extra energy. This extra heat is usually called the heat of sorpion. Different methods for calculating the heat of sorption of timber have been published in the literature (Skaar, 1980, Kelsey and Clarke, 1956, Smith and Van, 1975, Stamm and Loughborough, 1935). Pang, Langrish and Keey (1993) believe that the method of Skaar is the most reliable which can be expressed as a function of moisture content by

$$\Delta H_{wv} = 1.17x10^6\ exp(-14X) \qquad (5.24)$$

Therefore, the total heat for the vaporization of bound water is given by

$$H_{bv} = 2.792x10^{6} - 160\,T_G - 3.43\,T_G^2 + 1.17x10^{6}\,exp(-14X) \qquad (5.25)$$

The other parameters can also been fitted from data in the steam tables and gas tables (Perry, 1984):

$$C_{PV} = -247.5 + 22.20\,T_G - 8.043x10^{-2}\,T_G^2 + 9.990x10^{-5}\,T_G^3 \qquad (5.26)$$

$$C_{PG} = 1038.1 - 0.2388\,T_G + 4.599x10^{-4}\,T_G^2 \qquad (5.27)$$

Now all of the physical properties and parameters of wood, air and water vapour used in the model have been discussed. Therefore the proposed model can be solved by using the numerical technique given in chapter 3. The details of the results will be described in the following chapter.

5.4 Notation

C molar concentration, mol m^{-3}

C_f skin friction coefficient, -

C_{PG} specific heat of air, J kg^{-1} K^{-1}

C_{PV} specific heat of water vapour, J kg^{-1} K^{-1}

C_{PY} specific heat of moist air, J kg^{-1} K^{-1}

D_{AB} molecular diffusivity of component A in component B, m^2 s^{-1}

F the external mass-transfer coefficient based on the molar concentration, mol m^{-2} s^{-1}

h heat transfer coefficient, W m^{-2} K^{-1}

H_{bv} heat of vaporization of bound water, J kg^{-1}

H_{wv} heat of vaporization of liquid water, J kg^{-1}

j_D mass transfer factor, -

j_H heat transfer factor, -

k thermal conductivity, W m^{-1} K^{-1}

K_c mass-transfer coefficient based on molar concentration, m s^{-1}

K_o mass-transfer coefficient based on humidity potential, kg m^{-2} s^{-1}

K_y mass-transfer coefficient based on molar fraction, kg m^{-2} s^{-1}

M_A molar weight of component A, kg mol^{-1}

M_B molar weight of component B, kg mol^{-1}

N_A mass transfer rate, kg m^{-2} s^{-1} (or mol m^{-2} s^{-1})

p pressure, Pa

R universal gas constant, 8.314 J mol^{-1} K^{-1}

q heat transfer rate, W m^{-2}

T temperature, K

u air velocity, m s^{-1}

x distance along air stream, m

Y humidity of moist air, kg kg^{-1}

y molar fraction, mol mol^{-1}

z distance normal to the plate surface, m.

Greek

β mass-transfer coefficient based on partial pressure, s m^{-1}

δ boundary thickness, m

ϕ humidity potential coefficient, -

μ dynamic viscosity, kg m^{-1} s^{-1}

ν kinematic viscosity, m^2 s^{-1}

ρ density, kg m^{-3}

σ psychrometric coefficient, -

τ_w wall shear stress, N m^{-2}

ψ relative humidity, -

Superscript

v vapour

Subscript

1 parameters at wall

∞ parameters in the main stream

A component A

B component B

G gas

GD dry-bulb

GW wet-bulb

s saturation

t total

Dimensionless numbers

P_r Prantl number, $P_r = (C_P \mu)/k$

R_{ex} local Reynolds number, $R_{ex} = (x\, u/\nu)$

S_c Schmidt number, $S_c = \nu/D$

Sh_x local Sherwood number, $Sh_x = (K_c x)/D$

S_{tT} Stanton number (heat transfer), $S_{tT} = h/(C_P\, u\, \rho)$

S_{tc} Stanton number (mass transfer), $S_{tc} = K_c/u$

5.5 References

1. Chilton, T.H. and Colburn, A.P. 1934. Mass Transfer Coefficients: Prediction from Data on Heat Transfer and Fluid Friction. *Ind. Eng. Chem.*, 26(11), pp1183-1187.

2. Colburn, A.P. 1933. A Method of Correlating Forced Convection Heat Transfer Data and Comparison with Fluid Friction. *Trans. AIChE.* Vol.29, pp174-209.

3. Keey, R.B. 1978. "*Introduction to Industrial Drying Operations*". Pergamon Press, Oxford.

4. Kelsey, K.E. and Clarke, L.N. 1956. The heat of Sorption of Water by Wood. *Australian J. of Applied Science*, 7(2), pp160-175.

5. Kho, P.C.S., Keey, R.B. and Walker, J.C.F., 1989. Effects of Minor Irregularities and Air Flows on Drying Rate of Softwood Timber Boards in Kilns. *Proc. 2nd IUFRO International Wood Drying Symposium.* Seattle, Washington. pp.150 - 157.

6. Kho, P.C.S., Keey, R.B. and Walker, J.C.F., 1990. The Variation of Local Mass-Transfer Coefficients in Streamwise Direction Over A Series of In-Line, Blunt Slabs. *Proc. of Chemeca'90*, Auckland, New Zealand, Vol.1, pp348-355.

7. Kayihan, F. 1982. Simultaneous Heat and Mass Transfer with Local Three-Phase Equilibria in Wood Drying. *Proc. of 3rd International Drying Symposium*, Vol.1, pp123-134.

8. Langrish, T.A.G., Keey, R.B., Kho, P.C.S. and Walker, J.C.F. 1993. Time-Dependent Flow in Arrays of Timber Boards: Flow Visualization, Mass-Transfer Measurement and Numerical Simulation. *Chem. Eng. Sci.*, 48(12), pp2211-2223.

9. Lee, H.S. 1990. Flow Visualization on High Temperature Wood Drying, B.E. Report (Chemical and Process Engineering), University of Canterbury, New Zealand.

10. Massey, B.S. 1970. "*Mechanics of Fluids*". (2nd edn.) Van Nostrand Reinhold Co., London.

11. Pang Shusheng, Langrish, T.A.G. and Keey, R.B. 1993. The Heat of Sorption of Timber. *Drying Technology,* 11(5), pp1071-1080.

12. Perry, R.H. and Chilton, C.H. 1973. "*Handbook of Chemical Engineers*". 5th Edition. Hemisphere. New York.

13. Rosen, H.N. and Simpson, W.T. 1981. Evaluating Humidity at Dry Bulb Temperature above the Normal Boiling Point of Water: A Research Note. *Wood and Fibre*, 13(2), pp97-101.

14. Schlichting, H.L. 1960. "*Boundary Layer Theory*". McGraw-Hill, New York.

15. Sherwood, T.K., Pigford, R.L. and Wilke, C.R. 12975. "*Mass Transfer*". McGraw Hill, New York.

16. Skaar, C. 1988. "*Wood Water Relations*". Springer-Verlag, Berlin.

17. Smith, J.M. and van Ness, H.C. 1975. "*Introduction to Chemical Engineering Thermodynamics*". 3rd Edition, McGraw Hill, New York.

18. Stamm, A.J. and Loughborough, W.K. 1935. Thermodynamics of the Swelling of Wood. *J. Phys. Chem.*, Vol.39, pp121-132.

19. Stanish, M.A., Schajer, G.S. and Kayihan, F., 1986. A Mathematical Model of Drying for Hygroscopic Porous Media. *AIChE J.*, Vol.32, No.8, pp.1301 - 1311.

20. Stevens, W.C., Johnston, D.D. and Pratt, G.H. 1956. An Investigation into the Effect of Air Speed on the Transference of Heat from Air to Water. *Timber Technology,* Vol.64, No.2208, pp537-539.

21. Treybal, R.E. 1968. "*Mass Transfer Operations*". (2nd edn.), McGraw-Hill, New York.

Chapter **6**

The Temperature and Moisture-Content Profiles in A Board during Drying

Since the physical properties and thermodynamic parameters of wood, air and water vapour as well as the transport process in the airstream are known, the mathematical model proposed in Chapter 3 can now be solved numerically. In this way, one can quantitatively predict the temperature and moisture-content profiles within a single board at any stage of drying. Separate experiments were carried out at the New Zealand Forest Research Institute (NZFRI). These experiments were to examine the temperature profiles at different depths from one surface of a board, to measure the average moisture content variations with elapsed time and to investigate the moisture gradient through the board. The experimental results have also been used to verify the model.

6.1 Experimental

An experimental study of high-temperature drying of *Pinus radiata* was carried out at NZFRI to investigate the temperature and moisture-content profiles within a single board of pure sapwood and pure heartwood respectively. The sample board was dried in a tunnel dryer. Local temperatures at 5 different depths in each board were measured using copper-constantin T-type thermocouples. The total mass variation of the sample was obtained by supporting the board on a balance installed above the tunnel, from which the average moisture content can be calculated. The dry-bulb and wet-bulb temperatures used in the experiment were 120/70, 120/90, 140/70 and 140/90 °C respectively, while the air velocity was fixed at 5 m s^{-1}. The local moisture content of both heartwood and sapwood boards were examined by drying the samples to different dryness at 120/70 °C, then taking them out of the dryer, putting into a deep freezer for 48 hours and finally cutting them into slices.

6.1.1 Preparation of the Experiment

Two timbers of 5.1m x 400mm x 50mm were cut from two green *Pinus radiata* logs two days before the experiment. The two trees were from a stand in Kaingaroa Forest at an

age of about 30 years. Then the timbers were covered with plastic and stored in the workshop. One timber contained mainly sapwood, and the other mainly heartwood. The timbers were initially flat-sawn (Figure 6.1). On the next day, 7 heartwood samples and 4 sapwood samples were sawn out from the central strips of the timbers, while another 8 sapwood samples from both sides of the central line. The drying samples were clear of knots with the dimensions of 100mm x 50mm x 600mm for heartwood and 100mm x 50mm x 350mm for sapwood. The samples for density and initial moisture content measurement were cut out from both ends of the drying boards to be dried. After sawing, these samples were marked and wrapped with plastic to prevent them drying out. All the specimens were weighed immediately on a laboratory balance (sensitivity: ± 0.1 g).

The green volume for initial moisture content and basic density were determined by immersion in water, after which the specimens were oven dried at a temperature of 105°C for 48 hours. They were then taken out and weighed at once to determine the oven-dry weight and hence the green moisture content. When measuring the green volume, great care was taken to avoid the formation of any air bubbles on the surface of the specimen. Also, the quick measurement of the oven-dry weight minimized adsorbing moisture from the air. The basic density was calculated from the oven-dry weight divided by the specimen volume. The greenwood moisture content was calculated for each sample by dividing the weight loss on oven-drying by the oven-dry weight.

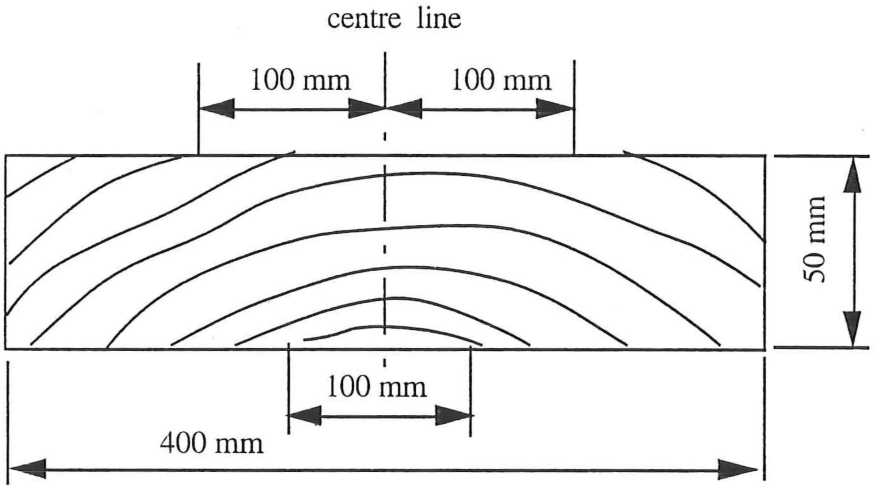

Figure 6.1. A flat-sawn timber from a green log.

The specimens prepared for drying were edge- and end-coated twice with a mixture of Altex Devoe Devshield 235 base aluminium paint and converter. The second coating was done 12 hours after the first time. Five hours after the second coating the samples were rewrapped in the plastic parcels and placed in a cool dark corner until the experiment. The end painting was adopted to prevent extra moisture loss along the grain since the samples

are much shorter than those in a commercial kiln. In this experiment, the moisture losses from sides are also believed to be significant by considering two factors: (1) the original samples were intentionally flat-sawn and (2) only a single board was to be dried. In the flat-sawn boards the edges are perpendicular to the tangential direction, so the wood is more permeable on their side edges. When drying a single board the eddies may form behind the specimen and these eddies will lead a higher turbulence and higher heat- and mass-transfer rates. Therefore, painting of the edge sides is also necessary.

For temperature monitoring, 4 holes of 40 mm depth and 2.5 mm in diameter were drilled from the back edge of the specimen at different positions (Fig 6.2). Silicon adhesive sealant was pumped into the holes by a hand pump during which the trapped air was bled out. After the holes were fully filled with the sealant, the copper-constantin thermocouple paired wires were inserted, with the jointed tip at the bottom of the hole to get a good thermal contact with the wood. The measuring points were chosen as 40mm away from the back edge since the external mass-transfer coefficient in this region is believed to be relatively uniform and can be taken as the representative value over the whole board (Kho, Keey and Walker, 1989). Therefore, the heat- and mass-transfer coefficient above this position can be used as the boundary values in the simulation of average moisture content across the whole board. Although the longitudinal permeability is much greater than the permeabilities in other directions, axial movement is of no consequence away from the sealed ends. Thus, the moisture transport along the grain (longitudinal) may also be neglected by locating the holes more than 100mm away from both ends of the specimen.

Thermocouples were installed for surface temperature measurement by inserting a knife tip to cut a slot about 0.5mm deep and pressing a thermocouple into the slot. Then the thermocouple paired wires were stapled on the surface of the board 15mm away from the slot to avoid the distortion of the moisture-content distribution around the thermocouple tip.

In the experiments, a dummy board was placed in front of the sample board so that the asymptotic mass-transfer coefficients were reached at the sample board (Fig 6.3). The dummy board was fixed by an adjustable supporter so that the level difference of these two boards could be adjusted within 3 mm.

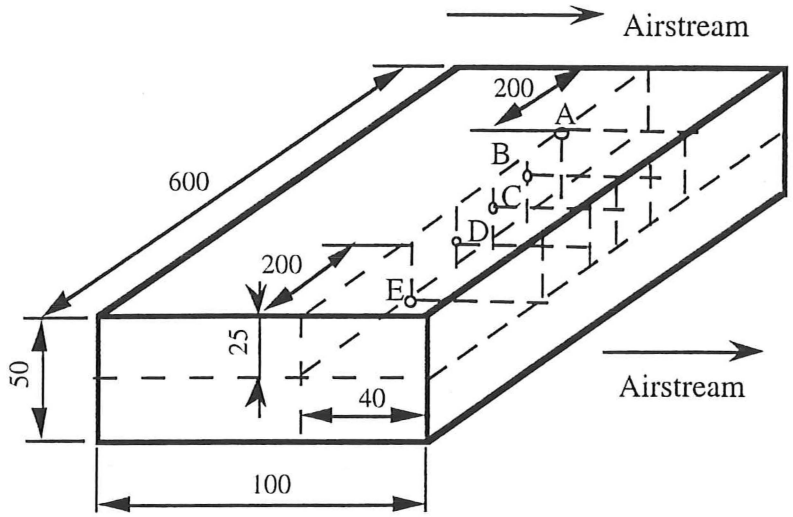

(a) heartwood specimen

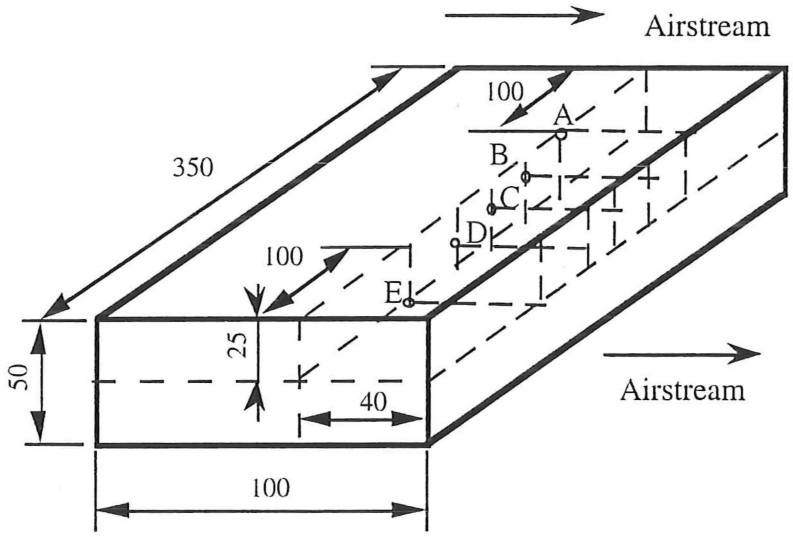

(b) sapwood specimen

Figure 6.2. The location of thermocouples in the specimens.

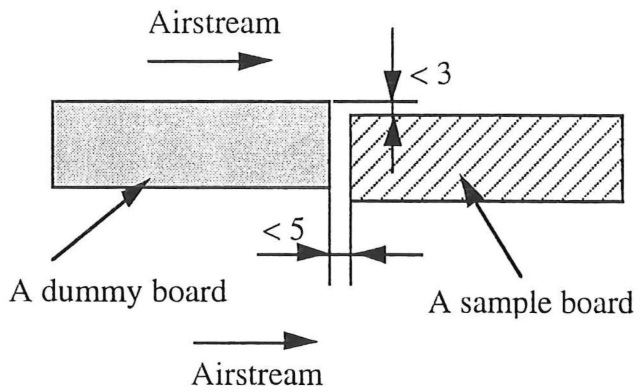

Figure 6.3. The layout of the sample board.

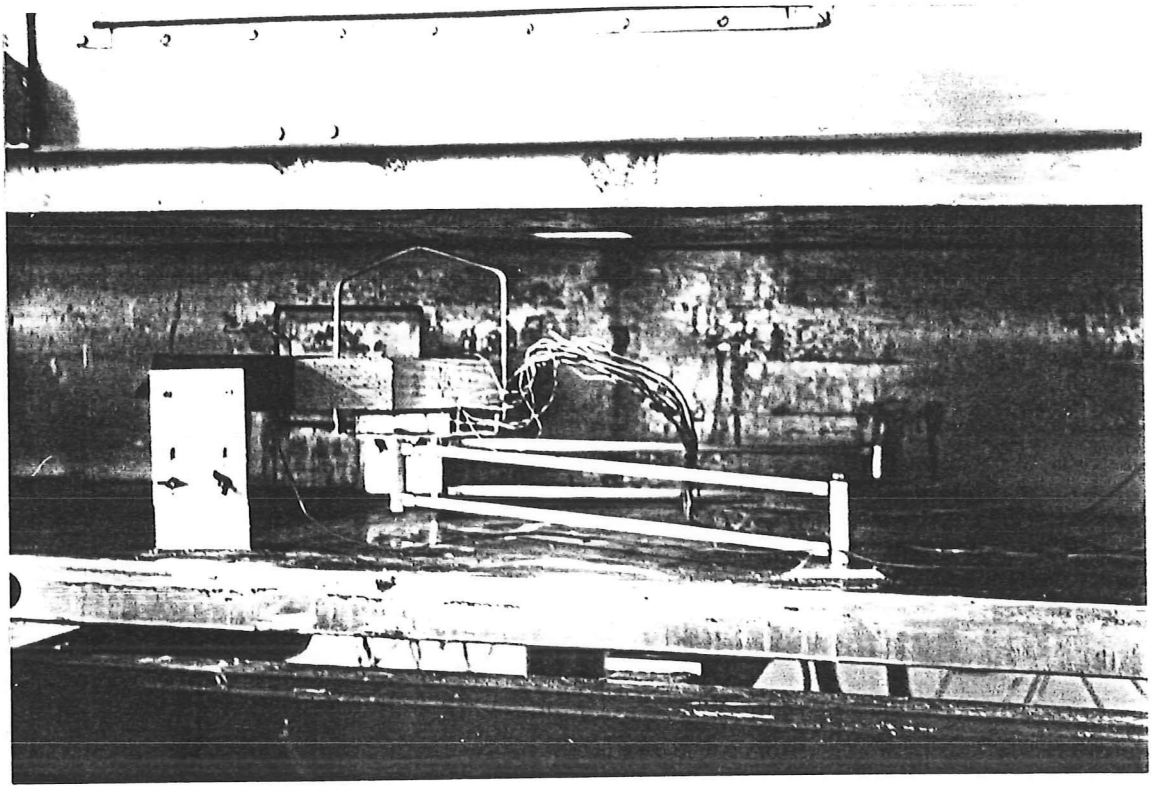

(a). Photograph of the cradle with a drying board on it and a dummy board in front of it.

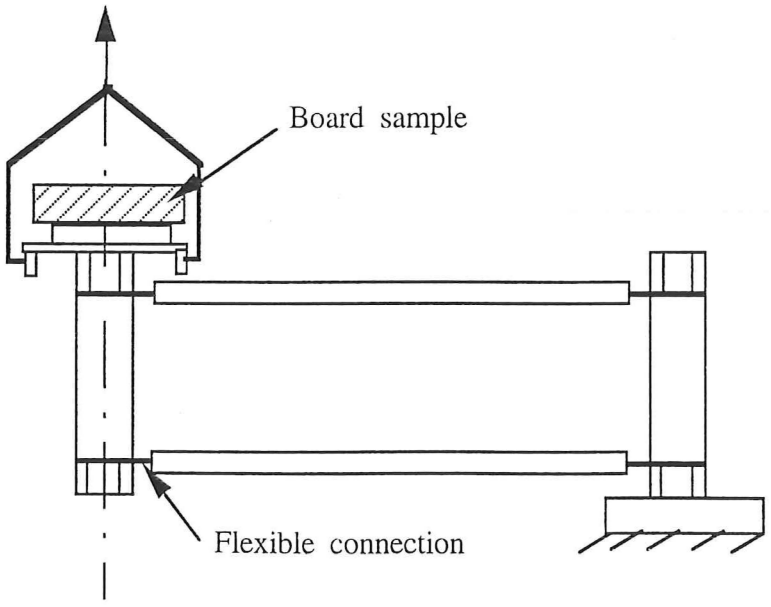

(b). Schematic diagram of the cradle.

Figure 4. Cradle for supporting the board.

Before the experiment, the tunnel was run under cool conditions to find the fan speed (1315 r.p.m.) corresponding to an air velocity of 5 m s^{-1}.

To avoid the sample board swinging in the airstream, the board was hung from the weighing balance and supported within a cradle as shown in Figure 6.4. The cradle allowed free vertical movement, but restrained any sideways shift.

6.1.2 The Drying Tests

Tests runs under various conditions were carried out in an electrically heated, steam-humidified tunnel dryer (Figure 6.5). The dry-bulb temperature and the wet-bulb temperature upstream of the sample were automatically controlled at fixed set points with maximum fluctuation of ±0.5 °C. Meanwhile, the dry-bulb temperature over the sample board and wet-bulb temperature downstream were monitored by thermocouples. Before commencing drying a board, the tunnel dryer was run for about 30 minutes to heat up the air to the required drying conditions (Figure 6.5).

For the temperature and average moisture-content measurements, when the dry-bulb and wet-bulb temperatures were stable, the heating and the fan were stopped. The sample was weighed free of the cradle and finally replaced on the cradle after weighing. Then the heating and the fan were switched on again and the data monitor and data logger were re-started to display and record the elapsed time, temperatures and sample weight. The process lasted for about 5 minutes. The data on the display screen gave the changing values every 30 seconds while the data logger recorded and printer printed the data every 10 minutes. When all the temperatures within the board were very close (in a range of 1-2°C) to the dry-bulb temperature, the test was stopped. The sample was weighed and placed in the oven to dry at a temperature of 105°C for 48 hours. The oven-dry weight was measured as the wood mass.

The thermocouple holes were intentionally drilled from back side edge at distances of 6mm, 12mm, 18mm and 25mm to upper surface. However, when drilling the holes by a hand drill it was found that some of them were inclined, so the bottom distances of these holes to the board surface were not the same as those at the openings. This problem was solved subsequently (for all the sapwood samples) by drilling the holes on a machine drill. Therefore, after oven-drying, the heartwood samples were cut into pieces through the holes to check the distances from the bottom of the hole to the board surface.

In the tests, the dry-bulb temperature and wet-bulb temperatures both for heartwood and for sapwood were set at 120/70, 120/90, 140/70 and 140/90 °C respectively. The air velocity was fixed as 5 m s^{-1} for each trial. The external conditions, the run numbers and sample marks are described in Table 1.

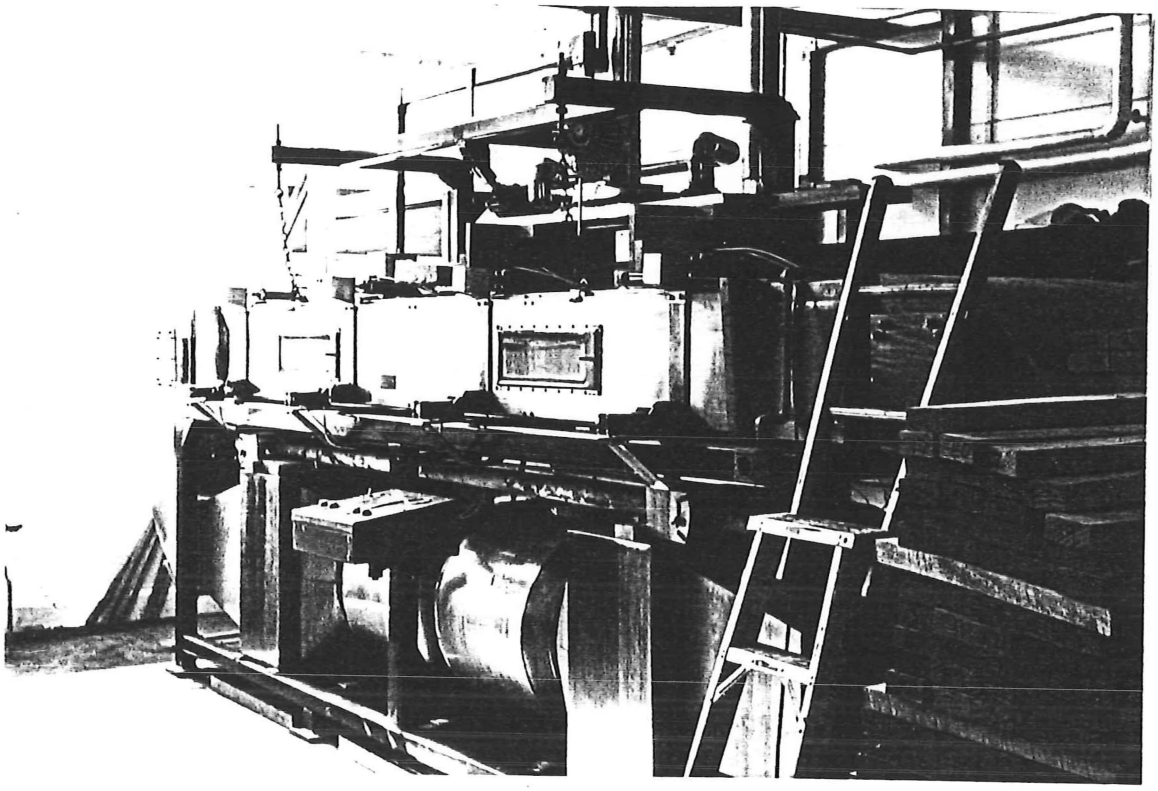

(a). Photograph of the outside view of the tunnel dryer.

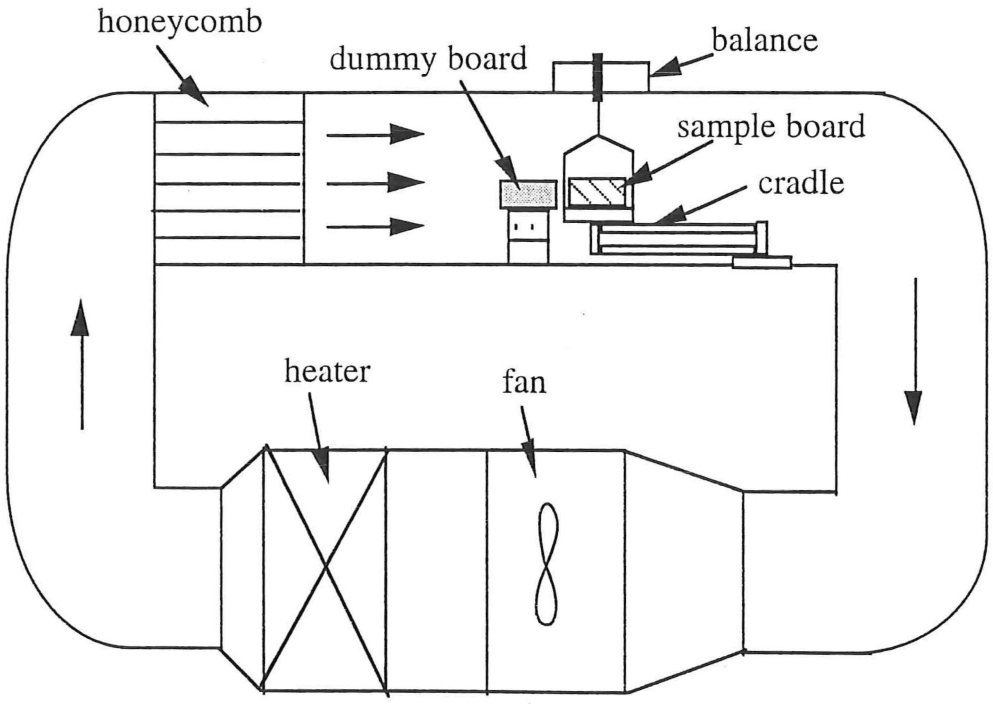

(b). Schematic diagram of the dryer.

Figure 6.5. The tunnel to dry a single board under high temperatures.

Table 6.1. The external conditions, the run numbers and samples

External Conditions (dry-bulb/wet-bulb temperatures, °C)	Run No.	Sample Numbers	Wood
120/70	Run 1	2H	Heartwood
120/90	Run 4	7H	Heartwood
140/70	Run 3	5H	Heartwood
140/90	Run 2	1H	Heartwood
120/70	Run 5	10B	Sapwood
120/70	Run 9	10G	Sapwood
120/90	Run 8	10J	Sapwood
140/70	Run 6	10E	Sapwood
140/90	Run 7	10L	Sapwood
140/90	Run 10	10A	Sapwood

For the local moisture content measurement, we put four sapwood and three heartwood samples in the tunnel dryer (Figure 6.6) and dried them at dry-bulb temperature of 120°C and wet-bulb temperature of 70°C with air velocity of 5 m s^{-1}. A maximum number of 3 samples was placed together to avoid differences in external condition due to moisture build up and temperature drop in drying. Two dry-bulb sensors were positioned at either side of the samples. With this arrangement, the temperature recording shows a difference from inlet to outlet of only approximately 1-2°C. By drying the samples to different dryness after 4 hours, 8 hours, 12 hours and 16 hours respectively, the heartwood and sapwood samples next to the dummy board were withdrawn. The rest of the samples were moved up next to the dummy board.

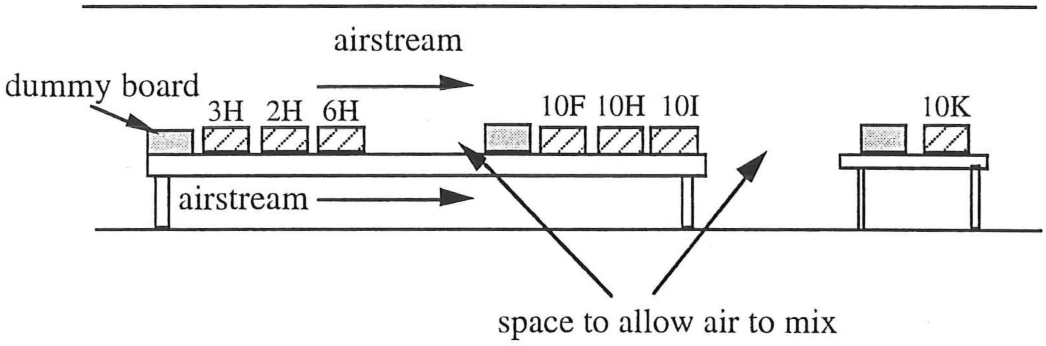

Figure 6.6. The layout of the samples for local moisture-content measurement.

As each board was taken out, it was cut on a portable circular saw to give: two 12mm thick cross-sections for moisture gradient determination, a 25mm thick cross-section for average moisture content, and another 25mm spare. The orientation of the samples is shown in Figure 6.7. The 12mm samples and one of 25mm thickness were placed in a deep freezer to minimize the moisture movement during further cutting the cross-sections into pieces. After freezing overnight, the cross-sections were cut on a multisaw into 9 separate slices (Figure 6.7). Then the slices were weighed and oven-dried at a temperature of 105 °C for 48 hours. The moisture content of each slice was determined by dividing the weight loss on oven-drying by oven-dry mass. Tests show that this practice caused little moisture changes.

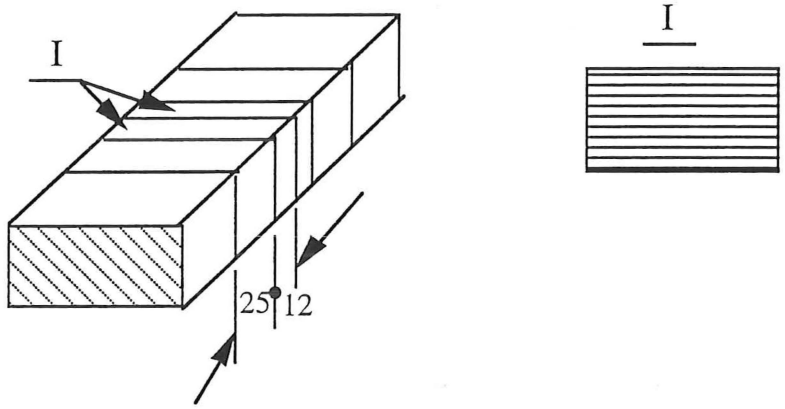

(a) Sawn-out the central portion of a test board (b) Sawn-out thin slices

Figure 6.7. The orientation of the thin slices for the local moisture-content measurement.

6.2 Results

6.2.1 Wood Density and Green Moisture Content

Wood density and green moisture content are two of the most variable properties of wood. Sapwood is much wetter than heartwood. Both of the density and green moisture content for heartwood and sapwood vary with factors such as the age of a tree, the field location , the orientation of a sample from the tree (different age ring, earlywood or latewood in a ring, different height, *etc.*), the month of felling and the environment (Cown and McConchie, 1983, Booker and Langrish, 1992). Therefore, the density and green moisture content were measured for each sample board. The results are shown in Table 2.

From the results obtained, it can be seen that for sapwood, the density varies from 419 to 488 kg m^{-3}, while the green moisture content falls in a range of 1.164 to 1.392 kg kg^{-1}. These values agree with data reported in literature (Cown and McConchie, 1983; Kininmonth, 1990). For the heartwood, the density ranges from 372 to 429 kg m^{-3} and green moisture content from 0.347 to 0.380 kg kg^{-1}. The density of the heartwood is also close to that measured by the above authors, although the moisture content is slightly less than the reported values. This may be due to the two days delay for the measurement or due to the location of the samples in a tree.

The slight reduction of moisture content just before drying is caused by the loss of moisture after the samples were sawn.

Table 6.2. The density and green moisture content of the samples

Sample No.	Wood	Density (kg m^{-3})	Green MC (kg kg^{-1})	MC Just Before Drying
1H	Heartwood	409	0.364	0.342
2H	Heartwood	372	0.380	0.332
3H	Heartwood	429	0.379	
4H	Heartwood	374	0.366	
5H	Heartwood	381	0.351	0.329
6H	Heartwood	392	0.358	
7H	Heartwood	387	0.347	0.325
10A	Sapwood	451	1.380	1.337
10B	Sapwood	443	1.392	1.383
10C	Sapwood	419	1.164	
10D	Sapwood	432	1.257	
10E	Sapwood	438	1.320	1.308
10F	Sapwood	428	1.342	
10G	Sapwood	452	1.315	1.320
10H	Sapwood	488	1.204	
10I	Sapwood	472	1.283	
10J	Sapwood	469	1.301	1.254
10K	Sapwood	464	1.287	
10L	Sapwood	447	1.272	1.272

6.2.2 The Temperature and Average Moisture-Content Profiles

The temperature profiles for the 10 trials at different conditions are shown in Figures 6.8 and 6.9. The shape of these profiles are similar to those reported by Beard *et al.* (1988) and Northway (1989). The average moisture content is also plotted on these temperature profiles.

Heartwood

The run numbers and external conditions are given beneath each diagram in Figures 6.8 and 6.9. For the heartwood at dry-bulb and wet-bulb temperatures of 120/70°C (Run 1), the surface temperature rises above 100°C and increases gradually towards the air temperature. During the first two hours, the interior of the board is heated up to about 100°C, after which the internal temperatures at different depths start to rise progressively as the drying proceeds. Before the internal temperatures increase they are very close to one other remaining at about 100°C. Finally, the central temperature increases and approaches the surface temperature of the board. Unfortunately, the data logger failed to record the sample weight after 7 hours drying due to a fault in the cradle, so the profile of average moisture content cannot be completed with time for this run. After 7 hours of drying the moisture content had fallen from the initial value of 33.1% to 13.7%.

For Run 4 (120/90°C), the temperature profile is similar to that of Run 1 (120/70°C). The moisture content decreases with elapsed time virtually from the beginning of drying except for a short induction time of about 10 minutes. During this period, the board adsorbs some moisture from the air and the sample weight increases a little since the surface temperature is below the wet-bulb temperature of the air. However, no constant drying rate period was observed throughout the whole process of drying. The final moisture content for this run is 4.0% after 18 hours of drying, while after 7 hours the value is 11.3% with the initial moisture content of 32.5%.

The feature of the temperature and moisture-content profiles discussed above is an envelope for the drying behaviour at higher temperatures of the air. In the two runs (140/70, 140/90 °C) at dry-bulb temperature of 140°C, the board surface temperature rises much more rapidly than that at 120°C. Within the first minute after the sample had been placed on the cradle and the fan and heater had been

switched on, the surface temperature was initially recorded as higher than 70°C. The average moisture content drops more quickly during drying at temperature of 140°C than that at the lower temperature of the air. However, for the same dry-bulb temperature, the drying rate at lower wet-bulb temperature (70°C) is higher than that at higher wet-bulb temperature (90°C). After 12 hours of drying, the moisture contents for Run 3 (140/70°C) and Run 2 (140/90°C) are 1.3% and 2.3% respectively, while the corresponding initial values are 32.9% and 34.2%. By comparison with these final values, the average moisture content for Run 4 (120/90°C) is 5.9% after 12 hours of drying.

Sapwood

The temperature and average moisture-content profiles are similar to those reported in earlier reports (Pang, Keey, and Langrish, 1991, 1992a) and also to what Northway (1989) measured for the same species of wood. However, Northway did not complete the whole process of drying. He stopped the drying before the central temperature started to increase above 100°C.

In the drying experiment for sapwood at dry-bulb temperatures of 120°C and 140°C, it has been observed that the surface temperature rises rapidly above the wet-bulb temperatures and then increases slowly towards the air temperature.

With the exception of Run 9 (120/70°C), all of the internal temperatures at different depths (6mm, 12mm, 18mm and 25mm beneath the surface) are very close to each other and remain at about 100°C for a substantial period of time. The length of this period depends on the external conditions, for example 8 hours for dry-bulb temperature of 120°C and 5-7 hours for that of 140°C. During this period the moisture content decreases linearly with drying time, corresponding to a constant drying rate period, although for a short initial period the board absorbs some moisture from the air. Following this constant drying-rate period, the wood dries in a similar way to that for heartwood. The drying rate falls and the temperatures at different depths start to increase progressively. Finally, all the temperatures approach the dry-bulb temperature as the moisture contents approach the equilibrium values.

As an exception for the sapwood, the temperature and moisture-content profiles in Run 9(120/70°C) are rather like heartwood. There is no significant period when all the internal temperatures are very close to each other, and the moisture content

decreases linearly with drying time. This difference may be due to the orientation of the grain in the sample or a singularity in the ring growth pattern or a slight portion of heartwood.

The average moisture contents over each board during final stages of drying are given in Table 6.3. Thus one can see how the external conditions (possibly together with the structural differences between boards) affect the drying behaviour of a board.

Table 6.3. The average moisture content during the final stages of drying

Drying time (h)	Run 5 (120 /70°C)	Run 9 (120 /70°C)	Run 8 (120 /90°C)	Run 6 (140 /70°C)	Run 7 (140 /90°C)	Run 10 (140 /90°C)
0	138.3%	132.0%	125.4%	130.8%	127.2%	133.7%
10.5	13.8%*	23.6%	14.9%	3.5%	4.6%	4.8%
11.5	-	19.3%	12.3%	2.4%*	3.9%*	3.7%
16.0	-	7.7%	5.6%	-	-	1.8%*
21.0	-	2.6%*	3.3%*	-	-	-

* the final value for the run

6.2.3 The Moisture-Content Gradient

The local moisture contents for both sapwood and heartwood boards during drying are shown in Figures 6.10 and 6.11. For heartwood, the boards were dried for 4, 8 and 12 hours and sapwood boards for 4, 8, 12 and 16 hours.

As expected, the layer close to the surface dries faster than those in the interior region. For sapwood (Fig 6.10) with initial moisture contents of 120.4-134.2%, the moisture content close to the surface falls to 21.1-25.5% after 4 hours, while the layer just 7mm beneath the surface is still quite wet with a moisture content of 45.1-67.2%. At this time, the moisture content in the central region is as high as 75.8-97.4%. This feature of moisture distribution persists with some reduction in the variation until 8 hours of drying. Now, the moisture content close to the surface has decreased to 9.3-14.2% and that in the mid-layer of the board to 39.1-45.9%. However, after 16 hours the moisture-content difference throughout the sample is greatly reduced to about 5%. The surface moisture content (2.9-3.8%) approaches the equilibrium value while the central moisture content has decreased to 6.1-8.2%.

The moisture distribution variations in heartwood (Figure 6.11) are similar to those in sapwood. As the initial value for heartwood is lower (34.7-38.0%) than sapwood, the moisture-content gradient in heartwood is not as great as that in sapwood. After 4 hours of drying, the moisture content close to the surface is 7.2-11.4% whereas that in the central area is 20.8-25.4%. The corresponding values after 12 hours of drying are 3.4-4.1% and 6.5-7.2% respectively.

Because of the difference in wood properties (mainly the green moisture content) between earlywood and latewood in a growth ring, the measured results show an irregular profile of moisture content after 4 hours of drying. Individual slices, of about 4mm thickness, contain varying proportions of earlywood which have a higher green moisture content than latewood. However, although the early part of a ring dries more easily than the late part, this irregularity in moisture content has vanished after 8 hours of drying. The asymmetrical distribution in moisture content over the thickness of the board can also be observed in Figures 6.10 and 6.11. This asymmetry may be due to the structural difference in the ring width (during growing) and ring angle (during sawing) within the upper part and lower part of the board.

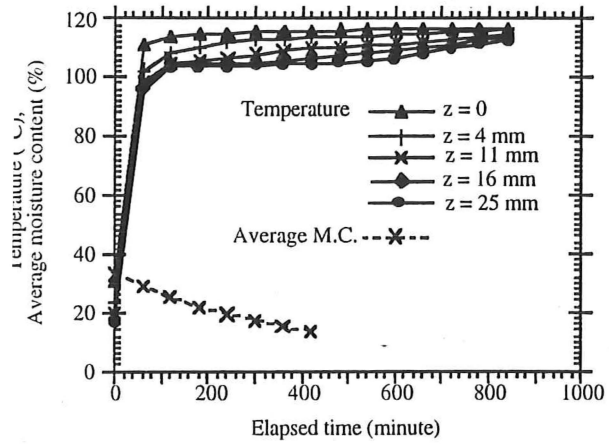

(a). Run 1 (120/70°C)

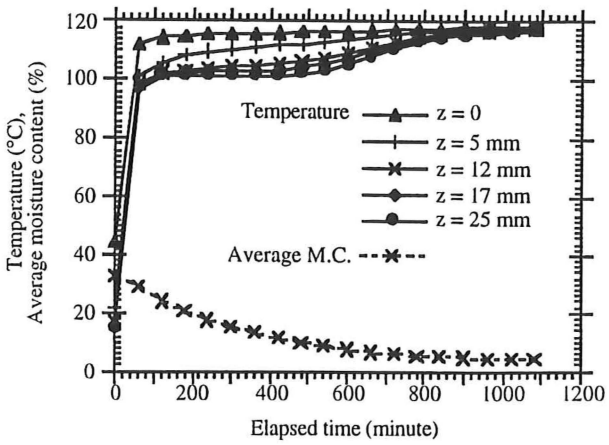

(b). Run 4 (120/90°C)

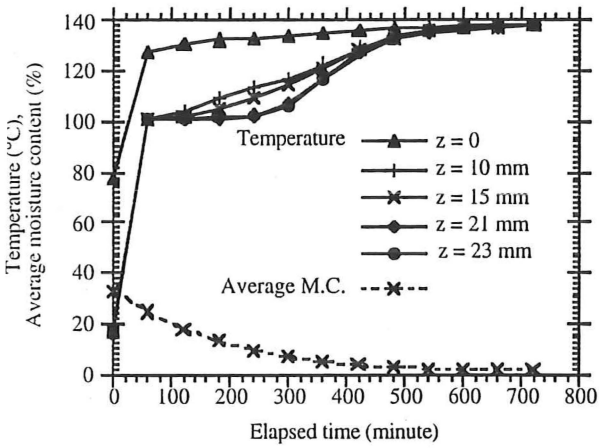

(c). Run 3 (140/70°C)

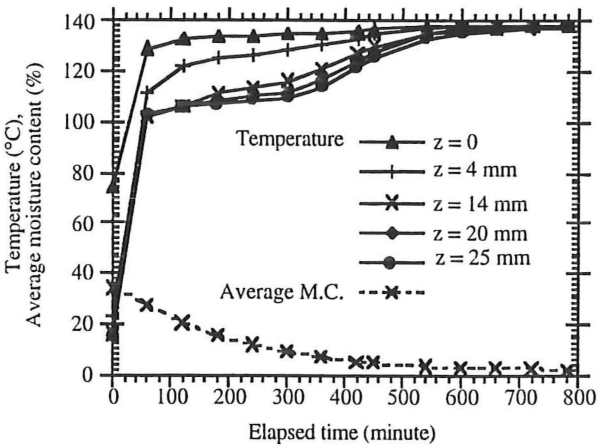

(d). Run 2 (140/90°C)

Figure 6.8 Temperature and moisture-content profiles within a heartwood board. Parameter z is the distance from upper surface of the board. Air velocity is 5 m s^{-1}.

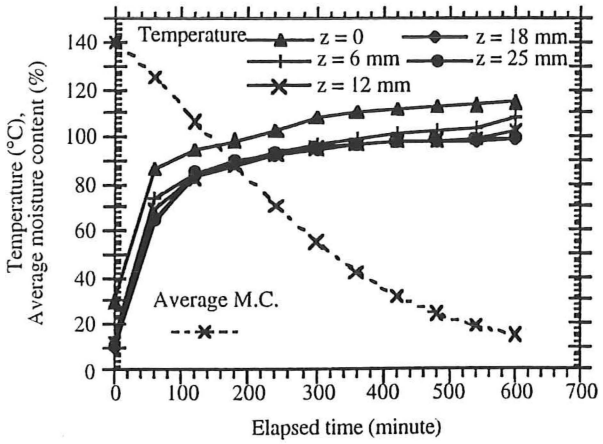

(a). Run 5 (120/70°C)

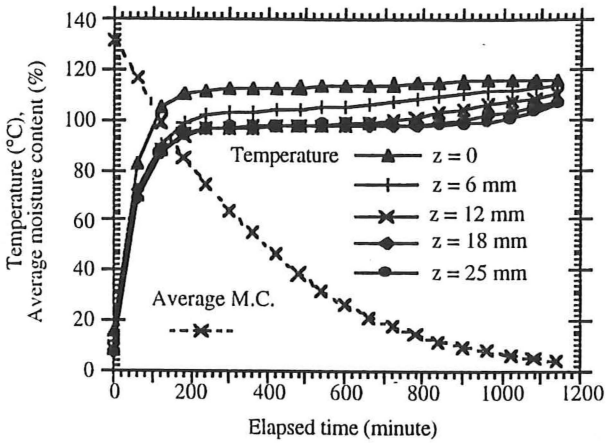

(b). Run 9 (120/70°C)

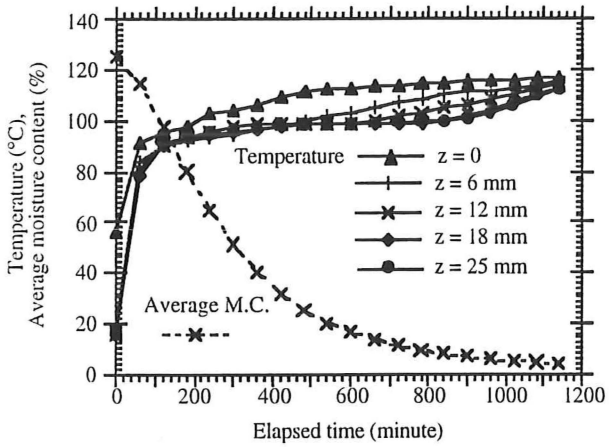

(c). Run 8 (120/90°C)

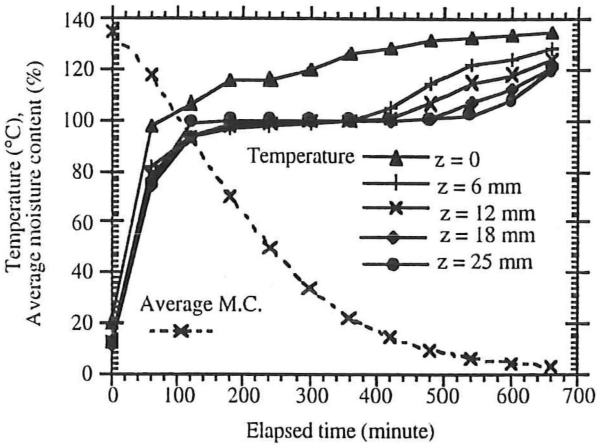

(d). Run 6 (140/70°C)

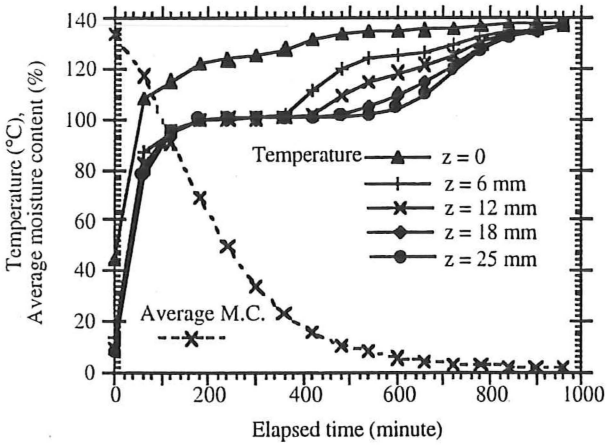

(e). Run 7 (140/90°C)

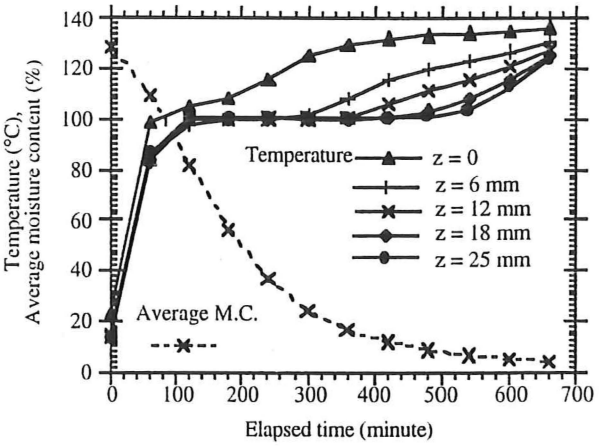

(f). Run 10 (140/90°C)

Figure 6.9 Temperature and moisture-content profiles within a saptwood board. Parameter z is the distance from upper surface of the board. Air velocity is 5 m s^{-1}.

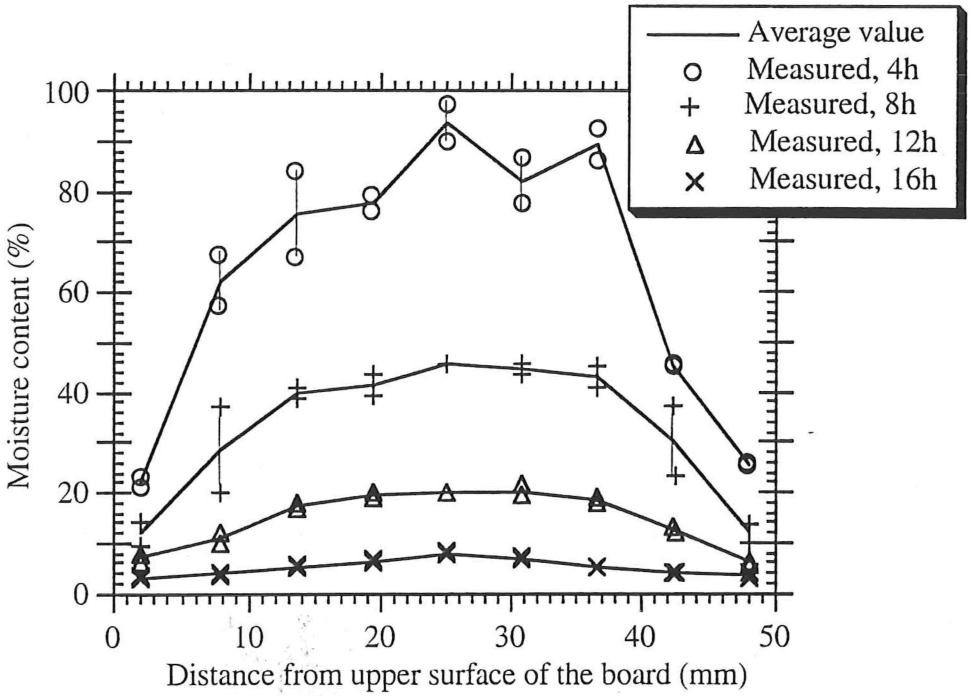

Figure 6.10 The moisture-content distribution within a sapwood board during drying. Drybulb/wet-bulb tem,peratures: 120/70°C; air velocity: 5 m s^{-1}.

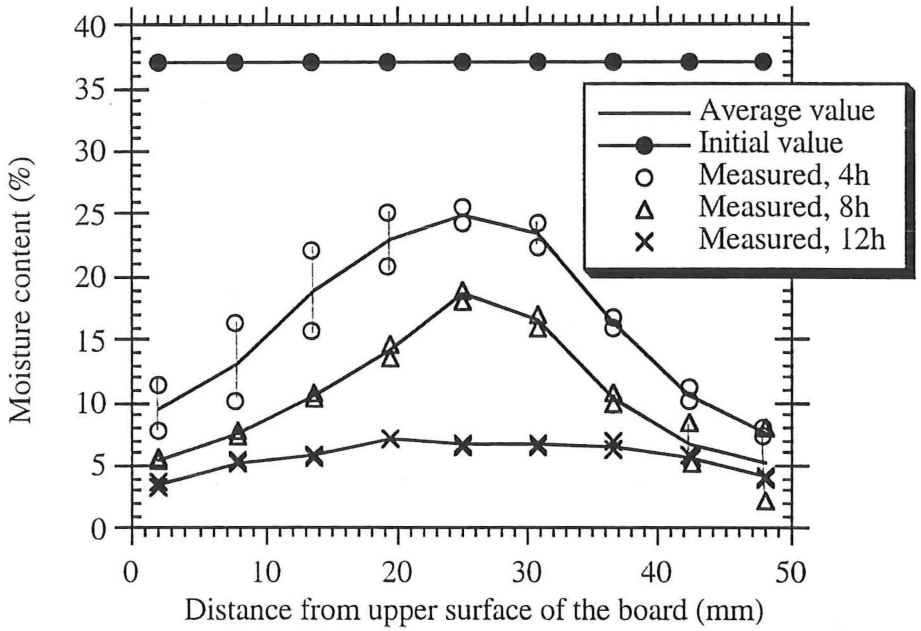

Figure 6.11 The moisture-content distribution within a heartwood board during drying. Drybulb/wet-bulb tem,peratures: 120/70°C; air velocity: 5 m s^{-1}.

6.3 Comparison of the Experimental Results with Predictions of A Mathematical Model

In Chapter 3, a model has been proposed to simulate the high-temperature kiln drying of *Pinus radiata* boards. In the model, the process of high-temperature drying of *Pinus radiata* heartwood are divided into three periods. During the initial stage of drying, an evaporation front is assumed to lie within the wood at which all of the liquid water evaporates during drying. Since the liquid flow is insignificant beneath the front due to the aspiration of the pits and the deposition of resins as the tree grows (Booker,1989), this evaporative front will recede into the material as drying proceeds. The front divides the material into two parts, a wet zone beneath the front and a dry zone above it. Above the front, moisture is assumed to exist as bound water and water vapour. Bound water will be in local thermodynamic equilibrium with the water vapour at the local temperature (Stanish *et al.*, 1986). In the wet zone, the moisture content remains at the initial value. This initial period, when the external transfer process controls the drying, may be called the first period of drying. However, as the evaporative front withdraws, the internal resistance becomes significant. Then the drying is internally controlled, the drying from this point on is called the second period.

After the evaporative front reaches the centre-layer of the board, drying is controlled by bound-water diffusion and water vapour flow. This is known as the third drying period.

In the drying of sapwood boards, the flow of liquid moisture close to the surface is insignificant because the surfaces of the board were damaged and the water column in green wood has been broken during the milling process. Therefore, at the beginning of the initial drying period of sapwood, the evaporative front quickly recedes in a short distance ξ_O within the material to produce cavitation to generate sufficient tension to for the liquid flow. However, at depths greater than ξ_O, most of the pits inside this position are not yet aspirated and the flow of liquid is no longer negligible. In green sapwood, these pits are required for the transport of liquid nutrients. They aspirate only when the sapwood is dried, and this aspiration is irreversible (Booker, 1989). The liquid flow towards the surface means that the evaporative front will remain at the position ξ_O until the moisture content at the front decreases to the minimum value for liquid continuity. Afterwards the front starts to recede into the material and the ongoing drying is similar to that for heartwood. The main difference between the drying behaviour of sapwood and

heartwood during this initial period is that the liquid flow in the wet zone for sapwood has a significant influence on the receding velocity of the evaporative front.

6.3.1 The Boundary Conditions and Chosen Physical Properties of Wood

The mass-transfer coefficients measured by Kho *et al.* (1989) have been used to define the external conditions above a board at the air velocity of 5 m s^{-1}. As the layout of the single board in this experiment is different from a stack of boards in a kiln, and also the surface of a wood board is not as smooth as the naphthalene layer in Kho's experiment, the airstream over the sample board is believed to be more turbulent than over the naphthalene layer. Therefore, we use a slightly different value (about 20% higher) for the external mass-transfer coefficient to simulate the drying process of a single board in the tunnel dryer. The external heat-transfer coefficient is estimated from the mass-transfer coefficient by using the Chilton-Colburn analogy. Higher values than those predicted from the analogy are chosen to take account of the radiation from the dryer shell to the board surface. In this case, the temperature of the dryer shell rises close to the air temperature very rapidly and the board surface is similar to a black one, so when the board surface-temperature is relatively low in the initial period of drying, the board absorbs more radiative heat from the dryer shell. Also, the hot airstream will radiate heat to the board surface beside the convection (Keey, 1991). To simulate this external heat-transfer process, we take the radiative heat as 20-30% of the convective heat when the surface temperature is more than 5°C lower than the air temperature, thereafter the radiation is taken as 10%.

For each experimental trial, the measured wood density and initial moisture content of the sample are used in the simulation. The values are the averaged ones over two pieces cut from both ends of the sample board. The initial temperature of the board is assumed to be 20°C, which is the typical ambient temperature in the laboratory. Although it was found that there was a temperature gradient within the board in the laboratory as the sample had been stored in a cool corner, the predictions of temperature and moisture-content profiles are not strongly sensitive to the initial temperature of the wood.

Again, the wood permeability both to gas flow in the dry zone and to liquid flow at saturation have been chosen so that the calculated temperature and moisture-content profiles agree with the experimental results. Booker (1989, 1990) has measured the permeability of *Pinus radiata* to both gas and liquid flow, in both the green and dry state for sapwood and heartwood in both radial and tangential directions. His values span a

considerable range. A comparison of the fitted values of the permeability with those measured by Booker provides a test of this mathematical simulation approach.

The calculations simulated the seasoning of each 100x50 mm *Pinus radiata* board dried in the tunnel dryer at various air temperatures. The values of the used parameters are set out in Table 6.4.

In Table 6.4, it can be seen that the fitted permeability for each board may be different. This could be due to the orientation of the grain in the sample or a singularity in the ring growth pattern or the effect of the air temperature. Temperature could affect the liquid permeability as the greenwood shrinks while heating (Pang *et al.*, 1992c). The variation in the external heat- and mass-transfer coefficients may be the result of the slight differences in thickness of each board or the configuration of each trial.

Table 6.4. Values of the parameters used in the simulation of high-temperature kiln drying of *Pinus radiata* boards

Chosen parameters	Run1	Run4	Run3	Run2	Run5	Run8	Run6	Run7
Wood permeability to gas, K_G, 10^{-15} m^2	0.2	0.4	0.6	0.5	1.0	1.3	1.2	1.3
Wood permeability to liquid, K_l^s, 10^{-16} m^2	—	—	—	—	14.0	10.0	10.0	14.4
External heat-transfer coefficient, h, W m^{-2} K^{-1}	35.1* 30.9+	35.1* 30.9+	35.1* 30.9+	35.1* 30.9+	65.0* 50.0+	55.0* 50.0+	55.0* 50.0+	60.0* 50.0+
External mass-transfer coefficient, β, 10^{-8} s m^{-1}	16.0	16.0	16.0	16.0	20.0	20.0	20.0	20.0
Thin dry layer thickness, ξ_o, mm	—	—	—	—	1.3	1.1	1.1	1.1

* the value used to account for higher radiative heat from the dryer cell to the board surface when the surface temperature is lower;
+ the value with 10% of radiative heat

6.3.2 The Simulation Results and Comparison with Experimental Data

As discussed in section 6.2, in the experiments the dry-bulb and wet-bulb temperatures of the air stream, the local temperatures within the board and the weight-variations of the sample with time were measured during drying. The air velocity was fixed at 5 m s^{-1}. Using the mathematical model developed in Chapter 3 and by Pang, Keey and Langrish (1991, 1992a, 1992b), the temperature and moisture-content profiles have been obtained within the boards for each trial. The physical properties and parameters are taken as those measured in the experiment or chosen by fitting the predicted temperature and moisture-content profiles to the measured ones (Table 6.4). The predicted variations are presented in Figs 6.12 and 6.13 as curves, while the experimental data are also plotted as discrete points to allow comparison with the predictions.

For heartwood, the predictions agree very well with the experimental data for the whole drying process especially for the match of moisture-content profiles, with a discrepancy of less than 1% (MC) between the measured and predicted values. The largest errors in temperature profile occur in the initial stage of drying, in which the measured surface temperature rises more rapidly than the predicted ones. The internal temperatures start to increase during drying in the same way as those measured. The maximum difference between the predicted temperature and measured one is 5°C, which occurs in the initial stages of drying.

The significant feature of sapwood drying is that the internal temperatures remain close to each other and the moisture loss is linear with time for a substantial period of time in the first stage of drying. This has been predicted from the model and verified by the experimental results. However, the discrepancy in moisture content between the predictions and the measured data is noticeable before the evaporative front (in the model) has reached the centre layer of the board. The predicted moisture contents are 5~15% higher in value than the experimental results during this period. This deviation is more significant when the higher air temperature (140°C) is used.

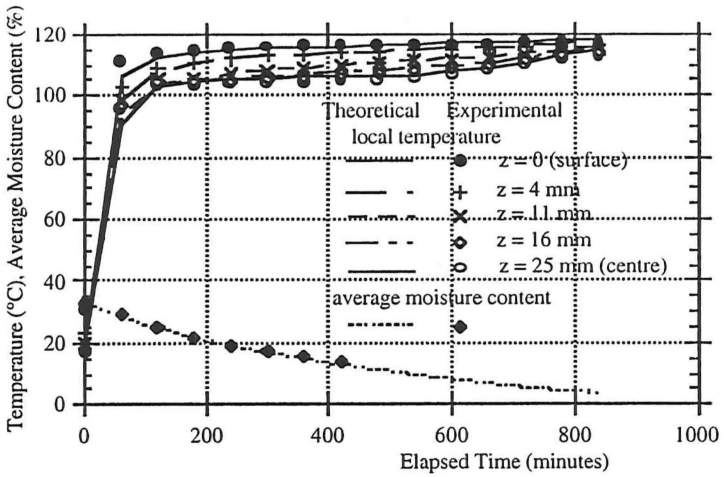

(a). dry-bulb/wet-bulb temperatures: 120/70 °C

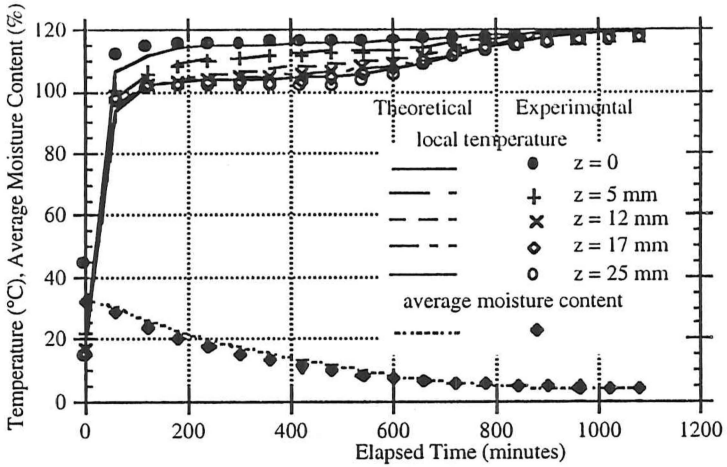

(b). dry-bulb/wet-bulb temperatures: 120/90 °C

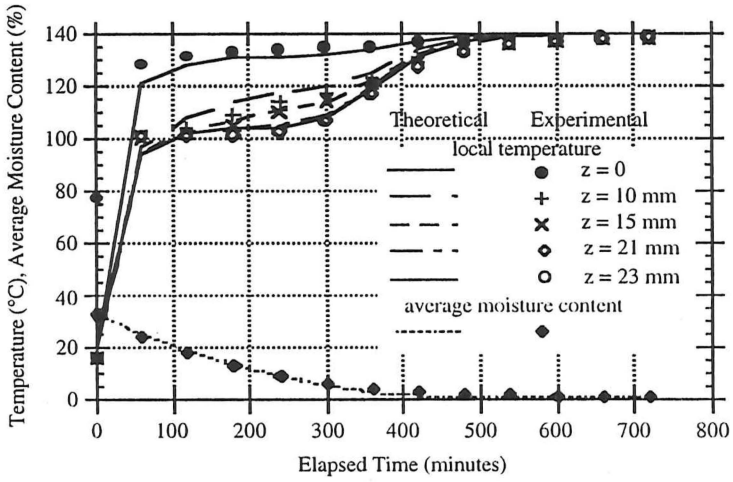

(c). dry-bulb/wet-bulb temperatures: 140/70°C

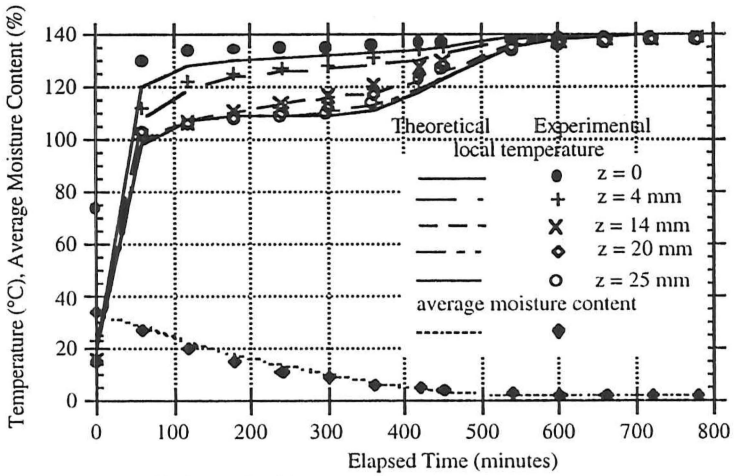

(d). dry-bulb/wet-bulb temperatures: 140/90°C

Figure 6.12. The temperature and moisture-content profiles within a heartwood board: the simulation results and the comparison with experimental data. Parameter z is the distance from upper surface of the board. Air velocity is 5 m s^{-1}.

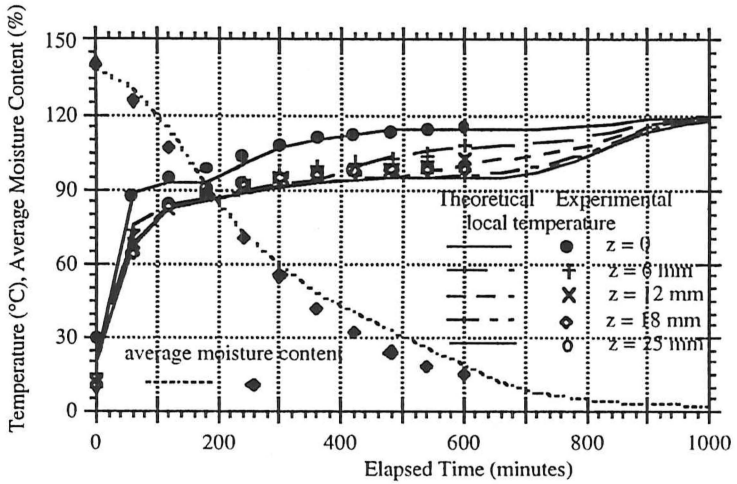

(a). dry-bulb/wet-bulb temperatures: 120/70 °C (Run 5)

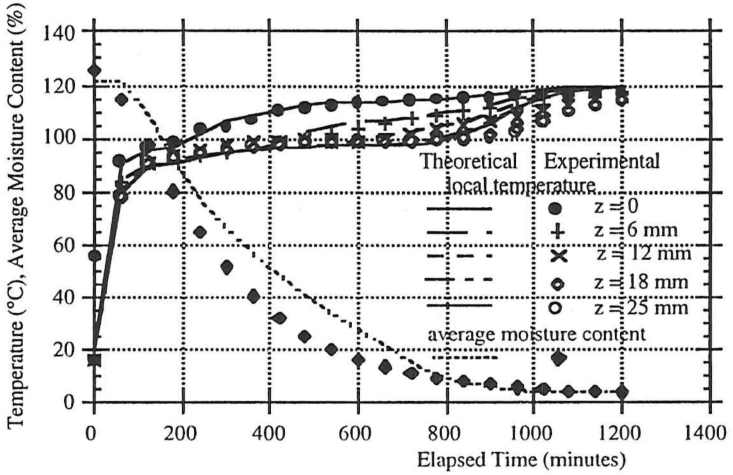

(b). dry-bulb/wet-bulb temperatures: 120/90 °C

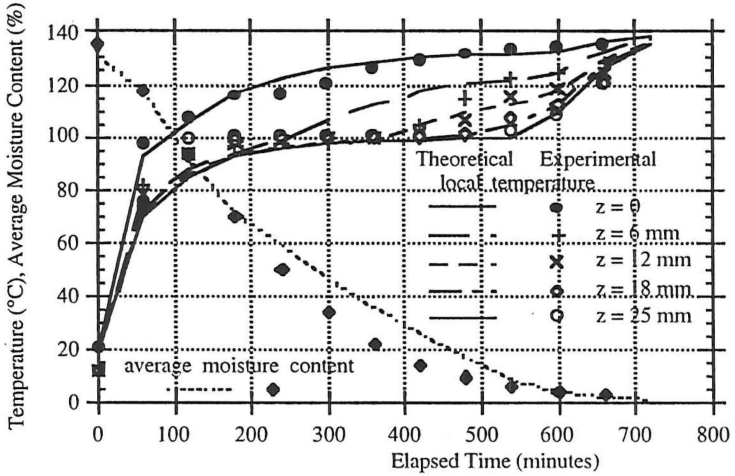

(c). dry-bulb/wet-bulb temperatures: 140/70 °C

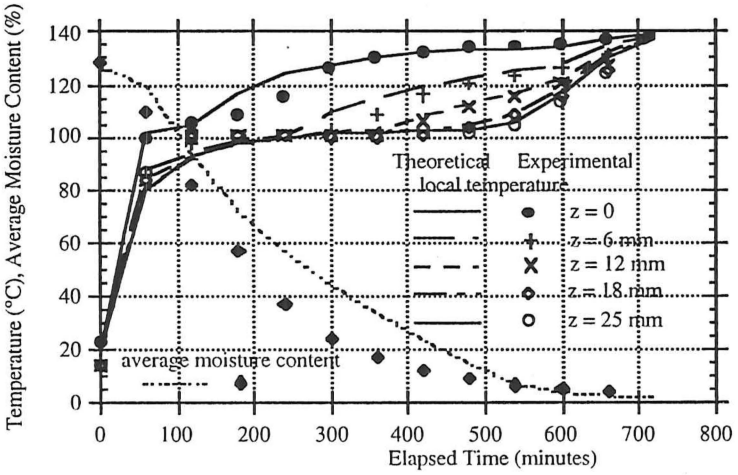

(d). dry-bulb/wet-bulb temperatures: 140/90 °C (Run 7)

Figure 6.13. The temperature and moisture-content profiles within a sapwood board: the simulation results and the comparison with experimental data. Parameter z is the distance from upper surface of the board. Air velocity is 5 m s^{-1}.

6.4 Discussion

6.4.1 The Experimental Results

When drying a heartwood board at dry-bulb temperature above 100°C (120°C and 140°C in these experiments), the surface temperature rises very rapidly to above 100°C, while the temperature at the centre-line remains at about 100°C until the average moisture content decreases to below 10%. During this period, the internal temperatures at different depths start to increase progressively, before which they remain close to the centre temperature. Finally, all the internal temperatures approach the surface temperature which is now only 2-3°C lower than the air temperature, while the average moisture content approaches the equilibrium value.

The progressive rise of the internal temperatures at different depths indicates an evaporative front receding from the surface to the centre-line during drying. As there is no significant liquid evaporation beneath the front, only a small amount of heat is conducted into this zone and the temperature gradient is negligible once the wood has been heated up to about 100°C. After all of the liquid water has evaporated, only bound water remains in the wood and it migrates to evaporate slowly within the whole material. At this stage the temperature at the centre of the board starts to increase.

The drying of a single heartwood board in the experiment is faster than predicted previously (Pang, Keey and Langrish, 1992a, 1992b). This difference can be attributed to two factors: (1) the initial moisture content of the sample is lower than that used before (50%); (2) the external heat- and mass-transfer coefficients are higher when drying a single board in tunnel dryer for this experiment compared with those on drying a stack of boards.

Steep temperature and moisture-content gradients near the surface (6°C mm^{-1} in temperature, 7.9% mm^{-1} above X_{FSP} and 2.2% mm^{-1} below X_{FSP} in moisture content) have been observed in these experiments. However, noticeable checking was not found, both by examining the surface and by cutting the board into pieces. This indicates that *Pinus radiata* is an elastic material to some extent (at least at high temperature), since brittle fracture is unlikely to occur while the material is stretched at the surface in the first stage of rapid drying and in the interior region during the later drying.

The feature of drying the sapwood board confirmed that there actually exists an evaporative front which remains close to the board surface during the initial period of drying. In the experiment, the fitted thickness of this thin dry layer is 1.1-1.3 mm, which is about 30 times that of a tracheid diameter. This idea of a thin dry layer can be further supported by the experimental data of Northway (1989). He measured temperatures on the surface and at the position 3 mm beneath. The surface temperature profile is similar to that found in this work, while the temperature 3 mm beneath the surface remains close to the centre temperature for 6 - 10 hours at the air temperature of 120/70 °C. This shows that the thickness of the thin dry layer is almost certainly less than 3 mm. However, the depth of this thin dry layer may be slightly different for different samples, for example, a depth of 0.3 - 0.5 mm have been predict in the previous work (Pang, Keey and Langrish, 1992a, 1992b) when comparing the predicted temperature with the experimental data by Miller and Simpson (1991). The depth of this thin dry layer may also be affected by the initial moisture content of green logs, the dryness of the environment and the method of sawing. The rapid drying of board surface in the environment and smoother surface will be expected to result in a thinner dry layer.

For the Runs at temperatures of 120/70 °C, it has been noticed that the temperature and the average moisture content for different samples may vary to some extent. The temperature profile in Run 9 using sample 10G is rather like heartwood, which indicates that the liquid flow towards the evaporative front is not high enough to keep the front near the surface during the initial stage of drying. By examining the sample, it was observed that the board was exactly flat-sawn and it is likely the board contained a small amount of heartwood. Since the tangential permeability is less than radial one and the permeability of heartwood is less than that of sapwood, both of these factors would reduce the liquid flow within board during drying.

During the experiments, some slight aerodynamic lift (or down draft) on the sample board was observed which somewhat affected the weight readings. For example, in Run10 (140/90 °C), the difference between the masses of sample with the air on and air off was 21.7g at the start of drying, but this difference decreased to 0.4g at the end of drying. These differences give an experiment error in the moisture contents of less 1% (M.C.).

6.4.2 Some Parameters in the Simulation

In the simulation, the wood permeabilities both for liquid and for gas flow are chosen to fit the predicted profiles to the measured ones of temperature and average moisture content. The permeability of the timber to vapour affects the drying behaviour

significantly. Highly permeable wood offers less resistance to vapour transport and has a lower inner temperature if other conditions are fixed. The fitted vapour permeability for heartwood varies from $0.2x10^{-15}$ m^2 to $0.6x10^{-15}$ m^2. This range of permeability is close to the value fitted by Stanish *et al.* (1986) for Douglas fir (*Pseudotsuga menziesii*) (1 x 10^{-15} m^{-2}). Also the values are recommended by Puiggali and Quintard (1992) who state "the best value (of intrinsic permeability) seems to be around $0.4x10^{-15}$ m^2" for unspecified pine wood. These fitted values are also close to separate findings ($0.5x10^{-15}$ m^2 for heartwood and $0.8x10^{-15}$ m^2 for sapwood) in previous reports (Pang, Keey and Langrish, 1992a, 1992b). Booker has given radial permeability of dry wood to gas flow (8.8 - $78.6x10^{-15}$ m^2) and he maintains that, for *Pinus radiata*, the tangential permeability of dry wood decreases by a factor 6 to 370 and is much lower than radial one. These differences are due to pit aspiration and influence of resin canals. When the pits have been aspirated, these paths are blocked for the moisture movement. However, on the other hand, the resin canals are cleared of deposits during high temperatures and a canal network forms for conveying the water vapour. Therefore, the dry wood will have a higher radial permeability and a lower tangential permeability under high temperatures. When the sample is sawn with the ring angle β (Chapter 4) greater than zero, the permeability normal to the drying surface may be less than the values on permeability in radial direction. Similar results have been obtained for the sapwood where both the fitted values normal to drying surface (1.0 - $1.3x10^{-15}$ m^2) and measured values in radial direction (32 - $138x10^{-15}$) are higher than those of heartwood. Booker (1990) finds that dry sapwood is much more permeable than dry heartwood. These fitted values are in agreement with this observation, but the present predictions suggest that the difference between the permeabilities of sapwood and heartwood to vapour flow is not as significant as that measured by Booker (1990). Possibly this is because the permeability of dry wood is strongly dependent on direction.

The fitted liquid permeability of green sapwood in direction normal to the drying surface (1.0 - $1.4x10^{-15}$ m^2) is close to the values measured by Kininmonth [tangential direction: $2.9x10^{-15}$ m^2; radial (earlywood): $3.8x10^{-15}$ m^2, radial (latewood): $3.1x10^{-16}$ m^2] (Kininmonth and Whitehouse, 1991). However, these are higher than the corresponding values reported by Booker (1990) (tangential direction: 1.69 to $7.74x10^{-16}$ m^2; radial direction: 0.18 to $1.68x10^{-16}$ m^2). This discrepancy may be understandable since the wood permeability is such a variable parameter that even the values measured by a single worker span a considerable range as reported by Booker (1989, 1990). Another reason for the higher liquid permeability in this work is that, when a single greenwood board is heated up, the fibre saturation point falls and the moisture is less bound (Pang, Keey,

Walker and Langrish, 1992c), so squeezing the liquid water free. This release of unbound water will increase the liquid permeability within the wood.

All permeabilities may vary from sample to sample due to the orientation of the board. Since the permeability in tangential direction is different from that in the radial direction, variation in the ring angle between radial (or tangential) direction and airstream direction will result in different nett permeabilities in the direction perpendicular to the airstream.

In the experiment at the air temperatures of 120/90 °C, the boards dried much more rapidly than the early measurement by Miller and Simpson (1991) who monitored the drying up to the point when the centre temperature starts to rise. Therefore, it is suspected that the external heat- and mass-transfer rates in this experiment are relatively higher than the drying in a commercial kiln. Further the radiation both from dryer shell and from the hot airstream affects the drying significantly in the initial period. The good match of the predicted profiles and the measured one by using higher external transfer coefficients supports this assumption.

In the simulation, the mass-transfer coefficients were chosen from the experimental values of Kho, Keey and Walker (1989, 1990). The convective heat-transfer coefficients were obtained from Chilton-Colburn analogy with radiation contribution of 20-30%. These higher values than the predictions from flat-plate experiments can be supported by the experiment of Stevens *et al.* (1956). For example, for the drying of sapwood boards in Runs from 5 to 8, values of heat-transfer coefficients of 50 to 65 (W m^{-2} K^{-1}) are used, which are in close agreement with that (55.50 W m^{-2} K^{-1}) calculated from equation (5.17). The fact that these values are higher than those used for heartwood may be due to the differences in configuration of the samples in the experiments.

When drying a sapwood board in the experiment, the board dried somewhat faster than predicted in the model by 5-15% in average moisture content between 3 to 8 hours from the start of drying. This difference is attributed to moisture loss in the grain direction at right angles to the assumed direction of moisture movement in the theoretical model.

6.5 Conclusion

From the experiment carried out at NZFRI on drying a single board in the tunnel dryer, the local temperatures, average moisture content variations and moisture gradient were determined both for heartwood and for sapwood. For heartwood, the surface temperature rises above 100°C very rapidly and the internal temperatures at different depths start to increase progressively, before which they remain close to the temperature at the centre-line of the board at about 100°C. Finally, the temperature in the centre of the board begins to rise and all the internal temperatures approach the surface temperature. The moisture content of the board decreases virtually from the beginning of the drying, except for a short induction period when the board adsorbs some water vapour from the air while the surface temperature is below the wet-bulb temperature. After 9-14 hours, depending upon the external conditions, the moisture content of the board falls close to the equilibrium value. Throughout the whole process, no period of constant drying rate has been observed.

For sapwood, the surface temperatures rise more sluggishly than heartwood and all internal temperatures (6mm, 12mm, 18mm and at mid-layer) remain close at about 100°C for a substantial period of time. The length of this period is from 6 to 8 hours according to the dry-bulb and wet-bulb temperatures of the air. During this period the moisture content decreases linearly with the elapsed time. Afterwards, the temperature and moisture content vary in the similar way to that for heartwood.

As an exception for sapwood, the temperature and moisture content profiles for Run 9 (120/90°C) are rather like heartwood, while the moisture content after 10 hours drying is 26% compared with that of 14.9% for another run (Run 5) at the same external conditions and same drying time. This clearly show the influence of the internal structural differences on the drying behaviour due to grain orientation within the sample.

The drying process of both heartwood and sapwood boards has been simulated by Pang, Keey and Langrish (1991, 1992a and 1992b) using a receding evaporative front model. The predictions are compared with the experimental data of temperature profiles at different depths and of the average moisture-content variation with time. The simulation and the measured results are in good agreement except that, in the initial stage of drying of heartwood, the predicted surface temperature rises more sluggishly. Also, the predicted moisture contents for sapwood between 3 to 8 hours from the start of drying are 5-15% higher than the measured values.

The local moisture-content profiles also agree with the predictions. For sapwood, the moisture content near the surface drops steeply below the fibre saturation point (X_{FSP}) within 8 hours while the interior is still above 40%. However, the moisture distributes more evenly after 16 hours of drying. For heartwood, the difference in moisture content between the surface and the centre of the board is less than that in sapwood since the initial moisture content for heartwood is much lower.

The simulation differs from the volume-averaged relationships derived by Southernland and colleagues (1992) in that they incorporate arbitrary fitting factors for their capillarity and diffusion coefficients to force agreement between experimental and theoretical profiles of temperature and moisture content. These fitting factors are many orders of magnitude different from unity. The receding front model we discuss, on the other hand, contains no fitting parameters apart from coefficients determined from other experiments and is based on a physical picture of pit aspiration.

6.6 References

1. Ashworth, J.C. 1977. The Mathematical Simulation of Batch-Drying of Softwood Timber. PhD. Thesis. Chemical Engineering, University of Canterbury, Christchurch, New Zealand.

2. Beard, J.N., Rosen, H.N. and Adesanya, B.A. 1985. Temperature Distribution in Lumber during Drying. *Wood Sci. and Tech.* 19: 277-286.

3. Booker, R.E. and Langrish, T.A.G. 1992. The Percentage Saturation of Sapwood and Heartwood from *Pinus radiata* on the Central Plateau of New Zealand. to be submitted to *the Journal of Experimental Botany.*

4. Booker, R.E. 1989. Hypothesis to Explain the Characteristic Appearance of Aspirated Pits. *Proc. 2nd Pacific Region Wood Anatomy Conference*, Forest Product Research and Development Institute, Laguna, Philippines.

5. Booker, R.E. 1990. Changes in Transverse Wood Permeability during the Drying of *Dacrydium cupressinum* and *Pinus radiata. New Zealand J. Forest Sci.* 20(20) pp231-244.

6. Cown, D.J. and McConchie, D.L. 1983. Radiata Pine Wood Properties Survey (1977-1982). New Zealand Forest Service, Forest Research Institute Bulletin No. 50, Rotorua, New Zealand.

7. Haslett, T. and Simpson, I. 1990. Multi-Client Drying Project Comparison HT and Conventional Drying. Wood Drying No. 10, Forest Research Institute, Rotorua, New Zealand.

8. Keey, R.B. 1991. "*Drying of Loose and Particulate Materials*". Hemisphere Publishing Co. New York.

9. Keey, R.B. and Ashworth, J.C. 1979. The Kiln Seasoning of Softwood Timber. *Chemical Engineer*, No.347, pp593-602.

10. Kho, P.C.S., Keey, R.B. and Walker, J.C.F. 1989. Effect of Minor Board Irregularities and Air Flows on the Drying Rate of Softwood Timber Board in Kilns. *Proc. 2nd IUFRO International Wood Drying Symposium*, Seattle, pp150 - 157.

11. Kininmonth, J.A. and Whitehouse, L.J. 1991. "*Properties and Use of New Zealand Radiata Pine, Vol. 1: Wood Properties*", New Zealand Ministry of Forestry, Forest Research Institute, Rotorua, New Zealand.

12. Kininmonth, J.A. 1970. An Evaluation of Timber Drying Problems in Terms of Permeability and Fine Structure. PhD Thesis, University of Melbourne, Australia.

13. Langrish, T.A.G., Kho, P.C.S., Keey, R.B. and Walker, J.C.F. 1992. Experimental Measurements and Numerical Simulation of Local Mass-Transfer Coefficients in Timber Kiln. *Drying Technology*, Vol.10 (3), pp753-782.

14. Langrish, T.A.G. 1993. Private Communication.

15. Northway, R. 1989. Moisture Profiles and Wood Temperature during Very High-Temperature Drying of *Pinus Radiata* Explain Lack of Degrade. *Proc. 2nd IUFRO International Wood Drying Symposium*, Seattle, pp24 - 28.

16. Pang Shusheng, Keey, R.B. and Langrish, T.A.G. 1991. Modelling of the High-temperature Kiln Drying of *Pinus radiata* Boards. Research Report No1, Chemical and Process Engineering, University of Canterbury, Christchurch, New Zealand (unpublished).

17. Pang Shusheng, Keey, R.B. and Langrish, T.A.G. 1992a. Modelling the Temperature Profiles within Boards during the High-Temperature Drying of *Pinus Radiata* Timber. in Mujumdar, A.S. (ed.): *Drying'92*, Elsevier, Part A: pp 417 - 433.

18. Pang Shusheng, Keey, R.B. and Langrish, T.A.G. 1992b. Moisture Movement in Softwood Timber at Elevated Temperatures. *Proc. 3rd IUFRO Wood Drying Symposium*, Vienna, Austria, pp112-122.

19. Pang Shusheng, Keey, R.B., Walker, J.C.F. and Langrish, T.A.G. 1992c. The Stress Development and Check Formation within Boards of *Pinus Radiata* during High-Temperature Drying. Research Report No3, Chemical and Process Engineering, University of Canterbury, Christchurch, New Zealand (unpublished).

20. Puiggali, J.R. and Quintart, M. 1992. Properties and Simplifying Assumptions for Classical Drying Model. in Mujumdar, A.S. (ed.): "*Advances in Drying*", Vol.5, Hemisphere Publishing Co. New York. pp109-143.

21. Stevens, W.C., Johnston, D.D. and Pratt, G.H. 1956. An Investigation into the Effect of Air Speed on the Transference of Heat from Air to Water. *Timber Technology,* Vol.64, No.2208, pp537-539.

22. Southernland, J.W., Turner, I.W. and Northway, R.L. 1992. A Theoretical and Experimental Investigation of the Convective Drying of Australia *Pinus Radiata. Proc. 3rd IUFRO Wood Drying Symposium*, Vienna, Austria.

23. Williams, D.H. and Kininmonth, J.A. 1984. High-Temperature Kiln Drying of Radiata Pine Sawn Timber. New Zealand Forest Service, Forest Research Institute Bulletin No. 73, Rotorua, New Zealand.

Chapter 7

Kiln-Wide Analysis of Drying A Stack of Boards

7.1 Introduction

For a designer or an operator of timber drying kilns, it is necessary to follow or re-evaluate the worth of batch-drying schedules. A reliable method is required to predict the moisture content and temperature fields as functions of time and various locations through the dryer. To dry the timbers, these are usually piled in stacks with a width of 2.4 m in a high-temperature kiln in New Zealand. The separating stickers are usually 25 mm or thicker (Walker, 1993). During drying, the variations in moisture content across a stack have been observed to be caused by the changes in external conditions as well as the differences in internal structure of the boards. As the air flows across over the boards, the hot air transfers heat to the boards to evaporate the moisture and at the same time carries away the moisture as vapour from the board. Thus, the dry-bulb temperature decreases and air humidity increases along the airflow direction. It is also observed that the external mean mass-transfer coefficient decreases and tends towards an asymptotic value over the following boards behind the front two or three rows whereas the mean mass-transfer coefficient over the first row of boards is the significantly higher than the second one in value (Kho, Keey and Walker, 1989; Langrish, *et al.*, 1992). Consequently, the boards in the front few rows of the stack dry rapidly while those towards the end of the stack dry slowly.

In an analysis of convective batch drying, van Meel (1958) suggested that a common normalised curve might describe the variation of drying rates with moisture content through the whole dryer. This curve has become known as *the characteristic drying curve.* Keey (1991) has reviewed recently drying kinetics data published by a number of workers and has found that the concept holds well for particulate materials below 20mm in diameter over a practical range in process variables (air temperature, humidity, velocity), but its application is uncertain for bulk materials. However, Ashworth (1977) found the concept useful for slabform material, such as timber boards, provided the characteristic drying curve is derived from data on material of the same thickness.

Conventionally, the characteristic drying curve describes a functional relationship between a *relative drying rate f* and a *normalised moisture content* Φ, which are defined by the expressions:

$$f = \frac{N_v}{N_{cr}} \tag{7.1}$$

$$\text{and } \Phi = \frac{(X - X_e)}{(X_{cr} - X_e)} \tag{7.2}$$

where N_v and X are the drying rate and mean moisture content at any location, the drying rate N_{cr} and moisture content X_{cr} are the values at the critical point and X_e is the equilibrium moisture content.

In the drying of timber in a batch kiln, by coupling the rate and conservation expressions and by introducing the dimensionless parameters for humidity potential Π, moisture content Φ, time of drying θ and distance ζ, Keey (1978, 1979) and Ashworth (1979) derive a set of equations to relate moisture content and drying rate to drying time and location in a dryer:

$$\frac{\partial \Phi}{\partial \theta} = \frac{\partial \Pi}{\partial \zeta} \tag{7.3}$$

$$-\frac{\partial \Phi}{\partial \theta} = \Pi f \tag{7.4}$$

If the relationship between normalised moisture content (Φ) and relative drying rate (f) is known, one can predict the kiln-wide variations of moisture content and drying rate by solving the above equations.

Recently, a number of mathematical models have been developed to simulate the drying process of timber in a kiln as discussed in chapter 3 and by other authors (Pang *et al.* 1992, Perré *et al.* 1988, Stanish *et al.* 1986). In these models, differential equations are set up to describe the heat and mass-transfer rates from which temperature and moisture-content profiles can be determined throughout the course of drying. However, coupling these equations with those to describe the varying air conditions within the kiln produces an equation set too complicated and computationally too slow for the purpose of analysing commercial kiln behaviour (Kayihan, 1993). So we need to explore a simplified method to model the kiln behaviour with sufficient accuracy for the evaluation or improvement of the kiln design and operation.

In this chapter, the drying kinetics of heartwood and sapwood will firstly be investigated and the simulation of drying process across a kiln will then be carried out. In this way, the changes in external conditions can be expressed quantitatively and the kiln-wide moisture-content variations through a stack predicted.

7.2 The Drying Kinetics of Heartwood Boards

7.2.1 The Drying-Rate Curve of Heartwood Boards

From the mathematical model discussed in Chapter 3, the process of drying 50 mm thick *Pinus radiata* heartwood boards under high temperatures can be simulated. One feature of the drying is that the liquid moisture movement on drying is negligible due to pit aspiration during the formation of heartwood while the tree was growing. A typical drying curve from these simulations is shown in Figure 7.1.

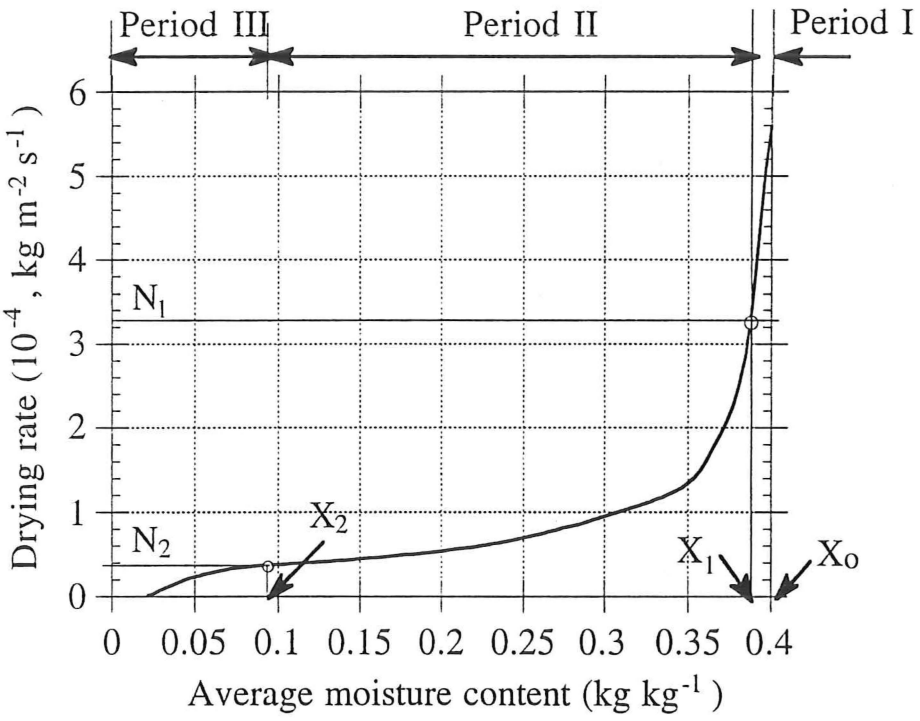

Figure 7.1 The drying curve for impermeable heartwood of *Pinus radiata* at dry-bulb/wet-bulb temperatures of 120/70°C. The air velocity is 5 m s^{-1}.

The whole process of the drying can be divided into three periods, preceded by a very short preheating period while the board is heated up. Initially, the surface temperature of the board reaches the wet-bulb temperature and the liquid moisture at the surface evaporates to diffuse into the airstream. At this time the drying rate is the maximum, but

as there is no liquid water flow towards the surface, the evaporative front quickly withdraws into the board. During the first period, the influence of internal resistance to moisture vapour transport gradually comes to dominate over the external resistance, and the drying rate drops sharply. By the end of this period, the evaporative front has withdrawn to a short distance from the surface (less than 1mm) and this period lasts only 5-15 minutes. The subsequent course of drying can be represented by two falling-rate periods, which are called period two and period three respectively in this thesis. In period two, the evaporative front continues to recede into the board at a rate which is not primarily determined by the external conditions. This period may last 8 to 14 hours according to the drying temperature. Finally, once the evaporative front reaches the mid-plane of the board, the drying is dominated by bound water diffusion. This is the third period of drying.

The first critical point is defined as the time when the evaporative front has withdrawn to a short distance from the surface (about 0.5 mm) where the internal resistance to moisture vapour flow becomes dominant. The corresponding mean moisture content for the whole board at this time is X_1 and the drying rate is N_1. The second critical point is defined when the front has reached the mid-plane, and the corresponding mean moisture content and drying rate are X_2 and N_2 respectively.

With the impermeable heartwood, since the duration of the first period is insignificantly short, it will not be distinguished from the second period except that the drying rate at the end of the first period is used as the initial value for the analysis. Therefore, the whole drying process can be described by two falling-rate periods. As discussed above, the physical characteristics of drying in the third period are different from that in the second period, and the drying rate drops rapidly when the average moisture content falls below the second critical point. In the following discussion, it will be postulated that two separate characteristic drying curves can be derived to express the drying in period two and period three.

Once the evaporative front has receded into the board, the moisture content within the outer drier zone is below the fibre-saturation point, whereas deeper within the board beyond the evaporative front, the moisture content will be still almost at the initial value, X_o. For simplicity, the relatively small moisture-content variations throughout each zone will be neglected, the moisture content everywhere being equal to the mean value in each zone. Let X_2 be the mean moisture content in the drier zone, and X_o be that in the wetter zone (Figure 7.2). When the evaporative front reaches the board's mid-plane the mean moisture content is X_2 and thereafter the mean moisture content is reduced progressively below X_2.

7.2.2 The Characteristic Drying Curves

With an impermeable timber, such as heartwood of *Pinus radiata*, the first period of drying is so brief that it can be ignored. Therefore the drying is considered to consist solely of period two and period three.

7.2.2.1 The second period of drying

In the second period of drying, the normalised moisture content and relative drying rate are defined as

$$\Phi_1 = \frac{X - X_2}{X_1 - X_2} \qquad X_2 < X < X_1 \tag{7.5}$$

$$f_1 = \frac{N_v - N_2}{N_1 - N_2} \qquad N_2 < N_v < N_1 \tag{7.6}$$

where X_1, X_2 and N_1, N_2 are the moisture contents and drying rates at the first and second critical points respectively.

During the second period of drying, the total moisture losses from a wet board are the sum of evaporation fluxes of liquid water at the evaporative front, N_E, and bound water in the dry zone, N_B. Since in the second period of drying the liquid water evaporation dominates, it is assume that the rate of bound water evaporation and the mean moisture content in the dry zone are the same as those at the right beginning of the third period of drying (the values at the second critical point). If the Fick's law is used to describe the moisture vapour movement and it is assume that by the end of first period the evaporative front has reached a short distance ξ_o from the board surface, then the drying rate at first critical point N_1 can be calculated to a first approximation as follows:

$$N_1 = N_{1E} + N_B = N_{1E} + N_2 \tag{7.7}$$

$$\text{and } N_1 = (p^v_{\xi_o} - p^v_G)/\left[\frac{1}{\beta} + \frac{\xi_o}{E_v'}\right] = \beta'(p^v_{\xi_o} - p^v_G) \tag{7.8}$$

$$\text{where } \beta' = 1/\left[(1/\beta) + (\xi_o/E_v')\right] \tag{7.8'}$$

From calculations in Chapter 6, it has been found that the drying rate at the second critical point can be related to that at the first critical point by:

$$N_2 = \alpha N_1 \tag{7.9}$$

where the factor α is from 0.09 to 0.13 with an average value of 0.11.

Therefore, the evaporation flux of liquid water at the first critical point is:

$$N_{1E} = N_1 - N_2 = (1 - \alpha)\,\beta'(p^v_{\xi o} - p^v_G) \tag{7.10}$$

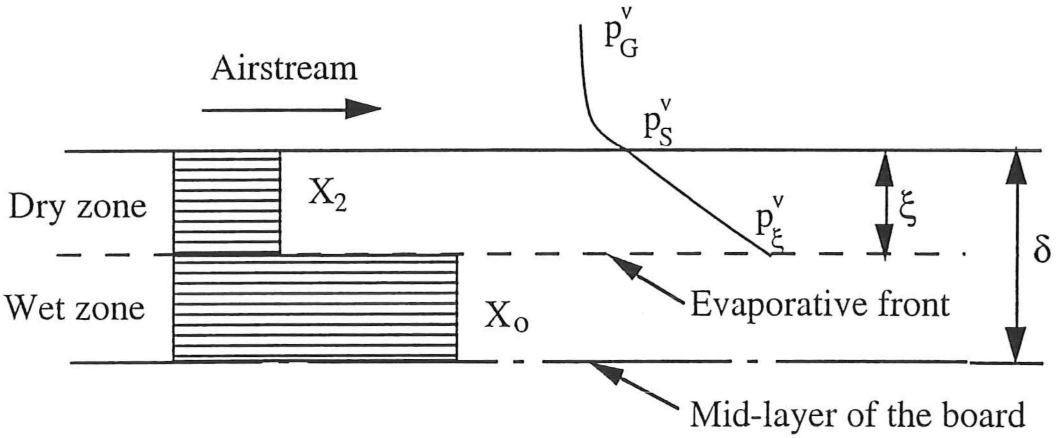

Figure 7.2 The receding evaporative front in a board during drying.

If the mass-transfer coefficient β' is considered as a hypothetical external mass-transfer coefficient, then the evaporation flux of liquid water is obtained in the second period as:

$$N_E = N_v - N_2 = \left\{ (p^v_\xi - p^v_G) / \left[\frac{1}{\beta} + \frac{\xi}{E_v} \right] \right\} - \alpha\,\beta'(p^v_{\xi o} - p^v_G) \tag{7.11}$$

From the above relationships, it is seen that the relative drying rate defined for the second period is equal to the ratio of evaporation of the liquid flux during drying to that at first critical point, so

$$f_1 = \frac{N_v - N_2}{N_1 - N_2} = \frac{N_E}{N_{1E}}$$

$$= \frac{1}{1 - \alpha} \left\{ (p^v_\xi - p^v_G) / \left[(p^v_{\xi o} - p^v_G)\,\beta' \left(\frac{1}{\beta} + \frac{\xi}{E_v} \right) \right] - \alpha \right\} \tag{7.12}$$

By using the relationship between β and β' in equation (7.8') the term $\beta'[(1/\beta) + (\xi/E_v)]$ in equation (7.12) can be rearranged for further calculation as:

$$\beta'\left[\frac{1}{\beta}+\frac{\xi}{E_v}\right] = 1 + \beta'\left[\frac{\xi-\xi_o}{E_v}\right] \qquad (7.12')$$

From Figure 7.2, where the initial moisture content is supposed to be uniformly distributed through the wet-zone and the mean moisture content in the dry zone is X_2, it is found that

$$\xi X_2 + (\delta - \xi)X_o = \delta X$$

and when $\xi = \xi_o$, $\xi_o X_2 + (\delta - \xi_o) X_o = \delta X_1$

$$\text{so, } \frac{\xi}{\delta} = 1 - (1 - \frac{\xi_o}{\delta})\Phi_1 \qquad (7.13)$$

If $\xi_o << \delta$, equation (7.13) becomes

$$\frac{\xi}{\delta} = 1 - \Phi_1 \qquad (7.13')$$

This relationship indicates that the normalised moisture content can be interpreted by the relative distance of evaporative front from the board surface which in turn reflects the resistance to moisture vapour movement in the drier zone.

By plotting p_ξ^v against the relative distance of the evaporative front from the board surface ξ/δ (Figure 7.3) for different external conditions, it is found that the curves have a similar shape, except that the values of the pressure are higher for higher dry-bulb and wet-bulb temperatures. This suggests that the term $(p_\xi^v - p_G^v)/(p_{\xi o}^v - p_G^v)$ in equation (7.12) may be correlated as a function of ξ/δ and independent of external conditions. If this ratio of vapour partial pressure differences is assumed to have the form of power function, then

$$\frac{p_\xi^v - p_G^v}{p_{\xi o}^v - p_G^v} = A(1 - \Phi_1)^m + B \qquad (7.14)$$

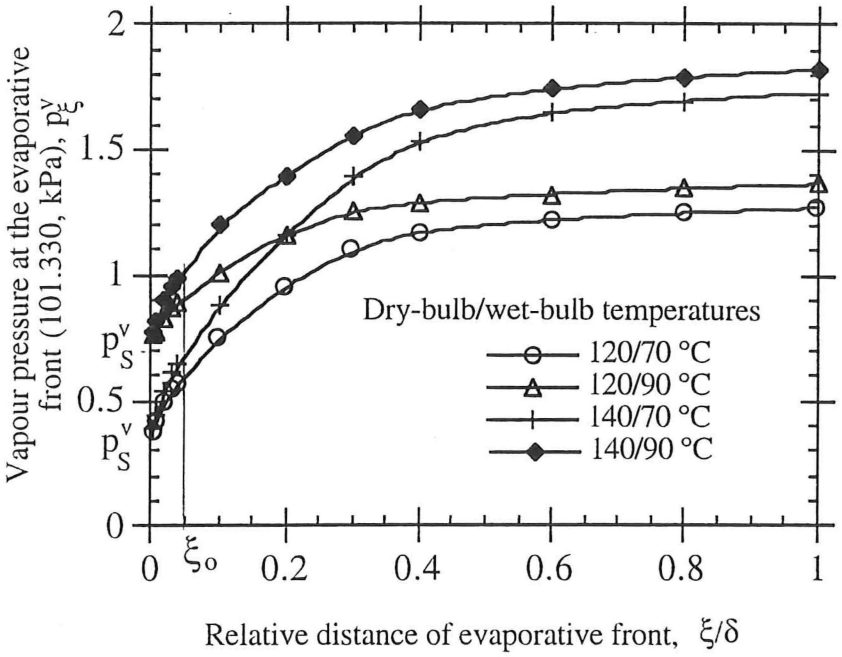

(a). the vapour partial pressure at the evaporative front as it withdraws in wood.

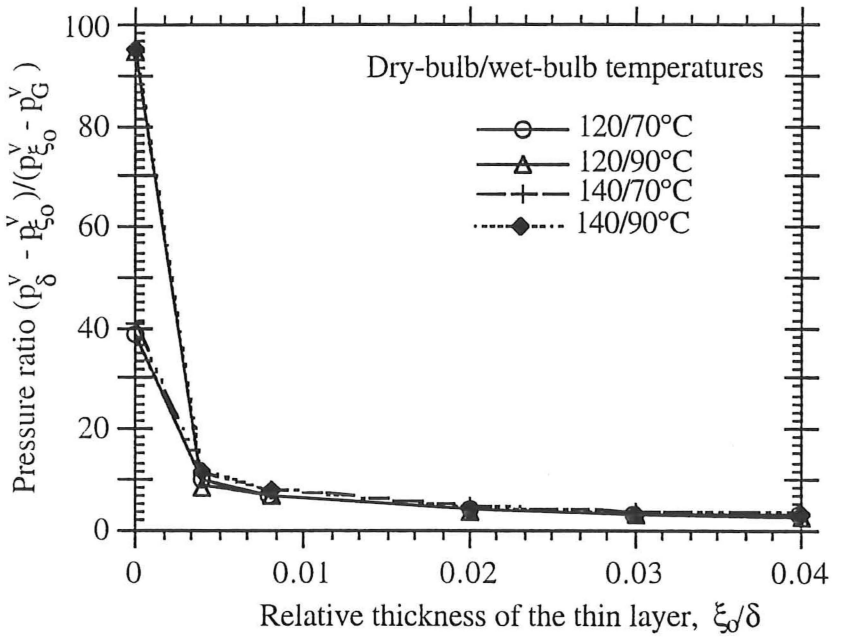

(b). the value of term *A* as a pressure ratio varies with the thickness of the thin layer

Figure 7.3 The vapour partial pressure at the evaporative front and the variation of term *A* as a pressure ratio in equation (7.16).

Using the initial condition $\Phi_1 = 1$ when $\xi = \xi_o$ at the start of second period of drying, equation (7.14) becomes

$$\frac{p^v_\xi - p^v_G}{p^v_{\xi o} - p^v_G} = 1 = B, \tag{7.15}$$

At the end of the second period $\Phi_1 = 0$, so

$$\frac{p^v_\delta - p^v_G}{p^v_{\xi o} - p^v_G} = A + B = A + 1$$

This equation can be rearranged as

$$A = \frac{p^v_\delta - p^v_{\xi o}}{p^v_{\xi o} - p^v_G} \tag{7.16}$$

In order to find the value of parameter A, the relative distance ξ_o/δ is varied over a possible range in values as shown in Figure 7.3b. Initially, when ξ_o/δ is zero, the values for A in equation (7.16) range widely from 38.8 to 95.6 depending on the external drying conditions, but as ξ_o/δ is increased, the values of A rapidly converge so that by $\xi_o/\delta =$ 0.02, A lies between 3.68 to 4.39. This condition corresponds to the end of the first period of drying which lasts only 5-15 minutes and at this point the evaporative front is 0.5 mm beneath the surface. Conceptually, the second period of drying starts from this point, although with heartwood it is not clearly distinguished from the first period which is so insignificantly short. To characterise the subsequent drying, it is sufficiently accurate to take $\xi_o/\delta = 0.02$ and A as 4.0 at the first critical point.

By using the above relationships, the relative drying rate can be related to normalised moisture content as

$$f_1 = \frac{1}{1 - \alpha}\left[\frac{4.0(1 - \Phi_1)^m + 1}{1 + \frac{\beta'\delta}{E_v}(1 - \Phi_1)\left(1 - \frac{\xi_o}{\delta}\right)} - \alpha\right] \tag{7.17}$$

In above discussion, E_v' and E_v are the effective permeabilities of wood at the beginning of the second period and at any time in subsequent drying respectively. These permeabilities can be related to the normally measured permeability K_v by the identities

$$E_v = \rho_v \frac{K_v}{\mu_v} \text{ and } E_v' = \rho_v' \frac{K_v}{\mu_v'} \tag{7.18}$$

in which ρ_v and μ_v are density and viscosity of the water vapour and ρ_v' and μ_v' are the values at temperature and pressure corresponding the beginning of the second period of drying.

At temperatures of 70 to 100°C which cover the range of inner temperature values for different external conditions applied, E_v' varies from 3.65×10^{-12} to 9.92×10^{-12} s for *Pinus radiata* heartwood. In this case, ξ_o/E_v' is 1.37×10^8 to 5.04×10^7 m s^{-1}. The external mass-transfer coefficient β is taken as 16×10^{-8} s m^{-1} which is the value directly measured by Kho *et al.* (1989, 1990) at the air velocity of 5 m s^{-1}. Since $1/\beta$ is only 0.05 to 0.12 times (with an average value of 0.083) that of ξ_o/E_v', then, the total resistance to moisture movement β' can be related to ξ_o/E_v' from equation (7.8') as

$$\beta' = \frac{1}{(0.083 + 1)\frac{\xi_o}{E_v'}} = 0.923 \frac{E_v'}{\xi_o}$$

Therefore, the term $\delta\beta'/E_v$ in equation (7.17) becomes

$$\frac{\delta\beta'}{E_v} = 0.923 \frac{\delta}{\xi_o} \frac{E_v'}{E_v} = 46.2 \frac{\rho_v' \mu_v}{\rho_v \mu_v'} = 46.2 \frac{(p^v_{\xi o})' T_\xi}{(p^v_\xi) T_{\xi o}'} \frac{\mu_v}{\mu_v'} = 46.2\, u\left(\frac{\xi - \xi_o}{\delta}\right) \tag{7.20}$$

If the function $u\left(\frac{\xi - \xi_o}{\delta}\right)$ is defined as

$$u\left(\frac{\xi - \xi_o}{\delta}\right) = 1 - C'\left[\frac{\xi - \xi_o}{\delta}\right]^n = 1 - C(1 - \Phi_1)^n \tag{7.21}$$

On inserting this relationship and the value of factor α (0.11) into equation (7.17) for the case of $\xi_o/\delta = 0.02$, it is obtained that

$$f_1 = \frac{4.53(1 - \Phi_1)^m + 1.12}{1 + 45.3\,[1 - C(1 - \Phi_1)^n]\,(1 - \Phi_1)} - 0.12 \tag{7.22}$$

By fitting the simulation results to the correlation of equation (7.22) using the least square technique, the coefficients m, C and n are found to be 0.34, 0.22 and 0.33 respectively. Therefore, the relative drying rate for heartwood board of *Pinus radiata* when dried at elevated temperatures in the range of 110 to 140°C can be related to normalised moisture content as follows:

$$f_1 = \frac{4.53(1 - \Phi_1)^{0.34} + 1.12}{1 + 45.3\,[1 - 0.22(1 - \Phi_1)^{0.33}]\,(1 - \Phi_1)} - 0.12 \qquad (7.23)$$

When the evaporative front has reached the mid-layer of the boards, the third period of drying starts. At this point, $N_v = N_2$ and $X = X_2$. Simulation results show that the values of X_2 vary from 0.071 kg kg^{-1} at 140/70°C to 0.12 kg kg^{-1} at 110/90°C. This range of moisture content is coincident with commonly required final values for commercial products. However, lower moisture contents are sought for certain boards grades or export markets. For this reason the third period of drying is explored.

7.2.2.2 The third period of drying

In this period, the normalised moisture content and relative drying rate are defined in the usual way, but the critical values are taken as those at second critical point:

$$\Phi_2 = \frac{X - X_e}{X_2 - X_e} \qquad X_2 > X > X_e \qquad (7.24)$$

$$\text{and } f_2 = \frac{N_v}{N_2} \qquad N_2 > N_v > 0 \qquad (7.25)$$

In equation (7.25), the the equilibrium moisture content, X_e, can be found from the literature (Kininmonth, 1992; USDA, 1988) or calculated by the correlation proposed in Chapter 4 for *Pinus radiata*. The magnitude of the values depends upon the temperature and the relative humidity of the air.

From the results of the mathematical simulation, a correlation has been fitted between normalised moisture content and relative drying rate as

$$f_2 = - a\,\Phi_2^2 + (1 + a)\,\Phi_2 \qquad (7.26)$$

where the coefficient a is found to be 1.017. Therefore, the relationship between relative drying rate and normalised moisture content in the second period of drying can be expressed as

$$f_2 = -1.017\,\Phi_2^2 + 2.017\,\Phi_2 \qquad (7.27)$$

7.2.3 The critical values

Since the drying time when the evaporative front reaches the distance ξ_o from the board surface is very short (only 5-15 minutes), the mean moisture content in board at the first critical point is almost the same as the initial value with a reduction of 0.006 - 0.010 kg kg^{-1} in value. Therefore the first critical moisture content X_1 is practically taken as the initial moisture content X_o without inducing significant error in the results.

If the drying rate at the first critical point is related to the humidity potential $(Y_S - Y_G^o)$ by the following equation,

$$N_1 = \beta'(p_{\xi_o}^v - p_G^v) = \varphi K_o\,(Y_S - Y_G^o) \qquad (7.28)$$

and the mass-transfer coefficient K_o is estimated from the expression given by Keey (1978) for the coefficient F based on molar fluxes,

$$K_o = F\,M_G \qquad (7.29)$$

then, the correction factor φ can be predicted as

$$\varphi = \frac{N_1}{K_o(Y_S - Y_G)} \qquad (7.30)$$

When F is taken as 0.8 mol m^{-2} s^{-1}, which has been directly measured by Kho Keey and Walker (1989, 1990) at the air velocity of 5 m s^{-1} and M_G as 0.0289 kg mol^{-1}, K_o is calculated to be 0.026 kg m^{-2} s^{-1}. From the predicted drying rate at $\xi = \xi_o$, the value of φ is found to be only a function of wet-bulb temperature and independent of the dry-bulb temperatures of the air. It can thus be expressed as

$$\varphi = -4.71x10^{-4}\,(T_{wK} - 273.15)^2 + 0.0673\,(T_{wK} - 273.15) - 1.99 \qquad (7.31)$$

The drying rate at the second critical point has been given in equation (7.9) with the averaged value of 0.11 for the factor α, so

$$N_2 = 0.11\, N_1 \tag{7.9a}$$

The critical moisture content X_2 varies with both the dry-bulb and wet-bulb temperatures. The influence of these is expressed in the following fitted equation

$$X_2 = 1.435x10^{-5}\, T_{DK}^2 - 0.003410 T_{DK} + 0.01092\, T_{wK} - 2.609x10^{-5}\, T_{DK}\, T_{wK} - 1.019 \tag{7.32}$$

7.3 The Drying Kinetics of Sapwood Boards

7.3.1 The Drying-Rate Curve of Sapwood Boards

The proposed mathematical model in Chapter 3 can also be used to simulate the drying process of sapwood boards. A plot of the averaged drying rate for a sapwood board against average moisture content predicted by the model is shown in Figure 7.4a, while the variation of drying rate with time is given in Figure 7.4b. In this example, the external conditions are: dry-bulb/wet-bulb temperatures are 120/70°C, the air velocity is 5 m s^{-1}. From the drying-rate curve, the drying process can be divided into three periods:

(a) The evaporative plane remains near to the surface and the drying rate remains relatively constant once the board has been warmed up to approximately the wet-bulb temperature (the first period).
(b) The evaporative plane recedes into the board and the drying-rate curve is concave downwards in form. This period is regarded as the first falling-rate drying period (second period).
(c) Bound water diffusion controls and the drying rate falls rapidly with diminishing moisture content until the drying rate is zero when the timber is at equilibrium with the airstream. This stage is called the second falling-rate drying period (period three).

On comparing Figure 7.4a with Figure 7.1, it can be seen that the first period of drying for sapwood is more extensive than for heartwood. Once the board has been warmed up, the drying rate is remained at a relatively high level. The drying rate in the second period for sapwood is higher than that for heartwood due to the liquid flow towards the evaporative front.

For sapwood drying, the first critical point is defined as a point when the evaporative plane starts to recede into the wood leaving the thin drying layer. This is the point when

the first falling-rate period starts. Similarly, we define the second critical point as the point when the first falling-rate period ends and the second falling-rate period starts. Then the characteristic drying curve for sapwood can be obtained in the same way as that for heartwood.

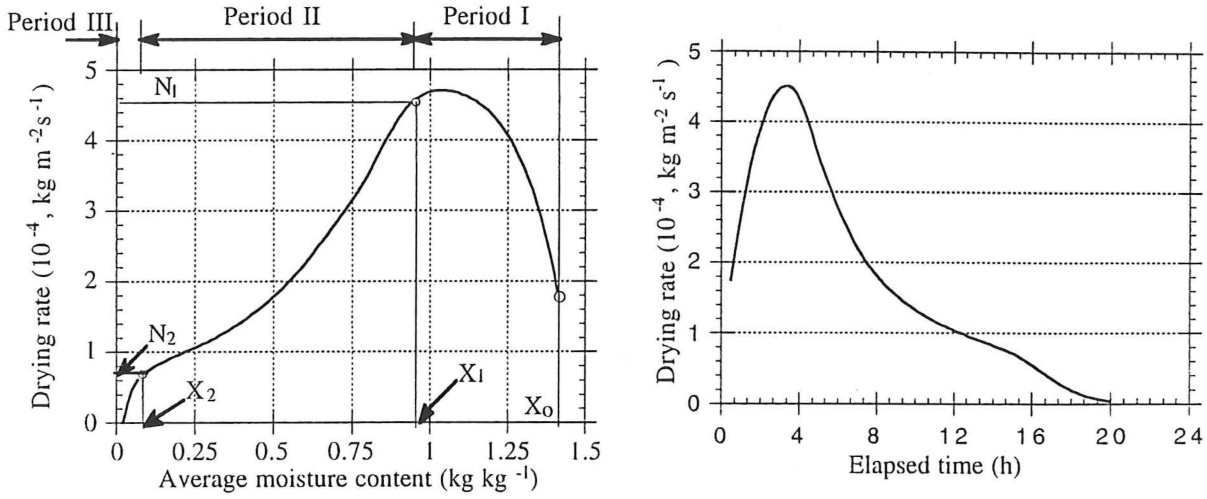

(a) variation of drying rate with average moisture-content

(b) variation of drying rate with elapsed time

Figure 7.4 The drying-rate curve for sapwood of *Pinus radiata* at dry-bulb/wet-bulb temperatures of 120/70°C. Air velocity is 5 m s^{-1}.

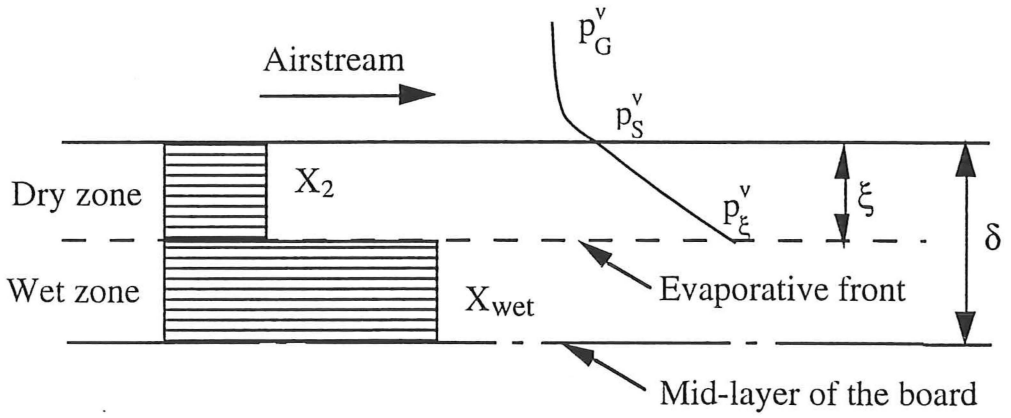

Figure 7.5 The receding evaporative front in a sapwood board during drying.

7.3.2 The Characteristic Drying Curve for Sapwood Boards

7.3.2.1 The first period of drying

If the normalised moisture content (Φ) and relative drying rate (f) in the first period of drying for sapwood are defined in the way as that of second period of drying for heartwood, then the values of Φ and f can be obtained as follows:

$$\Phi = \frac{X - X_2}{X_1 - X_2} > 1 \qquad X_o > X > X_1 \tag{7.33}$$

$$\text{and } f = \frac{N_v - N_2}{N_1 - N_2} = 1 \qquad N_v = N_1 \tag{7.34}$$

This procedure ignores the effect of thermal induction and the slow fall in drying rate from the maximum.

7.3.2.2 The second period of drying

In the second period of drying, the similar definition of normalised moisture content and relative drying rate as that for heartwood will also be used,

$$\Phi_1 = \frac{X - X_2}{X_1 - X_2} \qquad X_2 < X < X_1 \tag{7.5}$$

$$\text{and } f_1 = \frac{N_v - N_2}{N_1 - N_2} \qquad N_2 < N_v < N_1 \tag{7.6}$$

Thus the relationships of equations (7.7) to (7.11) can be applied to sapwood. The relative drying rate in this period is calculated by

$$\begin{aligned} f_1 &= \frac{N_v - N_2}{N_1 - N_2} = \frac{N_E}{N_{1E}} \\ &= \frac{1}{1 - \alpha}\left\{ (p^v_\xi - p^v_G) \Big/ \left[(p^v_{\xi o} - p^v_G)\, \beta' \left(\frac{1}{\beta'} + \frac{\xi - \xi_o}{E_v} \right) \right] - \alpha \right\} \\ &= \frac{1}{1 - \alpha}\left\{ \omega \Big/ \left[1 + \beta' \left(\frac{\xi - \xi_o}{E_v} \right) \right] - \alpha \right\} \end{aligned} \tag{7.35}$$

The ratio of vapour partial pressure differences $\omega = (p^v_\xi - p^v_G)/(p^v_{\xi_o} - p^v_G)$ can also be expressed as a function of normalised moisture content as follows:

$$\omega = 1.731\,(1 - \Phi_1)^m + 1 \qquad (7.36)$$

Since at the first critical point, the liquid water at the evaporative plane is no longer funicular, it may be assumed that the moisture content in the wet zone at this point is relatively uniformly distributed and remains unchanging in the first falling-rate period. Then from Figure 7.5, one has

$X = X_2$, when $\xi_o > \xi > 0$,
and
$X = X_{wet}$, when $\delta > \xi > \xi_o$

When the evaporative front remains at the position where $\xi = \xi_o$, the moisture balance over the half board yields

$$\delta X_1 = \xi_o X_2 + X_{wet}(\delta - \xi_o) \qquad (7.37)$$

With the evaporative front withdrawing further ($\delta > \xi > \xi_o$), the corresponding relationship is

$$X\delta = \xi X_2 + (\delta - \xi)X_{wet} \qquad (7.37a)$$

Therefore the relationship between normalised moisture content and the depth of the evaporative plane is obtained as:

$$\frac{\xi}{\delta} = 1 - (1 - \frac{\xi_o}{\delta})\,\Phi_1, \quad \frac{\xi - \xi_o}{\delta} = (1 - \frac{\xi_o}{\delta})(1 - \Phi_1) \qquad (7.38)$$

Using this relationship, the term $\beta'[(\xi-\xi_o)/E_v]$ in equation (7.12') can be rewritten as

$$\beta'\left[\frac{\xi-\xi_o}{E_v}\right] = \left[\frac{\xi-\xi_o}{E_v}\right]/\left\{\frac{1}{\beta} + \frac{\xi_o}{E_v'}\right\} = \left[\frac{\xi-\xi_o}{\xi_o}\right]/\left\{E_v\left[\frac{1}{\beta\xi_o} + \frac{1}{E_v'}\right]\right\}$$

$$= \left[\frac{\xi-\xi_o}{\delta}\right]\frac{\delta}{\xi_o}\,w'\left(\frac{\xi-\xi_o}{\delta}\right) = \left[\frac{\xi-\xi_o}{\delta}\right]\frac{\delta}{\xi_o}\,w(1 - \Phi_1)$$

$$= (1 - \frac{\xi_o}{\delta})(1 - \Phi_1)\frac{\delta}{\xi_o}\,w(1 - \Phi_1) \qquad (7.39)$$

The function $w(1 - \Phi_1)$ is assumed to have a form as follows:

$$w(1 - \Phi_1) = C' \exp[n(1- \Phi_1)] \tag{7.40}$$

In the drying of 50 mm thick sapwood board, α is taken as 0.181 and ξ_o as 1.1mm. On inserting these values and equations (7.39) into equation (7.35), the relationship between normalised moisture content and relative drying rate is obtained as:

$$f_1 = \frac{2.11\ (1 - \Phi_1)^m + 1.22}{1 + C\ (1- \Phi_1)\ exp[n(1- \Phi_1)]} - 0.22 \tag{7.41}$$

where $C = C' \delta / \xi_o$.

By fitting the above correlation to the simulation results from the mathematical model, the values of coefficients m, n and C are found to be 0.84, 0.98 and 3.80 respectively. Therefore, equation (7.41) becomes:

$$f_1 = \frac{2.11\ (1 - \Phi_1)^{0.84} + 1.22}{1 + 3.80\ (1- \Phi_1)\ exp[0.98(1- \Phi_1)]} - 0.22 \tag{7.42}$$

7.3.2.3 The third period of drying

If the normalised moisture content and relative drying rate for third period are defined in the same way as that for heartwood (equations 7.24 and 7.25), then the fitted correlation for relative drying rate against normalised moisture content is obtained as

$$f_2 = - 1.12\ \Phi_2^2 + 2.12\ \Phi_2 \tag{7.43}$$

7.3.3 The critical values

When the drying rate at the first critical point is related to the humidity potential $(Y_S - Y_G^o)$ by the equation (7.28) and the mass-transfer coefficient K_o is taken as 0.026 kg m^{-2} s^{-1} for the air velocity of 5 m s^{-1}, the influence of wet-bulb temperature of the airstream can be expressed by a correction factor φ, which is predicted as:

$$\varphi = 0.581 - 0.00563\ (T_{wK} - 343.15) - 0.00043\ (T_{wK} - 343.15)^2 \tag{7.44}$$

The moisture contents at the first and the second critical points are functions of both dry-bulb and wet-bulb temperatures of the airstream, which can be calculated from:

$$X_1 = -2.84\times10^{-5}\, T_{DK}^2 - 0.00160 T_{DK} - 0.0360\, T_{wK} + 8.32\times10^{-5}\, T_{wK}\, T_{DK} + 7.10 \quad (7.45)$$

$$X_2 = 9.47\times10^{-6}\, T_{DK}^2 + 0.00557\, T_{DK} + 0.0169\, T_{wK} - 4.06\times10^{-5}\, T_{wK}\, T_{DK} - 3.87 \quad (7.46)$$

The drying rate at the second critical point is only 18.1% of that at the first critical point, so

$$N_2 = 0.181\, N_1 \quad (7.47)$$

7.4 Modelling of Average Moisture-Content Variations and Temperature Profiles through A Stack of Boards

7.4.1 Constitutive Equations for Moisture Mass Balance

If it is assumed that the kiln is well-insulated and the air is distributed evenly over the boards, then only streamwise variations will be considered as the spanwise variations are negligible in comparison (Ashworth, 1977, Keey, 1991). There is some experimental evidence to suggest that in well-designed kilns the airflow is almost uniformly distributed over the entire stack surface (Wiedeman *et al.*, 1989). This assumption should be valid for the case within a stack while the surface temperatures among adjacent boards are approximately the same and the boards are neatly stacked (Figure 7.6).

Further, the mass-transfer coefficient over a single board is considered to be the distance-averaged value over this board. In this way, the local moisture content predicted is in fact the mean value over the board. The local drying rate is then calculated by the following equations, which are derived from equations (7.6) and (7.25):

$$N_v = f_1 (N_1 - N_2) + N_2 = [f_1(1 - \alpha) + \alpha] N_1 = f_1' N_1 = f_1' K_o \varphi (Y_S - Y_G) \quad (7.48)$$

where $X_1 > X > X_2$.

Whenever $X_2 > X > X_e$,

$$N_v = f_2 N_2 = \alpha f_2 N_1$$
$$= f_2' K_o \varphi (Y_S - Y_G) \qquad (7.49)$$

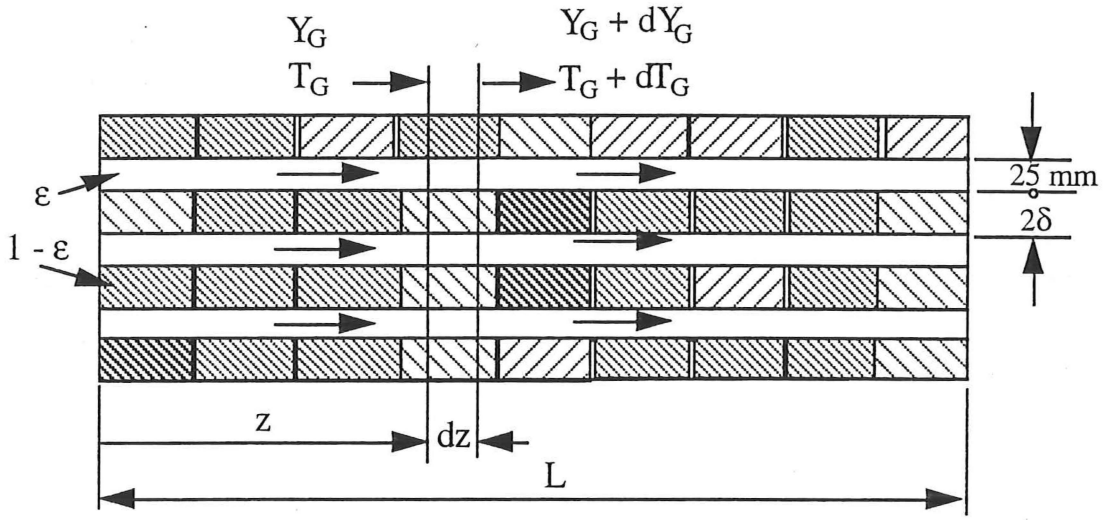

Figure 7.6 Schematic diagram of a well-insulated stack of boards.

From Figure 7.6, a moisture balance over an infinitesimally short zone of length dz in the direction of airflow for a short time interval $d\tau$ yields:

$$-\frac{\partial}{\partial \tau}[X \rho_S (1 - \varepsilon)\, dz]\, d\tau = \frac{\partial}{\partial \tau}(Y_G \rho_G \varepsilon\, dz)\, d\tau + \frac{\partial}{\partial z}(Y_G G\, d\tau)\, dz$$

$$\text{or, } -\frac{\partial}{\partial \tau}[X \rho_S (1 - \varepsilon) + Y_G \rho_G \varepsilon]\, dz\, d\tau = G \frac{\partial Y_G}{\partial z} d\tau\, dz \qquad (7.50)$$

where ρ_S is the basic density of wood, kg m^{-3};
ρ_G is the density of hot air, kg m^{-3};
ε is the void fraction in the board stack;
Y_G is the local humidity in the air;
and G is the specific dry gas flux, kg m^{-2} s^{-1}.

Since $\rho_G << \rho_S$ and $Y_G \sim X$, the second term in the above equation can be neglected and the equation reduces to the partial differential equation:

$$-\frac{\partial}{\partial \tau}[X \rho_S (1 - \varepsilon)] = G \frac{\partial Y_G}{\partial z} \qquad (7.51)$$

The loss of moisture with time is equal to the gain in humidity of the airstream with distance. The loss of moisture within a board may also be related to the drying rate:

$$-\frac{\partial}{\partial \tau}[X \rho_S (1 - \varepsilon)] = N_v a = f K_o \varphi a (Y_S - Y_G) \tag{7.52}$$

on introducing the expressions for drying rate (equations 7.48 and 7.49).

In equation (7.52), the function f is different for the two falling-rate periods:

$$f = f_1' = f_1(1 - \alpha) + \alpha \text{ when } X_1 > X > X_2 \tag{7.53}$$

$$\text{and } f = f_2' = \alpha f_2 \text{ when } X_2 > X > X_e \tag{7.54}$$

The parameter a is the exposed surface per unit volume of board stack, $m^2\ m^{-3}$.

Equations (7.51) and (7.52) can be used to specify the humidity in the airstream and moisture content in the board provided the expressions of f_1 and f_2 are known. These equations can be further simplified for the convenience in calculation by defining the following dimensionless parameters (Ashworth, 1977, Keey, 1978):

(a). The relative distance along the dryer (or *NTU*)

$$\zeta = \frac{K_o \varphi a}{G} z \tag{7.55}$$

(b). The relative drying time

$$\theta = \theta_1 = \frac{K_o \varphi a (Y_S - Y_G^o)}{\rho_S (1 - \varepsilon)(X_1 - X_2)} \tau, \text{ when } X_1 > X > X_2$$

$$\text{and } \theta = \theta_2 = \frac{K_o \varphi a (Y_S - Y_G^o)}{\rho_S (1 - \varepsilon)(X_2 - X_e)} \tau, \text{ when } X_2 > X > X_e \tag{7.56}$$

(c). The humidity potential relative to the value at the air inlet

$$\Pi = \frac{Y_S - Y_G}{Y_S - Y_G^o} \tag{7.57}$$

By substituting the above dimensionless parameters into equations (7.51) and (7.52), one finds

$$\frac{\partial \Phi}{\partial \theta} = \frac{\partial \Pi}{\partial \zeta} \tag{7.58}$$

$$\text{and } -\frac{\partial \Phi}{\partial \theta} = \Pi f \tag{7.59}$$

These two equations [(7.58) and (7.59)] have the same forms as those proposed by van Meel (1958), Ashworth (1977) and Keey (1978), except that in the equations the following relationships are used to define the dimensionless parameters:

$$\Phi = \Phi_1, f = f_1', \theta = \theta_1 \text{ when } X_1 > X > X_2 \tag{7.60}$$

$$\text{and } \Phi = \Phi_2, f = f_2', \theta = \theta_2 \text{ when } X_2 > X > X_e \tag{7.61}$$

7.4.2 Constitutive Equations for Heat Conservation

Along the course of drying through a stack of boards, the temperature of the air decreases as it provides heat to evaporate the moisture from the boards. On considering the heat conservation over a short distance *dz*, a heat balance equation can be obtained as:

$$Q_G + Q_R = Q_{wv} + Q_{HT} + Q_{LS} \tag{7.62}$$

where Q_G is the heat taken from the hot air by convection, W m^{-2};
Q_R is the heat by radiation, W m^{-2};
Q_{wv} is the heat used to evaporate moisture from board, W m^{-2};
Q_{HT} is the heat used to heat up the moist wood, W m^{-2};
and Q_{LS} is the heat losses, W m^{-2}.

After the board has initially been heated to approximately wet-bulb temperature, the heat for heating up the moist wood Q_{HT} can be negligible as the temperature increase is no longer significant. In a well-insulated stack of boards, the heat losses are very small compared with the thermal load for drying except towards the end of drying. Thus, to a first approximation,

$$Q_{HT} = 0$$

and $$Q_{LS} = 0$$

Let α_H be fraction of heat radiated from the kiln walls and gas compared with that provided by convection, that is

$$\alpha_H = \frac{Q_R}{Q_G} \tag{7.63}$$

Equation (62) can then be reduced to the expression:

$$-(1 + \alpha_H)\, G\, dI_G = H_{wv}\, N_v\, d(az) \tag{7.64}$$

On substituting the following the expressions for the calculations of Q_{wv} and Q_G,

$$Q_{wv} = H_{wv}\, N_v\, d(az) \tag{7.65}$$

and $$Q_G = G\, dI_G, \tag{7.66}$$

one gets an expression for the change of humid enthalpy of the damp gas with distance

$$\frac{dI_G}{dz} = -\frac{a}{G}\frac{1}{(1 + \alpha_H)} H_{wv}\, N_v \tag{7.67}$$

The humid enthalpy I_G is defined by

$$I_G = I_o + \int_{T_o}^{T_G} C_P dT = I_o + \int_{T_o}^{T_G} (C_{PG} + Y_G\, C_{PV})\, dT_G \tag{7.68}$$

$$\text{so, } \frac{\partial I_G}{\partial z} = \frac{\partial I_G}{\partial T_G}\frac{\partial T_G}{\partial z} = (C_{PG} + Y_G\, C_{PV})\frac{\partial T_G}{\partial z} \tag{7.69}$$

On introducing this relationship into equation (7.67), the temperature changes with distance along the airstream can be predicted by

$$\frac{\partial T_G}{\partial z} = -\frac{a}{G}\frac{1}{(1+\alpha_H)(C_{PG}+Y_G C_{PV})} H_{wv} N_v \tag{7.70}$$

By replacing the drying rate with

$$N_v = f K_o \varphi (Y_S - Y_G) \tag{7.71}$$

and using the dimensionless parameters of Π and ζ, equation (7.70) can be rearranged as

$$\frac{\partial T_G}{\partial \zeta} = -\frac{H_{wv}(Y_S - Y_G^o)\Pi f}{(1+\alpha_H)(C_{PG}+Y_G C_{PV})} \tag{7.72}$$

Also it follows that

$$\frac{\partial T_G}{\partial \zeta} = \frac{\partial T_G}{\partial \Pi}\frac{\partial \Pi}{\partial \zeta} = -\Pi f \frac{\partial T_G}{\partial \Pi} \tag{7.73}$$

Therefore,

$$\frac{\partial T_G}{\partial \Pi} = \frac{H_{wv}(Y_S - Y_G^o)}{(1+\alpha_H)(C_{PG}+Y_G C_{PV})} \tag{7.74}$$

Integration of the above equation yields:

$$T_G - T_{DK} = -\frac{H_{wv}}{(1+\alpha_H) C_{PV}} \ln\left(\frac{C_{PG}+Y_G C_{PV}}{C_{PG}+Y_G^o C_{PV}}\right) \tag{7.75}$$

This equation can be used to predict temperature changes in the direction of airflow provided the humidity in the air Y_G has been derived from the constitutive equations of moisture mass balance (equations 7.58, 7.59).

7.5 Calculation of the Drying Process

7.5.1 The Drying of Sapwood Boards

The whole process of drying a stack of sapwood boards can be represented as three stages. The first stage is taken as the period when the boards at any point dry at a relatively constant drying-rate. The second stage of drying starts when the moisture content at the air-intake drops below the first critical point and the drying rate begins to fall while the boards at other positions still dry at the constant drying-rate. Thus a front can be assumed corresponding to the first critical moisture content sweeping across the stack along the airflow direction until the end of the stack is reached. Mathematically, the first critical point sweeps through the whole stack, and then resides at distance greater than the stack width. A similar front at second critical moisture content to that at the first critical value can be suggested to move through the stack. When the moisture content at the air intake has decreased to the second critical point, the subsequent period of drying is defined as the third stage of drying.

7.5.1.1 First stage of drying

During the first stage of drying, the actual process is that the wood is firstly heated up to slightly above wet-bulb temperature by which time the significant drying is taking place. At first on drying with sapwood (initial stage of drying), the drying rate is relatively constant. The initial moisture-content distribution can be assumed to be uniform since the moisture-content variation due to the condensation of water vapour on the wet surface of board during the early stages of the warming-up phase is very small compared to the green moisture content for sapwood. Therefore, by using the unique value for function of f, one finds

$$\Phi(\zeta, \theta) = \frac{X - X_2}{X_1 - X_2} > 1 \tag{7.76}$$

$$f(\zeta, \theta) = \frac{N_v - N_2}{N_1 - N_2} = 1 \tag{7.77}$$

The initial condition is taken as

$$\Phi(\zeta, \theta = 0) = \Phi_o \tag{7.78}$$

In this case, the constitutive equations (7.58) and (7.59) can be solved analytically:

$$\frac{\partial \Pi}{\partial \zeta} = -\Pi, \quad \Pi(\zeta, \theta) = exp(-\zeta) \tag{7.79}$$

and

$$\frac{\partial \Phi}{\partial \theta} = -\Pi, \ \Phi(\zeta, \theta_1) = \Phi_o - \theta\, exp(-\zeta) \tag{7.80}$$

From these equations, the humidity in the air and the average moisture content in the board are calculated as:

$$Y_G = Y_S - (Y_S - Y_G^o)\, exp(-\zeta) \tag{7.81}$$

$$\text{and } X = X_1 + (X_1 - X_2)[\Phi_o - \theta\, exp(-\zeta)] \tag{7.82}$$

The temperature at any position can be calculated on knowing the humidity in the air:

$$T_G = T_{DK} - \frac{H_{wv}}{(1 + \alpha_H)\, C_{PV}}\, ln\left\{\frac{C_{PG} + [Y_S - (Y_S - Y_G^o)exp(-\zeta)]\, C_{PV}}{C_{PG} + Y_G^o\, C_{PV}}\right\} \tag{7.83}$$

This initial stage of drying ends when the moisture content within the boards lying in the front row decreases to the first critical moisture content, X_1. The duration of this stage is predicted as

$$\theta_{end}^I = \Phi_o - 1 \tag{7.84}$$

The real drying time τ^I for this stage of drying can be calculated accordingly. Equation (7.84) has been derived before (Ashworth, 1977; Keey, 1978), but the derivation is included here for completeness.

From equations (7.81) and (7.84), it is known that that in the first stage of drying for sapwood, the humidity and the temperature in airstream are only the functions of distance and independent on the elapsed time.

7.5.1.2 Second stage of drying

During this stage of drying, the moisture content is less than the first critical value in positions close to the air intake, but at the locations further into the stack, unhindered

drying takes place. Conceptually, this stage may be described initially in terms of the first critical point sweeping through the stack until the end of the stack has been reached. Afterwards, all the boards dry in the second period in which equations (7.42), (7.53), and constitutive equations (7.58), (7.59) and (7.75) are used to specify the external conditions and average moisture content through the stack. Since the function f is not a simple function of normalised moisture content, it is impossible to find an analytical solution to the problem. Therefore, a numerical method has been developed to solve the equations.

(a). The initial conditions:

Since the initial values of average moisture content in the board and the humidity in the airstream for second stage of drying are equal to those at the end of the first stage, the initial conditions are known as follows:

$$\Phi(\zeta, \theta=0) = \Phi(\zeta, \theta^{I}_{end}) = \Phi_o - (\Phi_o - 1)exp(-\zeta) \tag{7.85}$$

$$\Pi(\zeta, \theta=0) = \Pi(\zeta, \theta^{I}_{end}) = exp(-\zeta) \tag{7.86}$$

(b). The numerical solution

During the second period, since the variables of Π, Φ and f are the functions of both time θ and distance ζ, the grids of the time and distance for the changing of each variable are shown in Figure 7.7.

Suppose that each variable, F, can be represented by constant value determined by the values at 'old' and 'new' steps and positions, $F_{i,j}$, $F_{i,j+1}$, $F_{i+1,j}$ and $F_{i+1,j+1}$. On introducing the weighting factors κ and γ, the integration of each variable can be obtained:

$$\int_{j}^{j+1} F \, d\zeta = [(1 - \gamma) F_{i,j} + \gamma F_{i,j+1}] \, (\delta\zeta) \tag{7.87}$$

$$\int_{i}^{i+1} F \, d\theta = [(1 - \kappa) F_{i,j} + \kappa F_{i+1,j}] \, (\delta\theta) \tag{7.88}$$

$$\int_{i}^{i+1} \int_{j}^{j+1} F \, d\zeta \, d\theta$$

$$= [(1 - \kappa)(1 - \gamma) F_{i,j} + \kappa(1 - \gamma) F_{i+1,j} + \gamma(1 - \kappa) F_{i,j+1} + \gamma\kappa F_{i+1,j+1}] (\delta\zeta)(\delta\theta) \tag{7.89}$$

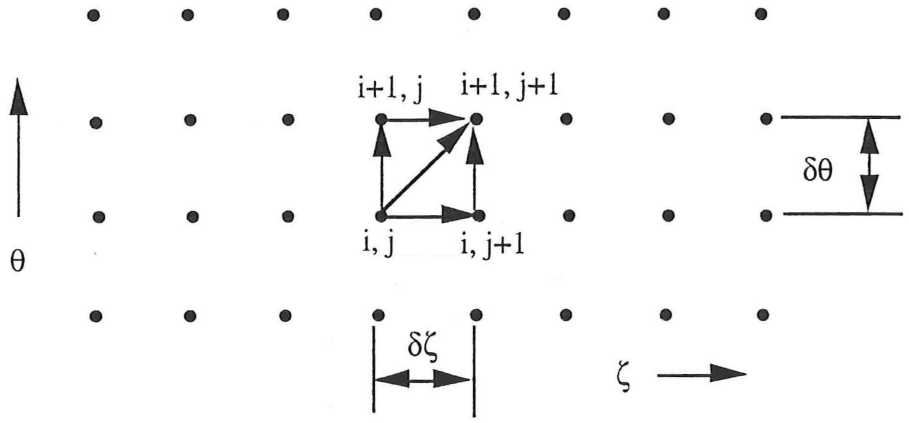

Figure 7.7 The grid layout and time changes for the numerical solution.

For specific values of the weighting factor γ and κ, the discretization equations reduce to the well-known schemes. In particular, $\gamma = 0$ and $\kappa = 0$ leads to the explicit scheme of Patankar (1980). By using this method, therefore, equations (7.58) and (7.59) are numerically solved as follows:

$$\int_{i}^{i+1} \frac{\partial \Phi}{\partial \theta} d\theta = \int_{i}^{i+1} - \Pi f \, d\theta \tag{7.90}$$

$$\Phi_{i+1,j} - \Phi_{i,j} = - \Pi_{i,j} f_{i,j} \, \delta\theta, \quad \Phi_{i+1,j} = \Phi_{i,j} - \Pi_{i,j} f_{i,j} \, \delta\theta \tag{7.91}$$

Similarly, on knowing the 'new' function $f_{i+1,j}$ from the 'new' normalised moisture content $\Phi_{i+1,j}$ the humidity potential for the 'new' step and 'new' position is predicted as:

$$\int_{j}^{j+1} \frac{1}{\Pi} \frac{\partial \Pi}{\partial \zeta} d\zeta = \int_{j}^{j+1} - f \, d\zeta$$

Integrating the above equation yields

$$ln\left[\frac{(\Pi_{i+1,j+1})}{(\Pi_{i+1,j})}\right] = -f_{i+1,j}\ \delta\zeta,\ \ \Pi_{i+1,j+1} = (\Pi_{i+1,j})\ exp(-f_{i+1,j}\ \delta\zeta) \qquad (7.92)$$

In the calculation, the value of $\Pi_{i+1,j}$ at the air intake ($j = 0$) is always 1.

In equations (7.91) and (7.92), f is initially taken as 1 when Φ is greater than or equal to 1. Otherwise f is determined by equation (7.53). When the normalised moisture content at air intake $\Phi(\zeta=0, \theta)$ equals zero, the second stage of drying ends. The duration of this stage θ^{II} can be estimated by accumulating the time intervals through the whole stage as $\Phi(\zeta=0)$ falls from 1 to zero. The corresponding real drying time is τ^{II}.

The solution to equation (7.92) is stable, since $(f_{i+1}\ \delta\zeta)$ is always positive. For equation (7.91), the condition for physically realistic results to be obtained is

$$\delta\theta < \frac{1}{\Pi_i} \qquad (7.93)$$

since f has the same order as Φ in quantity. If this condition is not met, $\delta\theta f_i\ \Pi_i$ may be greater than Φ_i, which will lead to the situation that the normalised moisture content has an unrealistic solution with a negative value. Equation (7.93), then, provides a criterion for the choice of time step. When the actual time step is chosen as about one second, this criterion can surely be met in the situation discussed in this thesis.

The temperature profile in the airstream along the flow direction can be calculated by using equation (7.75).

7.5.1.3 Third stage of drying

When the moisture content at the air intake falls to the second critical value the third stage of drying begins. At this time, however, the boards inside the stack along the direction of airstream are still drying above this value (second period of drying).

By applying the different functions of f and different definition of normalised moisture content and relative drying time to equations (7.86) and (7.87) for the cases above and below the second critical point, the humidity in the air and the moisture content in the boards can be predicted in the same way as that for the second stage of drying. The drying can be terminated using one of the following the criteria: whether the final moisture content at the air intake (the driest region) or at the air offtake (the wettest region) or the

mean moisture content through the whole stack has reached the required dryness. The drying time, θ^{III} (correspondingly τ^{III}) of third stage of drying can be estimated.

By now, the whole duration of drying of the sapwood boards can be calculated to be the sum of those in three stages:

$$\tau_{tot} = \tau^{I} + \tau^{II} + \tau^{III} \tag{7.94}$$

7.5.2 The Drying of Heartwood Boards

In order to predict the changes in air humidity and average moisture content in boards for the heartwood drying, the same procedure can be used as that for sapwood except that the initial relatively constant drying period no longer exists. Therefore, there are only two stages of drying for heartwood. The first stage starts when the moisture content everywhere is the initial value and finishes when the moisture content at air intake falls below second critical value. The second stage of drying for heartwood is identical to the third stage for sapwood drying. The problem can be solved with the initial and boundary conditions as:

$$\Phi(\zeta, \theta=0) = \Phi_o \tag{7.95}$$

$$\Pi(\zeta=0, \theta) = 1 \tag{7.96}$$

The function of f is calculated from equations (7.53), (7.54), (7.23) and (7.27).

7.5.3 The Worked Examples for High-Temperature Kiln Drying of *Pinus radiata* Boards

When a stack of sapwood boards and heartwood are respectively dried at dry-bulb/wet-bulb temperatures of 120/70°C and air velocity of 5 m s^{-1} in the batch kiln, the calculation can be carried out as follows.

7.5.3.1 The external mass-transfer coefficient

Kho, Keey and Walker (1989, 1990) has measured the external mass-transfer coefficient over a slab of boards in a pilot kiln-size stack. It is found that the board-averaged mass-transfer coefficient decreases and tends towards an asymptotic value over the boards just

behind the front two or three rows. Figure 7.8 shows such a profile developed from the data of Kho *et al.* (1989, 1990).

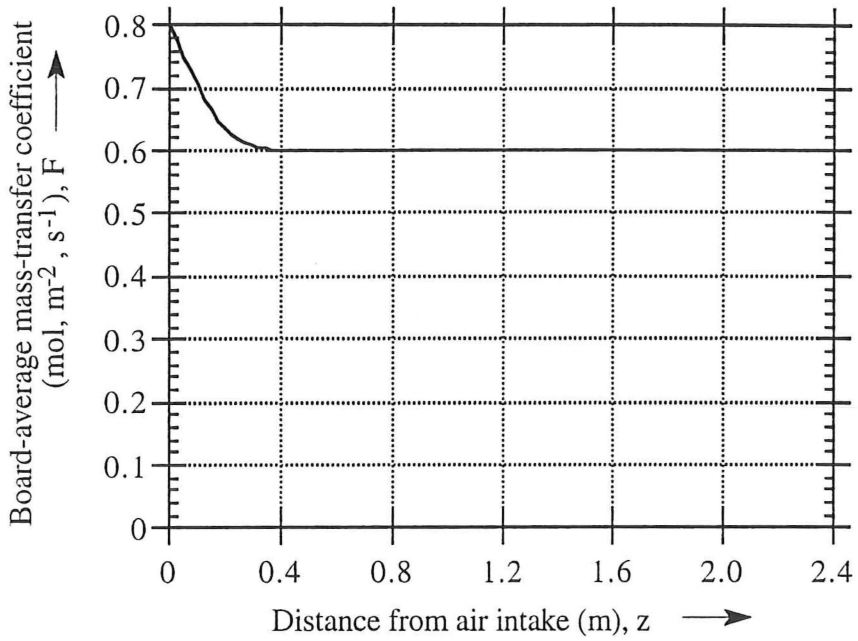

Figure 7.8 The board-average mass-transfer coefficient profile through a kiln stack. (After Kho, Keey and Walker, 1989, 1990)

7.5.3.2 The thermodynamic relationships and physical properties:

The thermodynamic relationships and physical properties to be used in the calculation are: the heat of vaporization of water, H_{wv}; specific heat of water vapour and that of air, C_{PV} and C_{PG}; and the air density ρ_G. These parameters vary with temperature and pressure.

The heat of vaporization of liquid water can be correlated with temperature from the data in steam tables using the polynomial given by Stanish (1986):

$$H_{wv} = 2.792x10^6 - 160\,T_{GK} - 3.43\,T_{GK}^2 \qquad (7.97)$$

When the moisture content is below the value at fibre saturation point, some extra heat is needed to evaporate the bound water as some energy is used to break the bond between water and wood. In this case, the heat of vaporization is the sum of heat for liquid vaporization and that for this extra energy. This extra heat is usually called the heat of sorption. Different methods for calculating the heat of sorption of timber have been

published in the literature (Skaar, 1980, Kesley and Clarke, 1956, Smith and Van, 1975, Stamm and Loughborough, 1935). It is believed that the method of Skaar is the most reliable which is expressed as (Pang, Langrish and Keey, 1993):

$$\Delta H_{wv} = 1.17x10^6 \exp(-14X) \tag{5.24}$$

Therefore, the total heat for the vaporization of bound water is

$$H_{bv} = 2.792x10^6 - 160\,T_{GK} - 3.43\,T_{GK}^2 + 1.17x10^6 \exp(-14X) \tag{5.25}$$

The other parameters have been fitted from data in the steam tables and gas tables (Perry, 1984):

$$C_{PV} = -247.5 + 22.20\,T_{GK} - 8.043x10^{-2}\,T_{GK}^2 + 9.990x10^{-5}\,T_{GK}^3 \tag{5.26}$$

$$C_{PG} = 1038.1 - 0.2388\,T_{GK} + 4.599x10^{-4}\,T_{GK}^2 \tag{5.27}$$

$$\rho_G = 2.967 - 8.288x10^{-3}\,T_{GK} + 7.594x10^{-6}\,T_{GK}^2 \tag{7.98}$$

7.5.3.3 The parameters in the calculation

(a). The superficial area per unit volume of the board stack

For the stack of 50mm thick boards and 25mm sticks, the superfacial area is given by

$$a = \frac{S}{V} = \frac{2\,Z\,L\,n}{n(0.025 + 0.05)\,Z\,L} = 26.67\ (\mathrm{m^2\ m^{-3}})$$

where Z is the length of the stack, L is the width and n is the number of layers.

(b). The void space in the stack

$$\varepsilon = \frac{0.025\,n\,Z}{(0.025 + 0.050)\,n\,Z} = 0.3333$$

(c). The humidity of the air at the air intake at the dry-bulb/wet-bulb temperatures of 120/70°C

Y^o_G = 0.2458 kg kg^{-1}

Y_S = 0.2770 kg kg^{-1}

so, $Y_S - Y^o_G$ = 0.0312 kg kg^{-1}

(d). The flow rate of the dry air

ρ_G = 0.8824 kg m^{-3}

$G = \varepsilon u \rho_G$ = 1.471 kg m^{-2} s^{-1}

(e). The number of transfer units

$$NTU = \frac{(K_o\varphi)\, a\, L}{G} = 0.657$$

(f). The relative distance

$$\zeta = \frac{(K_o\varphi)\, a\, z}{G} = 0.274\, z$$

(g). The relative drying time

Sapwood: X_o = 1.40 kg kg^{-1}

X_1 = 0.94 kg kg^{-1}

X_2 = 0.093 kg kg^{-1}

X_e = 0.0215 kg kg^{-1}

ρ_S = 450 kg m^{-3}

$$\theta_1 = \frac{K_o\varphi\, a\, (Y_S - Y^o_G)}{\rho_S\, (1 - \varepsilon)\, (X_1 - X_2)}\, \tau = 4.94\text{x}10^{-5}\, \tau$$

$$\theta_2 = \frac{K_o\varphi\, a\, (Y_S - Y^o_G)}{\rho_S\, (1 - \varepsilon)\, (X_2 - X_e)}\, \tau = 6.80\text{x}10^{-4}\tau$$

Heartwood: X_o = 0.40 kg kg^{-1}

X_1 = 0.40 kg kg^{-1}

X_2 = 0.0883 kg kg^{-1}

X_e = 0.0215 kg kg^{-1}

$$\rho_S = 377 \text{ kg m}^{-3}$$

$$\theta_1 = \frac{K_o \varphi \, a \, (Y_S - Y^o_G)}{\rho_S \, (1 - \varepsilon) \, (X_1 - X_2)} \, \tau = 1.14 \times 10^{-4} \, \tau$$

$$\theta_2 = \frac{K_o \varphi \, a \, (Y_S - Y^o_G)}{\rho_S \, (1 - \varepsilon) \, (X_2 - X_e)} \, \tau = 5.32 \times 10^{-4} \, \tau$$

7.5.3.3 The simulation results for sapwood boards

By using the parameters and the physical properties given in the above sections, the predicted results from the simplified model in this chapter are shown in Figures 7.9 to 7.12. Figure 7.9 shows the variations of local humidity potential with time while Figure 7.10 is for the drying rate and Figure 7.11 gives the profiles of temperatures of the air through the stack. With these variations of external conditions, the average moisture contents across the stack are calculated as shown in Figure 7.12.

When the air flows across the stack in one direction only, the humidity potential at air intake is always 1. The potential decreases along the airflow direction as the air takes up moisture vapour. In the first stage of drying, the humidity potential is only a function of position with a reduction of 38% at the air offtake. When the second stage begins, after about 4 hours of drying, the humidity potential everywhere inside the stack starts to increase as the drying rates near the air intake decrease. Finally, after about 24 hours of drying, the wood is relatively dry and the air no longer gains much moisture, so the humidity approaches to the inlet value.

Since the external mass-transfer coefficient and humidity potential at the air intake are higher than those over the boards inside the stack along the airstream, the drying rates through the stack are uneven in the first stage of drying. The boards at the air intake dry faster, while those near the air offtake dry more slowly. The simulation indicates that, at this stage, the drying rate at the air intake (4.7×10^{-4} kg m^{-2} s^{-1}) is over twice that at the air offtake (2.2×10^{-4} m^{-2} s^{-1}). However, during the second stage (from 7 to 15 hours from the start of drying) the drying rates are virtually the same throughout the stack, decreasing progressively with drying times. Afterwards, the drying rate over the front row of boards starts to lag behind when the moisture content there has fallen below the second critical point. As the moisture content at air intake is close to the equilibrium moisture content, the drying rate has become almost zero.

The uneven drying rate in the first stage of drying through the stack of boards causes a nonuniform distribution of moisture content as shown in Figure 7.21. After about 3 hours of drying, the average moisture content at the air intake is 0.25 kg kg^{-1} lower than that over the trailing boards. The maximum difference occurs between 6 to 15 hours from the start of drying when the average moisture content is 0.37 kg kg^{-1} lower at the air intake. However, after 24 hours this difference is reduced to below 0.14 kg kg^{-1}, the average moisture contents ranging from 0.022 to 0.164 kg kg^{-1} across the kiln.

The dry-bulb temperature in the airstream has a similar profile to that of humidity potential with elapsed time since both are related to drying rates in a similar way. When the drying rate is high, more heat is needed and more moisture vapour is taken up by the air. This will result in a drop in both humidity potential and dry-bulb temperature in the air. When the dry-bulb temperature is controlled at 120°C, the temperatures over the boards at 0.6m, 1.2m, 1.8m and 2.4m from the air intake drop to 115.5°C, 111.4°C, 107.8°C and 104.5°C respectively during the first stage of drying. In the second stage and the third stage, the temperatures everywhere behind air intake increase with the decrease of drying rates. After 24 hours of drying, the temperature drop across the board stack between inlet and outlet is less than 4°C. Culpepper (1990), discussing American high-temperature kiln-drying practice, notes that with an inlet-air setpoint of 240°F (116°C), a peak temperature difference of 50°C (28°C) can occur across the kiln before setting down to a value in the 30 to 35°F (17 to 19°C) range.

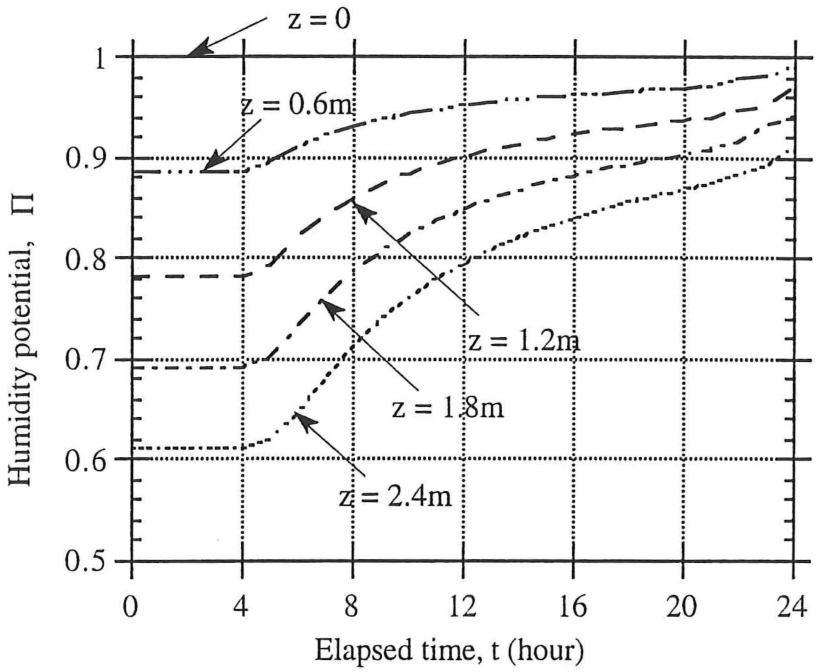

Figure 7.9 The humidity-potential variations relative to the air intake value with both position and elapsed time for the drying of *Pinus radiata* sapwood boards at 120/70 °C. Parameter z is distance from the air intake.

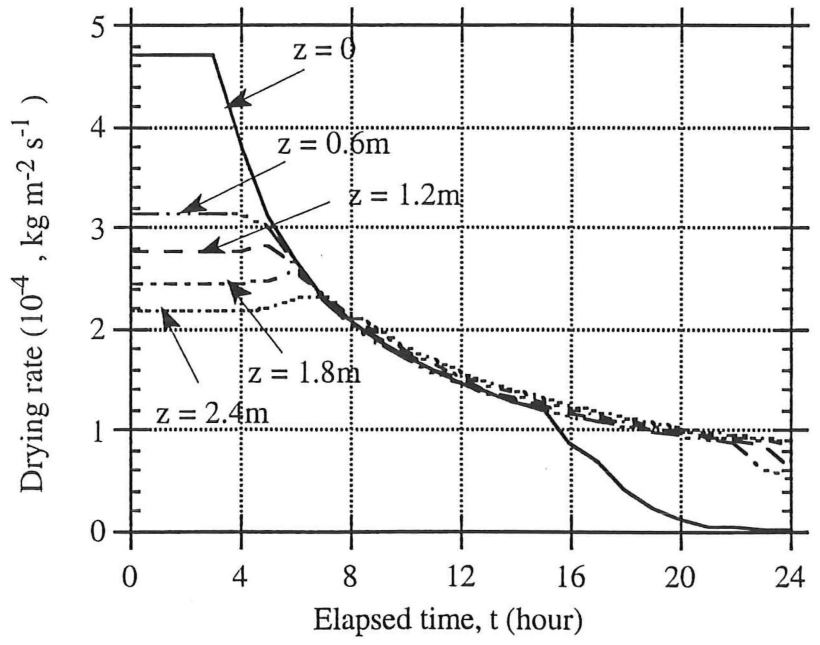

Figure 7.10 The variations of local drying-rates with elapsed time for the drying of *Pinus radiata* sapwood boards at 120/70 C. Parameter z is distance from the air intake.

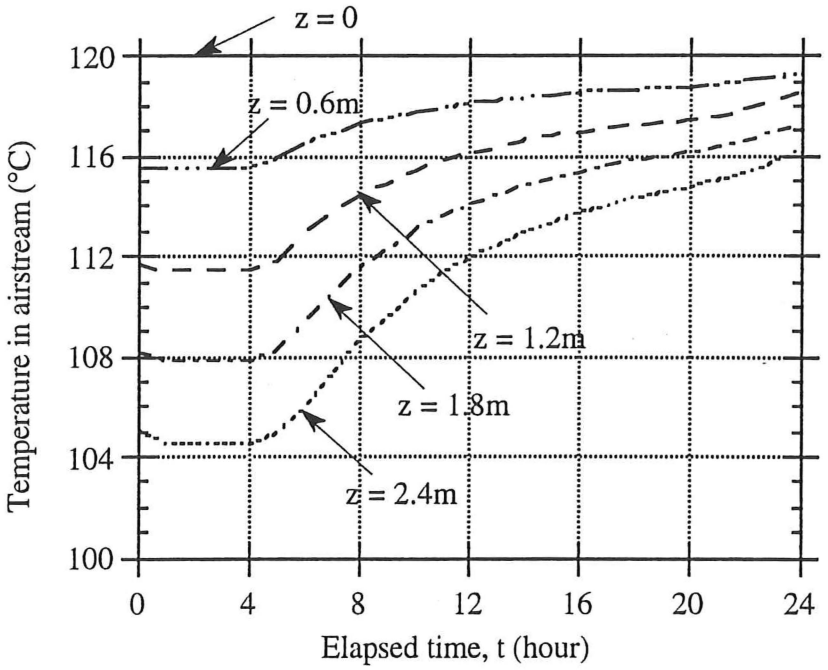

Figure 7.11 The temperature profiles in the kiln airstream for the drying of *Pinus radiata* sapwood boards at 120/70 °C. Parameter *z* is distance from the air intake.

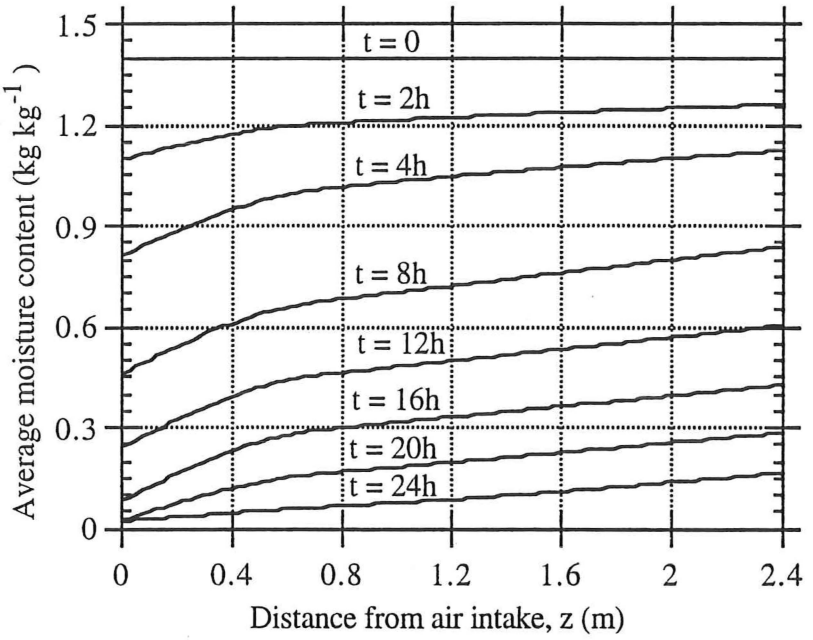

Figure 7.12 The distribution of average moisture-content across a stack of boards for the drying of *Pinus radiata* sapwood boards at 120/70 °C. Parameter *t* is the time of drying.

7.5.3.4 The simulation results for heartwood boards

The analysis for the drying of *Pinus radiata* heartwood boards can be carried out using the similar method to that for sapwood calculations. The results are given in Figures 7.13 to 7.16. As there is no constant drying-rate period for heartwood, the humidity potential and air temperature over the boards behind the air intake increase from the beginning of the drying. The drying rates over the boards from 0.6m to 2.4m along the airflow direction are very close, while the drying rate at air intake is initially higher than that along the down stream but becomes lower after about 12 hours of drying. The drying rates across the stack are nearly zero after 20 hours when the moisture content everywhere is below 0.03 kg kg^{-1}. The difference in average moisture-content is less than that for sapwood due to the much lower initial value in heartwood. The maximum difference in average moisture content is about 0.07 kg kg^{-1} during 6 to 15 hours from the start of drying.

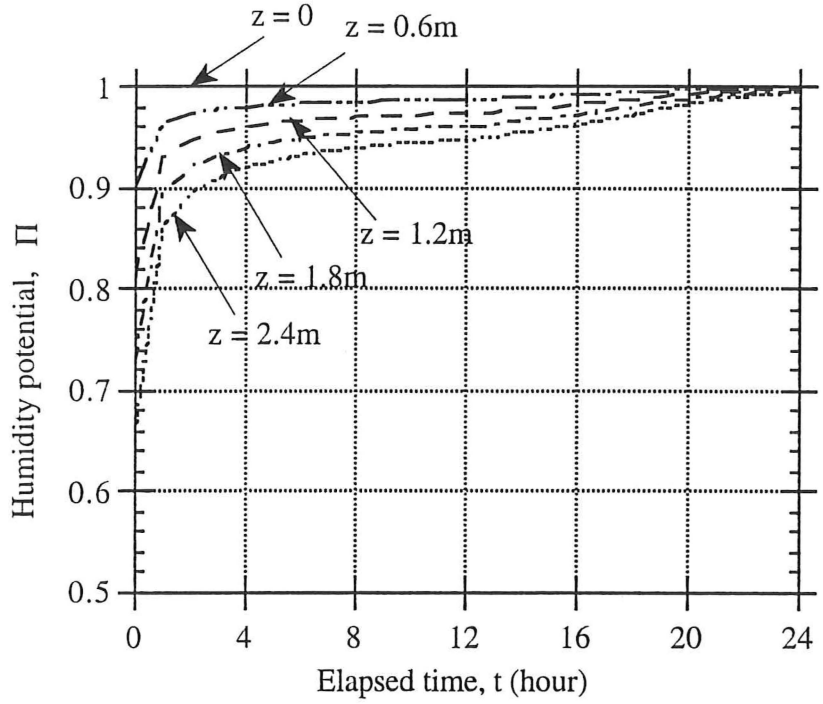

Figure 7.13 The humidity-potential variations with both positions and elapsed time for the drying of *Pinus radiata* heartwood boards at 120/70 °C. Parameter z is distance from the air intake.

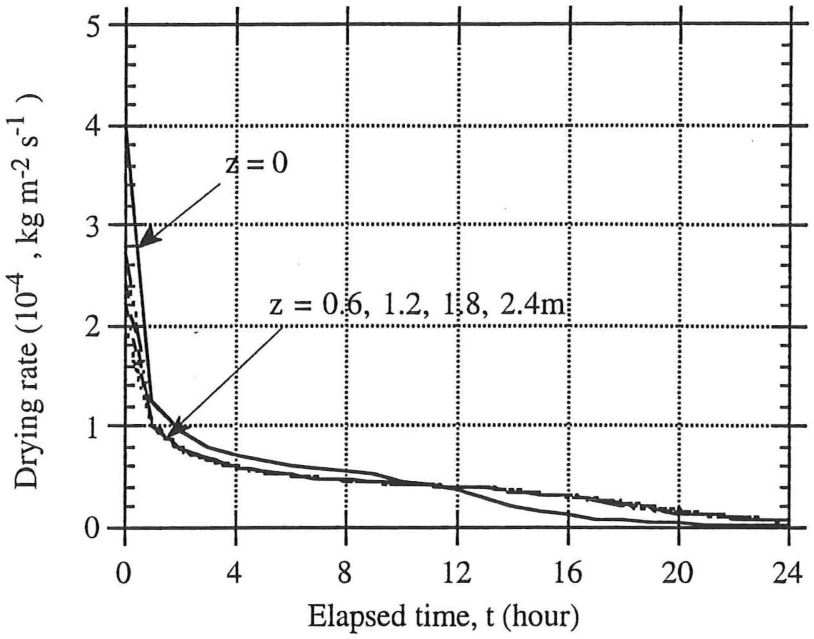

Figure 7.14 The variations of local drying-rates with elapsed time for the drying of *Pinus radiata* heartwood boards at 120/70 C. Parameter z is distance from the air intake.

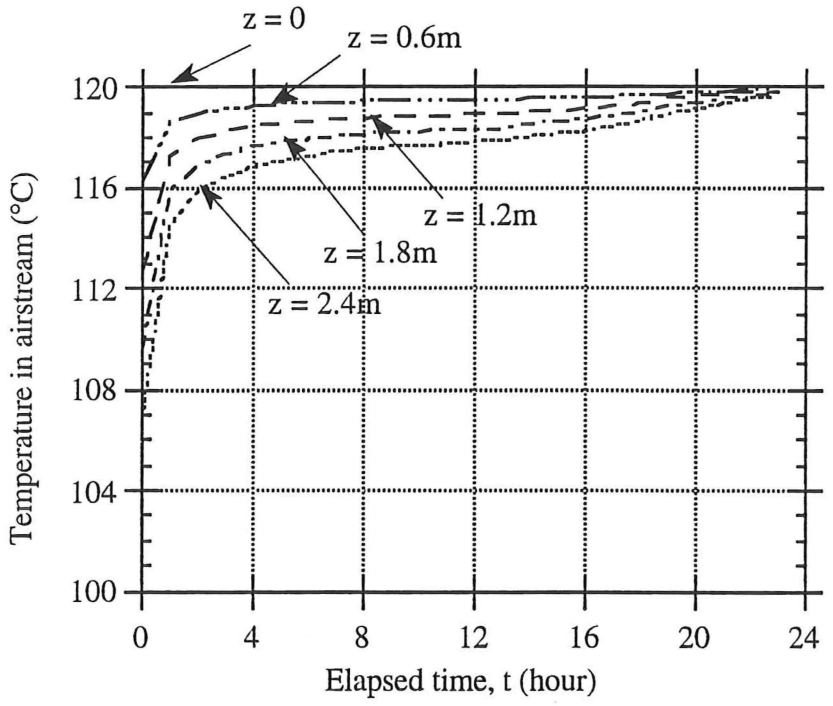

Figure 7.15 The temperature profiles in airstream for the drying of *Pinus radiata* heartwood boards at 120/70 °C. Parameter z is distance from the air intake.

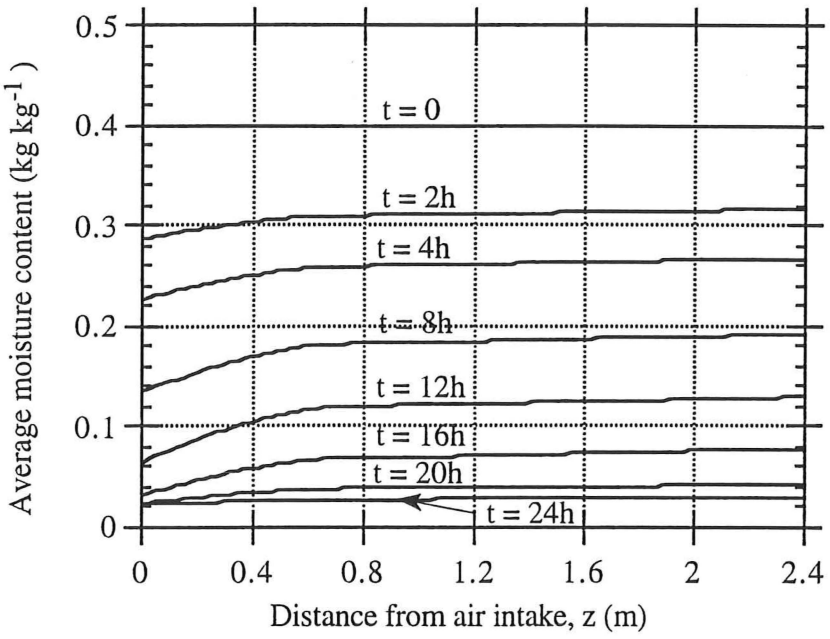

Figure 7.16 The distributions of average moisture-content across a stack of boards for the drying of *Pinus radiata* heartwood boards at 120/70 °C. Parameter *t* is elapsed time.

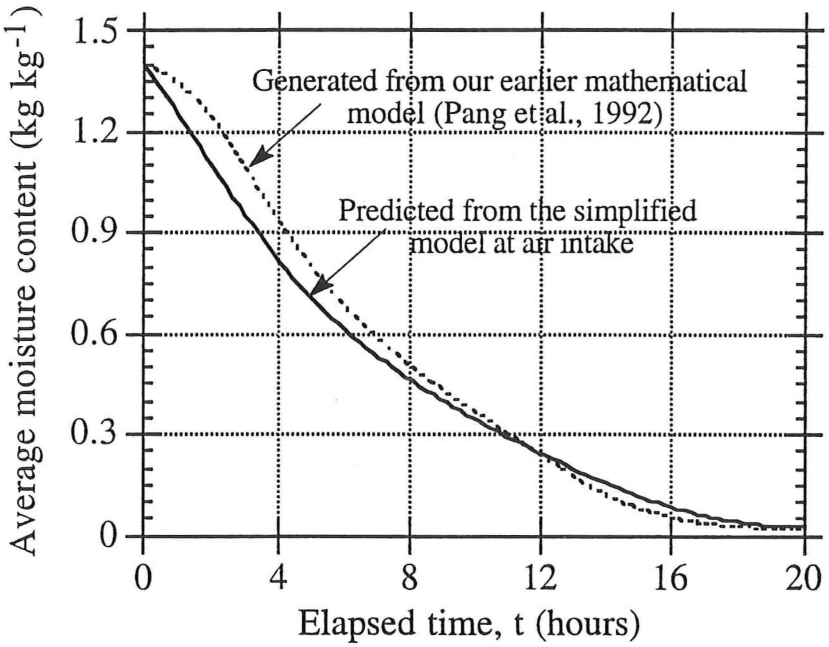

Figure 7.17 The comparison of average moisture-content for the drying of sapwood boards at air intake in a stack and that for drying a single board.

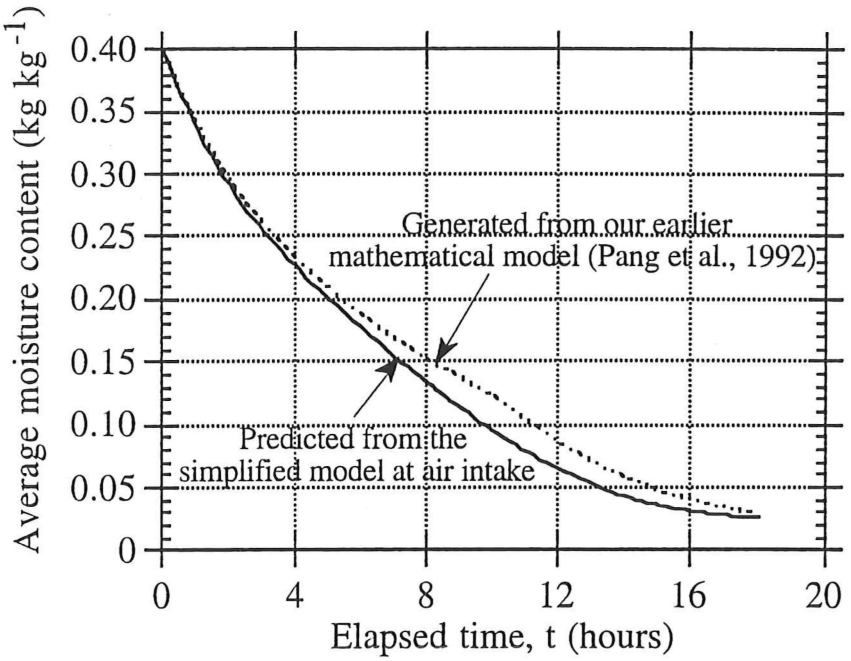

Figure 7.18 The comparison of average moisture-content for the drying of heartwood boards at air intake in a stack and that for drying a single board.

7.5.4 Discussion

The whole process of drying a stack of sapwood or heartwood boards may be divided into three stages, which enables the process calculations to be carried out by employing the simplified drying kinetics. In the calculations, the board size is assumed to be 100x50 mm and the dry-bulb/wet-bulb temperatures of 120/70°C with an air velocity of 5 m s^{-1} are used. From these simulations, the drying may be followed by checking the average moisture-content distribution across the stack. For the drying of sapwood boards, the drying time is predicted to be 16 hours when the final average moisture-content at intake is below 0.08 kg kg^{-1}, while for the whole stack to reach an average moisture-content of the same value the duration of drying is 24 hours. If all of the boards in the stack is dried to this dryness (0.08 kg kg^{-1} in moisture content) or below, the drying time should be extended to 27 hours. When drying the same size heartwood boards under the same external conditions as those for sapwood, the corresponding drying times are predicted to be 11, 15 and 16 hours respectively. If a different final moisture content is required, the drying time can also be predicted from the simulation results as shown in Figures 7.12 to 7.16.

From the profiles of humidity potential and temperatures across a stack, it is known that the drying conditions vary with distance and elapsed time. Since the external conditions over the boards at air intake are identical to those for the drying of a single board, the comparison of the average moisture-contents variations in these two cases has been made both for sapwood (Figure 7.17) and for heartwood (Figure 7.18). The results for the drying of a single board are generated from our earlier mathematical model, while the results for the drying at the air intake in a stack are predicted from the simplified method (using the relative drying rate functions *f*). For sapwood, the moisture content predicted from the simplified method drops more quickly than that predicted by the earlier mathematical model in the first stage of drying. This overprediction results from the constant drying rate in the first period of drying in the simplified method. However, after 12 hours of drying, the two curves converge, so similar drying times can be estimated from the two methods to determine when the wood is dried to required final dryness. For the drying of heartwood boards, the most significant deviation between these two curves occurs during 8 to 12 hours from the start of drying with a difference of 0.03 kg kg^{-1} in the average moisture content. This will cause an error of about 1 hour in estimating the drying times when the final moisture content is assumed to be 0.08 kg kg^{-1}. This error may be due to the imperfect fitting between two methods (Pang and Keey, 1994).

The close match as a whole between the result by our earlier mathematical model and that by the simplified method indicates that the simplified method may be used to replace the complicated mathematical model when the kiln average moisture content is of primary concern. Since the simplified method is much easier to use, it can be coupled with those to describe the varying air conditions within the kiln to directly analyse kiln-wide variations of average moisture content, drying rates and air temperatures. It could also be adapted to analyse the impact of air maldistribution through the kiln stack, by dividing the stack into various zones in which each has uniform air-inlet conditions but different from each other.

7.6 Notation

a	coefficient in equation (7.26), -
a	exposed surface per unit volume of dryer, $m^2\ m^{-3}$
$A,\ B$	coefficients in equation (7.14), -
C	coefficient in equation (7.21), -
C_{PG}	specific heat of air, $J\ kg^{-1}\ K^{-1}$
C_{PV}	specific heat of water vapour, $J\ kg^{-1}\ K^{-1}$
F	the external mass-transfer coefficient based on the molar concentration, $mol\ m^{-2}\ s^{-1}$
F	the representative variable, -
$E_v,\ E_v'$	effective permeability of wood, s
f	relative drying rate, -
f_1	relative drying rate in the first falling-rate period of drying, -
f_2	relative drying rate in the second falling-rate period of drying, -
G	specific dry gas rate, $kg\ m^{-2}\ s^{-1}$
H_{bv}	heat of vaporization of bound water, $J\ kg^{-1}$
H_{wv}	heat of vaporization of liquid water, $J\ kg^{-1}$
I_G	the enthalpy of air, $J\ kg^{-1}$
K_o	mass-transfer coefficient based on humidity potential, $kg\ m^{-2}\ s^{-1}$
K_v	wood permeability, m^2
L	the width of the kiln stack, m
m	coefficient in equation (7.22), -
M_G	molar weight of dry air, $kg\ mol^{-1}$
N_v	drying rate, $kg\ m^{-2}\ s^{-1}$
N_{cr}	drying rate at the critical point, $kg\ m^{-2}\ s^{-1}$
N_1	drying rate at the first critical point, $kg\ m^{-2}\ s^{-1}$
N_2	drying rate at the second critical point, $kg\ m^{-2}\ s^{-1}$
N_B	evaporation rate of bound water, $kg\ m^{-2}\ s^{-1}$
N_E	evaporation rate of liquid water, $kg\ m^{-2}\ s^{-1}$
N_{1E}	evaporation rate of liquid water at the first critical point, $kg\ m^{-2}\ s^{-1}$
p_G^v	vapour partial pressure in airstream, Pa
p_ξ^v	vapour partial pressure at the evaporative front, Pa
$p_{\xi o}^v$	vapour partial pressure at the evaporative front , when $\xi = \xi_o$, Pa
Q_G	the heat given off by the hot air, $W\ m^{-2}$
Q_{HT}	the heat used to heat up the moist wood, $W\ m^{-2}$
Q_{LS}	the heat losses, $W\ m^{-2}$

Q_R the heat by radiation, W m^{-2}

Q_{wv} the heat used to evaporate moisture from board, W m^{-2}

T_{DK} dry-bulb temperature of the air, K

T_{wK} wet-bulb temperature of the air, K

T_ξ temperature at the evaporative front, K

$T_{\xi o}$ temperature at the evaporative front when $\xi = \xi_o$, K

u function defined in equation (7.20), -

X average moisture content, kg kg^{-1}

X_{cr} average moisture content at the critical point, kg kg^{-1}

X_o initial moisture content of wood, kg kg^{-1}

X_{wet} average moisture content in the wet zone of sapwood, kg kg^{-1}

X_1 average moisture content at the first critical point, kg kg^{-1}

X_2 average moisture content at the second critical point, kg kg^{-1}

X_e equilibrium moisture content, kg kg^{-1}

Y_G humidity of the air, kg kg^{-1}

Y_G^o humidity of the air at the air intake, kg kg^{-1}

Y_S humidity of the air when saturated at wet-bulb temperature, kg kg^{-1}

z distance from air intake, m

Z the length of the kiln stack, m

Greek

α drying rate factor in equation (7.9), -

α_H the ratio of radiation to the heat transferred by the hot air, -

β mass-transfer coefficient based on the partial pressure difference, s m^{-1}

ε voidage of the boards stack in a kiln, -

δ half thickness of the board, m

μ viscosity of the vapour, N s m^{-2}

ξ distance of the evaporative front from board surface, m

ρ_v density of vapour, kg m^{-3}

ρ_S basic density of solid wood, kg m^{-3}

φ correction factor of temperatures on mass-transfer coefficient

Φ normalised moisture content

Φ_o initial value of the normalised moisture content

Φ_1 normalised moisture content in the first period of drying

Φ_2 normalised moisture content in the second period of drying

Π the dimensionless parameter for humidity potential

ζ the dimensionless parameter for distance

θ the dimensionless parameter for drying time

τ drying time, s

7.7 References

1. Ashworth, J.C. 1977. The Mathematical Simulation of Batch-Drying of Softwood Timber. PhD Thesis, University of Canterbury, New Zealand.

2. Culpepper, L. 1990. "*High Temperature Drying: Enhancing Kiln Operations*". Miller Freeman, San Fransisco.

3. Forest Product Lab., USDA. 1987. "*Handbook of Wood and Wood Based Materials for Engineers, Architects and Builders*". Hemisphere. New York.

4. Kayihan, F. 1993. Adaptive Control of Stochastic Batch Lumber Kilns. *Computers Chem. Engng.* Vol.17, No.3, pp265 - 273.

5. Keey, R.B. 1978. "*Introduction to Industrial Drying Operations*". Pergamon. Oxford.

6. Keey, R.B. 1991. "*Drying of Loose and Particulate Materials*". Hemisphere. New York.

7. Keey, R.B. and Ashworth, J.C. 1979. The Kiln Seasoning of Softwood Timber Boards. *The Chemical Engineers.* Aug./Sep. pp593 - 598.

8. Kesley, K.E. and Clarke, L.N. 1956. The heat of Sorption of Water by Wood. *Australian J. of Applied Science*, Vol.7(2), pp160-175.

9. Kho, P.C.S., Keey, R.B. and Walker, J.C.F. 1989. Effects of Minor Irregularities and Air Flows on Drying Rate of Softwood Timber Boards in Kilns. *Proc. 2nd IUFRO International Wood Drying Symposium.* Seattle, Washington. pp.150 - 157.

10. Kho, P.C.S., Keey, R.B. and Walker, J.C.F. 1990. The Variation of Local Mass-Transfer Coefficient in Streamwise Direction over A Series of In-Line, Blunt Slabs. *Proc. of Chemeca'90 Conference*, Auckland, New Zealand, Vol.1, pp348 - 355.

11. Kininmonth, J.A. and Whitehouse, L.J., 1991. "*Properties and Use of New Zealand Radiata Pine. Vol.1: Wood Properties*". NZ Ministry of Forestry, NZ Forest Research Institute. Rotorua, New Zealand.

12. Pang Shusheng, Keey, R.B. and Langrish, T.A.G., 1992a. Modelling of Temperature Profiles within Boards during the High-Temperature Drying of Pinus radiata Timber. in Mujumdar, A.S.(ed.): *Drying'92*, Elsevier, Part A: pp.417 - 433.

13. Pang Shusheng, Keey, R.B. and Langrish, T.A.G. 1992b. Moisture Movement in Softwood Timber at Elevated Temperatures. *Proc. of 3rd IUFRO International Wood Drying Symposium.* Vienna, Austria, pp112-122.

14. Pang Shusheng, Langrish, T.A.G. and Keey, R.B. 1993. The Heat of Sorption of Timber. *Drying Technology*, 11(5), pp1071-1080.

15. Pang Shusheng and Keey, R.B. 1994. The Drying Kinetics of An Impermeable Heartwood Board of *Pinus radiata* at Elevated Temperatures. Paper to be presented at International Drying Symposium, (August, 1994) Brisbane, Australia.

16. Patankar, S. 1980. "*Numerical Heat Transfer and Fluid Flow*". Hemisphere. New York.

17. Perré, P., Fohr, J.R. and Arnaud, G. 1988. A Model Applied to Softwood: the Effect of Gaseous Pressure below the Boiling Point. *Proc. 6th International Drying Symposium*, Versailles, pp279 - 286.

18. Perry, R.H. and Chilton, C.H. 1973. "*Handbook of Chemical Engineers*". 5th Edition. Hemisphere. New York.

19. Langrish, T.A.G., Keey, R.B., Kho, P.C.S. and Walker, J.C.F. 1992. Experimental Measurement and Numerical Simulation of Local Mass-Transfer Coefficients in Timber Kiln Drying. *Drying Technology*, Vol.10(3), pp753-782.

20. Skaar, C. 1988. "*Wood Water Relations*". Springer-Verlag, Berlin.

21. Smith, J.M. and van Ness, H.C. 1975. "*Introduction to Chemical Engineering Thermodynamics*". 3rd Edition, McGraw Hill, New York.

22. Stamm, A.J. and Loughborough, W.K. 1935. Thermodynamics of the Swelling of Wood. *J. Phys. Chem.* Vol.39, pp121-132.

23. Stanish, M.A., Schajer, G.S. and Kayihan, F. 1986. A Mathematical Model of Drying for Hygroscopic Porous Media. *AIChE J.*, Vol.32, No.8, pp.1301 - 1311.

24. van Meel, D.A. 1958. Adiabatic Convection Batch Drying with Recirculation of Air. *Chem. Eng. Sci.*, Vol.9, pp.36 - 44.

25. Wiedeman, H.G.R., Nassif, N.M. and Gostelow, J.P. 1989. Study of the Air Flow Profile Inside A Timber Drying Kiln. in Keey, R.B. (ed.): Heat and Mass Transfer'89 — *Proc. of 4th Australasian Conference on Heat and Mass Transfer*, Christchurch, New Zealand, pp693-701.

Chapter **8**

Influence of the Airflow Reversals

As the air flows through a stack of boards in a kiln, the external mass- and heat-transfer coefficients over each board vary with distance from the leading edge. The board-averaged value also changes over the first two or three rows of boards reaching an asymptotic value onwards. During drying, particularly in the early stages of drying, the external conditions change with distance from the air intake. As the airstream sweeps over the boards, moisture is picked up by the air, hence the humidity of the air increases and its temperature drops. These variations in the external conditions and in the external transfer coefficients will result in nonuniform distribution of moisture content both within a single board and through a kiln stack.

From the simulation of kiln-wide drying with unidirectional airflow, it was noted that the moisture content in the wood at the air offtake is higher than that at the air intake throughout the whole course of drying. The boards near the air offtake dry more slowly than those closer to the air intake. This nonuniformity in drying rates across a kiln stack can affect the timber's quality if the drying schedule is terminated according to the dryness of the boards at air intake. Alternatively, if all of the boards are to be dried to the required final moisture content, the boards at the front rows will be overdried and some extra energy will be consumed.

When the drying process of a single board in the stack is examined, a similar problem can also be found mainly due to the nonuniform local heat- and mass-transfer coefficients over the board. The peak values of the transfer coefficients close to the leading edge of the board will result in the greatest drying rate at a given moisture content. Therefore, the portion near the leading edge of a board dries faster than that close to the trailing edge. This uneven moisture content in a single board along the airflow direction will increase stress-related degrade, thus limiting the external conditions which can be chosen to maintain board quality.

To mitigate the problems described above, periodic reversals of the airflow have been practised by switching the fan direction. This switchover has the effect of enhancing the drying over the wetter section of the boards, and retarding the transfer over the drier portion. In this way, the extreme variations between both the drying at the leading edge

and trailing edge of each board, while the differences in the drying at the air inlet and that at the air outlet of the kiln stack can be smoothed out to some extent. However, in practical operations the frequency and the length of the period between reversals are mainly determined by trial and error.

In the United States where the steam heated kilns are widely used, most mills reverse their fans every 3 hours, although occasionally a 2- and 4-hour reversal may be found (Culpepper, 1990). Some mills reverse only once, two-thirds or so through the schedule. Culpepper (1990) argues that reversal periods appear to have little impact on drying and tend to be a matter of personal preference. In New Zealand conventionally, the airflow is reversed every 4-hour to dry the timber of *Pinus radiata*. This frequency of reversals is convenient as a double reversal is consistent with 8-hour shift change. However, recently the policy of reversing airflow every 3 hours has been employed in newly designed kilns. This policy is believed to be more effective in smoothing the final moisture content through a kiln stack.

Although airflow reversals have been employed in timber drying and the benefits are recognised, little attention has been attracted to the theoretical basis, except for the work by Ashworth (1977) and Stevens and Johnston (1957). Stevens and Johnston (1957) made some empirical observations in an examination of flow-reversing during timber drying. They suggest that if the direction of airflow is switched over frequently the drying rates on both inlet and outlet sides can be intensified and readjusted to that of the inlet side attained for one-way circulation. Ashworth (1977), in his analysis, used arbitrary characteristic drying curve functions ($f = \Phi$ *and* $f = \sqrt{\Phi}$) to express the drying behaviour in the falling-rate period, and the variation in external transfer coefficients in the airflow direction were not taken into account. It thus appears the the conclusion regarding the usefulness of a single early flow reversal in not sensitive to specific drying behaviour of the timber species.

Whether a given schedule employed is the best one, and how the temperature and moisture content change at different stages of drying with different strategies of airflow reversals are not yet thoroughly understood. This chapter will firstly cover the calculation of the changes of external heat- and mass-transfer coefficients both over a single board and across a stack when reversing the flow direction. Then the temperature and moisture-content profiles within a single board with airflow reversals will be predicted. For the kiln-wide analysis, the variations of the local average moisture content will be investigated through a stack. By comparing these profiles and variations by using different strategies,

such as reversing airflow every 3 hours, 4 hours and 8 hours, or only single reversal, recommendations can be made for kiln operations.

8.1. The Changes of External Heat and Mass Transfer Coefficients with Airflow Reversals

Kho, Keey and Walker (1989, 1990) show that the local mass-transfer coefficient over each single board in a kiln stack has a maximum value over the leading edge of the board, reaching an asymptotic value from about the middle region of the board onwards.(Figure 8.1). This variation arises from the inevitable small gaps between adjacent stacked boards throughout the whole stack (Langrish *et al.*, 1993).

In Figure 8.1, the variation of mass-transfer coefficients with distance in the flow direction is shown for an air velocity of 5 m s^{-1} and a board dimension of 100x50 mm. The sticker thickness is taken as 25 mm which is representitative of thickness used in high-temperature kiln seasoning (Walker, 1993). Sticker thickness may be larger under high-temperature kiln conditions (25-32mm), but difference is probably not significant in influencing the mass-transfer coefficient. The curve in Figure 8.1 is taken as representative for the uniformly level of boards lying adjacent to one another with a 1 mm board gap. However, minor irregularities and varying air velocities will have some minor effects on the mass-transfer coefficient profiles as investigated by Kho, Keey and Walker (1989, 1990).

If the driving force for the external mass-transfer is expressed by the vapour partial pressure difference, the corresponding mass-transfer coefficient, β, can be transformed from the mass-transfer coefficient, F, based on the molar concentration differences (Kho *et al.*, 1989, 1990) by the following equation (Table 5.1):

$$\beta = F\frac{M_v}{p_{BM}} \tag{5.14}$$

In this expression, M_v is the vapour molar mass (0.018 kg mol^{-1}) and p_{BM} is the logarithmic mean partial pressure difference of air (Pa), which is calculated by:

$$p_{BM} = \frac{p_{B\infty} - p_{BI}}{ln(p_{B\infty}/p_{BI})} \tag{5.15}$$

For the air at dry-bulb temperature of 120 °C and wet-bulb temperature of 70°C, it is known that:

p_s^v = 31250 Pa, p_∞^v = 28727 Pa

So, p_{BI} = 70080 Pa, $p_{B\infty}$ = 72603 Pa

and $p_{BM} = \frac{72603 - 70080}{\ln(\frac{72603}{70080})}$ = 71334.1 (Pa)

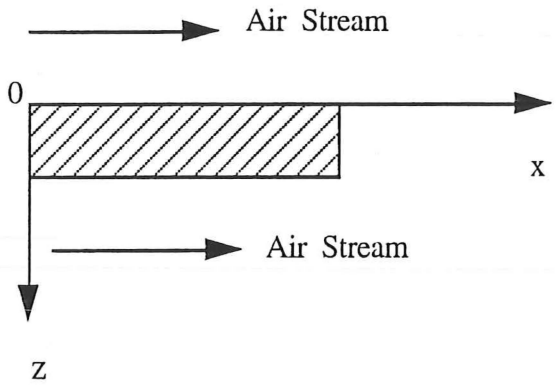

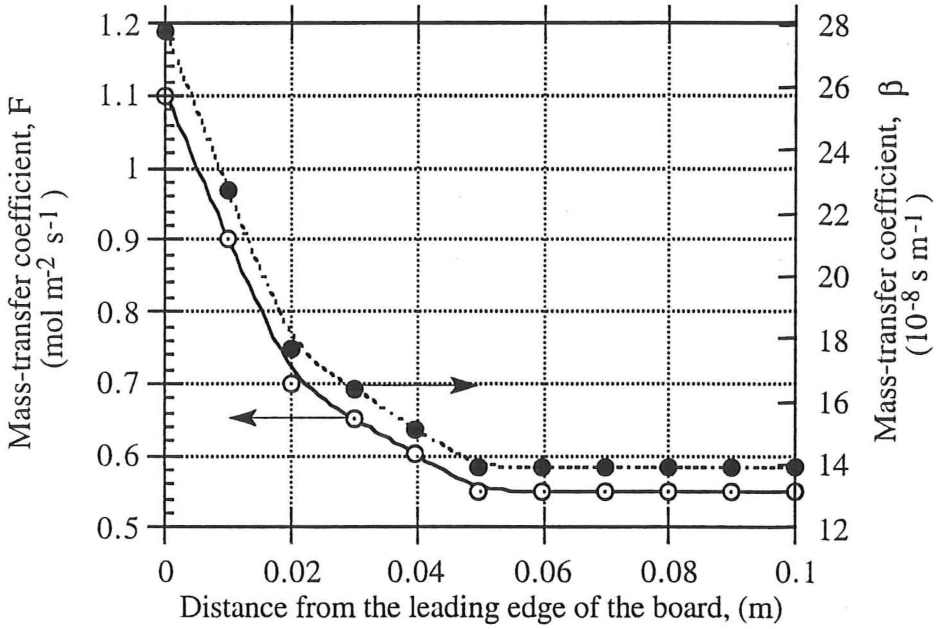

Figure 8.1. The variation of mass-transfer coefficient with distance through the board in the air flow direction from the leading edge. (After Kho, Keey and Walker, 1989, 1990)

The two mass-transfer coefficients can be related to each other by this set of working conditions by

$$\beta = 2.52\text{x}10^{-7}\, F \qquad (8.1)$$

Since M_V/p_{BM} is essentially constant within the kiln, both kinds of the local mass-transfer coefficient (β and F) have similar profiles through the board (Figure 8.1).

If radiation is taken to be 15% of the convective heat transfer in a large-scale commercial kiln (Pang, Keey and Langrish, 1992a), the heat-transfer coefficient can be related to the mass-transfer coefficient by the expression (Keey, 1991):-

$$h = 1.15\, C_{PY}\, K_o \qquad (8.2)$$

where C_{PY} is the humid specific heat of moist air, which is a function of the air humidity Y_G and the specific heat of the gas C_{PG} and of the vapour C_{PV}:-

$$C_{PY} = C_{PG} + C_{PV}\, Y_G \qquad (8.3)$$

With the schedule given above (120/70°C), the values of the thermal parameters for gas and vapour have been calculated to be

C_{PG} = 1015.3 J kg^{-1} K^{-1}
C_{PV} = 2119.3 J kg^{-1} K^{-1}
and Y_G = 0.2614 kg kg^{-1}

So, C_{PY} = 1569.3 J kg^{-1} K^{-1}

In equation (8.2), K_o is the mass-transfer coefficient based on the humidity differences and this can be related to the original defined mass-transfer coefficient F by the expression (Table 5.1):

$$K_o = M_G\, F \qquad (8.4)$$

in which M_G is the molar mass of the dry air (0.0289 kg mol^{-1}).

It follows that the profile of the local heat-transfer coefficients are similar to those of the mass-transfer coefficients with the coefficient of 1.15 C_{PY}.

$h = 1804.7\, M_G\, F = 52.16\, F$ (S.I. units) (8.5)

In the case when the airflow is reversed, the heat- and mass-transfer coefficients will follow the airflow change correspondingly. If the boards are symmetrically stacked, the new profiles of the coefficients will be mirror images of the old ones. Figure 8.2 illustrates the asymptotic profiles across each board away from the air inlet.

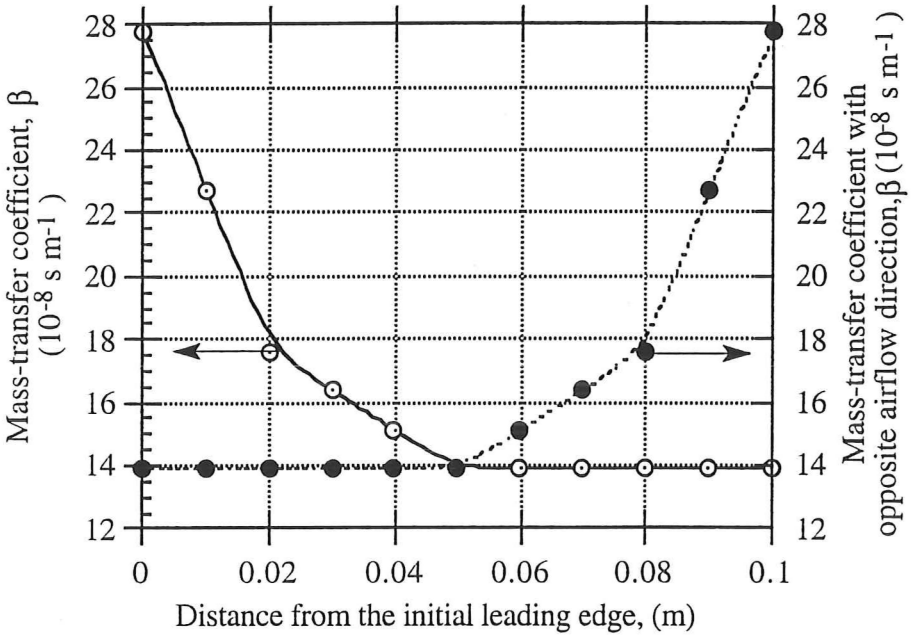

Figure 8.2. Local external mass-transfer coefficient variation through the board when the air flow is reversed every four hours.

Air velocity = 5 m s^{-1}. Boards: 100x50 mm. Sticker thickness (board gap): 25 mm.

The average mass-transfer coefficient over each board, $<\beta>$, may be calculated from the local values of the coefficient, β. If the vapour diffuses from a saturated surface of a wet board with a width of L_x and a length of L_y, then the total amount of the vapour transferred from the board surface, N_{tot}, is

$$N_{tot} = \int_0^{L_x} \beta\, (p_s^v - p_G^v)\, L_y\, dx = <\beta>\, L_x\, L_y\, (p_s^v - p_G^v) \qquad (8.6)$$

Therefore the average mass-transfer coefficient can be calculated by integration,

$$<\beta> = \frac{1}{L_x} \int_0^{L_x} \beta \, dx \tag{8.7}$$

or by accumulation,

$$<\beta> = \frac{1}{L_x} \sum_{i=1}^{n} \beta_i \, \Delta x_i \tag{8.8}$$

Figure 7.8 in Chapter 7 is an example of such a board-averaged mass-transfer coefficient profile over each board in a stack. When the airflow direction is altered with the air inlet becoming the outlet, this profile of external mass-transfer coefficients will be reversed.

In the following sections of this chapter, the external mass-transfer coefficients presented above will be used and the relationship between heat- and mass-transfer coefficients will be employed to define the external conditions both over a single board and through a kiln stack. By solving the model proposed in Chapter 3 the temperature and moisture-content profiles within a board will be predicted, while for kiln wide calculations the method presented in Chapter 7 will be used. In the calculations, the air is taken as at dry-bulb temperature of 120°C and wet-bulb temperature of 70°C. The air velocity will be assumed to be 5 m s^{-1}. These calculations will present a picture of the temperature and moisture content profiles within a single board at different stages of drying while for the drying of a kiln stack the distribution of local average moisture content will be given.

The strategies for the airflow reversals in the simulation are as follows:

Strategy A: the airflow is reversed every 3 hours;
Strategy B: the airflow is reversed every 4 hours;
Strategy C: the airflow is reversed every 8 hours;
Strategy D: the airflow is reversed only once after 4 hours of drying.

Strategy A and Strategy B have been practised in commercial kiln drying in New Zealand. Strategy C is used to investigate the influence of extending the interval length for reversing the airflow. Strategy D is proposed to investigate the effects of only a single reversal.

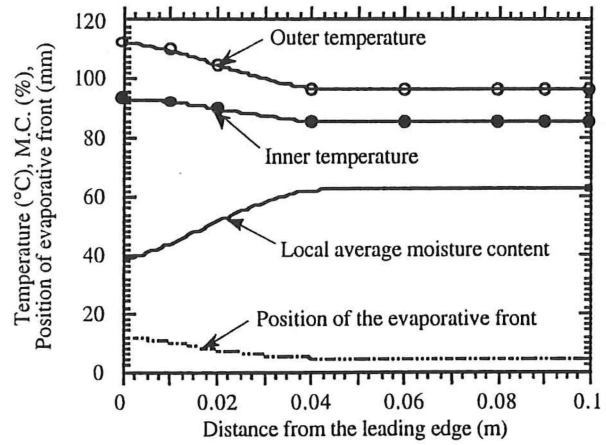

(a). Airflow is undirectional.

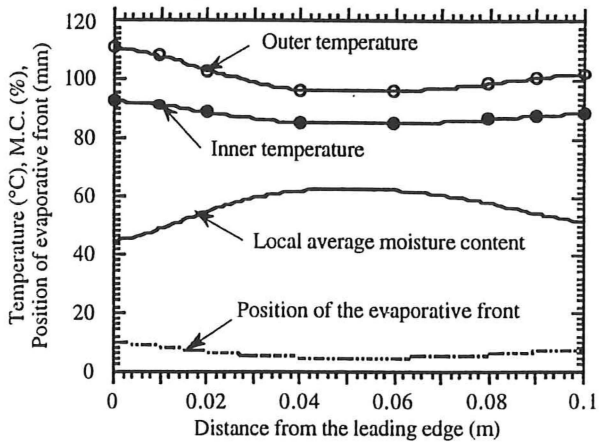

(b). Airflow is reversed every 3 hours.

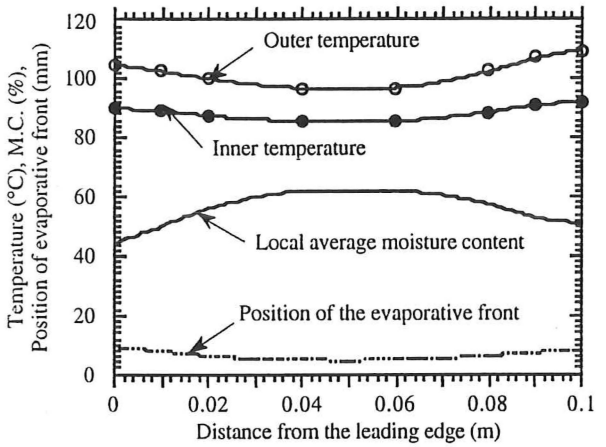

(c). Airflow is reversed every 4 hours.

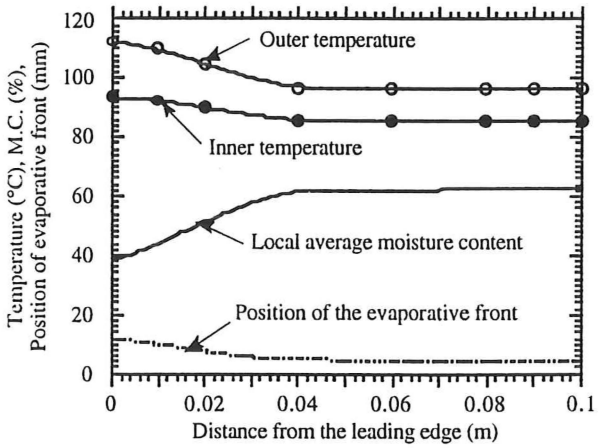

(d). Airflow is reversed every 8 hours.

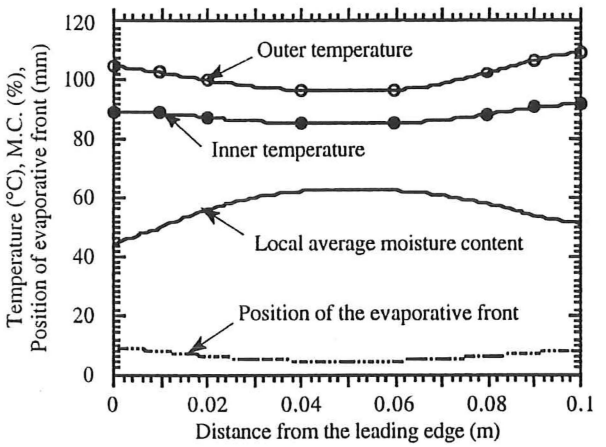

(e). Airflow is reversed only once after 4 hours.

Figure 8.3 The variations of the surface and centre temperatures, local average moisture content and the position of the evaporative front with distance along board from the leading edge: sapwood; after 8 hours of drying.

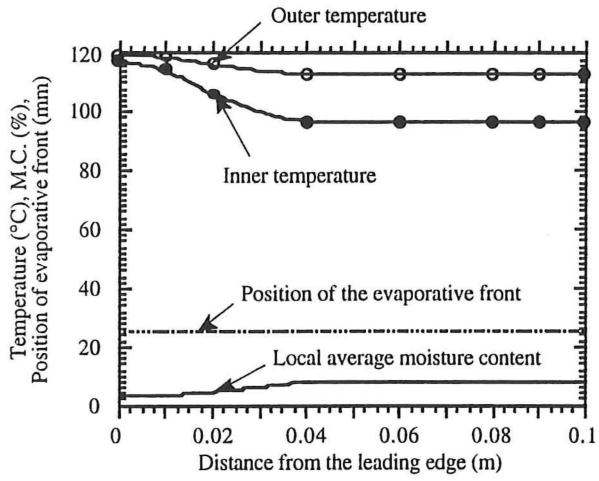

(a). Airflow is unidirectional.

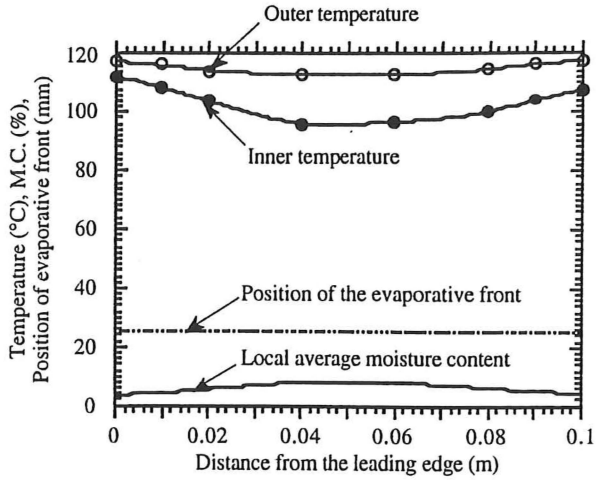

(b). Airflow is reversed every 3 hours.

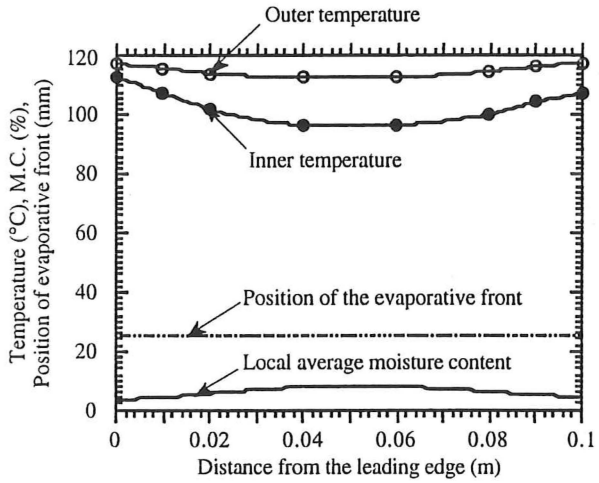

(c). Airflow is reversed every 4 hours.

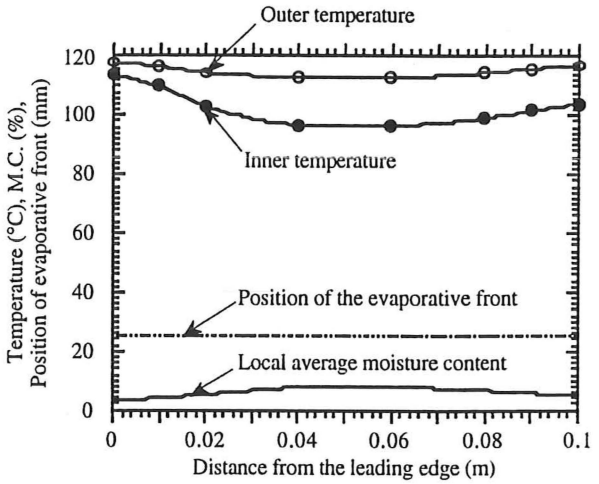

(d). Airflow is reversed every 8 hours.

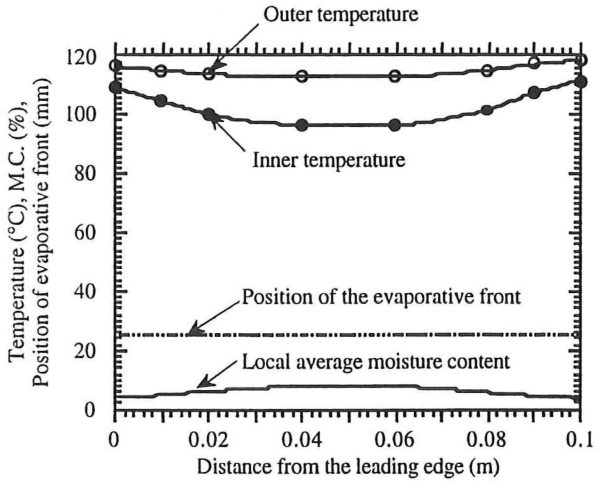

(e). Airflow is reversed only once after 4 hours.

Figure 8.4 The variations of the surface and centre temperatures, local average moisture content and the position of the evaporative front with distance along board from the leading edge: sapwood; after 16 hours of drying.

8.2 Temperature and Local Moisture-Content Profiles within A Single Board

8.2.1 Initial Conditions and Physical Properties of the Wood

In the simulation, the initial moisture content and basic density will be taken as those measured by the author (Chapter 4). The values of these two parameters are within the ranges reported by Cown *et al.* (1991) although these vary considerably between heartwood and sapwood. The wood permeabilities will be the same as those fitted in the single board simulation in Chapter 6. Other parameters will be determined using the methods from Chapters 4 and 5. Some of these properties and parameters are set out in Table 8.1.

Table 8.1 Values of parameters used in the simulation of drying a *Pinus radiata* single board

Parameters	Heartwood	Sapwood
Wood basic density, ρ_S, kg m^{-3}	377	450
Initial moisture content, X_o, kg kg^{-1}	0.40	1.40
Wood permeability to gas flow, K_G, 10^{-15} m^2	0.4	1.2
Wood permeability to liquid flow, K_l^S, 10^{-16} m^2	—	12.0
Thickness of the thin dry layer, ξ_o, mm	—	1.2

8.2.2 Results

By using the values given in Table 8.1 and on considering the variations in the heat- and mass-transfer rates with distance (Figure 8.1), the local temperature and average moisture-content profiles have been calculated both for a sapwood and heartwood board. Figures 8.3 - 8.4 show the results for a sapwood board: the variations of the temperatures at the surface and centre-line of the board, the local moisture contents and the position of the evaporative front with distance through the board. Heartwood has similar profiles to

sapwood, but the extent of the variations are less than those for sapwood due to the lower initial moisture content for heartwood. In Figures 8.3b to 8.3e, the simulation results are presented for drying after 8 hours with different reversal strategies. These results are compared with those with unidirectional airflow in Figure 8.3a. Figures 8.4a to 8.4e show similar results for the drying after 16 hours.

In Figures 8.3 and 8.4, the surface and centre temperatures within the wood are given to show the overall temperature differences between the surface and the centre-line of the board. In fact, the temperature changes across the thickness of the board are not uniform. In the wet zone, the temperature differences at positions perpendicular to the surface are not significant because the evaporation of water is negligible and the heat requirement for heating up the material is small. Therefore, the temperatures in the wet zone are close to that at the evaporative plane. During the initial period of drying when the wood is relatively cool, the temperature gradients in this zone have the largest value, but the temperature at the centre-line is only about 3°C lower than that at the evaporative plane.

In the dry zone, however, the temperature drop spans for most of the overall differences in temperature. The quantitative prediction of the temperature distribution is complex due to the non-linear variation of water vapour flux in this zone. As more water evaporates at a given location (liquid water at the evaporative front and bound-water at other points), more heat is required, resulting in a steep change in temperatures about this location. Normally, this situation occurs near the timber surface, since all the heat required to heat up the material and to evaporate the moisture (both bound- and unbound-water) will be transferred through the external surface.

The local average moisture contents in the board represent some volume-smoothed values at a position while the moisture contents vary both with the distance from the leading edge and with the depth from the board surface. In the dry zone the moisture is in equilibrium with local temperature of water vapour. At the position just above the evaporative front, the moisture content equals the fibre saturation value X_{FSP} (about 0.2 kg kg^{-1} at high temperatures), while near the surface the moisture content will decreases from X_{FSP} (when the evaporative front starts to recede) towards the equilibrium moisture content (during the second period of drying). The value of the equilibrium moisture content at operating conditions of 120°C/70°C is about 0.022 kg kg^{-1}.

In the wet zone, the moisture content profile will obey equation (3.32). If the apparent diffusion coefficient in this equation is taken as a constant in a small region, then the local

moisture content can be estimated by assuming a penetration process. The relative moisture content takes an error function:

$$\frac{X - X_{min}}{X_{cent} - X_{min}} = erf(u) \tag{8.9}$$

where X_{cent} is the moisture content at the centre-line, and u is a variable defined as:

$$u = \frac{z - \xi}{\sqrt{4\eta\tau}} \tag{8.10}$$

The parameter u is the non-dimensional extent of the drying process.

Therefore, the profile of the moisture content X against distance from the evaporative plane $(z - \xi)$ has approximately the shape of the error function. The relationship is only approximate because the apparent diffusion coefficient η is not actually independent of moisture content and temperature.

8.2.3 Discussion

In Figures 8.3 and 8.4, the profiles of temperature and local average moisture-content and the position of the evaporative front are shown at the same elapsed time (after 8 and 16 hours of drying). Thus the comparison in the temperature and moisture-content profiles within a board during drying can be clearly made between the results of unidirectional airflow and those with airflow reversals .

For sapwood drying with unidirectional airflow (Figures 8.3a and 8.4a), there is an initial period when the liquid flow outwards keeps the evaporative front near the surface for a variable length of time, depending upon the position from the leading edge of the board. The extent of the first period of drying will depend on both the external heat- and moisture mass-transfer rates and the initial moisture content of the green sawn wood. In this simulation where the initial moisture content is taken as 1.4 kg kg^{-1}, the first period lasts 4 hours for the wood at the leading edge, while in the material near the trailing edge this period extends to about 6 hours.

After the first period ends, the evaporative front will withdraw into the wood leaving the thin dry layer and, once this occurs, the internal resistance to vapour flow through the wood will increase significantly. Since the wood at the leading edge dries faster and the evaporative front starts to leave the thin dry layer earlier than that at other positions, the

moisture content at the leading edge drops more quickly (with 27 % M.C. lower than other positions after 4 hours of drying). In subsequent drying, this difference persists with only 2% difference in moisture content until the evaporative front at the leading edge has reached the mid-layer of the board after 12 hours of drying. Afterwards, the moisture content difference is reduced as the drying in the driest zone is retarded with only wood cell diffusion taking place. After 16 hours of drying, the difference in local average moisture content is 4% only between the leading edge and trailing edge. This difference may be further reduced to less than 0.5% with another 4 hours of drying. The duration of 24 hours drying was recommended by Williams and Kininmonth (1984) to dry New Zealand *Pinus radiata* boards of 100x50mm with the schedule considered, although recently shorter drying times are used commercially by employing higher air velocities than 5 m s^{-1}.

The greatest difference of surface temperature across the board also occurs between the leading edge and the trailing edge, with a value of 25°C after 6 hours of drying. This difference is reduced to 16°C after 8 hours and to 7°C after 16 hours of drying.

The inner temperatures everywhere are close to each other, with a difference of 5°C before the evaporative front at the leading edge has reached the centre-line of the board after 12 hours of drying. After this time, the centre temperature at the leading edge starts to rise while the centre temperatures at other positions still remain at around the boiling point (100°C). The largest difference of 20°C in inner temperature occurs after 16 hours of drying when the evaporative front near the trailing edge has just reached the centre line of the board. The differences both for surface and inner temperatures are reduced to less than 3°C after 20 hours of drying.

The above features of sapwood drying with unidirectional airflow can also apply to heartwood except that for heartwood drying the evaporative front will withdraw continuously into the material virtually from the start of drying (Pang, Keey and Langrish, 1992b). During this period of drying, at positions near the leading edge the temperatures rise more swiftly, the evaporative planes recede more deeply and the average moisture contents decrease more quickly than those at other places across the board in the airflow direction. After 4 hours of drying, the temperature near the leading edge begins to rise slowly due to the loss of the moisture at the surface and the mass-transfer rate falls. After 12 hours when the evaporative plane everywhere has reached the board's centre-line, the moisture contents at surface are almost at the equilibrium moisture content and the surface temperatures approach the dry-bulb temperature of the air. During the final period, the heat- and mass-transfer rates at any point become much lower than those in the

initial period of drying, and the differences in temperatures and average moisture contents through the board finally become insignificant.

The largest temperature difference occurs on the surfaces between the leading edge and the trailing edge with a value of about 10°C after 2 hours drying, while after 12 hours (when the evaporative plane everywhere has reached the centre-line of the board) the surface temperature at the trailing edge is 5°C lower than that at the leading edge. After 20 hours of drying, this temperature difference is estimated to be only 0.1°C.

The average moisture-content difference between the leading edge and the trailing edge is stable during the first period of drying and remains about 3% before the evaporative plane has reached the centre-line of the board everywhere. This difference with distance through the board in moisture content is mainly due to the variation in the depth of the evaporative plane at various positions across the board, because the moisture content in dry zone is much lower than that in the wet zone. Therefore, during the second period of drying (after the evaporative plane everywhere has reached the centre-line of the board) this moisture-content variation is reduced, reaching equilibrium after 20 hours drying.

For practical operation in a commercial kiln where the airflow is usually reversed periodically, the profiles of local temperature and moisture-content will change with these reversals. Before the first change in the flow direction, the temperature and moisture content profiles are the same as those with the unidirectional airflow discussed above. However, when the airflow is reversed, the previous leading edge becomes the trailing one and *vice versa.* The heat- and mass-transfer coefficient profiles are also inverted. The temperatures and moisture-contents profiles will now track these changes.

When the fan direction is changed every 4 hours in a kiln, the differences in the temperatures and moisture contents can be reduced greatly some time after the first flow reversal. For sapwood, the most non-uniform profiles of the temperatures and the average moisture contents occur after 4 to 12 hours of drying. Just before the airflow is to be reversed (after 4 h), the surface temperature at the leading edge is 14°C higher and the moisture content there is 27% lower than the corresponding values near the trailing edge. However, after the airflow has been reversed once, these differences fall to 8°C for the temperatures and 13% for the average moisture contents. After 8 hours the temperatures at the positions near both edges are close and higher than those in the middle-area of the board (Figure 8.3c). Likewise, the moisture contents at both edges also have a similar profiles, but are lower than those in the middle-area. This feature persists, even with continuing airflow reversals (Figure 8.4c). The lower temperatures and the higher

moisture contents in the middle-area are due to the lower average external heat- and mass-transfer rates even though the airflow has been reversed several times. The reason for this persistence lies in the fact that the airflow reversals only influence the magnitude of the transfer coefficients at the leading and trailing edges of each board. The drying conditions through the central strip of the board are barely changed. The final differences in temperature and average moisture content are 3°C and 1% respectively after 20 hours of drying.

The same tendency seen in sapwood drying is evident in the predictions for heartwood drying, but the profiles of the temperatures and the average moisture contents are relatively uniform because of the lower initial moisture content of heartwood (Pang, Keey and Langrish, 1992b).

In the case of airflow reversal every 8 hours, Figure 8.3d illustrates the result without reversing the airflow for sapwood before 8 hours: large temperature gradients are set up across the board with a wide variation of moisture content. However, after 8 hours the variation in these profiles with distance through the board are reduced and similar profiles to those for airflow reversals every 4 hours can be achieved.

A remarkable feature for reversing the airflow every 3 hours is that the maximum differences in moisture content and temperatures will be reduced since the first reversal after 3 hours of drying is before the greatest differences would have occurred when using the unidirectional airflow. With the airflow reversals every 3 hours, the largest difference in moisture content is 20% between 3 and 10 hours of drying. the maximum differences in surface and inner temperatures are 15°C (after 8 hours) and 16°C (after 16 hours) respectively. However, this strategy for airflow reversals produces a similar final results as those with airflow reversals every 4 hours after 20 hours of drying.

With only one airflow reversal (after 4h), the similar profiles of local temperature and moisture-content to those with reversals every 4 hours have been observed after 8 hours and 16 hours of drying. Hence further reversals are of only marginally benefit (Figures 8.3e and 8.4e). However, this conclusion is only valid for the drying of a single board. In the kiln-wide drying, the only one reversal may introduce some differences when the changes in external conditions throughout the kiln are taken into consideration.

For the drying of heartwood, the airflow reversals will also change the profiles of temperature and local average moisture content within a board, but the benefit is not as significant as for sapwood due to the much lower initial moisture content in heartwood.

The details of the simulation results with the airflow reversals for heartwood can be found elsewhere (Pang, Keey and Langrish, 1992b)

8.3 Local Average Moisture-Content Profiles through A Kiln Stack

8.3.1 Results

In the previous chapter, the profile of the local averaged external mass-transfer coefficient with distance through the airstream across a kiln stack has been presented. By using this profile, the local average moisture contents have been calculated for different stages of drying. In those calculations the airflow was assumed to be unidirectional. When the airflow direction is reversed, however, the external condition through a stack will be reversed and the drying rate at most of the positions except for the mid-region will be changed. As a result, the boards near the new air intake (the old air offtake) now dry faster that those close to the new air offtake (the old air intake). In this way the local average moisture contents in both sides of a stack can be smoothed out. The simulation results of sapwood drying for each strategy are shown in Figures 8.5a to 8.5e. In these figures, the variations of local average moisture contents with distance through airstream from the original leading edge are presented for different stages of drying. To describe the uneven distribution of local average moisture contents across a kiln stack, the maximum differences through a kiln-stack with drying time are given in Figures 8.6 and 8.7 for the comparison by using different strategies of airflow reversals. Figure 8.6 shows the results using different time interval for uniform airflow reversals, compared with that of unidirectional airflow while in Figures 8.7 the results of reversing the airflow only once after 4 hours of drying is compared with that with reversals every 4 hours. In all these calculations, the base case is taken of a kiln operating at dry-bulb/wet-bulb temperatures of 120/70°C and an air velocity of 5 m s^{-1}. In Figure 8.7, another curve is plotted for the airflow reversals after 2 and 6 hours from the start of drying.

A similar evaluation for heartwood drying is shown in Figures 8.8 to 8.10. As the initial moisture content for heartwood is much lower than that for sapwood, the differences in local average moisture contents are much less than that of sapwood at the same elapsed time of drying.

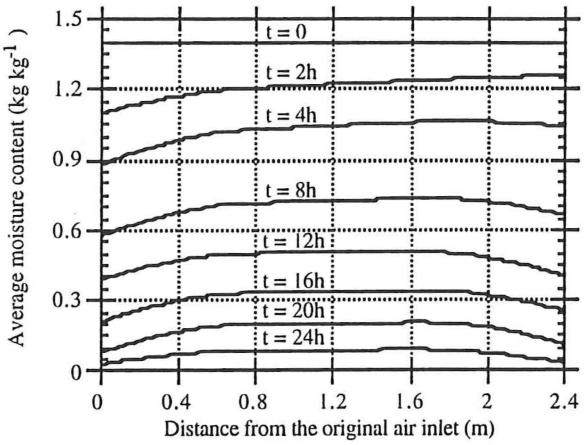

(a). Strategy A: Airflow is reversed every 3 hours.

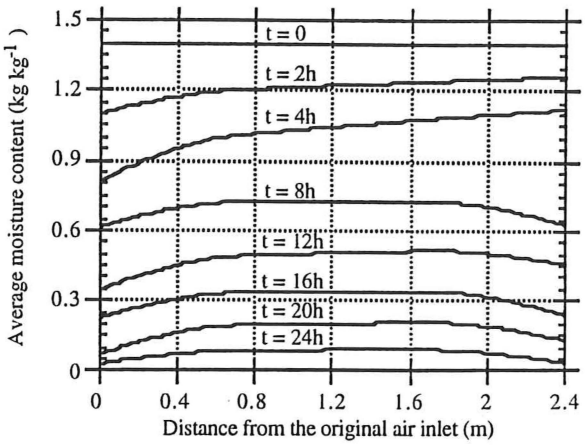

(b). Strategy B: Airflow is reversed every 4 hours.

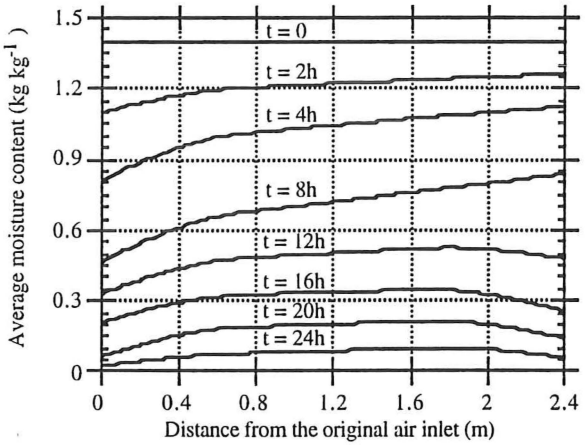

(c). Strategy C: Airflow is reversed every 8 hours.

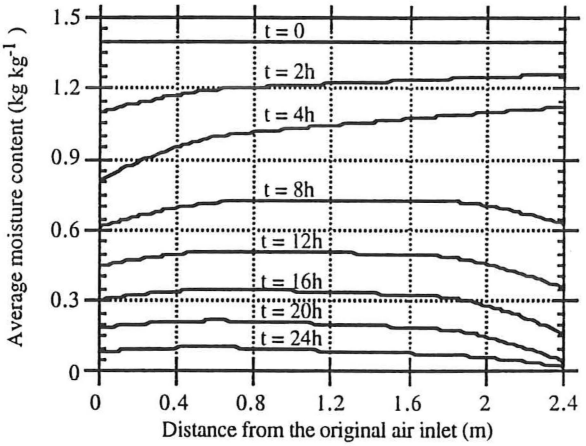

(d). Strategy D: Airflow is reversed only once after 4 hours of drying.

Figure 8.5 The distribution of local average moisture content through a kiln stack of sapwood boards with different airflow strategies. Dry-bulb/wet-bulb temperatures are 120/70°C. Air velocity is 5 m s^{-1}.

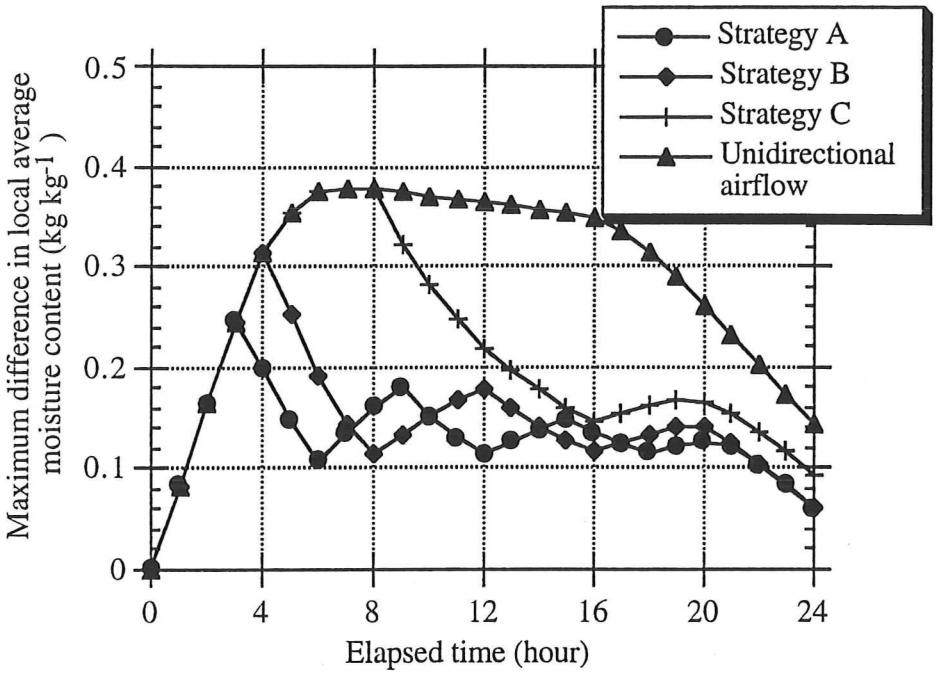

Figure 8.6 The comparison of maximum differences in local average moisture content for sapwood with different time intervals for airflow reversals and that with unidirectional airflow.
Dry-bulb/wet-bulb temperatures are 120/70°C. Air velocity is 5 m s^{-1}.

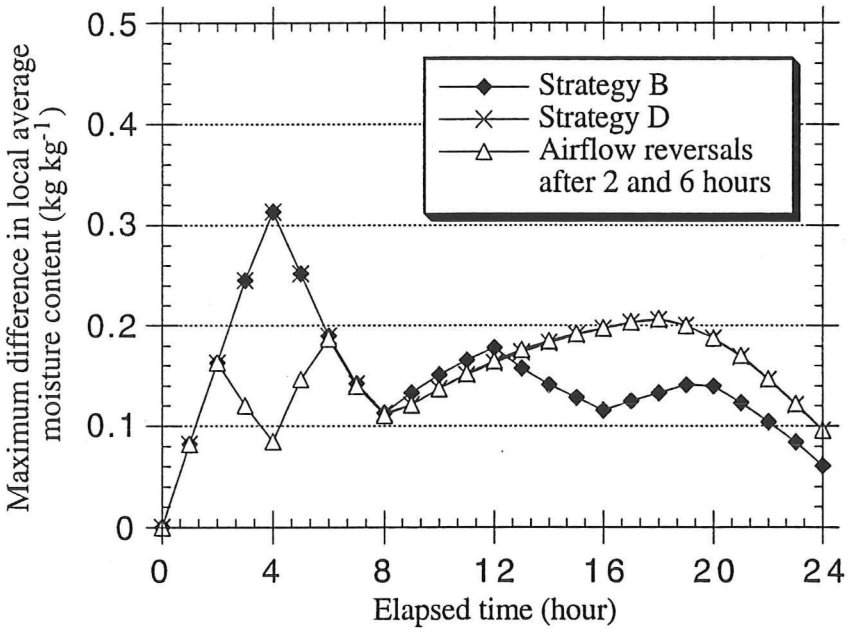

Figure 8.7 The comparison of maximum differences in local average moisture content for sapwood with airflow reversals every 4 hours and that with only once after 4 hours.
Dry-bulb/wet-bulb temperatures are 120/70°C. Air velocity is 5 m s^{-1}.

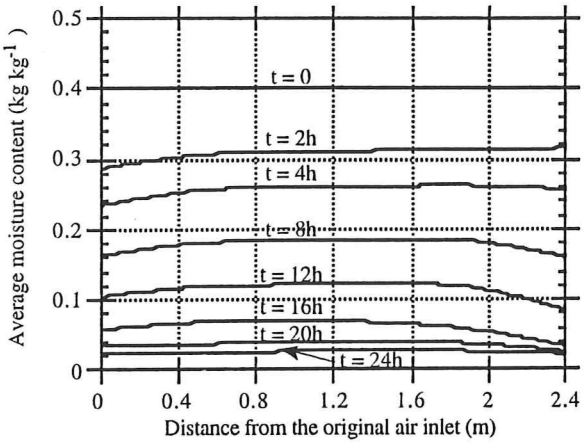

(a). Strategy A: Airflow is reversed every 3 hours.

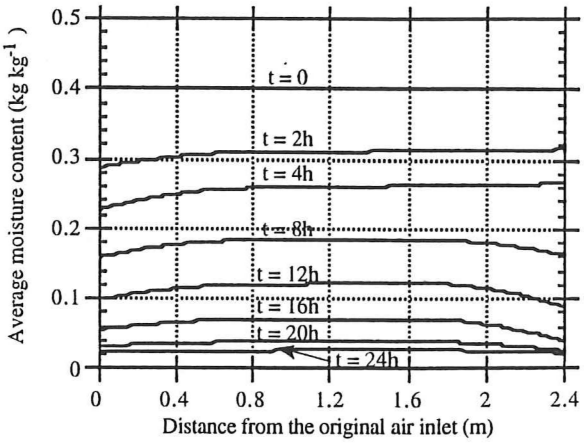

(b). Strategy B: Airflow is reversed every 4 hours.

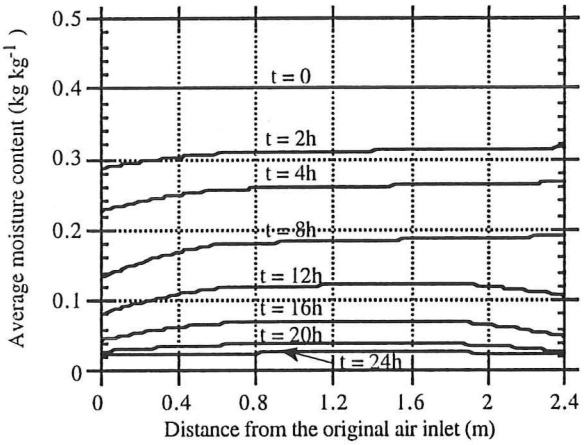

(c). Strategy C: Airflow is reversed every 8 hours.

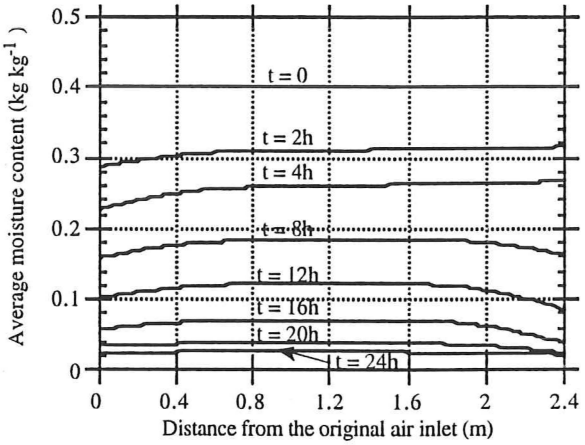

(d). Strategy D: Airflow is reversed only once after 4 hours of drying.

Figure 8.8 The distribution of local average moisture content through a kiln stack of heartwood boards with different airflow strategies. Dry-bulb/wet-bulb temperatures are 120/70°C. Air velocity is 5 m s^{-1}.

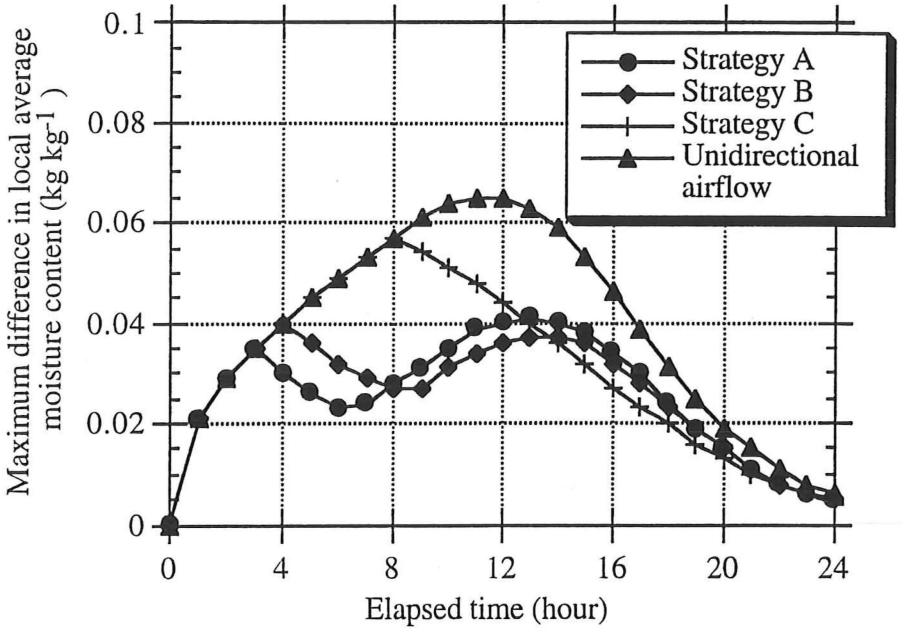

Figure 8.9 The comparison of maximum differences in local average moisture content for heartwood with different time intervals for airflow reversals and that with unidirectional airflow. Dry-bulb/wet-bulb temperatures are 120/70°C. Air velocity is 5 m s^{-1}.

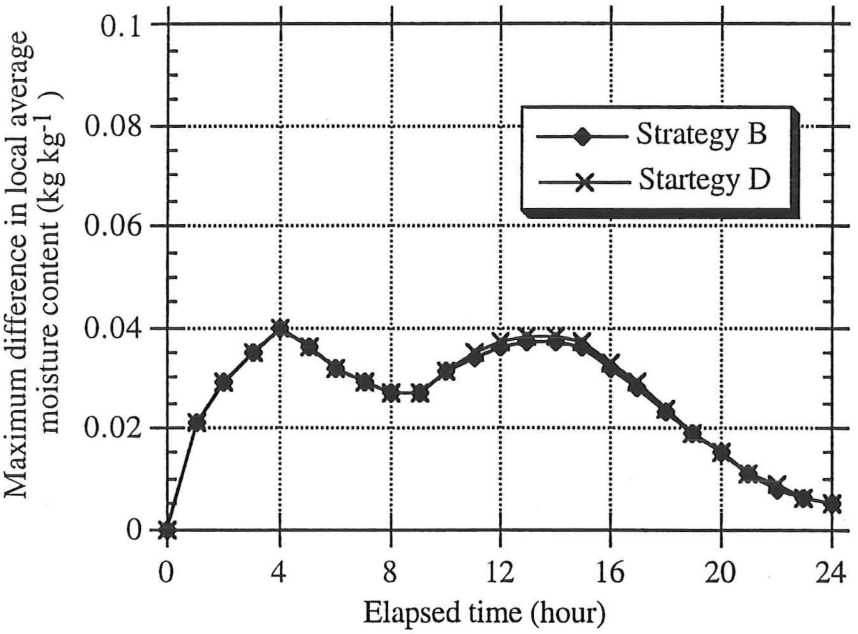

Figure 8.10 The comparison of maximum differences in local average moisture content for heartwood with airflow reversals every 4 hours and that with only once after 4 hours. Dry-bulb/wet-bulb temperatures are 120/70°C. Air velocity is 5 m s^{-1}.

8.3.2 Discussion

8.3.2.1 Sapwood

Initially, the moisture content is assumed to be uniformly distributed. As drying starts, the boards at air intake dry faster than those behind along the airstream as discussed in Chapter 7. However, when the airflow direction is reversed, the wettest zone at the old air offtake, which now becomes the air intake, gains the highest drying rates due to the favourable external conditions. This process is repeated when further airflow reversals are performed, hence the average moisture contents in both sides of the stack achieve essentially similar values. Soon after the first airflow reversal, the mid-area in the kiln stack becomes the wettest zone since the external conditions over this area are virtually unchanged if the airflow has been reversed several times.

With the unidirectional airflow as discussed in Chapter 7, the maximum differences in local average moisture content across a stack has peak values in the range of 36 to 38% moisture content (MC) during 6 to 16 hours of drying (Figure 8.6). Therefore for the airflow reversals every 8 hours, the peak value cannot be reduced. However, with the airflow reversals, the duration of the peak values is reduced to 4 hours. For other strategies of airflow reversals with uniform time intervals, the greatest values of maximum differences in local average moisture content are reduced to 30% (MC) for 4-hour reversals and to 25% (MC) for 3-hour reversals. These peak values with airflow reversal occur just before the first-time reversal and are not long-lasting. With further reversals, the maximum differences in moisture content remains between 10% (MC) and 20% (MC) without significant variations with different reversal strategies. This means that the first reversal is critical to minimize the uneven distribution on local average moisture content through a kiln stack of sapwood boards.

After 20 hours of drying, the maximum differences in local average moisture content for each strategy of uniform reversals are between 12% to 16% (MC), while the actual values of the average moisture contents across a kiln stack vary from 6% to 22% (MC). With another 4 hours of drying, the maximum difference in local average moisture content can be reduced to be less than 8% (MC). Since at this stage of drying the driest zones, at both sides of the stack, approach the equilibrium value, the moisture contents across the stack fall in a range of 3% to 11% (MC). The values of variations in average moisture contents for each strategy are as follows: 3.0% to 9% (MC) for reversals every 3 hours; 3.0% to 9.1% (MC) for reversals every 4 hours and 2.4% to 10.3% (MC) for reversals every 8

hours. This range of average moisture contents is consistent with the specified final moisture contents for ordinary timber products, bearing in mind that a condition stage is usually applied after drying..

In Figure 8.7, the result for only a single reversal is compared with that for uniform reversals every 4 hours. From this comparison, it is observed that the single reversal strategy can produce an essential similar result to that with uniform reversals during the first 12 hours from the start of drying. However, after this time the maximum difference in moisture content with the single reversal strategy becomes greater. After 24 hours of drying, the local average moisture contents with the single reversal strategy vary from 2.2% to 11% (MC), while the values with uniform reversals every 4 hours are from 3% to 9% (MC). When the airflow is reversed after 2 and 6 hours, the maximum difference in moisture content during the initial stages of drying can be further reduced to below 0.2 kg kg^{-1}.

8.3.2.1 Heartwood

The nonuniformity in the local average moisture content of heartwood boards through a kiln stack is significantly less than that for sapwood at the same drying time with the same airflow reversal strategy. With the unidirectional airflow as discussed in Chapter 7, the greatest value for moisture content differences is 6.5% (MC) after 10 hours of drying. For the drying with uniform airflow reversals, this value is reduced to 5.5% (MC) for reversals every 8 hours, and to 4.0% (MC) for reversals every 3 or 4 hours respectively. For reversals every 4 or 8 hours, the greatest differences in local average moisture content occur just before the first-time reversal, while with the reversals every 3 hours the greatest nonuniform distribution occurs between 8 and 14 hours from the start of drying. After 16 hours of drying the greatest differences with each uniform reversal strategy are reduced to less than 3.8% (MC), with the actual average moisture content ranging from 3.3 to 7.1%. The strategy with only a single airflow reversal has virtually the same results as that with uniform reversals.

8.4 Conclusion and Recommendations

Using the measured local mass-transfer coefficient profiles from Kho, Keey and Walker (1989, 1990), the local temperatures and moisture contents within a single board during the high-temperature drying of *Pinus radiata* can be predicted from the mathematical model developed in Chapter 3. When the air flows in one direction only, the temperatures are higher and the moisture contents are lower at the leading edge than in other positions due to the variations in the local heat- and mass-transfer rates. In the case of airflow reversals, these differences can be reduced and more uniform temperature and moisture-content profiles can be obtained. This should reduce the number of drying-related defects.

In the drying of a kiln stack of boards, a similar analysis can be performed by employing the simplified model proposed in Chapter 7. With unidirectional airflow, the local average moisture content at air inlet is significantly lower than that near the air outlet. This nonuniform distribution in average moisture content between two sides can be smoothed out by reversing the airflow. Some recommendations are given as follows:

• The first reversing of the airflow is critical to reduce the maximum differences in average moisture-content through a kiln-stack. The maximum difference in average moisture-content occur just before the airflow is first reversed when the drying lasts longer than 2 hours.

• Not many reversals are needed. Only twice reversals after 2 and 6 hours may be adequate to give a reasonable degree of uniformity in the temperature and moisture-content profiles within the boards and within a kiln stack.

8.5 Nomenclature

C_{PG} specific heat capacity of humid air, J kg^{-1} K^{-1}

C_{PV} specific heat capacity of water vapour, J kg^{-1} K^{-1}

C_{PY} specific heat capacity of moist air, J kg^{-1} K^{-1}

f relative drying rate, -

F external mass-transfer coefficient, mol m^{-2} s^{-1}

h external heat-transfer coefficient, W m^{-2} K^{-1}

N_{tot} the total moisture flux from the surface of a board to the airstream, kg m^{-2} s^{-1}

K_G permeability of wood to gas, m^2

K_l^s permeability of saturated wood, m^2

K_o external mass-transfer coefficient based on the humidity difference, kg m^{-2} s^{-1}

L_x width of a single board, m

L_y length of a single board, m

M_G molar mass of dry air, kg mol^{-1}

M_v molar mass of water vapour, kg mol^{-1}

P_t total pressure of the air stream, Pa

p_{BM} logarithmic mean partial pressure difference of component B, Pa

p_{BI} partial pressure of component B at board surface, Pa

$p_{B\infty}$ partial pressure of component B in the main stream, Pa

p^v vapour pressure, Pa

p_∞^v partial pressure of water vapour in the air stream, Pa

p_S^v partial pressure of water vapour at the surface of a board, Pa

X local moisture content , kg kg^{-1}

X_{cent} moisture content at the centre line of a sapwood board, kg kg^{-1}

X_{FSP} moisture content at the fibre saturation point, kg kg^{-1}

X_{min} minimum value of moisture content for liquid continuity within wood, kg kg^{-1}

Greek

Φ characteristic moisture content, -

β external mass-transfer coefficient, s m^{-1}

$<\beta>$ average mass-transfer coefficient over a single board, s m^{-1}

ξ distance of the evaporative plane from the surface, m

8.6 References

1. Ashworth, J.A. 1977. The Mathematical Simulation of the batch Drying of Softwood Timber. PhD Thesis, University of Canterbury, New Zealand.

2. Cown, D. J., McConchie, D. L. and Young, G.S. 1991. Radiata Pine Wood Properties Survey (1977 - 1982). New Zealand Forest Service, Forest Research Institute Bulletin No. 50 (rev.), Rotorua, New Zealand (unpublished).

3. Culpepper, L. 1990. "*High Temperature Drying: Enhancing Kiln Operations*". Miller and Freeman, San Fransisco.

4. Keey, R. B. 1991. "*Drying of Loose and Particulate Materials*". Hemisphere Publishing Co. New York.

5. Kho, P. C. S., Keey, R. B. and Walker, J. C. F. 1989. Effect of Minor Board Irregularities and Air Flows on the Drying Rate of Softwood Timber Board in Kilns. *Proc. IUFRO International Wood Drying Symposium*, Seattle, pp 150-157.

6. Kho, P. C. S., Keey, R. B. and Walker, J. C. F. 1990. The Variation of Local Mass-Transfer Coefficients in Streamwise Direction over A In-Line, Blunt Slabs. *Proc. Chemeca'90 Conf.*, Auckland, New Zealand, Vol.1, pp348-355.

7. Langrish, T. A. G., Keey, R. B., Kho, P. C. S. and Walker, J. C. F. 1993. Time-Dependent Flow in Arrays of Timber Boards: Flow Visualisation, Mass-Transfer Measurement and Numerical Simulation. *Chem. Eng. Sci.*, 48(12), pp2211-2223.

8. Pang Shusheng, Keey, R. B. and Langrish, T. A. G. 1992a. Modelling the Temperature Profiles within Boards during the High-Temperature Drying of *Pinus Radiata T*imber. in Mujumdar, A.S. (edr): *Drying'92*, Part A, pp417-433.

9. Pang Shusheng, Keey, R. B. and Langrish, T. A. G. 1992b. The Influence of Airflow Reversals during the High temperature Kiln Drying of *Pinus radiata* Boards. *Proc. Chemeca'92*, Canberra, Australia, Vol.2, pp153-2-160-2.

10 Stevens, W.C. and Johnston, D.D. 1957. Temperature Drop across A Pile of Green Timber and Its Effects on Drying Rates. *Timber Technology*, 65(2212), pp73-75.

11. Walker, J.C.F. 1993. "*Primary Wood Processing: Principles and Practice*". Chapman and Hall, London.

12. Williams, D. H. and Kininmonth, J. A. 1984. High Temperature Kiln Drying of Radiata Pine Sawn Timber. New Zealand Forest Service, Forest Research Institute Bulletin No.73, Rotorua, New Zealand (unpublished).

Chapter **9**

The Drying of Mixed Sap and Heartwood Boards

In Chapter 3, a mathematical model has been proposed to simulate the high-temperature drying of softwood boards. This model has been applied to both sapwoods board and heartwood boards respectively to predict temperature and moisture content profiles within a board during drying. In practice, however, the boards sawn from a green log fall into three categories according to their composition: (1) an entirely sapwood board; (2) an entirely heartwood board and (3) a mixed-wood board which contains both sapwood and heartwood. In the mixed sap and heartwood boards, the moisture movement becomes more complicated than in the entirely sapwood and the entirely heartwood.

In the case where the thickness of the heartwood layer is less than that of the sapwood within the board, the moisture in the sapwood close to the sap/heartwood transition layer either flows through a greater distance (more than half the thickness of the board) in the sapwood or across a shorter distance in the heartwood with much higher resistance (lower permeability than that of sapwood). As the sapwood is very wet in green wood, this part of the sapwood dries slowly and is likely to be the wettest region in a board in the later stages of drying.

Another difference between mixed-wood boards and sapwood or heartwood boards is that the mixed-wood boards contain a transition layer between sap and heartwood. Physiologically, this layer of wood differs from heartwood in that its ray parenchyma cells are alive and it is not impregnated with polyphenols, but it differs from sapwood in that much moisture has been lost and the pits have been aspirated in this transition zone. For *Pinus radiata*, Booker (1990) has found that the transition layer is only about one growth ring wide, which is too narrow for its actual permeability to be measured. Harris (1954) gives some experimental data on the percentage of aspirated bordered pits in green wood from the last-formed annual growth layer to the centre of the pith. He observed that the transition zone between sapwood and heartwood has almost the same percentage of aspirated pits as that in heartwood. The moisture content in the transition layer drops abruptly to a value similar to that in heartwood.

If the permeability and initial moisture content in this layer are assumed to be the same as those in heartwood, the drying of the mixed-wood boards can be simulated by employing simultaneously the earlier mathematical models for both sapwood and heartwood.

When the thickness of heartwood layer is equal to that of sapwood, the drying of such a board is similar to the drying of an entirely sapwood board and an entirely heartwood board separately. If the heartwood layer is greater than that of sapwood in thickness, the added difficulty in drying is still not significant compared with that for an entirely sapwood board. Since sapwood has a higher permeability and heartwood has a lower initial moisture content, the middle zone of such a board may dry slightly faster than an entirely sapwood board. As these two situations do not cause any significantly added difficulties with drying, the investigation here will focus on the drying of boards in which the heartwood layer is thinner than sapwood.

The whole drying of such a board can be considered as three phases, with an initial preheating period in which the board is heated up.

PHASE 1. Initially, the evaporative fronts on both the heartwood and the sapwood sides start to recede into the board. When the evaporative front on the sapwood side moves a short distance from the surface, forming a thin dry layer, the liquid water beneath the front flows towards it. This movement of liquid water keeps the front at this position until the liquid water just beneath this front is no longer funicular. Then the front recedes further towards the transition layer between the heartwood and sapwood. During this same period, the evaporative front from the heartwood side continues to move until the transition layer between sapwood and heartwood is reached. PHASE 1 is defined as the period before the evaporative front from heartwood reaches the transition layer.

PHASE 2. Once the evaporative front from the heartwood side has reached the transition layer, the liquid water in sapwood will flow towards this layer and evaporate. After some time, the liquid just beyond this layer will no longer be funicular either and this front starts to withdraw into the sapwood part. In subsequent drying, two fronts move in sapwood towards each other, one originally from the sapwood side and the other one from the heartwood side. Finally, they meet somewhere in the sapwood and PHASE 2 concluded.

PHASE 3. As soon as the two evaporative fronts have met, all the liquid water has evaporated. Thenceforth, the bound water diffusion and water vapour movement control the drying. This period of drying is called PHASE 3.

9.1 The Equations for Temperature and Moisture-Content Profiles

In the drying of a mixed sap and heartwood board (Figure 9.1), the heat and moisture mass conservation equations can be applied within the whole board. In order to solve the problem, each term in the equations needs to be specified for the different phases by using the corresponding boundary and initial conditions. These equations are:

$$C_P \rho_S \frac{\partial T}{\partial \tau} = \frac{\partial}{\partial z}[\lambda \frac{\partial T}{\partial z}] + \Phi \qquad (9.1)$$

$$- \rho_S \frac{\partial X}{\partial \tau} = \frac{\partial}{\partial z}(j_{wv} + j_{wf} + j_{wb}) \qquad (9.2)$$

where

C_P is the specific heat of moist wood, J kg^{-1} K^{-1}

X is the local moisture content, kg kg^{-1}

ρ_S is the basic density of wood, kg m^{-3}

T is the temperature, K

τ is the time, s

z is the space coordinate measured normal to the upper surface of the board, m

λ is the thermal conductivity of the moist wood, J m^{-1}

j_{wv} is the water vapour flux, kg m^{-2} s^{-1}

j_{wf} is the liquid water flux, kg m^{-2} s^{-1}

j_{wb} is the flux of bound water, kg m^{-2} s^{-1}

and Φ is the source term involving the latent heat of vaporization.

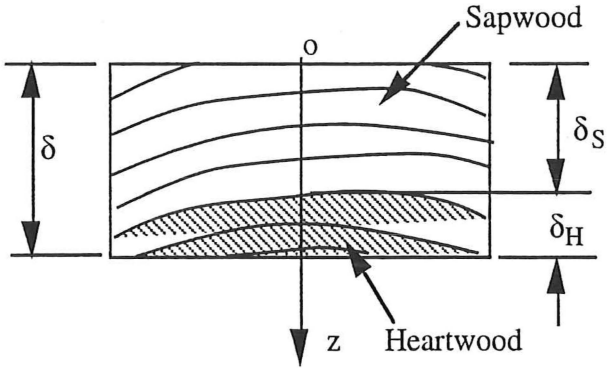

Figure 9.1. The mixed-wood board containing sapwood in the upper part and heartwood in the lower part.

In the following discussion, it is assumed that the heartwood is in the lower part with a thickness of δ_H and the sapwood in the upper side with a thickness of δ_S ($= \delta - \delta_H$) as shown in Figure 9.1.

9.1.1 Preheating Period

In this period, the wood is heated up while some water vapour in the airstream may be condensed on the board surfaces as the surface temperature is relatively low. During this period, the boundary conditions are:

(a). The convective heat transferred from airstream to board surfaces

$$q_S = \pm h\,(T_G - T_S) \tag{9.3}$$

(b). The vapour fluxes towards the board surfaces

$$j_{wv} = \pm \beta\,(p_G^v - p_S^v) \tag{9.4}$$

In equations (9.3) and (9.4),
q_S is the heat transferred through the surface, W m^{-2}
h is the external heat-transfer coefficient, W m^{-2} K^{-1}
T_G is the dry-bulb temperature of the airstream, K
T_S is the temperature at the surface, K
β is the external mass-transfer coefficient based on partial pressure difference, s m^{-1}
p_G^v is the vapour partial pressure in the airstream, Pa
and p_S^v is the vapour partial pressure at the board surface, Pa.
The positive sign is used for $z = 0$ and when $z = \delta$, the negative sign is taken.

(c). The source term in equation (9.1) is given by

$$\Phi = \Delta H_{wv} j_{wv} \text{ at } z = 0 \text{ and } z = \delta \tag{9.5}$$

in which ΔH_{wv} is the latent heat of vaporization of water.

Since the water and vapour flows within wood are negligible in the preheating period, the terms j_{wv}, j_{wf}, j_{wb} and Φ are taken as zero in region of $0<z<\delta$. When solving the above

equations, the wood properties, such as wood density, initial moisture content are taken as those of heartwood for heartwood layer and those of sapwood for sapwood part. The values in sap/heartwood transition layer are assumed to be those of heartwood.

9.1.2 Drying in PHASE 1

Since the physical properties of the wood vary substantially from sapwood to heartwood, the drying of sapwood and heartwood will be considered separately. It has been observed that the manner of liquid movement in green sapwood is significantly different from that in green heartwood due to the different state of pit aspiration. This has made it possible to develop a model to simulate the drying of both sapwood and heartwood. In the drying of mixed-wood boards, this idea will be employed again but here the sapwood and heartwood appear within one single board.

In PHASE 1, it is assumed that there exist two evaporative fronts, in the sapwood and the heartwood zones respectively, at which all the liquid water evaporates. By defining each term in equations (9.1) and (9.2) for sapwood and heartwood respectively, the equations can be solved with appropriate boundary conditions.

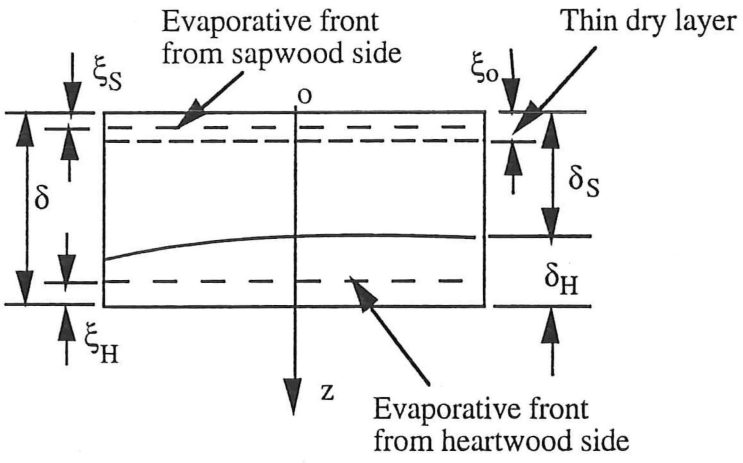

Figure 9.2 Drying in phase 1 with the two evaporative fronts receding from both the sapwood and the heartwood sides.

Let ξ_o be the thickness of the thin dry layer in the sapwood side, ξ_S the distance of the evaporative front from the sapwood side and ξ_H the distance of the evaporative front from the heartwood side (Figure 9.2). The water vapour fluxes in the dry zones ($0<z<\xi_S$ and $\delta-\xi_H<z<\delta$) can be predicted using Darcy's law

$$j_{wv} = -E_v \frac{\partial p^v}{\partial z} \tag{9.6}$$

in which p^v is the vapour partial pressure and E_v is the effective permeability to vapour flow which can be related to the normally measured permeability, K_G, by the equation:

$$E_v = \frac{K_v \rho_v}{\mu_v} \tag{9.7}$$

Here ρ_v and μ_v are the density and viscosity of the vapour respectively.

In the mixed-wood board, the permeability in the sapwood zone, K_{vS}, is different from that in the heartwood zone, K_{vH}, so the effective permeability will be calculated for both sides respectively as:

$$E_{vS} = \frac{K_{vS} \rho_v}{\mu_v} \quad \text{when } 0 < z < \delta_S \tag{9.7a}$$

$$E_{vH} = \frac{K_{vH} \rho_v}{\mu_v} \quad \text{when } \delta - \delta_H < z < \delta \tag{9.7b}$$

The vapour partial pressure can be calculated as a function of local temperature and moisture content using the relationship given in Chapter 4 for the wood of *Pinus radiata*. The boundary conditions for heat-transfer and moisture vapour flow at the surfaces of board are the same as expressed by equations (9.3) and (9.4). However, the vapour partial pressure at the surfaces is higher than that in the airstream at this stage of drying.

For the movement of bound water, the chemical potential has been used as the driving force and it has been assumed that the chemical potential of bound water is equal to that of water vapour (Stanish *et al.*, 1986). The bound water fluxes in the dry zones can be estimated by employing the expression of Stanish and his colleagues (1986):

$$j_{wb} = -\frac{D_b(1 - \varepsilon)}{M_v} \left\{ - \left[187 + 35.1 \ln\left(\frac{T}{298.15}\right) - 8.314 \ln\left(\frac{p^v}{101325}\right) \right] \frac{\partial T}{\partial z} + 8.314 \frac{T}{p^v} \frac{\partial p^v}{\partial z} \right\} \tag{9.8}$$

where D_b is the bound water diffusion coefficient, M_v is the molar mass of the water vapour and ε is the void fraction of the solid wood.

Since the bound water diffusion occurs within the wood tissue irrespective of the state of pit aspiration, the bound water diffusion coefficient of sapwood is the same as that of heartwood for the same species of wood such as *Pinus radiata.*

With the discontinuity of wood material at the surfaces of a board, the bound water cannot flow out of the board, so one can get

$j_{wb} = 0$ when $z = 0$ and $z = \delta$

In the wet zone since there are no significant vapour and bound water flows, both of these fluxes are taken as zero ($j_{wv} = 0, j_{wb} = 0$) when $\xi_S < z < \xi_H$.

In the wet region of the heartwood part, the liquid flow is also negligible, so

$j_{wf} = 0$ when $\delta - \xi_H < z < \xi_H$

As soon as the evaporative front from the sapwood side has reached a distance of ξ_o the liquid flow towards the front becomes significant. This liquid flow can also be described by Darcy's law. The pressure gradient is assumed to be a consequence of capillary action between the liquid and gas phases within the voids of wood. Thus this flux can be calculated from the earlier expression (Chapter 3):

$$j_{wf} = -\frac{A\ B\ E_l\ (X_{max} - X_{FSP})^B}{(X - X_{FSP})^{(1+B)}} \frac{\partial X}{\partial z} \quad \text{when } \xi_S < z < \delta_H. \tag{9.9}$$

where A and B are constants
E_l is the effective permeability of wood to liquid water flow, s m^{-1}
X_{FSP} is the moisture content at the fibre saturation point, kg kg^{-1}
and X_{max} is the moisture content of the wood if the entirely void structure were filled with liquid water, kg kg^{-1}.

In order to solve the above equation together with equations (9.1) and (9.2), it is necessary to know the boundary conditions at transition layer and at the evaporative front. Since no liquid water flows across the transition layer, the liquid flux is zero wherever $z = \delta - \delta_H$. At the other boundary when $z = \xi_S$, the local moisture content just above the front is at fibre saturation point, X_{FSP} and the moisture content just beneath the front can be estimated by adjusting the moisture content to satisfy mass conservation within the wet zone. The total moisture (liquid) losses from the wet zone during a time interval, $\Delta\tau$,

should equal the liquid flux just beneath the evaporative front multiplied by this time interval.

9.1.3 Drying in PHASE 2

In phase 2, as the evaporative front from the heartwood side withdraws into the sapwood just beyond the transition layer, liquid water will flow towards it. In this stage, equation (9.9) can also be used to predict the liquid flux in the wet zone between the two evaporative fronts. The moisture mass-conservation at this front is taken as the second boundary condition to solve the equation. The local moisture (liquid water) losses from the whole wet zone during a time interval, $\Delta\tau$, should equal the liquid fluxes just inside the two fronts multiplied by this time interval. On the heartwood side, when the liquid flux just inside the front equals the vapour flux just outside this front, this front remains stationary at the intermediate wood/sapwood boundary. Once the liquid in the adjacent sapwood is no longer funicular, this front will recede into the sapwood.

The same equations (9.6 to 9.8) and boundary conditions as those given in PHASE 1 can be used to describe the vapour and bound water movement in the drier zones. In this way equations (9.1) and (9.2) can be solved to predict the moisture-content and temperature profiles within a mixed board for this stage of drying.

9.1.4 Drying in PHASE 3

After the two evaporative fronts meet somewhere in the sapwood zone, all of the liquid water will have evaporated and the liquid flux everywhere will be zero in equation (9.2). This point is defined as the beginning of PHASE 3. For drying in PHASE 3, the equations and boundary conditions used in PHASE 1 and PHASE 2 for the dry zones apply for the entirely board. In this stage of drying, bound water diffusion and vapour flow control the movement of moisture.

9.1.5 Solving the Heat and Mass Transfer Equations Using A Numerical Method

In order to solve the equations described above using a numerical method, the whole board has been divided into J separate nodes. The sapwood is distinguished from heartwood at the point

$$J_{SH} = \frac{\delta_S}{\delta}(J\text{-}1) + 1 \tag{9.10}$$

The equation for the movement of liquid water in the wet zone has been rearranged as follows so that the local moisture content is directly related to distance and time

$$\rho_S \frac{\partial X}{\partial \tau} = \frac{\partial}{\partial z}\left(\eta \frac{\partial X}{\partial z}\right) \tag{9.11}$$

where η is the apparent moisture-content coefficient given by

$$\eta = \frac{A\ B\ E_l\ (X_{max} - X_{FSP})^B}{(X - X_{FSP})^{(1+B)}} \tag{9.12}$$

Equation (9.11) has a similar form as that for heat conduction, so it can be solved by the technique developed by Patankar (1980).

A similar technique as that presented in Chapter 3 will be employed to solve the equations for the drying of a mixed sap/heartwood board, but here the whole board instead of half of the board is considered and the board contains both sapwood and heartwood simultaneously. First, the heat conservation equation (9.1) will be solved for the temperature profiles within the whole timber. This enables the water vapour flux (j_{wv}) and bound water flux (j_{wb}) to be calculated in the drier zones, so the mass-conservation equation (9.2) can be solved in these zones. For sapwood, the moisture content in the wetter zone can be estimated from equations (9.11) and (9.12). These equations are non-linear and inter-linked. For example, the water vapour flux appears in the heat conservation equation. Therefore, the above procedure was repeated until all the temperatures changed between iterations by less than 0.001 K.

9.2 The Temperature and Moisture Content Profiles: Comparison of Simulation Results and Experimental Data

9.2.1 Experimental Results

A separate experiment was undertaken at New Zealand Forest Research Institute (NZFRI) to dry the mixed sap/heartwood boards under high temperatures. The objectives of the experiment were to investigate the temperature and moisture content profiles within a board during drying and to examine the local moisture-content gradient across a board. The dimensions of the drying specimens were 100x50x350 mm, which were sawn out from two larger boards with twice the specimens' thickness (100mm) and cut from a *Pinus radiata* stand of around 30 years old. Flat-saw specimens were cut with the boundary layer between sapwood and heartwood parallel to the drying surfaces (the two flat surfaces of the board). The thickness of the heartwood layer in the specimens was less than half of the board with the average thickness of the heartwood layer varying from board to board. The observed thickness of the heartwood layer ranges from 4 mm to 25 mm due to the irregularities in ring curvature and the variations of heartwood proportion with tree height. Small pieces were cut from each end of the specimen to determine the initial moisture content and basic density. The procedures for the tests were similar to that for drying of the sapwood and heartwood boards described in Chapter 6.

After the specimens were edge-painted, these were dried in the tunnel dryer at dry-bulb/wet-bulb temperatures of 120/70°C (Run 2) and 140/90°C (Run 3) respectively. The air velocity was 5 m s^{-1}. In the tests, five drying boards were placed in the dryer. One board was put on the cradle to monitor the temperatures on both surfaces and at depths of 8.3, 16.7, 25, 33.3, 41.7 mm from the upper surface. Meanwhile, the weight variations of this sample was recorded during drying. The other 4 boards were placed elsewhere for the local moisture contents measurement at different stages of drying. A single board was removed after drying for 6, 10, 14 and 19 hours from the start of drying in Run 2 (120/70°C) and for 3, 6, 10 and 12 hours in Run 3 (140/90°C). Immediately after the sample was taken from the dryer, three pieces 25 mm thick normal to the drying surface were sawn from the middle section of the board. One of these pieces was sawn immediately into slices, another was sawn 20 minutes later and the last one was put first in a deep freezer overnight and then sawn into slices. Finally all the slices were oven-dried to determine the local moisture content.

The experimental results are given in Figures 9.3 to 9.5. Figure 9.3 shows the variations of initial moisture contents with growth ring. These curves are similar to those reported by Cown *et al.* (1991). The moisture content in the heartwood ranges from 0.38 to 0.52 kg kg^{-1}, while the values in the sapwood vary in a range between 0.9 and 2.0 kg kg^{-1}, depending both on the ring position from the boundary between the heartwood and the sapwood and on the wood density. Since sapwood has a uniform saturation in green wood (Booker and Langrish, 1993), the initial moisture content is higher in low-density wood and lower in high-density wood. For sapwood with low density, the green moisture content is relatively constant differing less than 0.1 kg kg^{-1} from the zone boundary between sapwood and heartwood to the 5 growth rings away from this position. For sapwood with high density, this variation is 0.4 kg kg^{-1} with the moisture content of 1.0 kg kg^{-1} at the zone boundary and that of 1.4 kg kg^{-1} at the position 5 growth rings away.

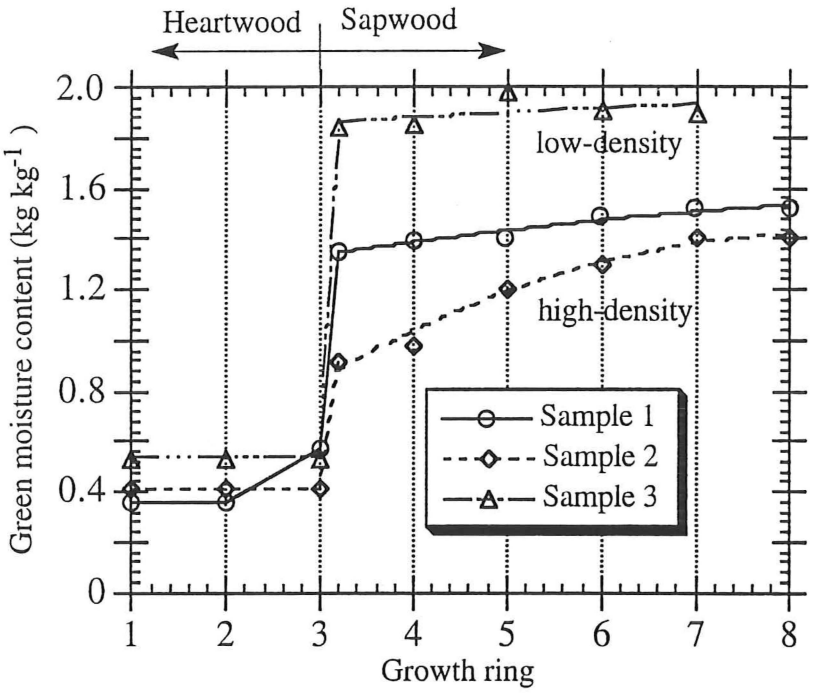

Figure 9.3 The green moisture content variations with growth ring from heartwood to sapwood (measured).

The temperature profiles within a board both for drying at 120/70 °C (Figure 9.4a) and for drying at 140/90°C (Figure 9.4b) reveal an asymmetrical profile across the thickness of the board before 10 hours of drying. In Run 2 (120/70°C), after 1 hour from the start of drying, the surface temperature on the heartwood side is 12 °C higher than that on the sapwood side although the initial values are very close after 1 or 2 minutes from the start of drying when the data were initially recorded. This difference persists until 10 hours

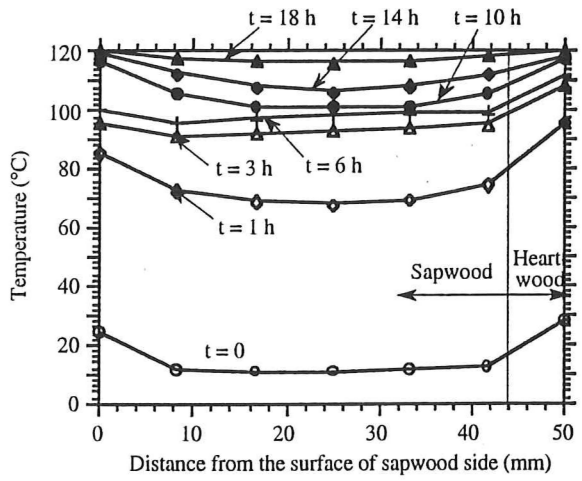

(a). Drying at 120/70°C.

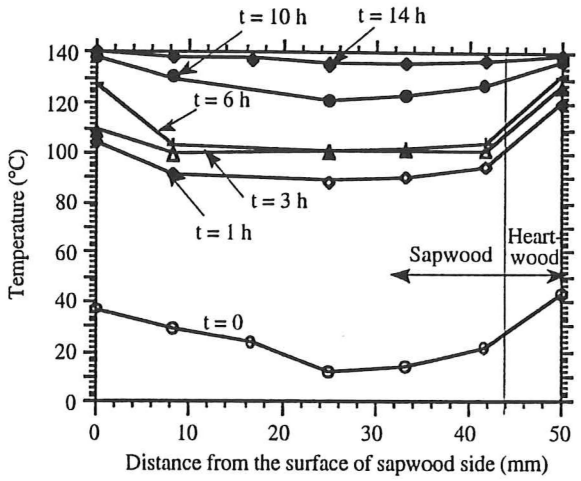

(b). Drying at 140/90°C.

Figure 9.4 Temperature profiles within a mixed sap/heartwood board.
Parameter *t* is the drying time.

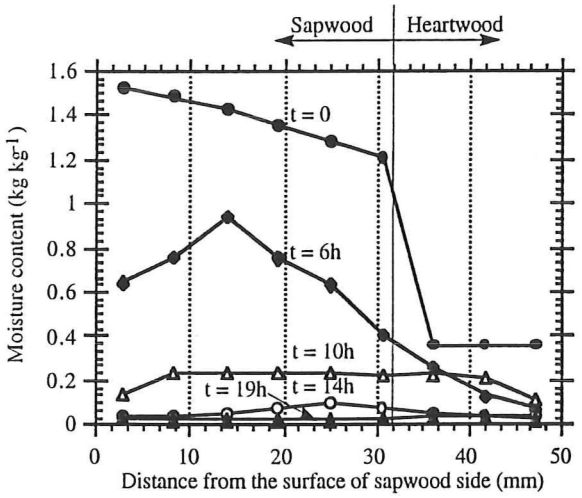

(a). Drying at 120/70°C.

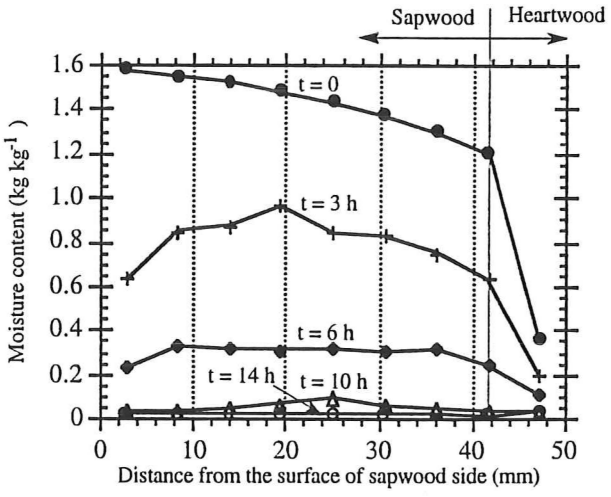

(b). Drying at 140/90°C.

Figure 9.5 Local moisture content gradient in a mixed sap/heartwood board.
Parameter *t* is the drying time.

from the start of drying although the interior temperatures rise towards the surface temperatures during this period. After 10 hours, these temperature profiles tend to be symmetrical across the board. In Run 3 (140/90°C), a similar temperature profile to that of Run 2 can be found, except that in Run 3 the asymmetrical feature persists only 6 hours from the start of drying.

The local moisture content profiles (Figures 9.5a and 9.5b) show that surfaces on both sides dry faster in the first stage of drying. For the drying at 120/70°C, after 6 hours from the start of drying the moisture content 3 mm beneath the sapwood surface drops from 1.50 kg kg^{-1} to 0.60 kg kg^{-1}, while on the heartwood side the moisture content 3 mm beneath is as low as 0.08 kg kg^{-1}. The maximum value at this time is 0.90 kg kg^{-1} and occurs at a position 15 mm beneath the sapwood surface. With 10 hours of drying, the moisture content is relatively even, with a moisture content of about 0.2 kg kg^{-1} in the sapwood, while the wood near the two surfaces is much drier with moisture content of about 0.08 kg kg^{-1}. After 14 hours from the start of drying, the moisture content near the mid-layer of the board decreases to 0.1 kg kg^{-1}, while the values at other positions vary from 0.03 to 0.07 kg kg^{-1}. With further 5 hours of drying, the wood becomes very dry with the average moisture content of 0.023 kg kg^{-1}. A similar profile of moisture content for the drying in Run 3 (140/90°C) to that of Run 2 (120/70°C) can be found, but the board dries faster with the higher air temperature. After 14 hours of drying, the wood can be expected to be very dry, with average moisture content of 0.03 kg kg^{-1}, while the surfaces are at equilibrium with the environment.

For the moisture content profiles given in Figure 9.5, the moisture content 3 mm beneath the surface is in fact the value averaged over 6 mm from the surface. The surface was observed to be dry with a lighter colour when the sample was just taken out of the dryer. This means the local moisture content at the board surface should be lower than this average value. However, the moisture content at the surface was not able to be determined due to difficulties in obtaining such a measurement. Since the moisture contents at different elapsed times were obtained from different samples (each time with one sample), the measured values may be not entirely self-consistent due to small variations between individual samples. For example, for the drying at 120/70°C, the moisture content at depths 3 and 9 mm from the heartwood surface after 10 hours are higher than those found in another sample after 6 hours. This inconsistency may be due to the differences in initial moisture content and proportions of heartwood in the two samples.

In regard to the local moisture content measurement, three methods were investigated, the influence of freezing the sample and the effects of the exposure time on the moisture

content gradient. The three methods were: (1) the sample was immediately sawn into slices for oven-drying; (2) the sample was first put in the freezer overnight and then sawn into slices and (3) the sample was sawn into pieces 20 minutes after the sample was taken from the dryer. It has been found that the three methods produce the essential similar results for the samples taken out in the last stages of drying. However, with the samples taken out in the early period of drying, the moisture content near the surfaces were measured to be lower by method 1 than that obtained using the other two methods. This difference is attributed to a slight loss of the moisture on slicing the sample.

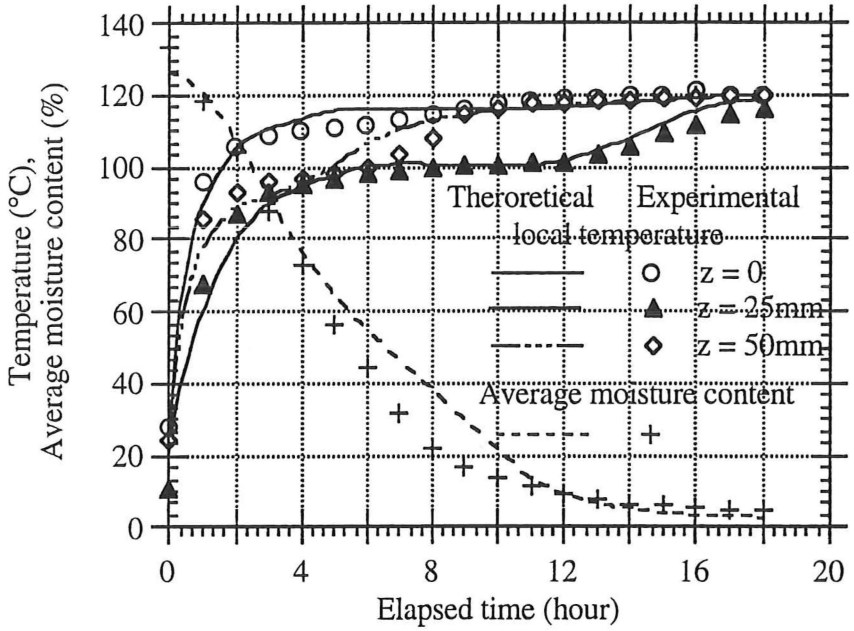

Figure 9.6 The predicted variations with time of temperatures at the board surfaces and board centre and the average moisture-content in comparison with experimental data. The parameter z is the distance from the board surface on the heartwood side. The dry-bulb/wet-bulb temperatures are 120/70°C. Air velocity is 5 m s^{-1}. The values of other parameters are given as follows:

Liquid permeability of sapwood:	$K_l^s = 2.0\text{x}10^{-15}$ m^2
Gas permeability of sapwood:	$K_{GS} = 1.4\text{x}10^{-15}$ m^2
Gas permeability of heartwood:	$K_{GH} = 0.6\text{x}10^{-15}$ m^2
The average thickness of heartwood:	$\delta_H = 6$ mm
The heat-transfer coefficient:	$h = 60$ W m^{-2} K^{-1}
The mass-transfer coefficient:	$\beta = 20$ s m^{-1}

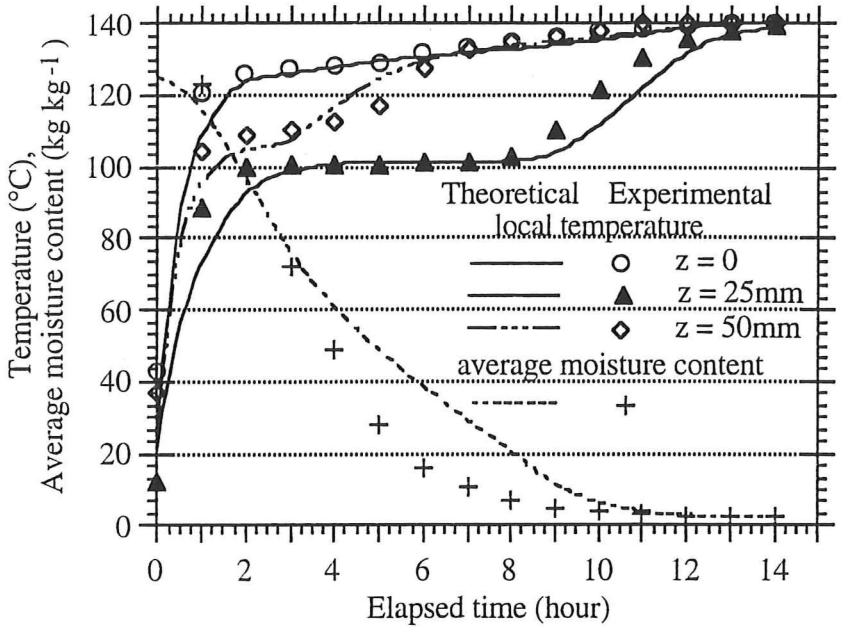

Figure 9.7 The predicted variations with time of temperatures at the board surfaces and board centre and the average moisture-content in comparison with experimental data. The parameter z is the distance from the board surface on the heartwood side. The dry-bulb/wet-bulb temperatures are 140/90°C. Air velocity is 5 m s^{-1}. The values of other parameters are given as follows:

Liquid permeability of sapwood:	$K_l^s = 2.6\text{x}10^{-15}$ m^2
Gas permeability of sapwood:	$K_{GS} = 2.0\text{x}10^{-15}$ m^2
Gas permeability of heartwood:	$K_{GH} = 0.8\text{x}10^{-15}$ m^2
The average thickness of heartwood:	$\delta_H = 6$ mm
The heat-transfer coefficient:	$h = 65$ W m^{-2} K^{-1}
The mass-transfer coefficient:	$\beta = 20$ s m^{-1}

9.2.2 Simulation Results

By employing the method presented in section 9.2, the temperatures at both surfaces and at the center-line of the board have been calculated as shown in Figures 9.6 and 9.7. Also the variations of average moisture content with drying time are given in the figures. Figure 9.6 is for drying under dry-bulb/wet-bulb temperatures of 120/70°C and Figure 9.7 for 140/90°C. The air velocity used in the simulation is 5 m s^{-1}. The values of the parameters used in the model are given below each figure in the legend. In the figures, the

predictions are shown as solid curves, while the experimental data are shown as discrete points for the comparison.

From the simulation results and comparison with the experimental data, some noticeable features can be observed:

• The surface temperature on the sapwood side is much lower than that on the heartwood side during the first 8 hours for air temperatures of 120/70°C and for the first 6 hours with the air temperatures of 140/90°C. The centre temperature remains at about 100°C for about two-thirds of the whole period of drying. This is in agreement with the measured asymmetrical profiles of temperature in the board.

• The surface temperature on the sapwood side is similar to that for an entirely sapwood board. However, the surface temperature on the heartwood side rises more sluggishly than that for the drying of an entirely heartwood board (Chapter 6). For example, for drying at dry-bulb/wet-bulb temperatures of 120/70°C, the surface temperature for the entirely heartwood board rises to 115°C after 2 hours, while for the mixed-wood board, the surface temperature on the heartwood side after 2 hours is 106°C and reaches 115°C after 5 hours. This indicates that in the drying of a mixed board more moisture has evaporated near the surface of the heartwood side compared to a entirely heartwood board. This supports the assumption that some liquid water in sapwood evaporates at the heartwood front.

• The predicted moisture content is higher than the measured value between 4 and 11 hours for air temperatures of 120/70°C and between 3 and 9 hours for air temperatures of 140/90°C from the start of drying. This can be attributed to the moisture losses from the edge sides of the board. As the evaporative fronts withdraw into wood, the drying rates fall, thus the moisture losses become significant. However, the predicted moisture contents are in close agreement with the measured value towards the end of drying when the drying of the board is very slow.

9.2.3 The Comparison between the Drying of A Mixed Sap/heartwood Board and That of An Entirely Sapwood Board or An Entirely Heartwood Board.

If the same values of the parameters as given in previous section (below Figures 9.6) are used to simulate the drying of an entirely heartwood and sapwood board respectively, the drying curves for these three cases can be compared as shown in Figure 9.8. In the calculations, the thickness of the board is taken as 50mm, while for the mixed-wood board the heartwood layer is assumed to be 6 mm. From the comparison, it can be seen that the mixed-wood board dries slower than either an entirely sapwood board or an entirely heartwood board. When the boards are dried to a moisture content of 6%, the drying time is 10 hours for an entirely heartwood board and 11 hours for an entirely sapwood board, whereas for the mixed sap and heartwood board the drying time will have to be extended to 14 hours.

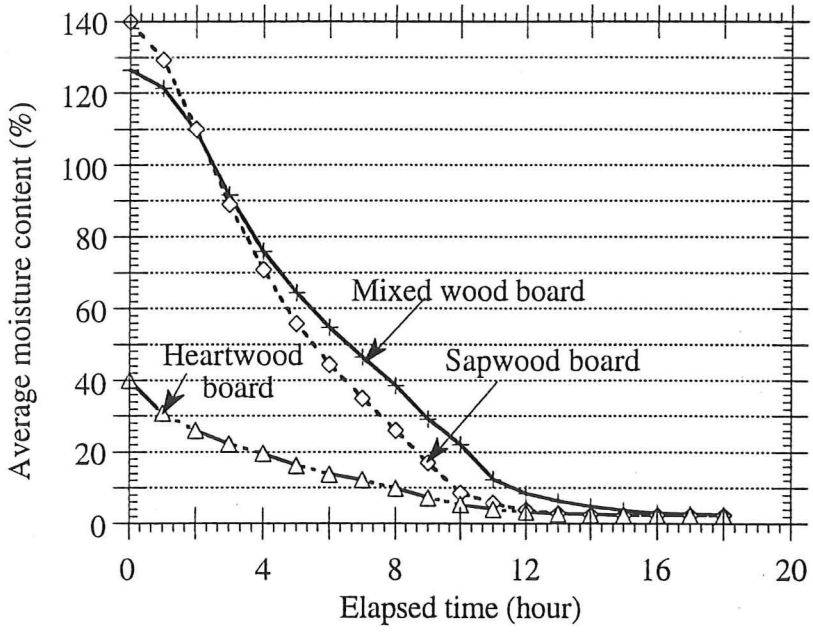

Figure 9.8 The predicted variations of average moisture contents with drying time for an entirely heartwood board, an entirely sapwood board and for a mixed-wood board. The dry-bulb/wet-bulb temperatures are 120/70°C. The air velocity is 5 m s^{-1}.

9.3 Summary

Mixed-wood boards, which contain both heartwood and sapwood, comprise a significant portion of a kiln stack in commercial drying. By employing the physical model of moisture movement proposed, the moisture-content and temperature profiles within *Pinus radiata* mixed-wood are predicted for conditions when the dry-bulb/wet-bulb temperatures are 120/70°C and 140/90°C respectively. The intermediate layer between the sapwood and heartwood is assumed to be as impermeable as the heartwood itself because of the blocked pathways for liquid movement and lower initial moisture content.

In the first stage of drying, an evaporative front recedes from each of the two exposed faces, but the front on the sapwood side remains close to the surface for an initial period while liquid moisture is drawn to it. Whenever the thickness of the heartwood portion is less than that of the sapwood, as soon as the heartwood evaporative front reaches the sapwood boundary, liquid moisture begins to move to that boundary as well as to migrate to the evaporative zone near the surface on the sapwood side. When the liquid moisture in the wet zone is no longer funicular, both fronts withdraw into the sapwood until they meet at a position near the intermediate layer. Thenceforth, the drying is maintained by bound water and water vapour movement.

The duration of drying such a mixed board is longer than that for drying a board composed entirely of either heart or sapwood under the same external drying conditions of air temperature, humidity and velocity.

9.4 Notation

A	constant in equation (9.9)
B	constant in equation (9.9)
C_P	specific heat of moist wood, J kg^{-1}
D_b	bound water diffusion coefficient
j_{wv}	water vapour flux, kg m^{-2} s^{-1}
j_{wf}	liquid water flux, kg m^{-2} s^{-1}
j_{wb}	flux of bound water, kg m^{-2} s^{-1}
E_l	effective permeability of wood to liquid water flow, s m^{-1}
h	external heat-transfer coefficient, W m^{-2} K^{-1}
ΔH_{wv}	latent heat of vaporization of water.
K_{vS}	gas permeability of sapwood, m^2
K_{vH}	permeability of heartwood, m^2
K_l^S	liquid permeability of sapwood at saturation, m^2
M_v	molar mass of the water vapour, kg mol^{-1}
p_G^v	vapour partial pressure in the airstream, Pa
p_S^v	vapour partial pressure at the board surface, Pa
q_S	heat transferred through the surface, W m^{-2}
T	temperature, K
T_G	dry-bulb temperature of the airstream, K
T_S	temperature at the surface, K
X	local moisture content, kg kg^{-1}
X_{FSP}	moisture content at the fibre saturation point, kg kg^{-1}
X_{max}	moisture content of the wood if the entirely void structure were filled with liquid water, kg kg^{-1}
z	space coordinate measured normal to the upper surface of the board, m

Greek

β	external mass-transfer coefficient based on partial pressure difference, s m^{-1}
ρ_S	basic density of wood, kg m^{-3}
τ	time, s
λ	thermal conductivity of the moist wood, J m^{-1}

ρ_v	density of the vapour kg m^{-3}
μ_v	viscosity of the vapour
η	apparent moisture-content coefficient in equation (9.11)
ε	void fraction of the solid wood
Φ	source term involving the latent heat of vaporization, J kg^{-3}
ξ	position of the evaporative front within the wood, m
ξ_o	thickness of the thin dry layer in sapwood side, m
ξ_S	distance of the evaporative front from sapwood side, m
ξ_H	distance of the evaporative front from heartwood side, m
δ	thickness of a half board, m
δ_H	thickness of the heartwood layer, m
δ_S	thickness of the sapwood layer, m

9.5 References

1. Booker, R.E. 1990. Changes in Transverse Wood permeability during Drying of *Dacrydium cupressinum and Pinus radiata*. *New Zealand J. Forest Sci.*, 20(2) pp231-244.

2. Booker, R.E. and Langrish, T.A.G. 1993. The Percentage Saturation of Sapwood and Heartwood from Pinus radiata on the Central Plateau of New Zealand. submitted to *J. of Experimental Botany.*

3. Cown, D.J. and McConchie, D.L. 1980. Wood Property Variations in an Old Crop Stand of Radiata Pine. *New Zealand J. of Forest Science*, 10(3) pp508-520.

4. Harris, J. M. 1954. Heartwood Formation in *Pinus radiata* (D. Don.). *New Phytol*, 53(3) pp517-524.

5. Pang Shusheng, Keey, R.B. and Walker, J.C.F. 1994. Modelling of the High-Temperature Drying of Mixed Sap and Heartwood Boards of Pinus radiata. Proc. 4th IUFRO Wood Drying Symposium. Rotorua, New Zealand.

6. Patankar, S. 1980. "*Numerical Heat Transfer and Fluid Flow*". Hemisphere Publishing Co., New York.

7. Stanish, M.A., Schajer, G.S. and Kayihan, F. 1986. A Mathematical Model of Drying for Hygroscopic Porous Media. *AIChE J.*, 32(8) pp1301-1308.

Chapter **10**

Conclusions and Suggestions for Further Work

10.1 Conclusions

From the studies presented in this thesis, some conclusions can be drawn:

(1) The moisture in the wet wood is present in three states: liquid water in wood cell cavities, bound water in wood cell walls and moisture vapour in wood void space. The movement of the moisture on drying can be described by the physical characteristics of wood and the thermodynamic relationships between wood, water and water vapour: the liquid water movement can be expressed by the capillary action; bound water diffusion by the differences in chemical potential of bound water, which equals that of water vapour at equilibrium; the transfer of water vapour by the gradient in vapour partial pressure. The ease of liquid water and water vapour movement can be reflected by the wood permeability and the state of pits aspiration. The green sapwood has a higher initial moisture content than heartwood, but is much more permeable to liquid water flow due to the pits in green wood remaining unaspirated On the other hand, in heartwood the liquid flow is greatly retarded due to the aspirated state of the pits between tracheids.

(2) The proposed mathematical model can be used to predict the profiles of temperature and moisture-content within a board during drying. From the simulation results, the drying of a single heartwood board can be interpreted using three periods. In the first period, the internal resistance to moisture movement becomes dominant after a short time from the start of drying (5-15 minutes). In subsequent drying, the drying rates decrease as a function of moisture content, which can be expressed by two separate curves. These correspond respectively to the drying when the evaporative front is withdrawing into the wood and to the drying when the movement of bound water and water vapour controls. For sapwood drying, in the first period of drying a relatively constant drying rate can be found when the evaporative front remains close to the drying surface. Afterwards, the drying is similar to that of the heartwood board and the falling-rate drying is also described by two periods.

(3) From the experimental results, the temperature profile in a heartwood board shows that centre temperature remains at about 100°C for a substantial period of time, while the temperature at surface continues to rise above 100°C and towards the dry-bulb temperature of the air. The temperatures at other positions start to rise above 100°C progressively, before which they remain close to the temperature at the board centre. A similar temperature profile to heartwood can be found for the drying of a sapwood board, except that with sapwood an initial period is observed when the surface temperature is only 3 to 5°C higher than 100°C. This feature of temperature profiles is in close agreement with the predictions of the mathematical model.

(4) Although the green sapwood contains over three times as much moisture as the heartwood, the drying time for a sapwood board is slightly longer than for heartwood, to the same final moisture content of about 6%. However, the drying of a mixed-wood board, where the heartwood layer is thinner than the sapwood, is predicted to take two to three hours longer for the wood to dry to the same final moisture content.

(5) In the kiln drying of a stack, the boards at the air inlet dry faster than those towards the air outlet. The nonuniform distribution of moisture content through the stack is believed to be caused by the changes in external conditions (humidity and temperature of the air) along the airflow direction and the variations in the board-averaged transfer coefficients across the first two or three rows of boards. A similar problem can also be found for the drying of a single board due to the variation in transfer rates over the board.

(6) The above uneven drying of a kiln stack and a single board can be smoothed to some extend by reversing the airflow direction. Such flow reversals are of limited usefulness in reducing the extent of the variations, particularly at the centre zone of the kiln. However, a single reversal after 4 hours from the start of drying is adequate to give a reasonable degree of uniformity in the drying. On considering the efficiency of a reversible fan, twice reversals after 4 and 16 hours is recommended.

The studies presented in this thesis have provided a means to understand and describe high-temperature drying process. Since the moisture content of the wood and the external conditions through a kiln-stack can be calculated, drying schedules can be evaluated or a better one chosen to dry the timber more efficiently in terms of the final moisture content distribution.

10.2 Suggestions for Further Work

As was pointed out in Chapter 1, some defects occur when using the faster drying methods under high-temperature conditions. These stress-related defects restrict the choice of operating conditions to maintain timber quality. Since these defects can be traced to uneven distributions of local moisture content and temperature within a board, further studies should be carried out based on the studies of this thesis to express the development and the impact of the drying-related stresses and shrinkage, as follows:

(1) Further drying tests of the mixed sap/heartwood boards. These tests should include the drying of entirely sapwood or heartwood boards sawn from the same tree as the mixed-wood boards and under the same conditions. In this way, the difficulties in drying a mixed-wood board can be clearly illustrated from the experimental results.

(2) Design of optimal drying schedules using the results of kiln-wide analysis and considering the influence of the airflow reversals.

(3) Mathematically modelling of the stress development and the formation of stress-related defects during drying, based on the predicted moisture-content gradient and temperature profile.

(4) Determination of some physical and mechanical properties of the wood of *Pinus radiata*, such as the modulus of elasticity and the loading behaviour of the wood. These properties may vary with moisture content and temperature.

(5) The assessment of the schedules by evaluating the risk of degrade of the damage. This can be undertaken by defining the conditions where the stresses are the greatest.